

# **DIRECTED ASSEMBLY OF HIERARCHICAL SUPRAMOLECULAR BLOCK COPOLYMERS**

**Thesis Submitted to AcSIR for the Award of the Degree of DOCTOR  
OF PHILOSOPHY in Chemical Sciences**



by

**DEEPTHI KRISHNAN**

**Registration No: 10CC14J39018**

**Under the Supervision of**

**Dr. E. BHOJE GOWD**



**CSIR-NATIONAL INSTITUTE FOR INTERDISCIPLINARY SCIENCE  
AND TECHNOLOGY (CSIR-NIIST)  
THIRUVANANTHAPURAM-695 019, KERALA, INDIA**

**2020**



## DECLARATION

I hereby declare that the work incorporated in the thesis entitled: “**Directed Assembly of Hierarchical Supramolecular Block Copolymers**” is the result of the investigations carried out by me at the Materials Science and Technology Division, CSIR-National Institute for Interdisciplinary Science and Technology (CSIR-NIIST), Thiruvananthapuram, under the supervision of Dr. E. Bhoje Gowd and the same has not been submitted elsewhere for any other degree. Due acknowledgements have been made wherever anything has been borrowed from other sources.

  
**Deepthi Krishnan**





राष्ट्रीय अंतर्विषयी विज्ञान तथा प्रौद्योगिकी संस्थान  
NATIONAL INSTITUTE FOR INTERDISCIPLINARY SCIENCE & TECHNOLOGY

वैज्ञानिक तथा औद्योगिक अनुसंधान परिषद्  
इंडस्ट्रियल इस्टेट पि. ओ., पाणपनकोड, तिरुवनंतपुरम- 695 019

Council of Scientific & Industrial Research  
Industrial Estate P.O., Thiruvananthapuram - 695 019

**Dr. E. BHOJE GOWD**  
Principal Scientist &  
Associate Professor (AcSIR)  
Materials Science & Technology Division

+91471-2515474  
+919048427911

## CERTIFICATE

*This is to certify that the work incorporated in this Ph.D. thesis entitled “Directed Assembly of Hierarchical Supramolecular Block Copolymers” submitted by Mrs. Deepthi Krishnan to Academy of Scientific and Innovative Research (AcSIR), in partial fulfilment of the requirements for the award of the Degree of Doctor of Philosophy in Chemical Sciences, embodies original research work under my supervision and guidance at the Materials Science and Technology Division of the CSIR-National Institute for Interdisciplinary Science and Technology (CSIR-NIIST), Thiruvananthapuram. I further certify that this work has not been submitted to any other University or Institution in part or full for the award of any degree or diploma. Research material obtained from other sources has been duly acknowledged in the thesis. Any text, illustration, table etc., used in the thesis from other sources, have been duly cited and acknowledged.*

  
**Deepthi Krishnan**

  
**Dr. E. Bhoje Gowd**  
(Thesis Supervisor)

Thiruvananthapuram  
January, 2020



## ACKNOWLEDGEMENTS

*First, and foremost, it is my great pleasure to express the deep sense of gratitude and indebtedness to Dr. E. Bhoje Gowd, my research supervisor, for his guidance, fruitful discussions, inspiration, constant support and encouragement throughout my research career. I was greatly inspired by his positive attitude and enthusiasm for research and that has greatly motivated me and helped me to build confidence in my work. It has been an honour working as a PhD student under his guidance.*

*I am grateful to Dr. A. Ajayaghosh, Director, NIIST, and former Directors Dr. Suresh Das and Dr. Gangan Pratap, for providing the necessary facilities and infrastructure to carry out this investigation.*

*I wish to thank Dr. Savithri. S (Head, Materials Science and Technology Division), Dr. Harikrishna Bhat, Dr. P. Prabhakar Rao, Dr. M.L.P. Reddy and Dr. M.T. Sebastian (former Heads, MSTD) for their valuable help and suggestions.*

*My sincere thanks also goes to Dr. C. H. Suresh, Dr. R. Luxmi Varma and Dr. Mangalam S. Nair, present and former AcSIR coordinators and Dr. Vijayakumar C. Nair, Dr. Narayanan Unni, and Dr. Saju Pillai, DAC members for their valuable comments and suggestions.*

*I would like to acknowledge Prof. Manfred Stamm, Leibniz Institute of Polymer Research Dresden, Germany for sharing his expertise and for the sincere and valuable guidance extended to me.*

*I thank all the scientists and technical staff of Materials Science and Technology Division for their timely help. Especially I convey my sincere thanks to Mr. Kiran Mohan, Mr. Robert Philip, Mr. Aswin M, Mr. Vishnu, Mr. Rajeev V. R, Mrs. Remya A. N, Mrs. Suchithra, Mrs.*

*Saumini Mathew, Mrs. Viji, Ms. Sreedevi. P. Muraleedharan, Ms. Greeshma, Ms. Anju. P and Mr. John for their timely help in various characterizations.*

*I'd like to acknowledge the valuable suggestions and indispensable helps received from my seniors Dr. S. Nagarajan, Dr. Nisha Kumari, Dr. P.Shaiju, and Dr. Baku Nagendra.*

*A special word of thanks to Mr. Amal Raj R. B, my naughty and lovable brother, sincere team-mate and my friend. He stood up with me in all the problems I faced during my research work as well as in my personal life.*

*I want to thank present and past group members Dr. Angel Mary Joseph, Mrs. Sijla Rosely C. V, Mr. Sivaprasad V, Ms. Praveena N. M, Dr. Jerin K. Pancrecios, Mr. Vipin G. Krishnan, Mr. Gandu Virat, Dr. Lakshmi V, Mrs. Sruthi Suresh, Ms. Ashitha George, Mr. Gokul, Ms. Drisya, Mrs. Kajal Francis, Mr. Palmurukan, Ms. Namitha Ashokan, Ms. Amrutha Krishnan, and Mr. Sujith.*

*I feel myself lucky to have besties like Dr. Fathimath Salfeena, Ms. Soumya M.P, Mrs. Susmitha. A, Ms. Lakshmi M. Nair, Dr. Molji.C, Mrs. Suhailath, Mrs. Lekshmi D. R, the stay and all the fun and the long chit-chat with them are surely going to be one of the most loving memories of my Ph.D life.*

*No acknowledgments would be complete without giving thanks to my parents; they've taught me the value of hard work and self-respect. I extend my deepest gratitude to my father Mr. K. Dana Krishna Pillai and my mother Mrs. G. Krishnakumai Amma for always encouraging and believing me to achieve my dream. I remember my heavenly grandparents, Mr. Janardhanan Pillai and Mrs. Jagadhamma whose role in my life was, and remains, immense. I sincerely thank my husband, Dr. Syam S Nair for his unconditional care and support.*

*I extended my thanks to all my teachers, my dear friends and other family members who stood as the source of inspiration in my early days and who taught me many things at different stages of my academic career.*

*I would like to thank University Grants Commission, New Delhi and Council of Scientific and Industrial Research for the financial support.*

*Finally, I thank God, for letting me through all the difficulties.*

**Deepthi Krishnan**



# CONTENTS

	<b>Page No.</b>
<b>Declaration</b>	iii
<b>Certificate</b>	v
<b>Acknowledgements</b>	vii
<b>Contents</b>	xi
<b>List of Abbreviations</b>	xvii
<b>Preface</b>	xxiii
<hr/>	
<b>CHAPTER 1:</b>	<b>Introduction</b>
	<b>1-47</b>
<hr/>	
<b>1.1.</b> Block Copolymers and their Self-Assembly	1
<b>1.2.</b> Phase Behaviour of Block Copolymers	3
<b>1.3.</b> Supramolecular Block Copolymers	7
<b>1.3.1.</b> Supramolecular Chemistry	7
<b>1.3.2.</b> Combination of Supramolecular Chemistry with Block Copolymers	8
<b>1.4.</b> Phase Behaviour of Block Copolymer Based Supramolecules in Bulk and in Thin Films	12
<b>1.4.1.</b> In Bulk	13
<b>1.4.2.</b> In Thin Films	13
<b>1.5.</b> Factors Influencing Block Copolymer Supramolecules	14

1.5.1.	Mole Fraction	14
1.5.2	Effect of Small Molecules	16
1.5.3.	Annealing	17
1.5.3.1.	Thermal Annealing	17
1.5.3.2.	Solvent Vapor Annealing	18
1.6.	Method to Determine the Morphology of BCP Supramolecules	19
1.6.1.	Small-Angle X-ray Scattering (SAXS)	20
1.6.2.	Transmission Electron Microscopy (TEM)	21
1.6.3.	Atomic Force Microscopy (AFM)	23
1.7.	Functional Small Molecules Based BCP Supramolecules	23
1.7.1.	Surfactant Based BCP Supramolecules	24
1.7.2.	Liquid Crystalline (LC) Based BCP Supramolecules	25
1.7.2.1	Azo Molecule (LC) Based BCP Supramolecules	27
1.7.3.	Organic Semiconductor Based Supramolecules	29
1.7.4.	Polymer Based Supramolecules	32
1.8.	. Applications of Block Copolymer Supramolecules	34
1.8.1.	Nanotemplates and Nanopatterning	34
1.8.2.	Membrane	37
1.8.3.	Photovoltaic Applications	38
1.9.	References	39

<b>CHAPTER 2:</b>	<b>Topochemical Polymerization of Hierarchically Ordered Diacetylene Monomers within the Block Copolymer Domains</b>	<b>49-79</b>
-------------------	--	--------------

2.1.	Abstract	49
2.2.	Introduction	50
2.3.	Experimental Section	52
2.3.1.	Materials	52
2.3.2.	Sample Preparation	52
2.3.3.	Annealing Methods	53
2.4.	Characterization	54
2.5.	Results and Discussion	55
2.5.1.	Hierarchical Assembly of PCDA Monomers within the Block Copolymer Microdomains	55
2.5.2.	Topochemical Polymerization of PCDA within the Block Copolymer Microdomains	63
2.6.	Conclusions	76
2.7.	References	76

**Directed Assembly of Hierarchical  
Supramolecular Block Copolymers: A  
CHAPTER 3: Strategy to Create Donor- Acceptor Charge  
Transfer Stacks** **81-110**

3.1.	Abstract	81
3.2.	Introduction	82
3.3.	Experimental Section	85
3.3.1.	Materials	85

<b>3.3.2.</b> Sample Preparation	85
<b>3.4.</b> Characterization	86
<b>3.5.</b> Results and Discussion	88
<b>3.6.</b> Conclusions	107
<b>3.7.</b> References	107

---

**Co-assembly of Functionalized Donor-  
ACCEPTOR MOLECULES WITHIN THE BLOCK  
CHAPTER 4: Copolymer Domains via Supramolecular  
Approach**

---

<b>4.1.</b> Abstract	111
<b>4.2.</b> Introduction	112
<b>4.3.</b> Experimental Section	115
<b>4.3.1.</b> Materials	115
<b>4.3.2.</b> Synthesis of Functionalized Naphthalene Diimide (FNDI)	115
<b>4.3.2.1.</b> Synthesis of Compound-1	115
<b>4.3.2.2.</b> Synthesis of Compound-2	116
<b>4.3.3.</b> SMA Preparation	116
<b>4.4.</b> Characterization	117
<b>4.5.</b> Results and Discussion	118
<b>4.5.1.</b> Characterization of Functionalized Naphthalene Diimide (FNDI)	118
<b>4.5.2.</b> Hierarchical Assembly of D-A Molecules within the Block Copolymer Domains	119

4.5.3.	Formation of Charge-Transfer Complex	126
4.6.	Conclusions	132
4.7.	References	133

---

**CHAPTER 5: Factors Influencing the Formation of Block Copolymer-based Supramolecular Assemblies in Bulk and Thin Films 137-165**

---

5.1.	Abstract	137
5.2.	Introduction	138
5.3.	Experimental Section	142
5.3.1.	Materials	142
5.3.2.	Sample Preparation	142
5.4.	Characterization	143
5.5.	Results and Discussions	144
5.5.1.	Effect of Small Molecules on the SMA Formation in Bulk	146
5.5.2.	Effect of Small Molecules on the SMA Formation in Thin Films	153
5.6.	Conclusions	161
5.7.	References	162

---

**CHAPTER 6: Overall Summary 167-171**

---

6.1.	Summary	167
6.2.	Future Perspectives	170

---

<b>Papers Presented at Conferences</b>	173
<b>List of Publications</b>	177

---

## List of Abbreviations

$\lambda$	Wavelength
$\varepsilon_{AA}$	Interaction energies
$\mu m$	Micro meter
$\Delta G_p$	Gibbs free energy
$^{\circ}C$	Degree Celsius
$^1H$ NMR	Proton nuclear magnetic resonance spectra
2D	Two-dimensional
3-NDP	3-nonadecylphenol
4HB	4-Hydroxybiphenyl
4T	5'''-(3,7-Dimethyloctyl)-5-(3-(3-hydroxyphenyl)propyl)-[2,2';5',2'';5'',2''']quaterthiophene
4VP	4-vinyl pyridine
A	Active device area
$\text{\AA}$	Angstrom
AC	Alternating current
AFM	Atomic force microscopy
Al	Aluminium
$Al_2O_3$	Aluminium oxide
BCP	Block copolymer
BHAB	4-butyl-4' hydroxyazophenol
BHJ	Bulk-heterojunction
BP4T	Bis-phenol quarterthiophene
BPCA	Biphenyl-4-carboxylic acid

C	Hexagonally packed cylinders
C <sub>60</sub>	Fullerene
CDCl <sub>3</sub>	Deuterated chloroform
CholHS	Cholesteryl hemi succinate
Cm	Centimeter
CO <sub>2</sub>	Carbon dioxide
CT complex	Charge transfer complex
D	Domain spacing
D-A	Donor-Acceptor
DBSA	Dodecyl benzenesulfonic acid
DCM	Dichloromethane
DI water	Deionized water
DSC	Differential scanning calorimetry
eV	Electron volt
<i>F</i>	Volume fraction
FETs	Field-effect transistors
FNDI	Functionalized naphthalene diimide
FTIR	Fourier transform infrared spectroscopy
FWHM	Full width half maximum
G	Bicontinuous gyroids
G	Gram
GISAXS	Grazing-incidence small-angle X-ray scattering
H	Planck constant
HABA	2-(4(-hydroxybenzeneazo) benzoic acid
HBCA	4'-hydroxy-4-biphenylcarboxylic acid

<i>Hkl</i>	Miller indices
Hrs	Hours
I	Current
I <sub>2</sub>	Iodine
IPA	Isopropyl alcohol
ITO	Indium tin oxide
K <sub>B</sub>	Boltzmann constant
<i>kV</i>	Kilovolt
L	Stacked lamellae
LC	Liquid crystals
LED	Light-emitting diodes
mA	Micro ampere
m <sub>e</sub>	Mass of electron
MHz	Mega hertz
Min	Minutes
Mm	Millimeter
Mn	Number average molecular weight
MSA	Methane sulfonic acid
Mw	Weight average molecular weight
N	Degree of polymerization
NCOOH	Naphthoic acid
NDI	Naphthalene diimide
Nm	Nanometer
NOH	Naphthol
OLEDs	Organic light-emitting diodes

OPVCN-OH	Oligo(phenylenevinylene)
OPVs	Organic photovoltaics
OsO <sub>4</sub>	Osmium tetroxide
P3HT- <i>b</i> -P4VP	Poly(3-hexylthiophene)- <i>block</i> - poly(4-vinylpyridine)
P4VP	Poly(4-vinyl pyridine)
P4VP- <i>b</i> - PAPI	Poly(4-vinylpyridine)- <i>block</i> -poly(N-acryloylpiperidine)
P4VP- <i>b</i> -PDMA	Poly(4-vinylpyridine)- <i>block</i> -poly(N,N-dimethylacrylamide)
P4VP- <i>b</i> -PS- <i>b</i> -PAPI	Poly(4-vinylpyridine)- <i>block</i> -poly(styrene)- <i>block</i> -poly(N-acryloylpiperidine)
Pa	Pascal
PAA	Poly(acrylic acid)
PAPI	Poly(N-acryloylpiperidine)
PBA	Pyrenebutyric acid
PBLG- <i>b</i> - PLL	Poly( $\gamma$ -benzyl-L- glutamate)- <i>block</i> -poly(L-lysine)
PCBM	[6,6]-phenyl-C <sub>61</sub> -butyric acid methyl ester
PCDA	10,12-pentacosadyonic acid
PDA	Polydiacetylene
PDI	Polydispersity index
PDMAEMA- <i>b</i> -PMA	Poly(2-(dimethylamino) ethyl methacrylate)- <i>b</i> -poly(sodium methacrylate)
PDP	3-pentadecylphenol
PEO- <i>b</i> -PS	Poly(ethylene oxide)- <i>block</i> -poly(styrene)
p <sup>H</sup>	Potential of hydrogen
PL	Photoluminescence
PLCPs	Photoresponsive liquid crystalline polymers

PMAA	Poly(methacrylic acid)
PMMA	Poly(methyl methacrylate)
pNIPAM	Poly (N-isopropyl acrylamide)
Ppm	Parts per million
PS	Poly(styrene)
PS- <i>b</i> -P4VP	Poly(styrene)- <i>block</i> -poly(4-vinyl pyridine)
PS- <i>b</i> -PAA	Poly(styrene)- <i>block</i> - poly(acrylic acid)
PS- <i>b</i> -PMMA	Poly(styrene)- <i>block</i> -poly(methyl methacrylate)
Q	Scattering vector
R	Ratio
R	Resolution
R <sub>g</sub>	Gaussian gyration radius
RuO <sub>4</sub>	Ruthenium tetroxide
S	Body-centered cubic arranged spheres
S	second
SA	Solvent vapor annealing
SAXS	Small-angle X-ray scattering
SCFT	Self-consistent mean field theory
SCLC	Space charge limited current
SiMe <sub>4</sub>	Tetramethylsilane
SMA	Supramolecular assembly
T	Temperature
TA	Thermal annealing
TEM	Transmission electron microscopy
T <sub>g</sub>	Glass transition temperature

THF	Tetrahydrofuran
$T_m$	Melting temperature
$T_{ODT}$	Order-disorder transition temperature
UPBI-PDP	Pentadecyl phenol based asymmetric perylenebisimide
UV Light	Ultraviolet light
UV-visible	Ultraviolet-visible
$V$	Potential difference
$V$	Voltage(Volt)
WAXS	Wide angle X-ray scattering
Xe lamp	Xenon lamp
$Z$	Number of adjacent monomers
$\delta$	Chemical shift
$\Delta H_p$	Enthalpy of demixing of polymer blocks
$\Delta S_p$	Configurational entropy
$\epsilon_0$	Permittivity of free space
$\epsilon_r$	Dielectric constant
$\theta$	Bragg angle
$\mu_{eff}$	Effective electron mobility
$\chi$	Flory-Huggins interaction parameter

## PREFACE

Supramolecular block copolymers are becoming the most attractive materials to achieve nanoscale structures for advanced applications such as nanopatterning, optoelectronic and catalytic technologies. This concept was first introduced by the Ikkala's group, which was produced by combining block copolymer (BCP) with a low molecular weight additive via secondary interactions, such as hydrogen bonding,  $\pi$ - $\pi$  stacking, electrostatic interactions, etc. These supramolecular assemblies (SMA) offer advantages over the covalently linked analogues since different functionalities can be incorporated into the assemblies simply by substituting the low molecular weight additives. This will reduce the burden of synthesizing entirely new families of BCP. Another major advantage of SMA strategy is that the additive can be removed easily from the SMA by selective dissolution to obtain a nanoporous material. These nanopores or nanochannels that are lined with functional groups are readily available for further applications.

Several thermodynamic and kinetic factors affect the overall assembly of the supramolecules. These include polymer-small molecule interactions, BCP microphase separation, interaction parameter, polymer chain deformation, melting, crystallinity and packing of the small molecule, etc. The polymer may affect the small molecules crystal structure or its ability to crystallize. Conversely, the incorporation of the small molecules can affect the BCP chain architecture, stiffness, interaction parameter ( $\chi$ ). Kinetically, the distribution and diffusion rate of the small molecules can depend on the melting temperature ( $T_m$ ) of the small molecules and the relative interaction parameter ( $\chi$ ) between the small molecules and each block of the BCP at the given annealing temperature.<sup>7,8</sup> With all of these considerations, it is clear that the phase behavior of the small molecules is of critical importance in its coassembly with the BCP, especially for highly crystalline

functional small molecules. The potential application of supramolecules mainly focused in the field of photovoltaics, transistors, optical devices, and stimuli-responsive materials, etc.

The conjugated block copolymers demonstrate some advantages due to their ability for self-assembly and solution processing. However, the synthesis of conjugated blocks with precise control of molecular weight required for ordering and alignment is extremely challenging. To overcome these difficulties, considerable attention has been devoted in the field of block copolymer supramolecular assemblies. It can combine the properties of the block copolymer as well as the functional small molecules. The small molecules such as organic semiconductors, liquid crystalline materials, etc. with optical, electronic, or stimuli-responsive properties can be used to incorporate functionality into the formation of BCP supramolecules. In the present thesis, we demonstrated several new aspects on BCP supramolecules, such as the incorporation of photopolymerizable small molecules and subsequent polymerization, the introduction of the three-component assembly to generate donor-acceptor stacks within the block copolymer microdomains and the effect of functionalization of small molecules on the BCP supramolecular assembly.

The thesis has been divided into six chapters. The first chapter gives a general introduction to the concept of supramolecular block copolymers. This chapter also explains the phase behavior of block copolymer supramolecules in bulk and thin films. Further, this chapter elucidates the factors affecting the block copolymer supramolecules and highlights the methods used for the determination of the morphology of supramolecules. A literature review on functional small molecule based supramolecules and the applications of these structures will also be discussed here in detail.

Chapter 2 deals with the incorporation of polymerizable diacetylene small molecules within the block copolymer domains. The photopolymerizable 10,12-

pentacosadiynoic acid (PCDA) molecule form supramolecular complex with poly(styrene)-*block*-poly(4-vinylpyridine) (PS-*b*-P4VP) block copolymer via H-bonding. We systematically investigate how the annealing conditions affect the hierarchical ordering and the molecular orientation of PCDA molecules within the block copolymer microdomains and subsequently the topochemical polymerization of PCDA. It was found that solvent vapor annealing is the most appropriate method to obtain the desired molecular orientation of PCDA for the effective topochemical polymerization compared to that of the thermal annealing method. The hierarchical ordering of the block copolymer supramolecules upon the UV irradiation and melt-cooling was investigated at multiple length scales by a combination of different techniques including small-angle X-ray scattering and wide-angle X-ray scattering.

In Chapter 3, we describe a three-component hierarchical self-assembly approach to generate stable alternate donor-acceptor (D-A) assemblies within block copolymer microdomains by involving the supramolecular approach in self-assembly of block copolymers. So far, the assembly between a single small molecule and block copolymer were explored to obtain block copolymer supramolecules. Here we report block copolymer supramolecules composed of two small molecules (donor and acceptor) and polystyrene-*block*-poly(4-vinylpyridine) (PS-*b*-P4VP). 1-Pyrenebutyric acid (PBA, donor) forms hydrogen bonding with P4VP and aromatic interactions with naphthalene diimide (NDI, acceptor) to generate charge-transfer (CT) complexes within the block copolymer domains in the solid state. Using FTIR, SAXS, WAXS, TEM, UV/Vis spectroscopy and photoluminescence spectroscopy measurements, we demonstrate the formation of hierarchical structures and charge-transfer complexes between PBA and NDI. Space charge limited current analysis showed the enhanced charge carrier mobility in PS-*b*-P4VP (PBA+NDI) supramolecules compared to the physical blends of PBA+NDI.

Chapter 4 describes the role of the functional groups on both the donor (PBA) and acceptor molecules (functionalized NDI) on the hierarchical assembly as well as the D-A stacking within the block copolymer domains. Here both the molecules can form the H-bonding with P4VP chains which is confirmed by FT-IR spectroscopy. Apart from this,  $\pi$ - $\pi$  stacking between D-A molecules is possible within the block copolymer domain. These noncovalent interactions lead to the formation of hierarchical structures and charge-transfer complexes between functionalized PBA and NDI within block copolymer microdomains. It was also observed that the introduction of functional group on NDI molecules favor the formation of stable D-A stacks in the physical blend as well.

Chapter 5 discussed the factors influencing the formation of supramolecular assemblies both in bulk and thin films using PS-*b*-P4VP and small molecules with different functional groups. The biphenyl molecules with monohydroxyl-functionalized (4HB), monocarboxylic acid-functionalized (BPCA) and both carboxylic acid and hydroxyl-functionalized groups (HBCA) are taken as the small molecules for the formation of supramolecular assembly. In bulk, it was observed that the glass transition temperature ( $T_g$ ) of the polymer plays a crucial role in the formation of SMA in the case of monohydroxyl-functional group (4HB). The improved long-range order was observed in the case of thin films in solvent-vapor annealed samples. In the case of SMAs with the carboxylic acid-functionalized small molecules, the macrophase separation is observed up to the melting temperature of small molecules, which may be due to the self-associated hydrogen bonds of carboxylic groups within small molecules. The corresponding solvent-vapor annealed samples, the selectivity of the solvent to the polymer and small molecules place a crucial role in the formation of SMAs. It was demonstrated that and a good solvent leads to effective formation of SMAs with well-defined morphology, and a bad solvent leads to

macrophase separated structures with disordered morphology irrespective of the functional groups present in the small molecules.

The salient features and summary of the research work carried out are described in 6th chapter, along with the future perspectives. The first three working chapters emphasize the development of BCP-based semiconductor supramolecules and the final working chapter deals with the effect of functionalization of the small molecules on the BCP-based supramolecular assembly.



## Introduction

---

---

### 1.1. Block Copolymers and their Self-Assembly

The term self-assembly stands for the design of complex structures obtained from spontaneous organization or arrangement of the smaller individual units of materials. Our nature becomes the finest sketch of self-assembly. It is a powerful tool for forming structures ranging from angstroms to meters. It has become a subject of tremendous interest in the research community, providing nano-structured materials with length scales beyond the crystallographic aspects. It is expected that these ordered assemblies will have applications in the field of lithography, especially when feature sizes are in the nanoscale.<sup>1-</sup>

<sup>5</sup> By tuning the size, shape, interactions, and surface characteristics of the building blocks, well-organized structures can be generated via self-assembly. The nanoscale entities pack into periodic arrangements in the self-assembly phase to reach minimum free energy by maximization of attractive and minimization of repulsive molecular interactions.<sup>6</sup>

Self-assembly of block copolymers (BCP) has gained enormous attention in the field of nanoscience and nanotechnology due to their ability to form a variety of periodic structures in the nanoscopic length scales.<sup>4, 7-11</sup> Block copolymers comprise of two or more chemically distinct polymer blocks associated together by covalent or non-covalent bonds in multiple architectures. The various BCP architectures are linear diblock, triblock, multiblock copolymers, star block copolymers, graft copolymers, etc.<sup>12, 13</sup> which are shown in Figure 1.1.

---

---

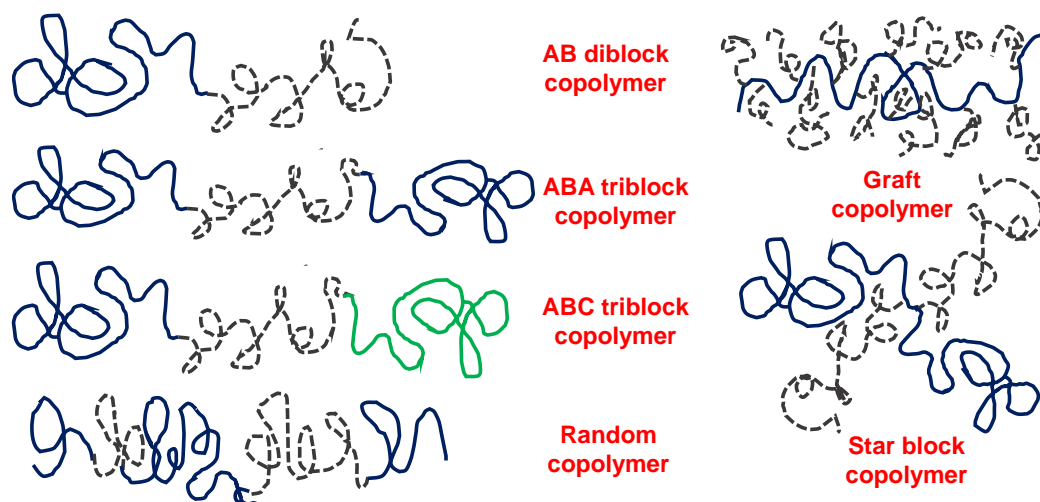


**Figure 1.1.** Typical architectures of block copolymers

Usually, when two chemically different polymers are mixed, they always get macrophase separated due to asymmetry in enthalpic and entropic contributions. Owing to the large number of repeating units in each polymer, the weak repulsive interactions between the repeating units in different polymers are intensified. These interactions typically control the thermal motion of polymer chains, instigating the macrophase separation. However, when these two different polymers are connected through a covalent bond, they can separate only up to certain local molecular scale leading to the formation of periodic nanostructures.<sup>14, 15</sup> It undergoes microphase separation in bulk as well as in thin films due to the intrinsic immiscibility of distinct polymer chains and results in various domain morphologies with dimension of about 10-100 nm. The BCP ordered phases such as body-centered cubic spheres, hexagonally packed cylinders, gyroid, and lamellae are shown in Figure 1.2. The obtained morphology depends on the ratio of block lengths, strength of interaction, the number of blocks, etc.<sup>16</sup> The variable factors such as the film thickness, post-deposition annealing processes, and interaction among the polymer blocks with the substrate can control the degree of long-range order and the microdomain orientation. Furthermore, self-assembly is an extremely parallel method that occurs spontaneously. The combination of these specific features make block copolymers

extremely attractive in several distinct areas for both basic research and technological applications including nanoparticle templates, nanoporous membranes, organic photovoltaics, nanostructured networks, drug delivery vehicles, and for next-generation lithography.<sup>17-19</sup>

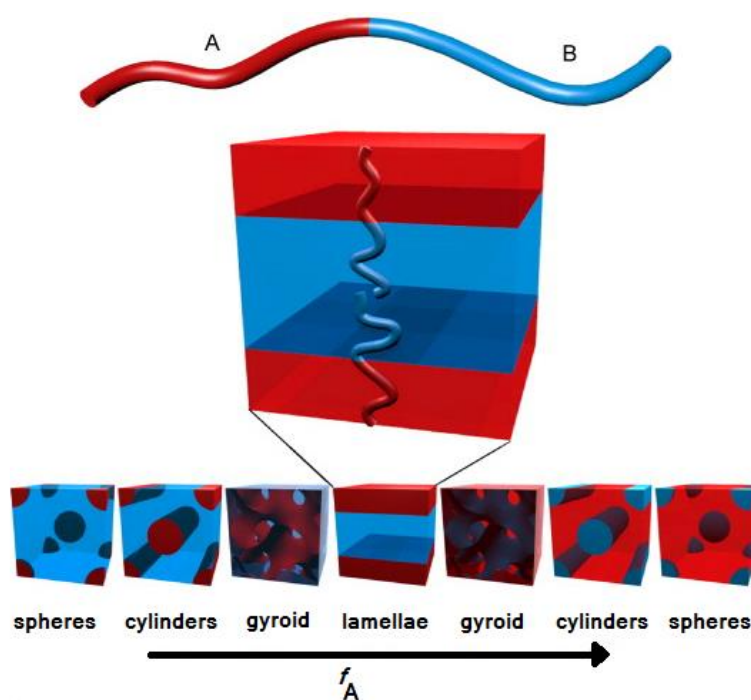


**Figure 1.2.** Different phases made by the diblock copolymer self-assembly. Reprinted with permission from ref. 3; copyright 2007 Elsevier.

Modern synthetic chemistry provides the option of using appropriate length scales and geometries to design these macromolecules. A fundamental understanding of the thermodynamics and kinetics of the self-assembly process of block copolymers, both in bulk and in thin films is required for the development of these materials. The ability to organize these nano-objects exactly on suitable substrates is a cherished tool for exploiting new developments in technology.

## 1.2. Phase Behaviour of Block Copolymers

The inherent quality of incompatibility of the polymer segments in block copolymers allows it to separate into two individual domains within the matrix, and it leads

to separation in the nanometer length scale. Due to the covalent linkage between the polymer blocks, the competition between bond connectivity and macrophase separation leads to the microphase separation.<sup>20</sup> This contributes to domain sizes in the range of 10–100 nm. The block copolymer microphase separation can be well-defined by considering two opposing factors, the repulsion between the different monomers and stretching of the polymer chains. The microdomain structures were obtained due to the incompatibility of blocks, whereas the microdomain interfaces are attained from the block junctions. Thermodynamically, this process is specified by the enthalpy of demixing of polymer blocks,  $\Delta H_p$ . As the surface-to-volume ratio increases, the BCP's microdomains size increases and thus the BCP system interfacial free energy decreases. Since the growth of the microdomain generates a density defect towards the microdomain centre, the BCP chains were stretched over the undisturbed Gaussian gyration radius  $R_g$  to fill space. This method, which is accompanied by a decrease in configurational entropy  $\Delta S_{p,conf}$ , is in contrast to the block separation. The extra loss in interfacial entropy  $\Delta S_{p,int}$  is due to confinement of the block junctions in the interfacial area. The change in Gibbs free energy was calculated by the equation,

$$\Delta G_p = \Delta H_p - T\Delta S_{p,int} - T\Delta S_{p,conf} \quad (1.1)$$

The Gibbs free energy determines the transition from homogenous blended blocks (disordered state) to an organized structure. If the enthalpic part dominates, i.e.,  $\Delta G_p > 0$ , the transition occurs from disordered state to ordered state.

One important thermodynamic parameter called the Flory-Huggins interaction parameter ( $\chi$ ) that describes the degree of incompatibility or the miscibility between the A and B blocks, drives the phase segregation or separation. In the case of a simple diblock copolymer system AB, the Flory-Huggins interaction parameter, ( $\chi_{AB}$ ) is defined by,

$$\chi_{AB} = \frac{z}{K_B T} \left( \varepsilon_{AB} - \frac{\varepsilon_{AA} + \varepsilon_{BB}}{2} \right) \quad (1.2)$$

where  $z$  is the number of adjacent monomers,  $T$  is the temperature,  $K_B$  is the Boltzmann constant and  $\varepsilon_{AA}$ ,  $\varepsilon_{BB}$ , and  $\varepsilon_{AB}$  stands for the interaction energies of the A-A, B-B and A-B interactions, respectively. The favourable positive  $\chi$  values are the result of adverse interactions between the distinct polymer constituents, whereas the negative  $\chi$  value specifies favourable mixing. The segregation strength of two chemically dissimilar polymer segments is represented as the product,  $\chi N$  (where  $N$  is the degree of polymerization), which controls the microphase separation status. The weak segregated polymer blocks having  $\chi N < 10$ , implies that the thermodynamic driving force is insufficient to control the entropic stretching combined with demixing that favours isotropic morphology or disordered morphology. The microphase separation arises when the  $\chi N > 10.5$ , and a series of structures can be exhibited depending on the relative volume fractions ( $f$ ) as well as the exact value of  $\chi N$  of the polymer blocks. It is essential to remind that the higher  $\chi N$  values are required for achieving the microphase separated structures.<sup>21, 22</sup>

The composition of the diblock copolymer will be expressed in terms of volume fraction of the A-component,

$$f_A = \frac{N_A}{N_A + N_B} = \frac{N_A}{N} \quad (1.3)$$

and for the B-component,

$$f_B = 1 - f_A = \frac{N_B}{N_A + N_B} = \frac{N_B}{N} \quad (1.4)$$

Where,  $N_A$  and  $N_B$  are the numbers of monomer units of A- and B-type and  $N$  is the total number of monomers. If  $N_A = N_B$ , we have a symmetric diblock. A schematic illustration of a symmetric and an asymmetric diblock copolymer is presented in Figure 1.3.

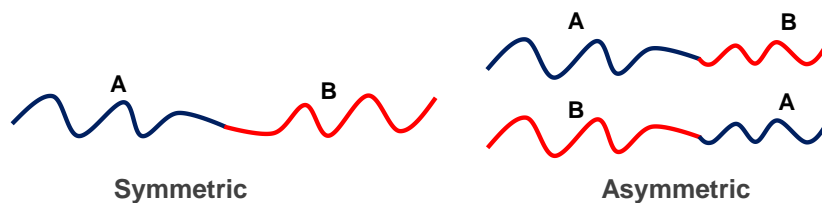


**Figure 1.3.** Schematic of symmetric and asymmetric AB diblock copolymers.

Based on the self-consistent mean-field theory (SCFT), Matsen and Bates proposed the phase diagram of diblock copolymer melt, which is the graph expressing phase balance between enthalpy and entropy of the block, plotted by the product ' $\chi N$ ' vs. ' $f$ ', volume fraction of one of the blocks. Figure 1.4 shows the diblock copolymer morphologies and the phase diagram.<sup>23</sup>

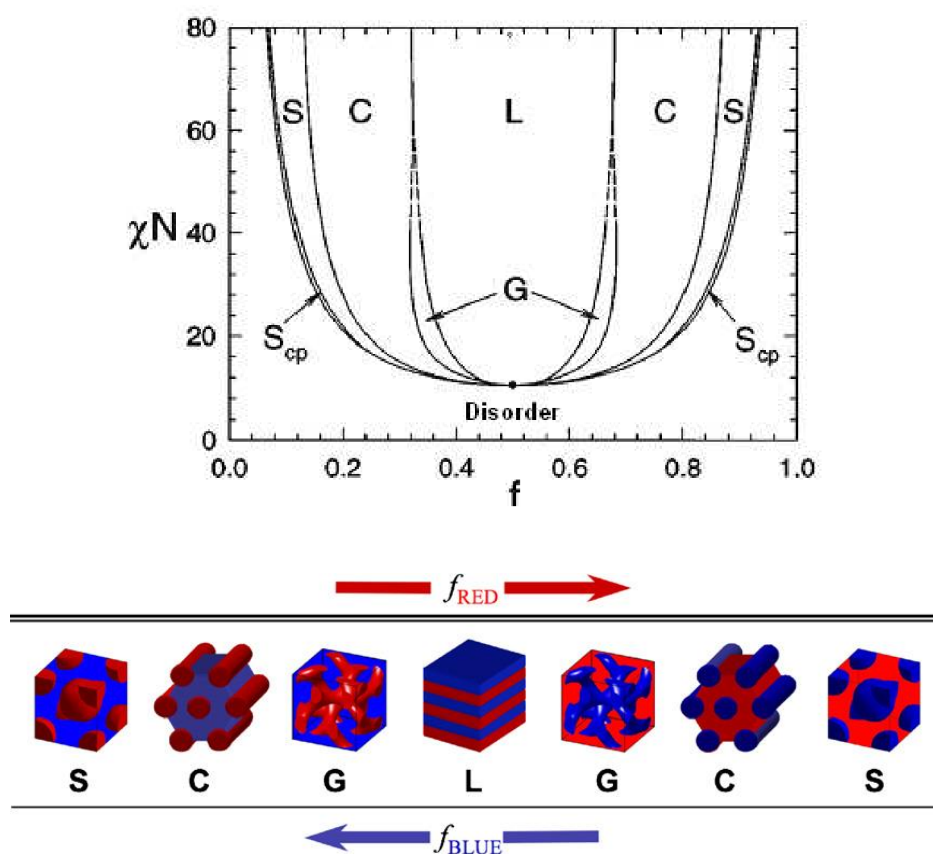


**Figure 1.4.** The phase diagram of a diblock copolymer and possible morphologies. Reprinted with permission from ref. 23; copyright 1996 American Chemical Society and from ref. 24; copyright 2008 Elsevier.

From Figure 1.4, as the volume fraction of A block increases, strongly segregated diblock copolymer produces body-centered cubic arranged spheres (S) ( $f_A \approx 5-21\%$ ), hexagonally packed cylinders (C) ( $f_A \approx 21-33\%$ ), bicontinuous gyroids (G) ( $f_A \approx 33-37\%$ ) and well stacked lamellae (L) ( $f_A \approx 37-50\%$ ) of A-phase in a matrix of B phase. For  $f_A > 50\%$ , the inversion of the morphology takes place, i.e., A-phase as the matrix and B-phase as the domains. The development of these diblock copolymer morphologies is strongly dependent on both  $f$  and  $\chi N$ . The  $\chi N$  value less than 10.5 should always end up in a disordered morphology neglecting the volume fraction. It can happen at a higher temperature and a lower degree of polymerization.<sup>5, 22, 23</sup>

### 1.3. Supramolecular Block Copolymers

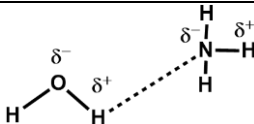
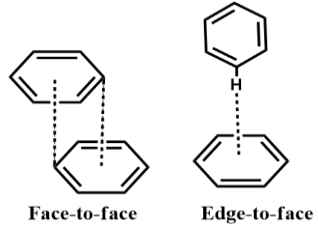
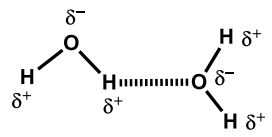
The combination of self-assembly of block copolymers and supramolecular chemistry is one of the most auspicious techniques in achieving nanoscale structures and thus an active ingredient for soft material nanotechnology.

#### 1.3.1. Supramolecular Chemistry

The field of supramolecular chemistry is the new branch of chemistry which is rapidly emerging and is defined as self-organization of molecular complexes by noncovalent interactions.<sup>24, 25</sup> A variety of noncovalent interactions are used in supramolecular chemistry including hydrogen bonding, ionic interactions,  $\pi-\pi$  interactions, metal coordination, van der Waals interactions, hydrophobic interactions, etc..<sup>26-28</sup> The non-covalent interactions are generally weaker than covalent bonds, therefore, supramolecular assemblies (SMAs) are more dynamic in nature compared to covalently-bonded molecules. The strength and other characteristics of different non-covalent interactions are summarized in Table 1.1.

---

**Table 1.1.** Characteristics of noncovalent interactions in supramolecular chemistry<sup>24</sup>

Interaction	Strength (kJ/mol)	Character	Example
Hydrogen Bonding	10-120	Selective, Directional	
$\pi$ - $\pi$ stacking	0-50	Directional	
Ionic (ion-ion)	100-350, comparable to covalent bonding	Non-selective, Non-directional	<b>Na<sup>+</sup> Cl<sup>-</sup></b>
Dipole-dipole	5-50	Directional	
Van der Waals	< 5 but depends on surface area	Non-selective, Non-directional	

### 1.3.2. Combination of Supramolecular Chemistry with Block Copolymers

The supramolecular block copolymers can be obtained by the fusion of self-assembly of the block copolymers and supramolecular chemistry. It is a simple, efficient, and feasible way to construct complicated and stimuli-responsive polymer self-assembly systems.<sup>18, 29, 30</sup> Ikkala's group has introduced this new class of materials by combining BCP and small molecule.<sup>29</sup> These can be generated via non-covalent interactions like van der Waals interaction, hydrogen bonding, ionic interaction,  $\pi$ - $\pi$  stacking, or metal-ligand

---

---

interaction by incorporating small molecule to one or more polymer blocks of the BCP.<sup>17, 29, 31-35</sup> Like BCP, the supramolecules also exhibit hierarchical assembly, which is arising from the BCP nanoscale ordering as well as from the order of packing of small molecules in few nanometers.<sup>17, 31</sup> These BCP SMAs give benefits over the covalently linked analogues as multiple functionalities can be readily integrated into the assemblies by replacing the small molecules. This will moderate the burden of synthesizing completely new families of BCP.<sup>25, 36</sup> Another foremost advantage of SMA approach is the removal of small molecules from the BCP SMA by selective dissolution to acquire a nanoporous material.<sup>37, 38</sup> The obtained nanopores or nanochannels that are arranged with functional groups are easily accessible for more applications.<sup>29, 30</sup> From the several kinds of SMAs, those containing hydrogen bonds have a prominent position in supramolecular chemistry due to their versatility and directionality. Extensive studies have been carried out on supramolecules based on functional alkyl-small molecules having no intrinsic electronic or optical characteristics.<sup>17, 29, 31, 34, 39</sup> But the noncovalent interaction between small molecules and polymers creates a thermally responsive elements within the system.<sup>17, 31, 34</sup> Figure 1.5 summarizes the potential advantages of supramolecules based on polymers and functional small molecules.

The overall assembly of the supramolecules is affected by several thermodynamic and kinetic factors. These consist of polymer-small molecule interaction, BCP microphase separation, interaction parameter, polymer chain deformation, melting, crystallinity, packing of the small molecule, etc. The polymer can influence the crystal structure of the small molecule or its capability to crystallize. On the other hand, the incorporation of small molecules can influence the architecture of the BCP chain, interaction parameter ( $\chi$ ), and stiffness. Kinetically, the diffusion and distribution rate of the small molecules can rely on the melting temperature ( $T_m$ ) of the small molecules and the comparative interaction

---

---

parameter ( $\chi$ ) between each block of the BCP and the small molecules at the specified annealing temperature.<sup>17, 31, 40</sup>

Considering all these factors, it is evident that the phase behaviour of small molecules has a crucial role in their co-assembly with the BCP, particularly for extremely crystalline small molecules. The potential application of supramolecules mainly focused in the fields of photovoltaics, transistors, optical devices, stimuli-responsive materials, etc.

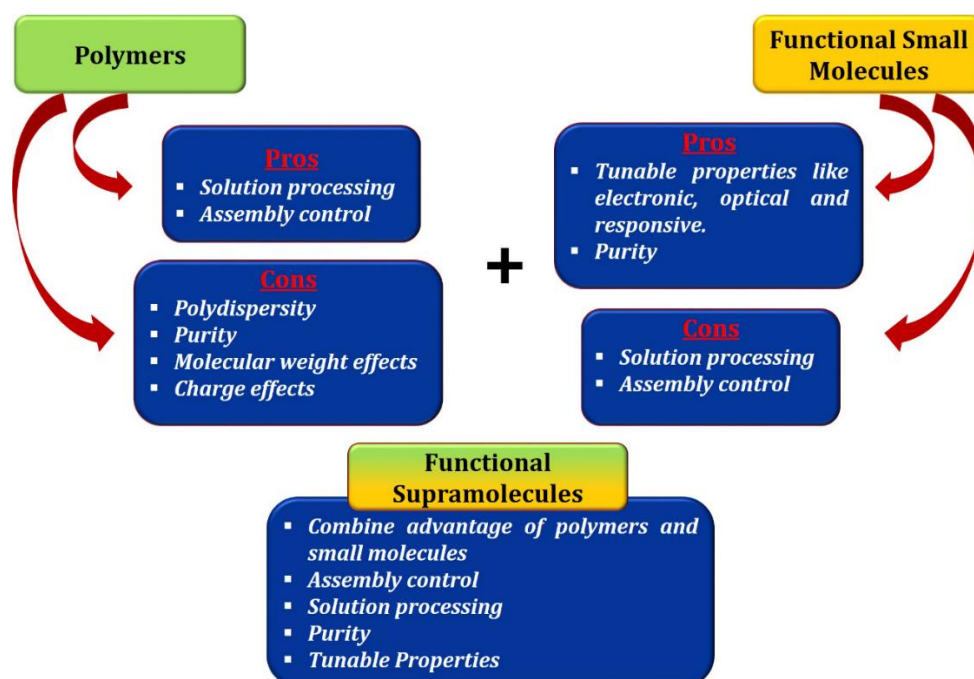


**Figure 1.5.** Advantages of functional small molecules-based supramolecules.

The most frequently researched diblock copolymer for the formation of supramolecules is poly(styrene)-*block*-poly(4-vinyl pyridine) (PS-*b*-P4VP). The prominence of this diblock copolymer is mainly due to two factors, one is its commercial accessibility with various  $N$  and  $f_{PS}$ , the range of self-assembled structures in bulk or thin film and the other one is the capability of hydrogen-bonding formation and basicity of the nitrogen in the pyridine group of P4VP block.<sup>41</sup> It allows the selective absorption of small molecules such as alcohols,<sup>42, 43</sup> phenols,<sup>34, 35, 44-46</sup> carboxylic acids,<sup>36, 47, 48</sup> sulfonic acids,<sup>49,</sup>

---

---

<sup>50</sup> etc. into the P4VP phase. The small molecules possess low miscibility within the hydrophobic PS domains and form hydrogen bonds or protonate the P4VP domains. When small molecules are selectively incorporated into P4VP domain in bulk, two primary effects can be anticipated. First, the protonation or improved polarity of the P4VP-small molecule complex contributing to increased  $\chi$  value between the PS and P4VP comb block phase. The increased  $\chi$  value enables sharper domain interfaces and obtains nanostructures at smaller length scales.<sup>51</sup> The second is with increasing in the small molecule content, the comb block volume fraction also increases. This can lead to the formation of different morphologies (order-order transitions).<sup>5</sup>

Recently, the supramolecular approach has been expanded to double-comb diblock copolymer complexes, in which both blocks behave as hydrogen-bonding acceptors. Adding small molecules into such a block copolymer like poly(4-vinylpyridine)-*block*-poly(N,N-dimethylacrylamide) (P4VP-*b*-PDMA) or poly(4-vinylpyridine)-*block*-poly(N-acryloylpiperidine) (P4VP-*b*-PAPI) would eventually leads to double comb diblock copolymer where the small molecules are linked via hydrogen bonding on both sides of the diblock copolymer.<sup>52, 53</sup> This leads to a complex structure in which the distribution of amphiphiles across both blocks depends on the strength of the hydrogen bonding interaction. This kind of system always gives two phase morphologies such as cylinders-in-lamellae or lamellae-in-lamellae.<sup>52, 54</sup>

---

---

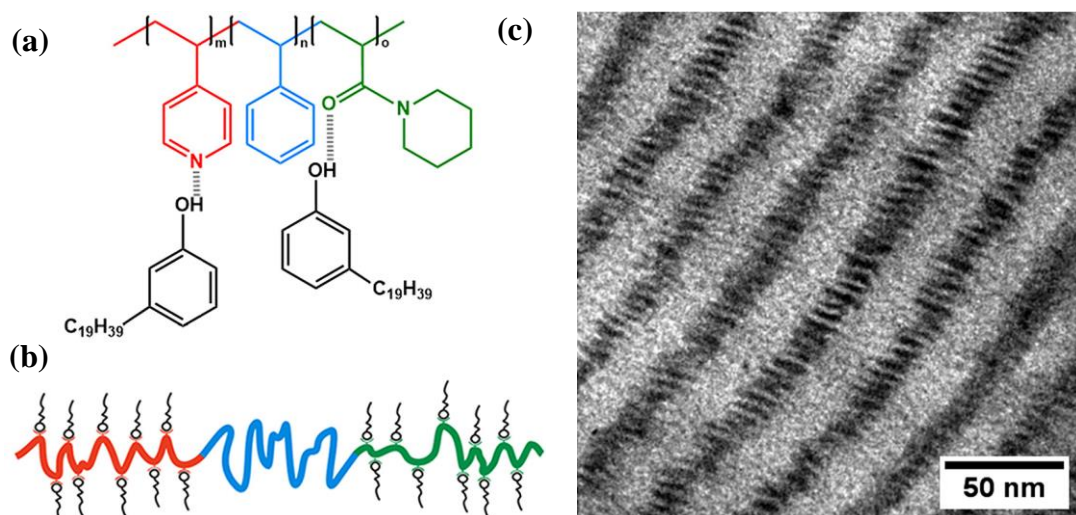


**Figure 1.6.** (a) Chemical structure and (b) schematic representation of the supramolecular  $(P4VP-b-PS-b-PAPI)(3-NDP)_x$  double-comb triblock terpolymer and (c) TEM image of  $P4VP-b-PS-b-PAPI(3-NDP)_1$  supramolecules, PS appears white, P4VP in dark and PAPI in grey. Reprinted with permission from ref. 47; copyright 2018 American Chemical Society

To get the three-phase morphologies, applying the supramolecular concept to triblock terpolymers, Hofman et al. described the double-comb triblock terpolymer self-assembly by introducing a PS block between the P4VP and the poly(*N*-acryloylpiperidine) (PAPI) blocks as shown in Figure 1.6. Here, the comb-coil-comb supramolecular triblock terpolymer was formed by the incorporation of 3-nonadecylphenol (3-NDP) molecule. By varying the structure or block sequence, the creation of more complex phase behaviours such as tetragonally packed diamond-shaped cylinders-in-lamellae, hexagonal core-shell cylindrical morphology, etc. can be obtained, which might be interesting for nanopatterning applications.<sup>46</sup>

#### 1.4. Phase Behaviour of Block Copolymer Based Supramolecules in Bulk and in Thin Films

---

---

### 1.4.1. In Bulk

The initial studies regarding the phase behaviour of supramolecular block copolymers in bulk were put forward by ten Brinke and Ikkala.<sup>17, 33, 55, 56</sup> Their aim was to build the self-organizing comb-coil BCPs with structures of two length-scales in a simple supramolecular manner, by mixing BCP with hydrogen-bonding amphiphiles.<sup>33, 55</sup> The most widely reported supramolecular system is the PS-*b*-P4VP block copolymer with 3-pentadecylphenol (PDP). This supramolecular system exhibits hierarchical structure (structure-within-structure) with larger-length scale formed by block copolymer self-assembly and the smaller length scale corresponding to the small molecules assembly within the block copolymer microdomains.<sup>29, 33, 55, 57</sup> The concept of BCP SMAs resulted in a wide range of nanoscale morphologies and their phase behaviour can be altered by varying the amount of the amphiphiles, block lengths, length of alkyl chain, strength of the hydrogen bonding, etc.<sup>29</sup> The same group presented the charging of comb-like blocks by protonating the 4VP groups by methanesulfonic acid (MSA), which is bonded to the P4VP blocks strongly via ionic interactions. This indicated that not only the H-bonding, the ionic interactions also come into the BCP supramolecules formation.<sup>29, 56</sup>

### 1.4.2. In Thin Films

The phase behaviour of the BCP-based supramolecules in thin films must be studied in order to make the supramolecular strategy for nanofabrication, nanotemplating, etc.<sup>30, 36, 58</sup> The interactions between polymer-substrate and air-polymer interfaces have a powerful impact on the BCP thin film morphology.<sup>59</sup> Besides, the orientation of the BCP microdomains also comes into the picture in thin films that rely on the surface energy of the coated substrate. The blocks having low surface energy tend to move on to the surface (air side) resulting the perpendicular orientation, whereas the blocks with a preference

---

---

towards the substrate side gives the parallel orientation.<sup>60</sup> Tung et al. demonstrated that increasing the weight ratio of the P4VP(PDP) comb blocks influence the supramolecular structure, and also leads to the vertical orientation of the microdomains in thin films.<sup>61</sup> In addition to ratio of small molecules, the selection of solvent used for annealing also affects the morphology, facilitates the interfacial interactions and the macroscopic alignment of the supramolecules in thin films and that will be discussed later.

## 1.5. Factors Influencing Block Copolymer Supramolecules

The comb-like supramolecules can be created by selectively incorporating the small molecule to one of the blocks of the BCP. This incorporation of small molecule into a polymer side chain could alter its architecture and improve the polymer rigidity, which eventually impacts the phase behaviour of supramolecular BCP in thin film and in bulk. These phases of supramolecules can form into well-defined microdomains comparable to those in BCPs alone and the ordered packing of the small molecules within the BCP microdomains. Below we discuss some of the critical factors that regulate the properties and hierarchical assembly of the BCP supramolecules.

### 1.5.1. Mole fraction

The stoichiometry (mole fraction) has a critical role in the creation of hierarchical assembly of block copolymer supramolecules. When the stoichiometry between the small molecule and the corresponding block is mismatched, the hierarchical assembly (structure-within-structure) could not be achieved. For example, if the stoichiometric ratio ( $r$ ) between the small molecule and the polymer block is 0.25, a non-uniform distribution of small molecules will be observed in the BCP supramolecules. When the ratio becomes 0.5, the distribution of small molecules is increased and the overall morphology of the supramolecular BCP will be changed. If the ratio is more than 0.5, i.e., 0.75 and 1, SMAs

---

---

exhibit perfect hierarchical assembly with a homogeneous distribution of small molecules. Xu and co-workers showed the change in the hierarchical morphology of PS-*b*-P4VP (bisphenol quarterthiophene, BP4T) supramolecules concerning the mole fractions. As the ratio becomes greater than 0.5 (i.e.,  $r=0.75$  and 1), a well aligned lamella-within-lamella structure is seen in TEM images<sup>62</sup>(Figure 1.7).

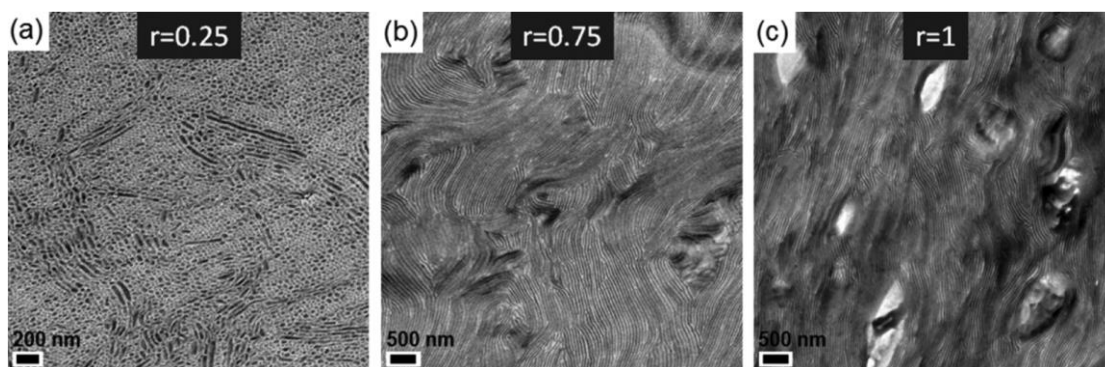


**Figure 1.7.** TEM images of the PS-*b*-P4VP(BP4T)<sub>r</sub> supramolecules with various 4VP:BP4T ratio ( $r = 0.25, 0.75,$  and 1) Reprinted with permission from ref. 63; copyright 2016 American Chemical Society

However, at higher loading ( $r > 1$ ), more phase-segregated small molecules were observed due to the excess of small molecules present in the sample. Once all the binding sites were occupied with small molecules via hydrogen bonding, the BCP supramolecules expel additional small molecules from the system and resulted in the macrophase separation of small molecules.

The volume fraction of the comb block will be altered either by using BCPs with distinct molecular weights of the functional block (like P4VP) or by changing the stoichiometry of the small molecule to functional block.<sup>59-61, 63</sup> Ten Brinke et al. reported a clear-cut correlation among the ratio of comb block and the orientation of the SMA thin films. They demonstrated that the BCP microdomains were aligned parallel to the surface for PS-*b*-P4VP(PDP)<sub>r</sub> supramolecules with  $f_{\text{comb}} < 0.5$ . By increasing the  $f_{\text{comb}} > 0.5$ , the

orientation of the BCP microdomains changes to perpendicular with respect to the surface and P4VP(PDP)<sub>r</sub> comb block lamellae aligned parallel to the surface.<sup>60</sup> Later, some other groups produced similar observations as well.<sup>37, 38, 64</sup>

### 1.5.2. Effect of Small Molecules

The morphologies of BCP supramolecules are more complex than BCPs. The secondary interaction of the small molecule with BCP depends on several factors including the binding strength used for attachment, the crystallization of the small molecules and their crystal structure, the conditions for sample preparation, etc. Kinetically, the small molecules diffusion and distribution rate can rely on the melting temperature ( $T_m$ ) and the relative  $\chi$  value between each block of the BCP and small molecules at the specified annealing temperature. Thus, the small molecules phase behaviour is critical in their co-assembly with the BCP.<sup>17, 31, 40</sup>

The stoichiometry between the polymer repeating unit and the small molecules may decrease due to the small molecules crystallization and may macrophase separate from the BCP matrix.<sup>64, 65</sup> The reduction in the stoichiometry changes the conformation of the polymer chain, interaction parameters, chain rigidity, and the volume fraction of the comb block. The hierarchical assemblies and the molecular arrangement of the attached small molecules may influence the chain architecture and mobility of the BCP that lead to kinetically trapped states or non-equilibrium nanostructures and can possibly intensify the thermal responsiveness of the material.<sup>66-68</sup>

It is shown that strongly interacting small molecules have a major impact on the architecture and packing of the BCP chain and morphology. Precisely, the small molecules crystallization can compress and elongate both BCP blocks, and also the crystal packing can affect the natural packing structure of the BCP. The packing and crystallinity of the

---

---

---

---

small molecules could be tuned by altering core of the crystalline molecule, the attachment site (side- vs end-functionalization) and also the structure (linear vs branched) of the alkyl solubilizing group, etc. which affect the polymer chain conformation along with the overall supramolecular morphology.<sup>44</sup>

The length of the small molecule also influences the SMAs. If the length of the molecule is sufficiently long, that will give the well-defined hierarchical morphologies.<sup>30</sup>

### 1.5.3. Annealing

The thermal annealing and solvent vapor annealing are the two significant and most frequently used techniques that enable BCP supramolecules to generate extremely ordered nanostructures.

#### 1.5.3.1. Thermal Annealing

It is the most frequently used technique consisting of heating the sample at temperatures above the glass transition temperature ( $T_g$ ) but below the decomposition temperature of polymers for a specific time to get an equilibrium morphology.<sup>69</sup> But in some cases, the temperature window between the  $T_g$  and the degradation temperature of the block concerned could only be very low in the thermal annealing method. Meanwhile, the order-disorder transition temperature ( $T_{ODT}$ ) increases greatly for high molecular weight BCP.<sup>70</sup> In the case of BCPs having a rigid backbone, the diffusion of polymer chains during thermal annealing is rapid and the long-range order improved rapidly even in higher molecular weight BCPs. On the other hand, in flexible BCPs, the diffusion of polymer chains is slow due to the chain entanglement and the improvement in long-range order is time consuming even at higher temperature. Also the blocks of many copolymers are prone to thermal degradation and are therefore undesirable for elevated temperatures and lengthier time of thermal annealing.<sup>71</sup> Thermal annealing can be carried out only over a

---

---

very limited temperature range for some supramolecules owing to the possible evaporation of the small molecules which can result in a significant structural change in BCP supramolecules.

### 1.5.3.2. Solvent Vapor Annealing

Considering the drawbacks of the thermal annealing process, solvent vapor annealing is the technique of choice for achieving long-range order in BCP supramolecules.<sup>72-75</sup> It involves the copolymer thin films subjected to a saturated atmosphere of one or more solvents that imparts mobility to particular blocks. The solvent exposure enables the polymer chains to be rearranged among the neighbouring domains. The solvent swells the BCP film during the annealing process that effectively decreases the  $T_g$  of the blocks and thus improves the chain mobility.<sup>69</sup> To obtain more orderly nanostructures, both supercritical CO<sub>2</sub> and low boiling point solvents were used.<sup>76</sup> Unlike thermal annealing, the solvent molecules are additional elements brought into supramolecules and, therefore, final morphology can be influenced by the interplay between polymers, small molecules and solvents. The BCP swelling can trigger the morphology owing to variations in solvent solubility to separate blocks, which alters interactions between the polymer blocks and the volume fractions of the components. If the swollen BCP stays as microphase separated, the lateral order will be dictated by enthalpic interactions between the block segments and entropic penalties related with the packing of the chains on the air and substrate interfaces.

The solvent used for annealing has a crucial role in achieving the ordered nanostructures. If both blocks are fairly soluble in a particular solvent which is called a neutral solvent, the solvent molecules track unfavourable interactions among the segments of the two blocks resulting in deviations in the configuration of the polymer chains attached

---

---

---

---

to the microdomain interfaces.<sup>77</sup> On the other hand, using a selective solvent to one block improves the unfavourable interaction.<sup>78, 79</sup> The concentration of the solvent in the BCP film will be different depending on the vapor pressure of the solvent. If the concentration of the solvent is higher, then the BCP can be forced into the disordered state, and as the solvent is removed, primarily the BCP orders on the air surface. Lateral ordering happens on the surface owing to the higher motion of the ordered surface layer structures, resulting in a quicker reaction of the BCP chains and allowing for bigger grain sizes. As the solvent is constantly removed, an ordering front propagates into the film, which can be templated on the initially formed microdomains on the surface, resulting in the lateral ordering and orientation of the BCP microdomains.<sup>69, 72</sup>

Solvent vapor annealing studies examined a range of parameters for achieving optimal morphologies, including solvent selectivity, swollen film thickness, solvent removal rate and annealing time. Stamm and co-workers discovered that both the solvent selectivity and the degree of swelling dictate on the alignment of the cylindrical comb block P4VP(HABA) microdomains in PS-*b*-P4VP(HABA) thin films. The cylinders turn into spherical domains at high swelling ratios, and solvent drying leads to the perpendicular orientation which is attributed to the merging of the spherical microdomains. It is observed that the orientation of the cylinders in a selective solvent such as 1, 4-dioxane was always perpendicular to the substrate, and in a non-selective solvent such as chloroform, the cylinders were aligned parallel to the substrate.<sup>80-82</sup>

## 1.6. Method to Determine the Morphology of BCP Supramolecules

Several techniques are available for understanding the morphology/microstructure of the block copolymer supramolecules, which are listed below.

---

---

### 1.6.1. Small-Angle X-ray Scattering (SAXS)

Small-angle X-ray scattering has been used as a crucial technique for characterizing the microstructure of block copolymers. In SAXS, the sample is irradiated by a monochromatic X-ray beam and scattering of the X-rays by the sample is measured at very small angles.

The diffraction of X-rays by a periodic structure is easily explained by Braggs Law

$$n\lambda = 2d_{hkl} \sin\theta \quad (1.5)$$

where  $n$  is an integer, indicating the order of the reflection,  $d_{hkl}$  stands for interplanar spacing between parallel planes with same Miller indices ( $hkl$ ), and  $\theta$  is the Bragg angle or half the scattering angle.

The scattering vector  $q$ , which is the vector difference between the wave propagation vectors of the scattered and the incident beam, is given by:

$$q = \frac{4\pi \sin\theta}{\lambda} \quad (1.6)$$

So, when the first order peak of a structure is found, the difference between lattice planes or the characteristic length scale,  $d$  is estimated by:

$$d = \frac{2\pi}{q} \quad (1.7)$$

For block copolymers, the comparative position of the higher-order reflections to the primary order reflection indicates the type of microstructure, as summarized in Table 1.2. Therefore, the microstructure of the block copolymer can be determined when sufficient peaks are observed.

---

---

**Table 1.2.** Relative peak positions ( $q/q^*$ ) in SAXS for most common block copolymer morphologies.<sup>83</sup>

Structure	Ratio ( $q/q^*$ )
Spherical	$1:\sqrt{2}:\sqrt{3}:\sqrt{4}:\sqrt{5}:\sqrt{6}\dots$
Hexagonally Packed Cylinder	$1:\sqrt{3}:\sqrt{4}:\sqrt{7}:\sqrt{9}\dots$
Gyroid	$1:\sqrt{4/3}:\sqrt{7/3}:\sqrt{8/3}:\sqrt{10/3}\dots$
Lamellar	$1:2:3:4:5\dots$

### 1.6.2. Transmission Electron Microscopy (TEM)

Structural imperfections or low contrast could reduce the scattering of self-assembled block copolymer structures and thus complicate the interpretation of SAXS patterns. In such cases, a supplementary method that offers real space lattice information could help to identify the equilibrium morphology. However, traditional light microscopy is unfit for two reasons in block copolymer system; one is the transparency of polymers in the visible spectrum which makes the different blocks indistinguishable, and the other is the fact that the structures are too small.

The resolution ( $R$ ) at a certain wavelength relies on the viewing medium with the refractive index  $n$  and the angle  $\theta$  at which the optical system can emit or accept the light.

$$R = \frac{0.61\lambda}{n \sin\theta} \quad (1.8)$$

By using the above equation, the resolution obtained was around 260 nm ( $\theta = 70^\circ$ ) when the light microscope was operated in the air ( $n = 1$ ) at the edge of the visible spectrum ( $\approx 400$  nm), which is higher than the typical size of morphologies found in self-assembled block copolymers.

Because of the wave-particle duality, the wavelength,  $\lambda_e$  for the accelerated electrons in an electric field with potential difference  $V$  is calculated by the equation,

$$\lambda_e = \frac{h}{\sqrt{2m_e eV}} \quad (1.9)$$

If the electrons are accelerated in a 100 kV field, the resolution  $R$  of an electron microscope is increased by a factor of  $10^5$  to 0.00252 nm ( $\lambda_e = 0.00388$  nm) when compared to photons in the visible range. So it is an ideal candidate for studying block copolymer self-assembly.

There are several sample preparation methods available to study the microphase separation in block copolymer-based materials by TEM; not every method enables for a proper interpretation of equilibrium morphology. In general, the simple and commonly used method is based on drop casting of a copolymer solution onto the sample holder (TEM grid), but rapid evaporation of the solvent could cause the kinetically trapped morphology. So the preferred route is that the sample was annealed either by selective solvent or by thermal annealing, which was further used for the TEM analysis.

To probe the exact morphology of the pre-treated bulk samples, thin sections of samples should be obtained by ultramicrotomy. In this method, first, a piece of the bulk film is embedded in resin for a support, and then trimmed into a suitable shape. Thus obtained sample is mounted in the ultramicrotomy and cut into thin slices. Such obtained thin slices can be transferred to a TEM grid by suitable procedures. Although this process is time-consuming and quite challenging, TEM analysis of such sections will provide information about the true bulk structure.

Selective staining agents can be used to improve the contrast of the sample and also to show increased stability in the electron beam during TEM analysis. Most commonly used staining agents for polymer blends and block copolymers include osmium tetroxide ( $\text{OsO}_4$ ),

---

ruthenium tetroxide (RuO<sub>4</sub>) and iodine (I<sub>2</sub>). The particular block which absorbs the vapors of the staining agent will appear dark in bright-field TEM. However, one should always be cautious while interpreting stained TEM micrographs, as a higher concentration of staining agents may alter or damage the structure.

### **1.6.3. Atomic Force Microscopy (AFM)**

Atomic force microscopy is the most popular method to study the thin film morphologies of the block copolymer supramolecules. This is a comparatively inexpensive method that enables the surface structure to be imaged. There are three types of AFM operation: non-contact, contact, and tapping modes. Usually, tapping mode is suitable for the polymer-based systems and the images can be obtained with higher resolution. In this mode, the sharp tip (generally a silicon or silicon nitride) is oscillating above the surface of the sample, which tracks the topography of the surface. The oscillation frequency is altered by the appearance of comparatively softer or harder surface characteristics, resulting in the so-called phase-contrast images. It is essential to recognize that the inside structures such as cylindrical domains can cause obvious topography of the surface in AFM tapping mode owing to differences in the indentation of the tip arising from differences in stiffness. Most AFM analyses are conducted on films coated on flat surfaces such as silicon wafers or mica at room temperature and are carried out in the air.

## **1.7. Functional Small Molecules-Based BCP Supramolecules**

A lot of small molecules with different characteristics such as electronic, optical, or stimuli-responsive characteristics are used to introduce functionality/features into the BCP supramolecules. Molecules having different nature such as surfactant molecules, liquid crystalline molecules, especially azo group containing molecules, organic semiconductors, etc. have been incorporated into the BCP supramolecules

---

---

### 1.7.1. Surfactant Based BCP Supramolecules

The first effective hydrogen-bonded P4VP-containing comb polymer was based on the alkylphenol surfactant molecule, i.e., 3-pentadecylphenol (3-PDP), which is the most frequently reported small molecule used for the formation of such supramolecular complexes.<sup>17, 29, 34, 40, 84</sup> Based on the composition of PS-*b*-P4VP block copolymer, the resulting PS-*b*-P4VP(PDP) blends may have morphologies of the sphere, cylinder, and lamella.

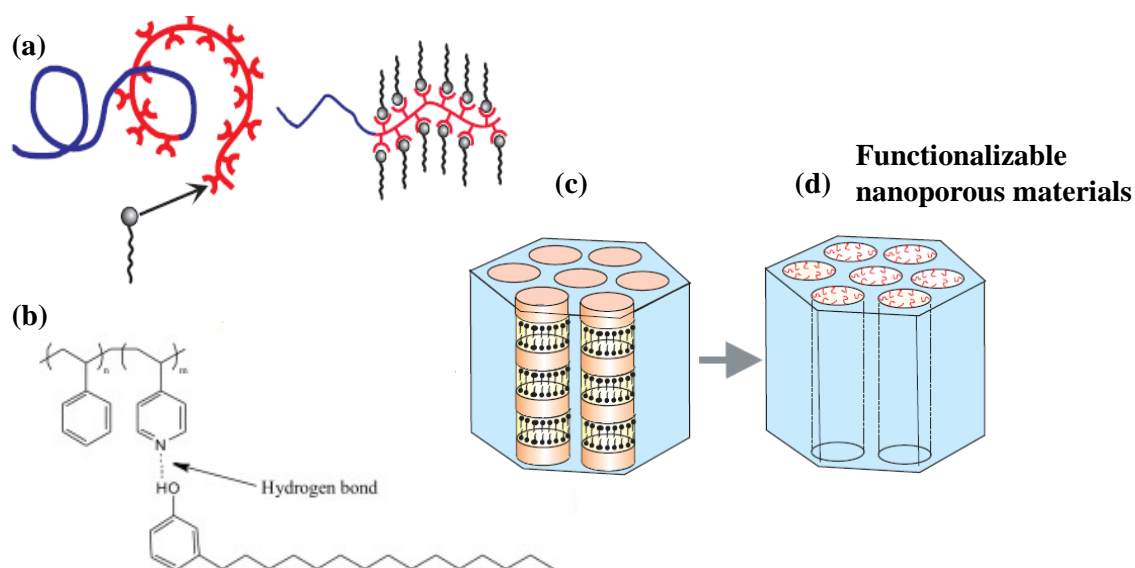


**Figure 1.8.** (a) Supramolecular self-organization was obtained by attaching amphiphiles to one of the blocks of a diblock copolymer, (b) chemical structure showing the hydrogen bonding between PS-*b*-P4VP and PDP molecule, (c) the lamellae-within-cylinders hierarchical structure and (d) functionalizable nanoporous materials. Reprinted with permission from ref. 30; copyright 2004 Royal Society of Chemistry

Special attention was given to the reports by Ten Brinke et al.<sup>60, 85</sup> and Tung et al.<sup>61, 86</sup>, which mainly focused on the hierarchical structures formed by the interaction of PDP with P4VP blocks in thin films as shown in Figure 1.8. They addressed how annealing conditions could affect the terrace formation and the phase behaviour of the system.<sup>60, 61</sup>

---

---

In 2006, Ikkala et al. demonstrated the formation of hierarchical structures using poly( $\gamma$ -benzyl-L-glutamate)-*block*-poly(L-lysine) (PBLG-*b*-PLL), a rod-coil diblock copolymer, and dodecyl benzenesulfonic acid (DBSA). The complexation occurs by transferring the proton from the acidic surfactant to the amine of PLL, leading to an electrostatically connected comb diblock copolymer.<sup>87</sup> Hong et al. discussed the complexation between the 4-dodecylbenzenesulfonic acid (DBSA) and PS-*b*-P4VP and suggested that the ionic bonding between DBSA and P4VP is stronger than the weak H-bonding in other systems, and such ionic interaction is persistent at elevated temperatures.<sup>88</sup>

### 1.7.2. Liquid Crystalline (LC) Based BCP Supramolecules

The main attractions of LC-based small molecules are the phase transitions and their interesting optical properties, which are due to the orientation and packing of the LC molecules. The incorporation of these LC molecules into supramolecules improves their processability by controlling the orientation and macroscopic alignment of the molecules, which is crucial in the device applications. A range of LC moieties were used in supramolecular systems, such as azobenzene,<sup>37, 89-91</sup> cholesterol,<sup>48, 92, 93</sup> (alkoxybenzoyloxy) benzoate,<sup>32</sup> and biphenyl,<sup>25, 94, 95</sup> etc.

The first supramolecular LC BCP was established by Gohy et al., where they used the poly(2-(dimethylamino) ethyl methacrylate)-*b*-poly(sodium methacrylate) (PDMAEMA-*b*-PMA) system. The first block, PDMAEMA was intended to provide electrostatic binding relations with cholesterol molecules and the second block PMA was intended to bind the molecules containing azobenzene.<sup>89</sup> Copolymers which contain both mesogens did not microphase separate at the same time, but a distinctive smectic mesophase was found. Depending on the composition of the BCP blocks and cholesteric molecules, a series of hierarchical morphologies were achieved.

---

---

Ikkala and co-workers disclosed that the hierarchical morphologies (structure-within-structure) when a mesogenic molecule, cholesteryl hemisuccinate (CholHS) is noncovalently complexed with PS-*b*-P4VP block copolymer (Figure 1.9). Depending on the corresponding block to CholHS ratio, smectic-within-lamellar order was observed.<sup>48</sup>

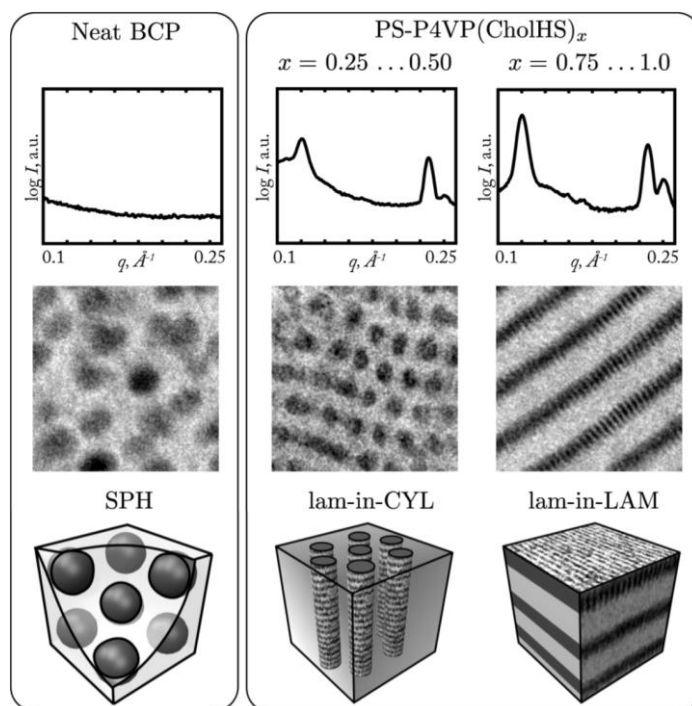


**Figure 1.9.** SAXS pattern of PS-*b*-P4VP(CholHS)<sub>x</sub> complexes shows the ordering of mesogens and TEM images show the larger morphologies. Reprinted with permission from ref. 49; copyright 2010 American Chemical Society.

Osuji et al.<sup>25, 94-96</sup> have published a series of works on homopolymers and BCPs attaching imidazole terminated-biphenyl-based LC small molecules, in which the carboxylic acid groups of poly(methacrylic acid) (PMAA) or poly(acrylic acid) (PAA) groups were hydrogen bonded with these LC based small molecules. These supramolecules were hierarchically assembled, and the small molecules brought interesting optical and thermal properties to the system. The mesogenic domains of PS-*b*-PAA based supramolecules and the alignment of the BCP may be driven in minutes by AC electrical fields<sup>25</sup> or magnetic fields<sup>96</sup> during melt cooling. The alignment of LC molecule containing

supramolecules could have an important impact on their optical characteristics. Hence the usage of magnetic and electric fields can be helpful for the development of these materials based products in devices.<sup>25</sup>

### 1.7.2.1. Azo Molecule (LC) Based BCP Supramolecules

The Azo group containing mesogen is also an example of a liquid crystalline molecule. A series of studies were carried out in the area of azo-containing supramolecular polymer complexes. In specific, block copolymers carrying azobenzene (Azo) units were an active part of research.<sup>97-100</sup> When azobenzene molecules are irradiated under UV light of adequate wavelengths, they are photoisomerized from trans to cis form. This method can be reversed, which means that either light irradiation or heat can return the cis form to the trans form.<sup>101, 102</sup> This photoresponsive characteristic makes it possible to use azo block copolymers for many applications, including photomechanical devices, photoswitches, photoinduced patterning, photoalignment materials, etc.<sup>97, 103-105</sup>

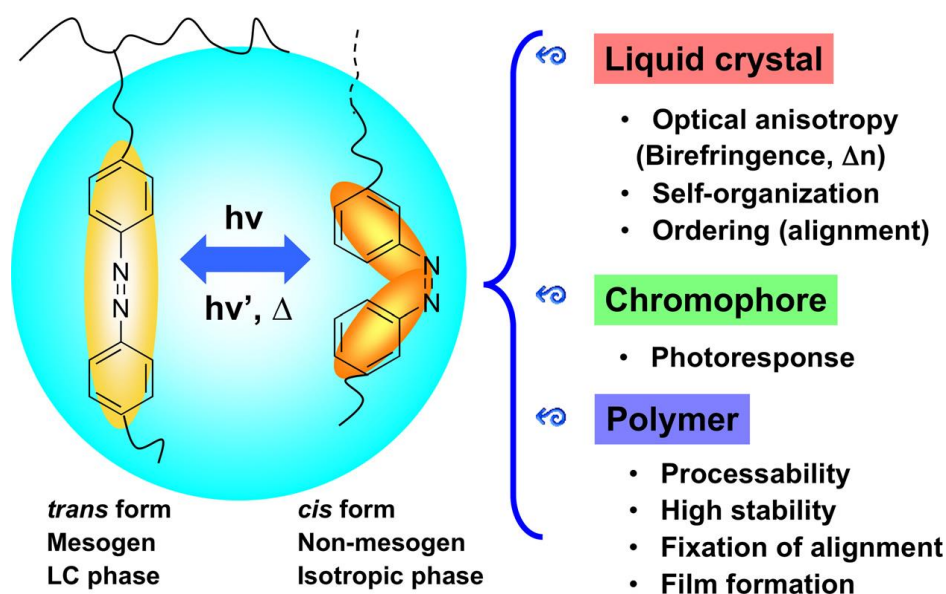


**Figure 1.10.** Properties of photoresponsive liquid crystalline polymers (PLCPs) with azobenzene as the side chain. Reprinted with permission from ref. 107; copyright 2014 Elsevier.

The research groups including Xu and co-workers,<sup>40</sup> Groschel and co-workers,<sup>45</sup> Stamm and co-workers,<sup>37, 58, 80</sup> and Bubeck and co-workers<sup>91, 106</sup> used azobenzene-containing hydrogen bonded side chains supramolecules, but they did not investigate the prospective photoresponsive characteristics of such complexes. A photo-induced control of the BCP phase structured materials containing azobenzene molecules is an extremely exciting phenomenon. For the first time, del Barrio et al. demonstrated that when photoinduced anisotropy is enrolled in self-assembled BCP structures composed of PS-*b*-P4VP and an azobenzene, the extent of photo-orientation depends on the morphology of block copolymer.<sup>107</sup>

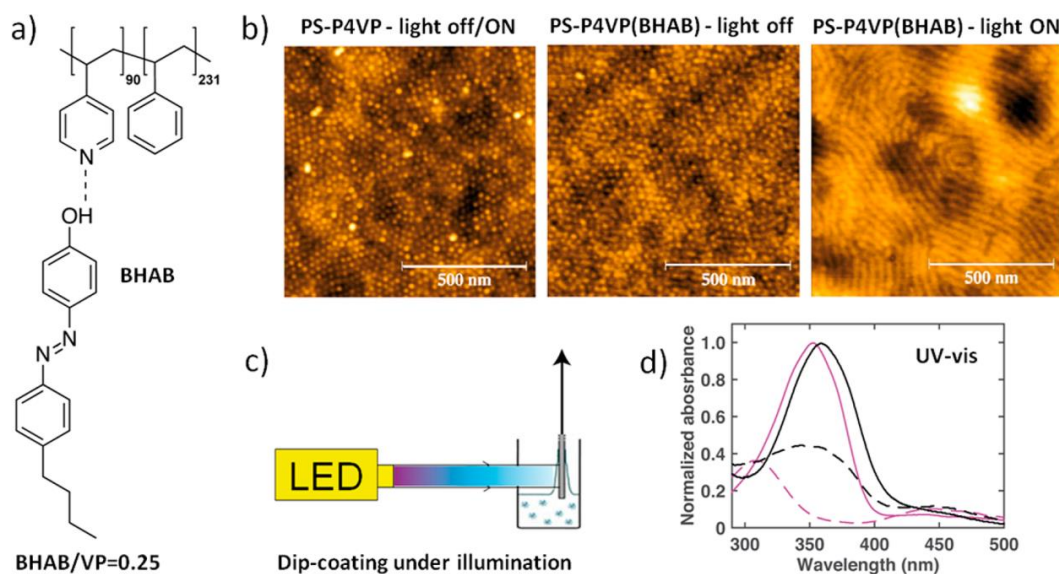


**Figure 1.11.** (a) Chemical structure showing the hydrogen bonding between PS-*b*-P4VP and BHAB molecules, (b) topographical AFM images ( $1 \times 1 \text{ mm}^2$ ) of thin films of PS-*b*-P4VP and PS-*b*-P4VP(BHAB) diblock copolymers dip-coated under dark condition, and PS-*b*-P4VP(BHAB) dip-coated under LED (365 nm) irradiation, (c) schematic of the dip-coater setup and (d) UV-visible spectra of PS-*b*-P4VP(BHAB) samples at different conditions. Reprinted with permission from ref. 110; copyright 2015 American Chemical Society.

---

---

Vapaavuori et al. have recently shown that the block-selective hydrogen-bonded azobenzene containing BCP thin film morphology can be operated with light. They compared the film patterns of the PS-*b*-P4VP/4-butyl-4' hydroxyazophenol (BHAB) (in a proportion of 0.25 molar to the pyridine-repeat-units), which prepared by dip-coating with and without the presence of light. By changing the dip-coating rate and the illumination of light, different surface morphologies were obtained as shown in Figure 1.11b. These observations indicated that the BCP supramolecular nanostructured morphology of dip-coated thin film can be controlled by light illumination.<sup>108</sup>

### 1.7.3. Organic Semiconductor Based Supramolecules

Organic semiconductor-based supramolecules have become an interesting subject in recent years. Due to the well-defined electronic properties of organic semiconductor small molecules, they offered distinctive possibilities for manufacturing low-cost, high-performance organoelectronic devices like organic photovoltaics (OPVs) or organic light-emitting diodes (OLEDs).<sup>109-113</sup> Owing to the dewetting and their rapid crystallization, it is difficult to form a uniform film with small molecules.<sup>114, 115</sup> The complexation of BCP with the organic semiconductor molecules can overcome these constraints and organize them into thinfilm nanoscopic structures to generate organic electronics, thus opening up a new avenue for tailoring electronic properties.<sup>116</sup>

The assembly of BCPs with a conjugated polymer and its optical and electrical features were examined by Hadziioannou et al. For example, the regioregular poly(3-hexylthiophene)-*b*-poly(4-vinyl pyridine) (P3HT-*b*-P4VP) rod-coil block copolymers with PCBM ([6,6]-phenyl-C61-butyric acid methyl ester) exhibit nanostructured thin films. The suitable interactions between PCBM and P4VP domains resulted in high thermal stability electron donor/electron acceptor networks.<sup>117</sup>

---

---

Another set of organic semiconductor based BCP supramolecules are formed by the complexation of perylene diimide-based and phenol-containing oligothiophene semiconductors with PS-*b*-P4VP block copolymer.<sup>118-122</sup> Tran et al. reported that by using the magnetic fields, the supramolecules formed between PS-*b*-PAA and the imidazole-functionalized perylene diimide were aligned macroscopically, which is helpful to monitor the macroscopic alignment of nanostructures in wide areas in organic semiconductor systems.<sup>118</sup> Nanostructured lamellar assemblies of the oligothiophene molecules were achieved in the thin films of oligothiophene-based supramolecules (Figure 1.12b), which is an ideal morphology for OPV devices.<sup>121</sup>

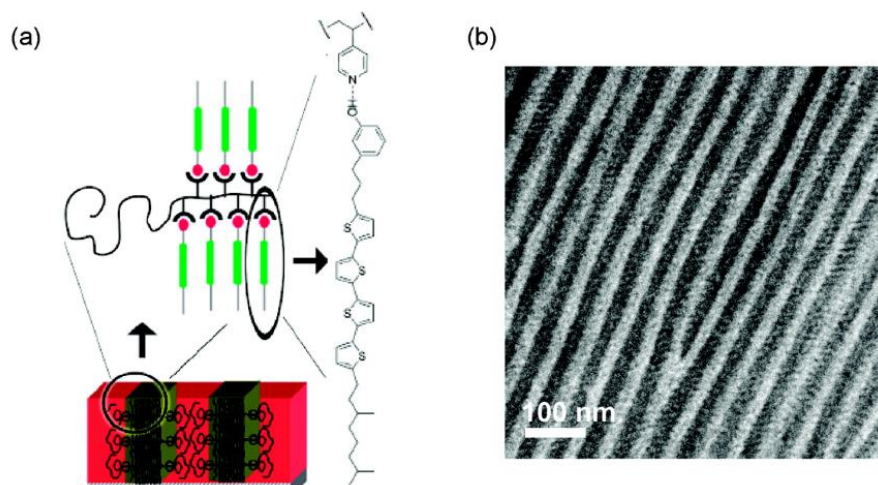


**Figure 1.12.** (a) Chemical structure and SMA of PS-*b*-P4VP(4T) and (b) TEM images of PS-*b*-P4VP(4T)<sub>1.5</sub> annealed at 155°C. Reprinted with permission from ref. 123; copyright 2010 American Chemical Society

Xu and co-workers described that in supramolecules, the crystallization tendency of the oligothiophene molecule possesses an impact on the entanglement of the polymer chain and the morphology of both BCP blocks and the small molecules guide the thermoresponsiveness of the material. In addition, when the small molecules form a crystalline state in supramolecules, the BCP periodicity is increased.<sup>44, 123, 124</sup>

---

---

Supramolecular films based on the pyrenebutyric acid (PBA) and PS-*b*-P4VP block copolymer was described by Kuila et al. The supramolecules with greater molar ratio result in a hierarchical structure by two length scales, where larger-length scale was formed by block copolymer self-assembly and the smaller length scale corresponding to the small molecules assembly within the comb block. The supramolecular orientation could be tailored by picking the selective or non-selective solvents, and the fluorescence emission increased in solution and thin films in comparison to the pure PBA, which may be significant for the luminescent sensing material applications.<sup>125</sup>

A few studies have been reported for the supramolecules based on  $\pi$ -conjugated polymers (which is also a class of organic semiconductors) and among them most of the studies were focused on the diacetylene molecule. This molecule undergoes topochemical polymerization under UV light to generate polydiacetylene (PDA), a well-known conjugated polymer and exhibit colour tunability with respect to external stimuli such as heat, stress, etc.<sup>126, 127</sup>

Lu and coworkers fabricated a colorimetric sensor based on PDA fibers using an electrospinning method, in which the PDA was embedded within the polystyrene-co-poly(4-vinyl pyridine) (PS-co-P4VP) polymer matrix. This hydrogen-bonded complex was used to detect the amine concentration even in the ppb level, indicated by the colour change that occurs due to the intensified stress on the backbone of PDA while partially breaking hydrogen bonding when exposed to amine vapor.<sup>128</sup>

Further, Zhu et al. outlined the use of noncovalent polymer side-chain modification to conduct the topochemical polymerization in BCP solutions and thin films. They exploited the SMA strategy for the complexation of imidazolyl diphenyl-diacetylene monomer with PS-*b*-PAA via hydrogen bonding. The microphase separation of the BCP was enhanced by using solvent vapor annealing, which in fact enhanced the orientation and

---

---

molecular packing of the monomer and as a consequence the topochemical polymerization was improved significantly.<sup>129</sup>

The primary focus of the research community in this field to date was the incorporation of a small molecule into the polymer chain via SMAs. In fact, the multicomponent assembly using more than one small molecule was rarely attained, may be due to the frequently faced issue of phase separation, even though it produces novel nanostructured materials with improved properties. Saibal et al. described the formation of random donor-acceptor (D-A) comb polymers through the complexation with P4VP domains via hydrogen-bonding. The hydroxyl functionalized oligo(phenylenevinylene) (OPVCN-OH) act as donor molecule and pentadecylphenol based asymmetric perylenebisimide (UPBI-PDP) act as the acceptor molecule. The supramolecular random D-A comb polymer shows a lamellar arrangement with a domain size of less than 10 nm. In order to check the self-organizing behaviour of the D-A assembly with and without the polymer template (P4VP domain), they prepare the D-A small molecular complex in the absence of P4VP. The D-A alone complex exhibit poor film-forming capability and possess very low electron and hole mobilities compared to the supramolecular system.<sup>120</sup>

#### 1.7.4. Polymer-Based Supramolecules

It would be more attractive when we simply blend various diblock copolymers like A-B/C-D, as it combines the physical characteristics and extend the processing space.<sup>130</sup>  
<sup>131</sup> However, in such systems, the uniform long-range order was not accomplished owing to their macrophase separation.<sup>132-134</sup> To limit the macrophase separation, researchers introduced the supramolecular interactions (mainly H-bonding) other than the non-specific diffusive interactions typically found in the copolymer alloy.<sup>29</sup> The supramolecular interactions among the functional groups suppress the macrophase separation in favour of

microphase separation, resulting in long-range ordered nanoscale structures. Only few studies were carried out in this area.

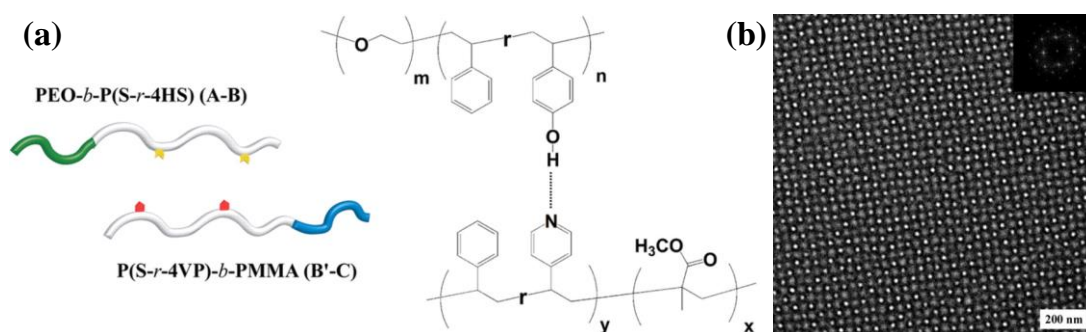


**Figure 1.13.** (a) Hierarchical self-assembly and target morphology of supramolecular A-B and B'-C diblock copolymers blend stabilized by H-bonding and (b) TEM image and related Fourier transform (inset) of a solvent-annealed supramolecular block copolymers blend film. Reprinted with permission from ref. 36; copyright 2008 The American Association for the Advancement of Science.

Tang et al. reported the block copolymers blend of poly(styrene)-*block*-poly(methyl methacrylate) (PS-*b*-PMMA) and poly(ethylene oxide)-*block*-poly(styrene) (PEO-*b*-PS). In such a system, they modified the PS segment with minor portions of randomly distributed 4-vinylpyridine and 4-hydroxystyrene units for supramolecular interaction, which generates the nanoscale square patterns as shown in Figure 1.13. This makes it possible to customize the amount of incorporated hydrogen-bonding entities and to regulate the molecular weight of each block accurately by simple random copolymerization.<sup>131</sup>

In 2010, the same group evaluated the blending of acid-cleavable PEO trityl-*b*-P(S-r-4HS) diblock copolymer (H-bond donor) with photodegradable P(S-r-4VP)-*b*-PMMA (H-bond acceptor). Here, they proved a unique strategy for generating various nanoscale templates such as cylindrical pores from the PEO and PMMA domains or blended nanostructure with nested arrangements of both pores made from the same starting system using orthogonal

degradation responses from a particular supramolecular copolymer lithographic system. This strategy offers an easy path to achieve the diverse and tunable nanoscale templates.<sup>135</sup>

## 1.8. Applications of Block Copolymer Supramolecules

The ability to produce multi-length scale structures of BCP supramolecules got more attention in the application point of view.<sup>29, 34, 136, 137</sup> The SMAs possess various morphologies, including the spherical-within-lamellar, cylindrical-within-lamellar, lamellar-within-lamellar, lamellar-within-cylinder, lamellar-within-spherical, etc.<sup>17, 33</sup> The BCP supramolecules offers an extensive use of functional materials for designing nanostructured materials and devices in optical, electrical, and other functionalities.<sup>25, 29, 30,</sup>

138

### 1.8.1. Nanotemplates and Nanopatterning

The patterning of bulk materials on a nanoscale may result in achieving new characteristics such as high surface area, enhanced electronic properties, etc. The various chemical functionalities and the capacity to phase-segregate on the nanoscale dimension made block copolymer as well as the BCP supramolecules ideal nanotemplates for various applications. To generate the template using block copolymer, one of the blocks is used to be removed by controlled degradation, but in the case of BCP supramolecules, the nanoporous membranes (nanotemplates) are simply created by removing small molecules by dissolution in a suitable solvent from the bulk or thin film.<sup>37, 38</sup> The small molecule can only be removed if the interaction of small molecules with polymer chain is a weak H-bonding. The polymeric nano-object or membrane walls are also covered by functional polymer chains and can also be used as templates for nanofabrication.<sup>139</sup>

Ikkala and co-workers examined the complex formation of PS-*b*-P4VP with 4-dodecylphenol. By the addition of small molecule, they could control the P4VP volume

fraction as well as the morphology that might be used for the  $\text{Al}_2\text{O}_3$  gas-phase deposition templates, shown in Figure 1.14. The hollow inorganic tubular and spherical  $\text{Al}_2\text{O}_3$  structures are produced after heating/pyrolysis followed by the removal of the block copolymer.<sup>140</sup>

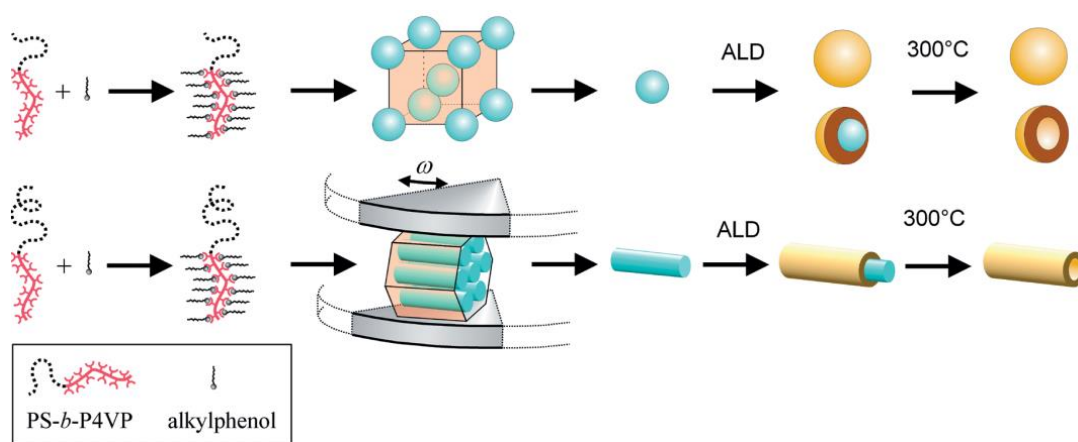


**Figure 1.14.** Method for the preparation of inorganic hollow nanospheres and nanotubes.

Reprinted with permission from ref. 142; copyright 2007 John Wiley and Sons.

Another use of block copolymer supramolecules is the structure-directing agents/patterning of nanoparticles or metal salts, which is the most appropriate way to organize hybrid bulk materials. Generally, the metal nanoparticles with a diameter in between 1-10 nm have distinctive and size-related properties connected with photonic, catalytic, magnetic, electrical, and chemical characteristics. The controlled immobilization and the nanoparticle assembly on the appropriate substrate are very much important for their unique characteristics which is applicable in molecular electronics, catalyst, etc.<sup>19, 141, 142</sup> But it's a challenge to assemble them on substrates in a nanometer-scale ordered fashion, and that patterning is significant for the next generation of electronic devices with smaller, quicker, and denser structures.

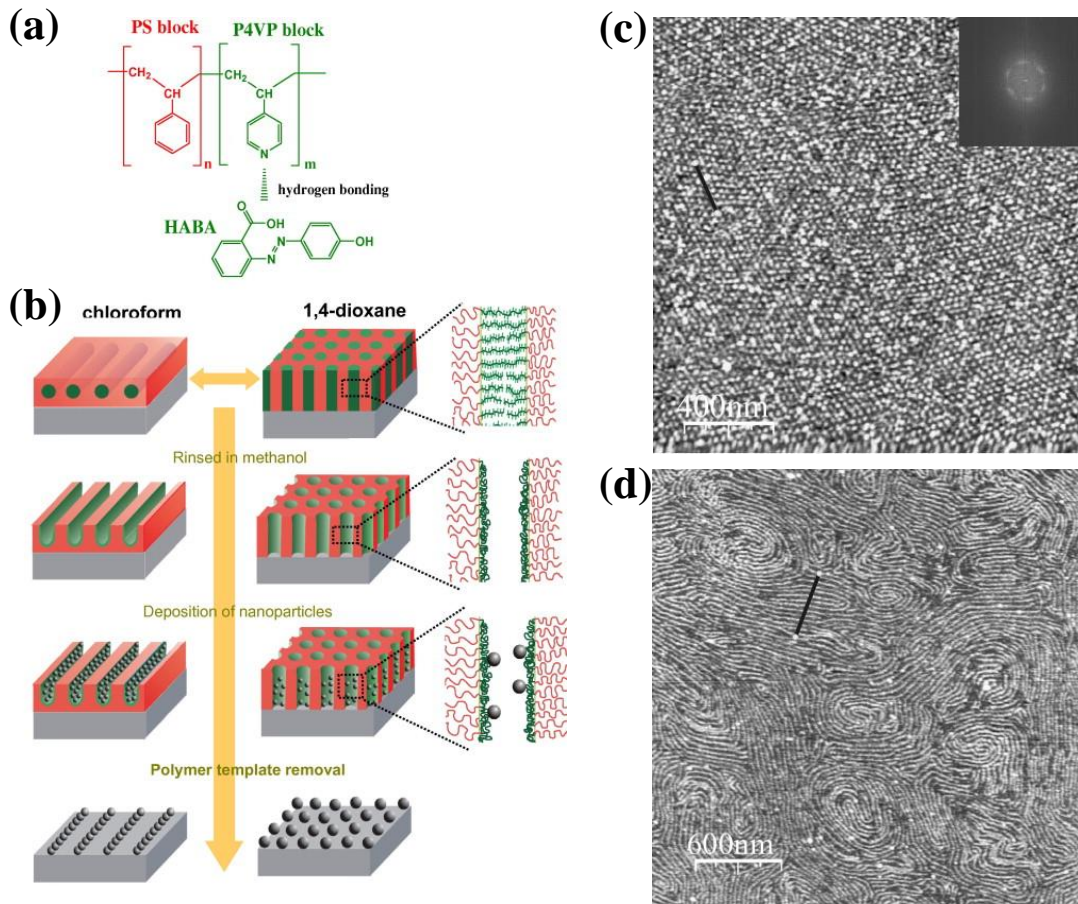


**Figure 1.15.** Schematic of (a) the formation of PS-*b*-P4VP (HABA) supramolecules (b) the preparation of inorganic nanowires and nanodots using BCP supramolecules nanotemplates. AFM height image of the palladium deposited nanoporous block copolymer (c) perpendicular template and (d) parallel template after polymer removal by pyrolysis. Reprinted with permission from ref. 59; copyright 2009 John Wiley and Sons.

In recent times, various methodologies have been used for patterning the metal nanoparticles via block copolymer or block copolymer supramolecules. This methodology is common and flexible so that it might simply be expanded for nanodot and nanowire arrays of metallic materials. Besides, the spacing and size of the nanostructures might readily altered by controlling the BCP molecular weight, and the stoichiometric ratio between the small molecule and the corresponding block.

---

---

For instance, Nandan et al. described the creation of highly dense arrays of palladium nanowires and nanodots via supramolecular assemblies of PS-*b*-P4VP block copolymer with 2-(4-(hydroxybenzeneazo) benzoic acid (HABA) as the nanotemplate as shown in Figure 1.15. Because of the preferential attraction of palladium nanoparticles to the P4VP block, which are directly placed in the nanoporous templates from an aqueous solution in the pores. Then pyrolysis or oxygen plasma etching removes the polymer template that results in palladium nanostructures.<sup>30, 58</sup>

### 1.8.2. Membranes

Membranes are selective barriers that allow the transport of gas, liquid, or substance from one section to other. The degree of membrane selectivity relies on the membrane pore size. The porous materials was categorized as microporous ( $\leq 2$  nm), mesoporous (2-50 nm) and macroporous ( $\geq 50$  nm) depending on the pore size.<sup>143</sup>

Over the last century, the membranes produced of block copolymer self-assembly have drawn excellent scientific interest. The extra functional groups inside the pores as well as on the membrane surface enable multiple opportunities to use these membranes for different filtration applications. So the functional molecules were attached via supramolecular interactions to the respective sites of the block copolymer. These block copolymer supramolecules have a tendency to form self-assembled arrays of nano-sized pores.<sup>144</sup> Madhavan et al. showed the self-assembly with a non-solvent induced phase-segregation method to generate the nanoporous supramolecular membrane using PS-*b*-P4VP and -OH/-COOH organic molecule with adjusted morphology. The organic molecules were comprising of -OH functional groups forming a hexagonally ordered framework, while -COOH comprising organic molecules form lamellar as well as hexagonal patterns.<sup>145</sup> By modifying the surface of the PS-*b*-P4VP (pH-responsive material) with poly (N-isopropyl acrylamide) (pNIPAM, temperature-responsive material),

---

---

Coldt et al. fabricated the temperature and pH responsive supramolecular membranes that can be used for separation of biomolecules.<sup>146</sup>

### 1.8.3. Photovoltaic Applications

Beyond the generation of nanopatterns and membranes, BCP supramolecules can also be used for photovoltaic applications. For OPV applications, the domain size must almost match with the exciton diffusion length (~10 nm), which can be easily achieved by block copolymers/block copolymer supramolecules. So it is considered as the ultimate candidate for the creation of bulk-heterojunction (BHJ) organic photovoltaics.<sup>147, 148</sup>

In the area of organic photovoltaics, the supramolecules based on fullerenes were extensively investigated.<sup>149, 150</sup> Fujita et al. have used the carboxylic acid-modified C<sub>60</sub> molecules to design the supramolecules with pyridine units of PS-*b*-P4VP. This BCP has an amphiphilic nature for the formation of the polymer micelles with P4VP(C<sub>60</sub>) core and PS shell, which results in the creation of C<sub>60</sub> nanoparticles with comparatively small distributions of size.<sup>151</sup> The SMA of PS-*b*-P4VP using C<sub>60</sub> molecules without functionalization was described by Laiho et al. in which the pyridine groups formed a charge transfer complex with the C<sub>60</sub> molecule. The formation of supramolecules based on fullerenes without having to synthesize the new functional moieties is an advantage.<sup>152</sup> In addition, this concept is extended to block copolymer with conjugated polymer blocks like P3HT and the other block bind the small molecule, which can be used to generate a donor-acceptor system with high thermal stability and controlled domain size for photovoltaic applications.<sup>117</sup>

Sary et al. proposed a new supramolecular route for solar cell applications by using rod-coil block copolymer. In this work, they design an electron donor (P3HT)-electron acceptor (P4VP: PCBM) system via supramolecular assembly of the bicontinuous P3HT-

---

---

---

---

*b*-P4VP rod-coil-based block copolymers with PCBM. This BCP supramolecular system makes the compositional/structural control much more than the copolymers with covalently connected electron-acceptor moieties and exhibit enhanced stability as well as improved optoelectronic properties.<sup>117</sup>

## 1.9. References

- [1] Whitesides, G. M.; Boncheva, M. *Proc Natl Acad Sci U S A* **2002**, 99 (8), 4769-4774.
  - [2] Hamley, I. W. *Angew. Chem. Int.* **2003**, 42 (15), 1692-1712.
  - [3] Darling, S. *Progress in Polymer Science - PROG POLYM SCI* **2007**, 32, 1152-1204.
  - [4] Bates, F. S.; Fredrickson, G. H. *Annu. Rev. Phys. Chem.* **1990**, 41 (1), 525-557.
  - [5] Bates, F. S.; Fredrickson, G. H. *Phys. Today* **1999**, 52 (2), 32-38.
  - [6] Whitesides, G. M.; Grzybowski, B. *Science* **2002**, 295 (5564), 2418-2421.
  - [7] Hamley, I. W., *The Physics of Block Copolymers*. Oxford University Press: 1998.
  - [8] Krausch, G.; Magerle, R. *Adv. Mater.* **2002**, 14 (21), 1579-1583.
  - [9] Bates, F. S.; Shefelbine, T. A.; Vigild, M.; Engineers, A. I. o. C.; Meeting, A. I. o. C. E. A., *Block Copolymers: Designer Soft Materials*. American Institute of Chemical Engineers: 1999.
  - [10] Chen, J. T.; Thomas, E. L.; Ober, C. K.; Mao, G.-p. *Science* **1996**, 273 (5273), 343-346.
  - [11] Thurn-Albrecht, T.; Schotter, J.; Kästle, G. A.; Emley, N.; Shibauchi, T.; Krusin-Elbaum, L.; Guarini, K.; Black, C. T.; Tuominen, M. T.; Russell, T. P. *Science* **2000**, 290 (5499), 2126-2129.
  - [12] Förster, S.; Antonietti, M. *Adv. Mater.* **1998**, 10 (3), 195-217.
  - [13] Forster, S.; Plantenberg, T. *Angew Chem Int Ed Engl* **2002**, 41 (5), 689-714.
  - [14] Kim, H.-C.; Park, S.-M.; Hinsberg, W. D. *Chem. Rev.* **2010**, 110 (1), 146-177.
  - [15] Förster, S.; Plantenberg, T. *Angew. Chem. Int.* **2002**, 41 (5), 688-714.
  - [16] Botiz, I.; Darling, S. B. *Mater. Today* **2010**, 13 (5), 42-51.
  - [17] Valkama, S.; Ruotsalainen, T.; Nykänen, A.; Laiho, A.; Kosonen, H.; ten Brinke, G.; Ikkala, O.; Ruokolainen, J. *Macromolecules* **2006**, 39 (26), 9327-9336.
  - [18] Kuila, B. K.; Stamm, M. *J. Mater. Chem.* **2011**, 21 (37), 14127-14134.
- 
-

- 
- 
- [19] Kuila, B. K.; Nandan, B.; Böhme, M.; Janke, A.; Stamm, M. *Chem. Commun.* **2009**, (38), 5749-5751.
- [20] G H Fredrickson, a.; Bates, F. S. *Annu. Rev. Mater. Sci.* **1996**, 26 (1), 501-550.
- [21] Matsen, M. W.; Schick, M. *Curr. Opin. Colloid Interface Sci* **1996**, 1 (3), 329-336.
- [22] Bates, F. S. *Science* **1991**, 251 (4996), 898-905.
- [23] Matsen, M. W.; Bates, F. S. *Macromolecules* **1996**, 29 (4), 1091-1098.
- [24] Phlip, D. *Adv. Mater.* **1996**, 8 (10), 866-868.
- [25] Chao, C.-Y.; Li, X.; Ober, C. K.; Osuji, C.; Thomas, E. L. *Adv. Funct. Mater.* **2004**, 14 (4), 364-370.
- [26] Aida, T.; Meijer, E. W.; Stupp, S. I. *Science* **2012**, 335 (6070), 813-7.
- [27] Ghosh, S.; Praveen, V. K.; Ajayaghosh, A. *Annu. Rev. Mater. Res*, **2016**, 46 (1), 235-262.
- [28] Steed, J.; Turner, D.; Wallace, K. **2007**.
- [29] Ikkala, O.; ten Brinke, G. *Chem. Commun.* **2004**, (19), 2131-2137.
- [30] Nandan, B.; Kuila, B.; Stamm, M. *Eur. Polym. J.* **2011**, 47, 584-599.
- [31] Valkama, S.; Kosonen, H.; Ruokolainen, J.; Haatainen, T.; Torkkeli, M.; Serimaa, R.; Ten Brinke, G.; Ikkala, O. *Nat Mater* **2004**, 3 (12), 872-6.
- [32] Kato, T.; Frechet, J. M. J. *Macromolecules* **1989**, 22 (9), 3818-3819.
- [33] Ruokolainen, J.; Saariaho, M.; Ikkala, O.; ten Brinke, G.; Thomas, E. L.; Torkkeli, M.; Serimaa, R. *Macromolecules* **1999**, 32 (4), 1152-1158.
- [34] Ruokolainen, J.; Mäkinen, R.; Torkkeli, M.; Mäkelä, T.; Serimaa, R.; Brinke, G. t.; Ikkala, O. *Science* **1998**, 280 (5363), 557-560.
- [35] Tang, C.; Lennon, E. M.; Fredrickson, G. H.; Kramer, E. J.; Hawker, C. J. *Science* **2008**, 322 (5900), 429-432.
- [36] Kuila, B. K.; Gowd, E. B.; Stamm, M. *Macromolecules* **2010**, 43 (18), 7713-7721.
- [37] Sidorenko, A.; Tokarev, I.; Minko, S.; Stamm, M. *J. Am. Chem. Soc.* **2003**, 125 (40), 12211-12216.
- [38] Tokarev, I.; Krenek, R.; Burkov, Y.; Schmeisser, D.; Sidorenko, A.; Minko, S.; Stamm, M. *Macromolecules* **2005**, 38 (2), 507-516.
- [39] Antonietti, M.; Conrad, J. *Angew. Chem. Int.* **1994**, 33 (18), 1869-1870.
- [40] Zhao, Y.; Thorkelsson, K.; Mastroianni, A. J.; Schilling, T.; Luther, J. M.; Rancatore, B. J.; Matsunaga, K.; Jinnai, H.; Wu, Y.; Poulsen, D.; Fréchet, J. M. J.; Alivisatos, A. P.; Xu, T. *Nat Mater* **2009**, 8 (12), 979-985.
- 
-

- 
- 
- [41] Kennemur, J. G. *Macromolecules* **2019**, 52 (4), 1354-1370.
- [42] Walish, J. J.; Kang, Y.; Mickiewicz, R. A.; Thomas, E. L. *Adv. Mater.* **2009**, 21 (30), 3078-3081.
- [43] Lin, E.-L.; Hsu, W.-L.; Chiang, Y.-W. *ACS Nano* **2018**, 12 (1), 485-493.
- [44] Rancatore, B. J.; Kim, B.; Mauldin, C. E.; Fréchet, J. M. J.; Xu, T. *Macromolecules* **2016**, 49 (3), 833-843.
- [45] Hiekkataipale, P.; Löbbling, T. I.; Poutanen, M.; Priimagi, A.; Abetz, V.; Ikkala, O.; Gröschel, A. H. *Polymer* **2016**, 107, 456-465.
- [46] Hofman, A. H.; Terzic, I.; Stuart, M. C. A.; ten Brinke, G.; Loos, K. *ACS Macro Lett.* **2018**, 7 (10), 1168-1173.
- [47] Bharatiya, B.; Schumers, J.-M.; Poggi, E.; Gohy, J.-F. *Polymers* **2013**, 5 (2), 679-695.
- [48] Korhonen, J. T.; Verho, T.; Rannou, P.; Ikkala, O. *Macromolecules* **2010**, 43 (3), 1507-1514.
- [49] Wang, J.; de Jeu, W. H.; Müller, P.; Möller, M.; Mourran, A. *Macromolecules* **2012**, 45 (2), 974-985.
- [50] Valkama, S.; Ruotsalainen, T.; Kosonen, H.; Ruokolainen, J.; Torkkeli, M.; Serimaa, R.; ten Brinke, G.; Ikkala, O. *Macromolecules* **2003**, 36 (11), 3986-3991.
- [51] Sinturel, C.; Bates, F. S.; Hillmyer, M. A. *ACS Macro Lett.* **2015**, 4 (9), 1044-1050.
- [52] Faber, M.; Hofman, A. H.; Polushkin, E.; van Ekenstein, G. A.; Seitsonen, J.; Ruokolainen, J.; Loos, K.; ten Brinke, G. *Macromolecules* **2013**, 46 (2), 500-517.
- [53] Hofman, A. H.; Reza, M.; Ruokolainen, J.; ten Brinke, G.; Loos, K. *Angew. Chem. Int.* **2016**, 55 (42), 13081-13085.
- [54] Hofman, A. H.; Reza, M.; Ruokolainen, J.; ten Brinke, G.; Loos, K. *Macromol. Rapid Commun.* **2017**, 38 (17), 1700288.
- [55] Ruokolainen, J.; Brinke, G. t.; Ikkala, O. *Adv. Mater.* **1999**, 11 (9), 777-780.
- [56] ten Brinke, G.; Ruokolainen, J.; Ikkala, O., Supramolecular Materials Based On Hydrogen-Bonded Polymers. In *Hydrogen Bonded Polymers*, Binder, W., Ed. Springer Berlin Heidelberg: Berlin, Heidelberg, 2007; pp 113-177.
- [57] Ikkala, O.; Knaapila, M.; Ruokolainen, J.; Torkkeli, M.; Serimaa, R.; Jokela, K.; Horsburgh, L.; Monkman, A.; Brinke, G. t. *Adv. Mater.* **1999**, 11 (14), 1206-1210.
- [58] Nandan, B.; Gowd, E. B.; Bigall, N. C.; Eychmüller, A.; Formanek, P.; Simon, P.; Stamm, M. *Adv. Funct. Mater.* **2009**, 19 (17), 2805-2811.
- 
-

- 
- 
- [59] van Zoelen, W.; ten Brinke, G. *Soft Matter* **2009**, 5 (8), 1568-1582.
- [60] van Zoelen, W.; Asumaa, T.; Ruokolainen, J.; Ikkala, O.; ten Brinke, G. *Macromolecules* **2008**, 41 (9), 3199-3208.
- [61] Tung, S.-H.; Kalarickal, N. C.; Mays, J. W.; Xu, T. *Macromolecules* **2008**, 41 (17), 6453-6462.
- [62] Lee, K. H.; Bai, P.; Rancatore, B. J.; He, B.; Liu, Y.; Xu, T. *Macromolecules* **2016**, 49 (7), 2639-2645.
- [63] van Zoelen, W.; Polushkin, E.; ten Brinke, G. *Macromolecules* **2008**, 41 (22), 8807-8814.
- [64] Morikawa, Y.; Nagano, S.; Watanabe, K.; Kamata, K.; Iyoda, T.; Seki, T. *Adv. Mater.* **2006**, 18 (7), 883-886.
- [65] Busch, P.; Krishnan, S.; Paik, M.; Toombes, G. E. S.; Smilgies, D.-M.; Gruner, S. M.; Ober, C. K. *Macromolecules* **2007**, 40 (1), 81-89.
- [66] Peet, J.; Kim, J. Y.; Coates, N. E.; Ma, W. L.; Moses, D.; Heeger, A. J.; Bazan, G. C. *Nat Mater* **2007**, 6 (7), 497-500.
- [67] Adams, J.; Gronski, W. *Die Makromol. Chem., Rapid Commun.* **1989**, 10 (10), 553-557.
- [68] Gallot, B. *Prog. Polym. Sci* **1996**, 21 (6), 1035-1088.
- [69] Gu, X.; Gunkel, I.; Hexemer, A.; Gu, W.; Russell, T. P. *Adv. Mater.* **2014**, 26 (2), 273-281.
- [70] Gu, W.; Huh, J.; Hong, S. W.; Sveinbjornsson, B. R.; Park, C.; Grubbs, R. H.; Russell, T. P. *ACS Nano* **2013**, 7 (3), 2551-2558.
- [71] Kim, E.; Ahn, H.; Park, S.; Lee, H.; Lee, M.; Lee, S.; Kim, T.; Kwak, E.-A.; Lee, J. H.; Lei, X.; Huh, J.; Bang, J.; Lee, B.; Ryu, D. Y. *ACS Nano* **2013**, 7 (3), 1952-1960.
- [72] Kim, S. H.; Misner, M. J.; Xu, T.; Kimura, M.; Russell, T. P. *Adv. Mater.* **2004**, 16 (3), 226-231.
- [73] Peng, J.; Xuan, Y.; Wang, H.; Yang, Y.; Li, B.; Han, Y. *J Chem Phys* **2004**, 120 (23), 11163-70.
- [74] Xuan, Y.; Peng, J.; Cui, L.; Wang, H.; Li, B.; Han, Y. *Macromolecules* **2004**, 37 (19), 7301-7307.
- [75] Fukunaga, K.; Hashimoto, T.; Elbs, H.; Krausch, G. *Macromolecules* **2002**, 35 (11), 4406-4413.
- 
-

- 
- 
- [76] Stafford, C. M.; Russell, T. P.; McCarthy, T. J. *Macromolecules* **1999**, 32 (22), 7610-7616.
- [77] Helfand, E.; Tagami, Y. *J. Chem. Phys.* **1972**, 56 (7), 3592-3601.
- [78] Lai, C.; Russel, W. B.; Register, R. A. *Macromolecules* **2002**, 35 (10), 4044-4049.
- [79] Wang, J.-Y.; Chen, W.; Roy, C.; Sievert, J. D.; Russell, T. P. *Macromolecules* **2008**, 41 (3), 963-969.
- [80] Nandan, B.; Vyas, M. K.; Böhme, M.; Stamm, M. *Macromolecules* **2010**, 43 (5), 2463-2473.
- [81] Luchnikov, V.; Kondyurin, A.; Formanek, P.; Lichte, H.; Stamm, M. *Nano Lett.* **2007**, 7 (12), 3628-3632.
- [82] Zschech, D.; Milenin, A. P.; Scholz, R.; Hillebrand, R.; Sun, Y.; Uhlmann, P.; Stamm, M.; Steinhart, M.; Gösele, U. *Macromolecules* **2007**, 40 (22), 7752-7754.
- [83] Hamley, I. W.; Castelletto, V. *Prog. Polym. Sci* **2004**, 29 (9), 909-948.
- [84] Hofman, A. H.; Chen, Y.; ten Brinke, G.; Loos, K. *Macromolecules* **2015**, 48 (5), 1554-1562.
- [85] van Zoelen, W.; Bondzic, S.; Landaluce, T. F.; Brondijk, J.; Loos, K.; Schouten, A.-J.; Rudolf, P.; Brinke, G. *Polymer* **2009**, 50 (15), 3617-3625.
- [86] Huang, W.-H.; Chen, P.-Y.; Tung, S.-H. *Macromolecules* **2012**, 45 (3), 1562-1569.
- [87] Hanski, S.; Houbenov, N.; Ruokolainen, J.; Chondronicola, D.; Iatrou, H.; Hadjichristidis, N.; Ikkala, O. *Biomacromolecules* **2006**, 7 (12), 3379-84.
- [88] Hong, J.-Y.; Hong, J.-L. *J. Polym. Res.* **2004**, 11 (2), 89-97.
- [89] Gohy, J.-F.; Sobry, R.; Bossche, G.; Jérôme, R. *Macromol. Chem. Phys.* **2000**, 201, 31-41.
- [90] de Wit, J.; van Ekenstein, G. A.; Polushkin, E.; Kvashnina, K.; Bras, W.; Ikkala, O.; ten Brinke, G. *Macromolecules* **2008**, 41 (12), 4200-4204.
- [91] Wu, S.; Bubeck, C. *Macromolecules* **2013**, 46 (9), 3512-3518.
- [92] Soininen, A. J.; Tanionou, I.; ten Brummelhuis, N.; Schlaad, H.; Hadjichristidis, N.; Ikkala, O.; Raula, J.; Mezzenga, R.; Ruokolainen, J. *Macromolecules* **2012**, 45 (17), 7091-7097.
- [93] Bai, P.; Kim, M. I.; Xu, T. *Macromolecules* **2013**, 46 (14), 5531-5537.
- [94] Osuji, C.; Chao, C.-Y.; Bitá, I.; Ober, C. K.; Thomas, E. L. *Adv. Funct. Mater.* **2002**, 12 (11-12), 753-758.
- 
-

- 
- 
- [95] Osuji, C. O.; Chao, C.-Y.; Ober, C. K.; Thomas, E. L. *Macromolecules* **2006**, 39 (9), 3114-3117.
- [96] Gopinadhan, M.; Beach, E. S.; Anastas, P. T.; Osuji, C. O. *Macromolecules* **2010**, 43 (16), 6646-6654.
- [97] Ding, L.; Mao, H.; Xu, J.; He, J.; Ding, X.; Russell, T. P.; Robello, D. R.; Mis, M. *Macromolecules* **2008**, 41 (6), 1897-1900.
- [98] Hayakawa, T.; Horiuchi, S.; Shimizu, H.; Kawazoe, T.; Ohtsu, M. *J. Polym. Sci. A* **2002**, 40 (14), 2406-2414.
- [99] You, F.; Paik, M. Y.; Häckel, M.; Kador, L.; Kropp, D.; Schmidt, H.-W.; Ober, C. K. *Adv. Funct. Mater.* **2006**, 16 (12), 1577-1581.
- [100] Breiner, T.; Kreger, K.; Hagen, R.; Häckel, M.; Kador, L.; Müller, A. H. E.; Kramer, E. J.; Schmidt, H.-W. *Macromolecules* **2007**, 40 (6), 2100-2108.
- [101] Vapaavuori, J.; Bazuin, C. G.; Priimagi, A. *J. Mater. Chem. C* **2018**, 6 (9), 2168-2188.
- [102] Yu, H.; Kobayashi, T. *Molecules (Basel, Switzerland)* **2010**, 15 (1), 570-603.
- [103] Tong, X.; Wang, G.; Soldera, A.; Zhao, Y. *J. Phys. Chem. B* **2005**, 109 (43), 20281-20287.
- [104] Tong, X.; Wang, G.; Yavrian, A.; Galstian, T.; Zhao, Y. *Adv. Mater.* **2005**, 17 (3), 370-374.
- [105] Yager, K. G.; Tanchak, O. M.; Godbout, C.; Fritzsche, H.; Barrett, C. J. *Macromolecules* **2006**, 39 (26), 9311-9319.
- [106] Wu, S.; Huang, J.; Beckemper, S.; Gillner, A.; Wang, K.; Bubeck, C. *J. Mater. Chem.* **2012**, 22 (11), 4989-4995.
- [107] del Barrio Lasheras, J.; Blasco, E.; Oriol, L.; Alcalá, R.; Sanchez Somolinos, C. *J. Polym. Sci. A* **2013**, 51.
- [108] Vapaavuori, J.; Grosrenaud, J.; Pellerin, C.; Bazuin, C. G. *ACS Macro Lett.* **2015**, 4 (10), 1158-1162.
- [109] Peumans, P.; Yakimov, A.; Forrest, S. R. *J. Appl. Phys.* **2003**, 93 (7), 3693-3723.
- [110] Peumans, P.; Uchida, S.; Forrest, S. R. *Nature* **2003**, 425 (6954), 158-62.
- [111] Riede, M.; Mueller, T.; Tress, W.; Schueppel, R.; Leo, K. *Nanotechnology* **2008**, 19 (42), 424001.
- [112] Matsuo, Y.; Sato, Y.; Niinomi, T.; Soga, I.; Tanaka, H.; Nakamura, E. *J. Am. Chem. Soc.* **2009**, 131 (44), 16048-16050.
- 
-

- 
- 
- [113] Roncali, J. *J. Acc. Chem. Res.* **2009**, 42 (11), 1719-1730.
- [114] Katz, H. E.; Bao, Z.; Gilat, S. L. *J. Acc. Chem. Res.* **2001**, 34 (5), 359-369.
- [115] Ma, B.; Woo, C. H.; Miyamoto, Y.; Fréchet, J. M. J. *Chem. Mater.* **2009**, 21 (8), 1413-1417.
- [116] Nelson, J. *Science* **2001**, 293 (5532), 1059-60.
- [117] Sary, N.; Richard, F.; Brochon, C.; Leclerc, N.; Lévêque, P.; Audinot, J.-N.; Berson, S.; Heiser, T.; Hadziioannou, G.; Mezzenga, R. *Adv. Mater* **2010**, 22 (6), 763-768.
- [118] Tran, H.; Gopinadhan, M.; Majewski, P. W.; Shade, R.; Steffes, V.; Osuji, C. O.; Campos, L. M. *ACS Nano* **2013**, 7 (6), 5514-5521.
- [119] Narayan, R.; Kumar, P.; Narayan, K. S.; Asha, S. K. *Adv. Funct. Mater.* **2013**, 23 (16), 2033-2043.
- [120] Saibal, B.; Chithiravel, S.; Asha, S. K. *J. Polym. Sci. A* **2016**, 54 (15), 2403-2412.
- [121] Rancatore, B. J.; Mauldin, C. E.; Tung, S.-H.; Wang, C.; Hexemer, A.; Strzalka, J.; Fréchet, J. M. J.; Xu, T. *ACS Nano* **2010**, 4 (5), 2721-2729.
- [122] Kumari, P.; Khawas, K.; Bera, M. K.; Hazra, S.; Malik, S.; Kuila, B. K. *Macromol. Chem. Phys.* **2017**, 218 (8), 1600508.
- [123] Rancatore, B. J.; Mauldin, C. E.; Fréchet, J. M. J.; Xu, T. *Macromolecules* **2012**, 45 (20), 8292-8299.
- [124] Kao, J.; Thorkelsson, K.; Bai, P.; Rancatore, B. J.; Xu, T. *Chem. Soc. Rev.* **2013**, 42 (7), 2654-2678.
- [125] Kuila, B. K.; Chakraborty, C.; Malik, S. *Macromolecules* **2013**, 46 (2), 484-492.
- [126] McQuade, D. T.; Pullen, A. E.; Swager, T. M. *Chem. Rev.* **2000**, 100 (7), 2537-2574.
- [127] Tashiro, K.; Nishimura, H.; Kobayashi, M. *Macromolecules* **1996**, 29 (25), 8188-8196.
- [128] Wu, J.; Lu, X.; Shan, F.; Guan, J.; Lu, Q. *RSC Adv.* **2013**, 3 (45), 22841-22844.
- [129] Zhu, L.; Tran, H.; Beyer, F. L.; Walck, S. D.; Li, X.; Ågren, H.; Killops, K. L.; Campos, L. M. *J. Am. Chem. Soc.* **2014**, 136 (38), 13381-13387.
- [130] Abetz, V.; Goldacker, T. *Macromol. Rapid Commun.* **2000**, 21 (1), 16-34.
- [131] Tang, C.; Hur, S.-m.; Stahl, B. C.; Sivanandan, K.; Dimitriou, M.; Pressly, E.; Fredrickson, G. H.; Kramer, E. J.; Hawker, C. J. *Macromolecules* **2010**, 43 (6), 2880-2889.
- 
-

- 
- 
- [132] Asari, T.; Matsuo, S.; Takano, A.; Matsushita, Y. *Macromolecules* **2005**, 38 (21), 8811-8815.
- [133] Frielinghaus, H.; Hermsdorf, N.; Sigel, R.; Almdal, K.; Mortensen, K.; Hamley, I. W.; Messé, L.; Corvazier, L.; Ryan, A. J.; van Dusschoten, D.; Wilhelm, M.; Floudas, G.; Fytas, G. *Macromolecules* **2001**, 34 (14), 4907-4916.
- [134] Jeon, H. G.; Hudson, S. D.; Ishida, H.; Smith, S. D. *Macromolecules* **1999**, 32 (6), 1803-1808.
- [135] Tang, C.; Sivanandan, K.; Stahl, B. C.; Fredrickson, G. H.; Kramer, E. J.; Hawker, C. J. *ACS Nano* **2010**, 4 (1), 285-291.
- [136] Mäki-Ontto, R.; de Moel, K.; Polushkin, E.; Alberda van Ekenstein, G.; ten Brinke, G.; Ikkala, O. *Adv. Mater.* **2002**, 14 (5), 357-361.
- [137] Ruotsalainen, T.; Torkkeli, M.; Serimaa, R.; Mäkelä, T.; Mäki-Ontto, R.; Ruokolainen, J.; ten Brinke, G.; Ikkala, O. *Macromolecules* **2003**, 36 (25), 9437-9442.
- [138] Kosonen, H.; Valkama, S.; Ruokolainen, J.; Torkkeli, M.; Serimaa, R.; ten Brinke, G.; Ikkala, O. *Eur. Phys. J. E* **2003**, 10 (1), 69-75.
- [139] Böhme, M.; Kuila, B.; Schlörb, H.; Nandan, B.; Stamm, M. *Phys. Status Solidi B* **2010**, 247 (10), 2458-2469.
- [140] Ras, R. H. A.; Kemell, M.; de Wit, J.; Ritala, M.; ten Brinke, G.; Leskelä, M.; Ikkala, O. *Adv. Mater.* **2007**, 19 (1), 102-106.
- [141] Lee, J. I.; Cho, S. H.; Park, S.-M.; Kim, J. K.; Kim, J. K.; Yu, J.-W.; Kim, Y. C.; Russell, T. P. *Nano Lett.* **2008**, 8 (8), 2315-2320.
- [142] Park, M.; Harrison, C.; Chaikin, P. M.; Register, R. A.; Adamson, D. H. *Science* **1997**, 276 (5317), 1401-1404.
- [143] Sing, K. S. W., Reporting physisorption data for gas/solid systems with special reference to the determination of surface area and porosity (Recommendations 1984). *Pure Appl. Chem.* 1985; Vol. 57, p 603.
- [144] Nabeel, F.; Rasheed, T.; Bilal, M.; Iqbal, H. M. N. *Sep. Purif. Technol.* **2019**, 215, 441-453.
- [145] Madhavan, P.; Peinemann, K.-V.; Nunes, S. P. *Appl. Mater. Interfaces* **2013**, 5 (15), 7152-7159.
- [146] Clodt, J. I.; Filiz, V.; Rangou, S.; Buhr, K.; Abetz, C.; Höche, D.; Hahn, J.; Jung, A.; Abetz, V. *Adv. Funct. Mater.* **2013**, 23 (6), 731-738.
- 
-

- [147] Riede, M.; Mueller, T.; Tress, W.; Schueppel, R.; Leo, K. *Nanotechnology* **2008**, 19 (42), 424001.
- [148] Tseng, Y.-C.; Darling, S. B. *Polymers* **2010**, 2 (4), 470-489.
- [149] Badamshina, E.; Gafurova, M. *J. Mater. Chem.* **2012**, 22 (19), 9427-9438.
- [150] Babu, S. S.; Möhwald, H.; Nakanishi, T. *Chem. Soc. Rev.* **2010**, 39 (11), 4021-4035.
- [151] Fujita, N.; Yamashita, T.; Asai, M.; Shinkai, S. *Angew Chem Int Ed Engl* **2005**, 44 (8), 1257-61.
- [152] Laiho, A.; Ras, R. H. A.; Valkama, S.; Ruokolainen, J.; Österbacka, R.; Ikkala, O. *Macromolecules* **2006**, 39 (22), 7648-7653.
- 
-



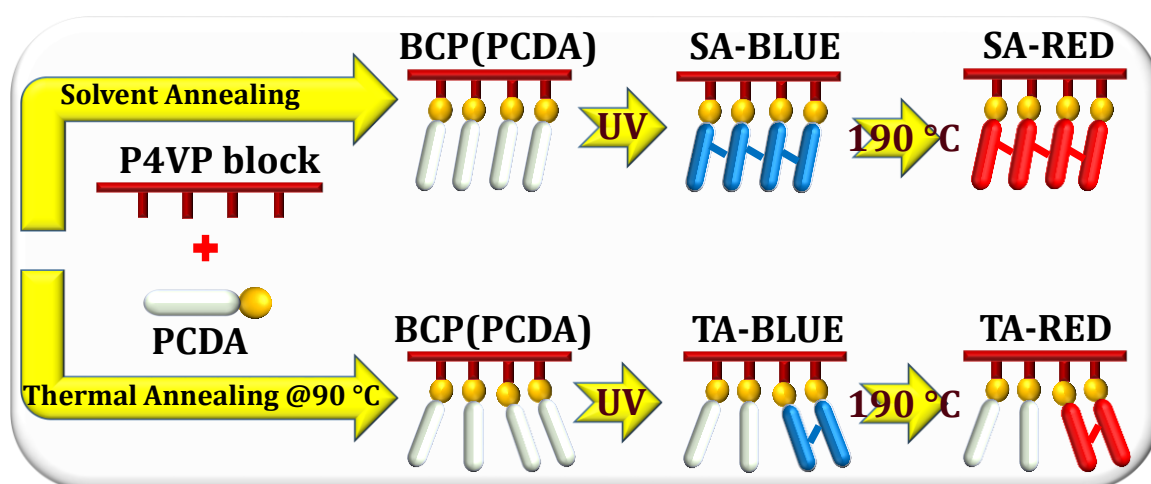
---

---

## Topochemical Polymerization of Hierarchically Ordered Diacetylene Monomers within the Block Copolymer Domains

---

---



### 2.1. Abstract

*The integration of polymerizable small molecules within the block copolymer based supramolecules provides a new strategy to generate functional materials. Herein, we report hydrogen-bonding complexes of photopolymerizable 10,12-pentacosadyonic acid (PCDA) and polystyrene-block-poly(4-vinylpyridine) (PS-*b*-P4VP). We systematically investigate how the annealing conditions affect the hierarchical ordering and the molecular orientation of PCDA molecules within the block copolymer microdomains and subsequently the topochemical polymerization of PCDA. It was found that solvent vapor annealing is the most appropriate method to obtain the desired molecular orientation of PCDA for the effective topochemical polymerization compared to that of the thermal*

---

---

*annealing method. The hierarchical ordering of the block copolymer supramolecules upon the UV irradiation and melt-cooling was investigated at multiple length scales by a combination of different techniques including small-angle X-ray scattering and wide-angle X-ray scattering.*

## **2.2. Introduction**

Chemical reactions in the solid state attract great interest of researchers because of their specificity, and these reactions often produce a single product without any solvent waste.<sup>1-3</sup> Some of these solid-state reactions have been used in polymerization reactions, like topochemical polymerization or solid state polymerization of monomers.<sup>4-11</sup> Among these, topochemical polymerization of diacetylenes has developed as one of the best investigated systems because of its unique structural, photophysical and electronic properties.<sup>9,11-14</sup> Stimuli-responsive colour changes of polymerized diacetylenes (PDAs) have been reported, and this intriguing property of nanostructured polydiacetylenes has made them useful in a myriad of applications such as sensors, molecular switches, bioelectronics materials, and other optoelectronic devices.<sup>6, 15-22</sup> It has been demonstrated that molecular packing and orientation of diacetylenes are crucial to produce polydiacetylenes by 1,4- addition. Several strategies have been developed to align monomers in ordered systems, such as monolayers,<sup>23</sup> crystals,<sup>6</sup> cages,<sup>24</sup> porous materials,<sup>19</sup> vesicles,<sup>25, 26</sup> electrospun fibers,<sup>27, 28</sup> etc., for effective topochemical polymerization. Photoinduced topochemical polymerization converts diacetylene monomers into polydiacetylenes with a blue colour. Heating induces the torsion of the polydiacetylene main chain and turns the blue phase to the red phase by shortening the effective conjugation length.<sup>29</sup> There is also an alternative explanation that the red phase may have a different geometry compared to the blue phase, and this colour change is closely connected to the structure of the side chain.<sup>30-32</sup> In the blue phase, the polymer backbone maintains a regular

---

---

---

---

trans-zigzag structure with all-trans alkyl side chains, and in the red phase, the regular structure changes to an irregular structure with gauche conformations in alkyl side chains.<sup>33</sup> In recent years, polymerization of diacetylene molecules has been carried out not only in crystalline states but also in mesomorphic states and amorphous states.<sup>34-37</sup> For example, Li et al. used topochemical polymerization to stabilize self-assembled structures in liquid-crystalline homopolymer–surfactant complexes.<sup>34</sup> Though a few examples are available, the ability of topochemical polymerization in constrained media, particularly in amorphous materials, is less explored due to the lack of control of the arrangement of monomers.

Polymer side-chain modification using noncovalent interactions has emerged as a powerful strategy for the creation of ordered nanostructured materials with hierarchical morphologies. Ikkala and ten Brinke demonstrated the complexation of a small molecule with the block copolymer by hydrogen bonding.<sup>38</sup> Later, this supramolecular assembly (SMA) approach has become attractive to generate nanostructured composites for diverse applications.<sup>39-43</sup> Among these, the supramolecules containing organic semiconductors attracted the attention of researchers as this approach opens up a new avenue to tailor the electronic properties of composites.<sup>39,40,44</sup> Zhu et al. exploited the use of noncovalent polymer side-chain modification to study topochemical polymerization in block copolymer solutions and thin films.<sup>35</sup> In their studies, the SMA approach exploits hydrogen-bonding interactions between the imidazolyl diphenyl-diacetylene monomer and acrylic acid on the block copolymer. Solvent vapor annealing was used to improve the microphase separation in the block copolymer in thin films, which in turn improved the molecular packing and orientation of the monomers. As a result, the rate of topochemical polymerization enhanced remarkably. However, their studies were limited to solvent vapor annealed thin films at room temperature. In this regard, understanding of hierarchical ordering of the monomers within the block copolymer microdomains in bulk at room temperature and close to the

---

---

melting temperature of the monomers is significantly important. The main question to be addressed here is whether the microphase separation of the block copolymers improves the topochemical polymerization of hierarchically ordered monomers. For that purpose, the microphase separation of the block copolymer supramolecules containing diacetylene monomers was improved by both solvent vapor annealing and thermal annealing methods.

In this work, in the first step, 10,12-pentacosadyonic acid (PCDA) molecules are hydrogen-bonded with P4VP of PS-*b*-P4VP to create hierarchically structured materials in bulk. The hierarchical ordering and the molecular orientation of PCDA molecules within the block copolymer microdomains are controlled by the microphase separation of the block copolymer supramolecules. In the second step, the hierarchically ordered PCDA molecules are then converted into an optoelectronically active material by photoirradiation followed by subsequent heating. The effect of topochemical polymerization on the hierarchical ordering at multiple length scales was investigated by a combination of different techniques including small-angle X-ray scattering, wide-angle X-ray scattering, and spectroscopy.

## 2.3. Experimental Section

**2.3.1. Materials:** PS (32900)-*b*-P4VP (8000) (PDI=1.06) was purchased from Polymer Source, Inc. 10,12-pentacosadyonic acid (PCDA) was purchased from Sigma Aldrich and further purified by dissolving in methylene chloride (DCM) and filtered through 0.25  $\mu\text{m}$  syringe filter to remove the poly-PCDA. Using a rotary evaporator, the solvent (DCM) was evaporated and the purified PCDA monomer was stored at -15 °C in the dark.<sup>17</sup> The solvents 1,4-dioxane and DCM (analytical grade) were purchased from Sigma Aldrich.

**2.3.2. Sample Preparation:** PS-*b*-P4VP(PCDA)<sub>r</sub> supramolecular complexes were prepared in 1,4-dioxane, where r denotes the molar ratio between PCDA monomer and 4VP

---

---

unit. The molar ratio ( $r$ ) of PCDA to 4VP unit was varied from 0.25, 0.5, 0.75, and 1. The block copolymer solution was added drop-by-drop to the PCDA solution while maintaining the mixing temperature close to the boiling point of the solvent with continuous stirring. Such prepared solution was stored 3 days for the complete hydrogen-bonding formation. After that, the solution was transferred into the petri dish, and the solvent was allowed to evaporate for a week slowly.

**2.3.3. Annealing Methods:** Two phases of annealing were used in this work. In the first phase, the samples were solvent-vapor annealed or thermally annealed at 90 °C. In the solvent-vapor annealing step, PS-*b*-P4VP(PCDA) solutions were drop-casted in a petri dish and the solvent was allowed to evaporate slowly in a desiccator under dark conditions. These samples were labeled as “solvent annealed”. In the thermal annealing step, PS-*b*-P4VP(PCDA) powder samples were annealed at 90 °C, which is above the melting temperature of PCDA monomer and then cooled to room temperature. These samples were labeled as “thermally annealed”. In the second phase, solvent-vapor annealed samples/thermally annealed samples (at 90 °C) were then exposed to UV irradiation for 20 min and this step leads to the topochemical polymerization of PCDA within the block copolymer microdomains to form the “blue phase”. Depending on the initial annealing conditions, samples were labeled as “SA blue” (solvent-vapor annealed) and “TA blue” (thermally annealed). These samples were then further heated to 190 °C (just above the melting temperature of red phase) and cooled to room temperature in order to study the blue phase to red phase transition of polymerized PDA within the block copolymer domains and also to understand the order-disorder transition of block copolymer supramolecules.<sup>39</sup>

<sup>54</sup> Again, depending on the initial annealing conditions, samples were labeled as “SA red” (solvent-vapor annealed) and “TA red” (thermally annealed).

---

---

## 2.4. Characterization

Wide-angle and small-angle X-ray scattering measurements (WAXS/SAXS) were carried out using Xeuss SAXS/WAXS system from Xenocs operated at 0.6 mA and 50 kV. The data were collected in the transmission mode geometry using Cu K $\alpha$  radiation with wavelength,  $\lambda = 1.54 \text{ \AA}$ . The 2D images were recorded on a Mar 345 detector (Image plate), processed using Fit2D software. Silver behenate was used as the standard sample for calibration of WAXS and SAXS. The sample-detector distance was set at 219.5 mm and 1044.5 mm for WAXS and SAXS data collections, respectively. Linkam THMS 600 hot stage was used to carry out the temperature-dependent measurements. The sample was heated from 30 to 190 °C at a rate of 10 °C/min. The X-ray patterns were obtained at the interval of 20 °C on holding the sample at that temperature for 10 min.

FTIR measurements were collected using PerkinElmer series Spectrum Two FT-IR spectrometer. The spectra were recorded by averaging 32 scans at a resolution of  $2 \text{ cm}^{-1}$  in the range of  $4000\text{--}400 \text{ cm}^{-1}$ . The morphologies of the prepared block copolymer supramolecules were analyzed with TEM, JEOL 2010 transmission electron microscope operating at 300 kV. UV-visible spectra were recorded with a PerkinElmer lambda 900, UV-visible-NIR spectrophotometer. Raman spectra was recorded using WI-Tec Raman microscope (WI-Tec, Inc., Germany, alpha 300R) with a laser beam directed to the sample through 20 $\times$  objective with 600 g/mm grating and a Peltier cooled CCD detector. Samples were excited with a 785 nm wavelength laser and the spectra were recorded in the range of  $1000\text{--}2500 \text{ cm}^{-1}$  with  $1 \text{ cm}^{-1}$  resolution. The TEM grids were directly coated with the PS-*b*-P4VP((PCDA)<sub>1</sub>) solution in 1,4-dioxane (2mg/ml). Iodine vapor was used to stain the samples to enhance the contrast, where the iodine molecules selectively interact with the P4VP domains.

## 2.5. Results and Discussion

### 2.5.1. Hierarchical Assembly of PCDA Monomers within the Block Copolymer Microdomains

The PCDA monomer was purified to remove the traces of polymerized part at ambient conditions prior to the formation of supramolecules with PS-*b*-P4VP. PS-*b*-P4VP(PCDA)<sub>r</sub> supramolecular complexes were prepared in 1,4-dioxane, where *r* denotes the molar ratio between the PCDA monomer and the 4VP unit. The molar ratio (*r*) of PCDA to the 4VP unit was varied from 0.25, 0.5, 0.75, and 1.

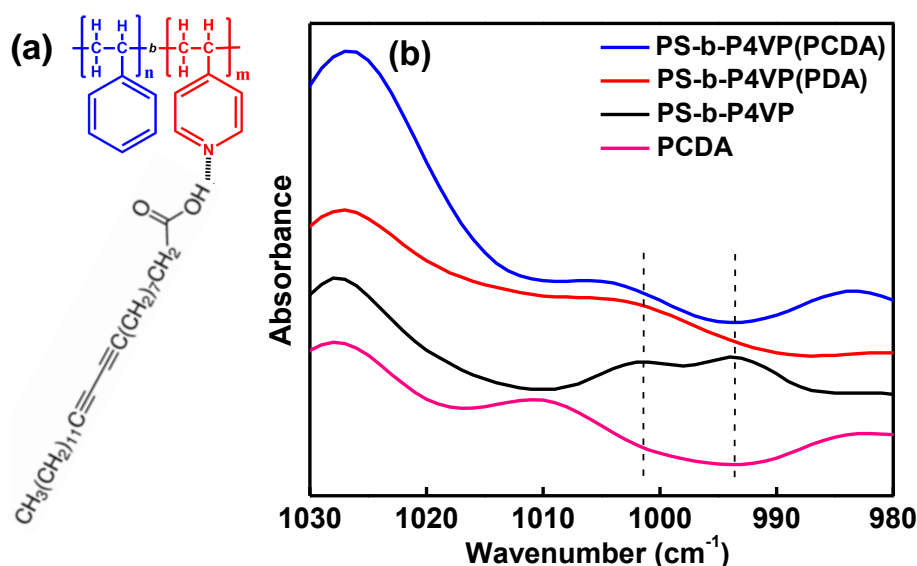


**Figure 2.1.** (a) Chemical structure indicating the formation of hydrogen bonding between PS-*b*-P4VP and PCDA; (b) FTIR spectra of PCDA, PS-*b*-P4VP, PS-*b*-P4VP(PCDA)<sub>1</sub>, and PS-*b*-P4VP(PDA)<sub>1</sub>.

For FTIR studies, the molar ratio between vinylpyridine units in the P4VP block and PCDA was fixed at 1 (PS-*b*-P4VP(PCDA)<sub>1</sub>). The formation of hydrogen bonding between carboxylic groups in PCDA and pyridine groups in P4VP was confirmed by infrared spectroscopy. Figure 2.1 shows the chemical structure of PS-*b*-P4VP(PCDA)<sub>1</sub> and FTIR spectra of PCDA, PS-*b*-P4VP, PS-*b*-P4VP(PCDA)<sub>1</sub> and PS-*b*-P4VP(PDA)<sub>1</sub>. The

absorption band at  $993\text{ cm}^{-1}$ , which corresponds to the symmetric ring stretching mode of free pyridine groups in the PS-*b*-P4VP block copolymer, shifted to a higher frequency after blending with PCDA indicating the formation of hydrogen bonding between PCDA and P4VP.<sup>42,45</sup>

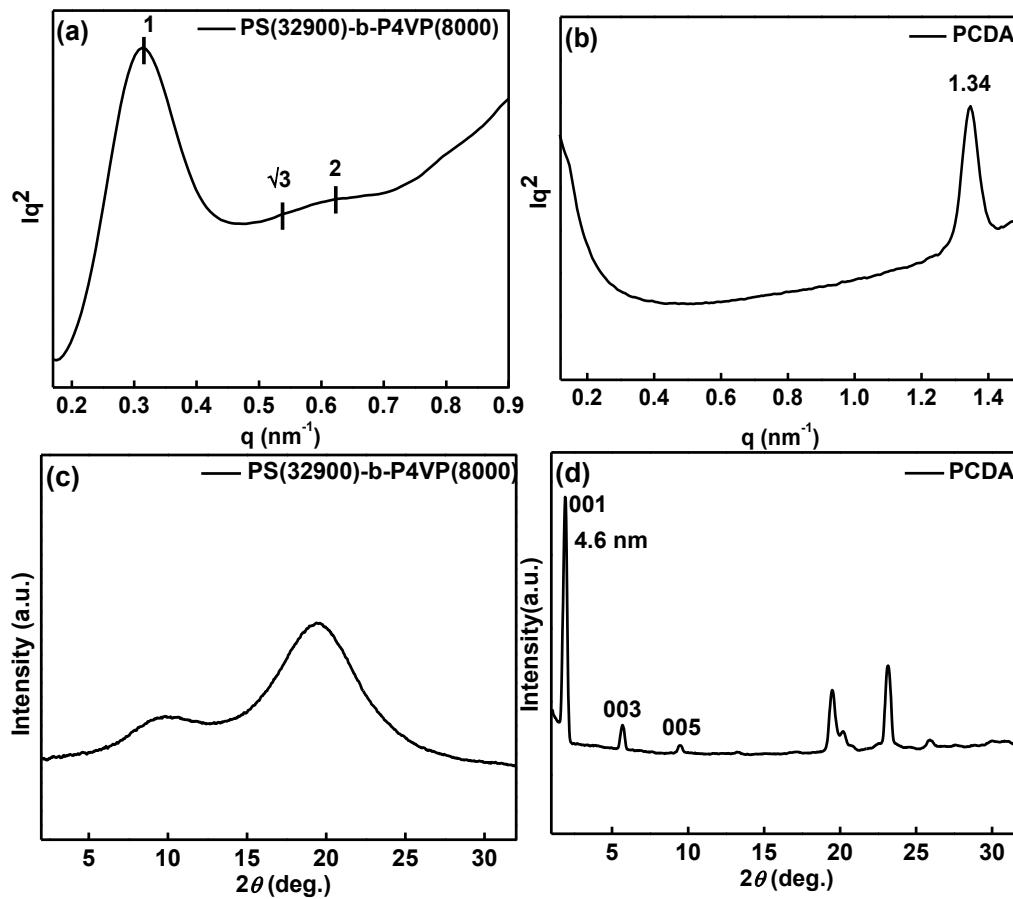


**Figure 2.2.** SAXS patterns of (a) PS-*b*-P4VP, (b) PCDA and WAXS patterns of (c) PS-*b*-P4VP, (d) PCDA.

The PS-*b*-P4VP block copolymer used for this study had weight fractions of two blocks ( $f_{\text{PS}} = 0.80$  and  $f_{\text{P4VP}} = 0.20$ ). The SAXS pattern shows peaks at  $q = 0.31, 0.54,$  and  $0.62\text{ nm}^{-1}$  with a ratio of  $1:\sqrt{3}:2$ , which confirms the formation of the hexagonally packed cylindrical structure ( $d = 20.0\text{ nm}$ ) shown in Figure 2.2a. The hierarchical self-assembly of PCDA monomers within the block copolymer microdomains was analyzed by SAXS and WAXS. Figure 2.3(a and b) shows Lorentz-corrected SAXS and WAXS patterns of the

---

---

solvent vapor annealed PS-*b*-P4VP(PCDA)<sub>1</sub>. The SAXS pattern of the solvent vapor annealed sample shows a peak at  $q = 0.2 \text{ nm}^{-1}$  ( $d = 31.4 \text{ nm}$ ) corresponding to the domain spacing of the block copolymer supramolecules. It has to be noted that the solvent-vapor annealed samples generally result in kinetically trapped structures in non-equilibrium.<sup>46</sup> No higher-order peaks corresponding to the microphase separation are observed, indicating the poor order of the block copolymer self-assembly. However, a peak at  $q = 1.36 \text{ nm}^{-1}$  ( $d = 4.6 \text{ nm}$ ) corresponding to the assembly of the PCDA monomers within the block copolymer microdomains is observed shown in Figure 2.2b. The TEM image obtained for the solution casted PS-*b*-P4VP(PCDA)<sub>1</sub> also confirms the formation of lamellar morphology (Figure 2.4) in agreement with the SAXS data. The corresponding WAXS pattern (Figure 2.3b) shows a series of (00*l*) peaks at lower  $2\theta$  which are contributed by the highly ordered layered structure of PCDA along the c-axis within the block copolymer microdomains and at higher  $2\theta$ , multiple crystalline reflections were observed corresponding to the crystal structure of PCDA.<sup>20</sup> As the block copolymer used in this work is amorphous (Figure 2.2c), the observed crystalline reflections can be assigned to the crystallization of the PCDA monomers within the block copolymer microdomains. This kind of crystallization of small molecules within the block copolymer microdomains is well known.<sup>39, 47, 48</sup> The *d*-spacing estimated from the (001) reflection is  $\sim 4.6 \text{ nm}$ , and it is assigned to the bilayer structure of PCDA.<sup>49,50</sup> This value is in good agreement with the spacing estimated from the SAXS pattern. The *d*-spacing estimated from the (00*l*) reflection of the pure PCDA WAXS pattern is  $\sim 4.6 \text{ nm}$  (Figure 2.2d). These results suggest that the molecular packing of PCDA in the solvent vapor annealed supramolecules is almost the same as that of the pure PCDA.

---

---

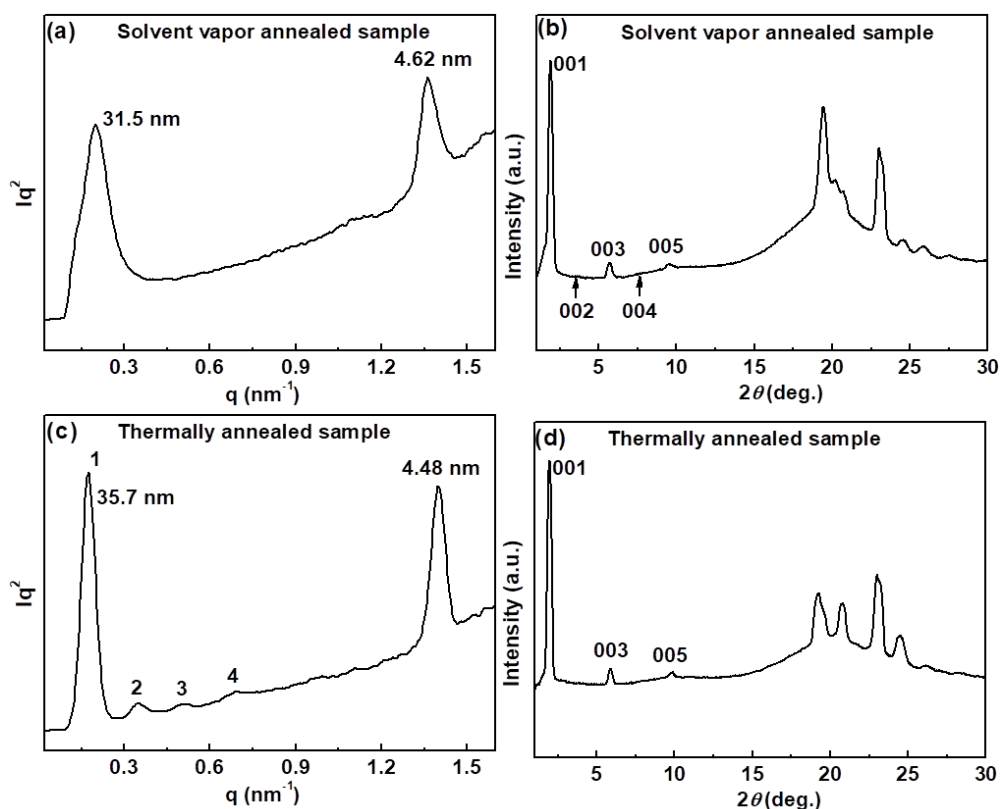


**Figure 2.3.** Lorentz-corrected SAXS and WAXS patterns of (a, b) solvent vapor annealed, and (c, d) thermally annealed PS-*b*-P4VP(PCDA)<sub>1</sub> complexes.

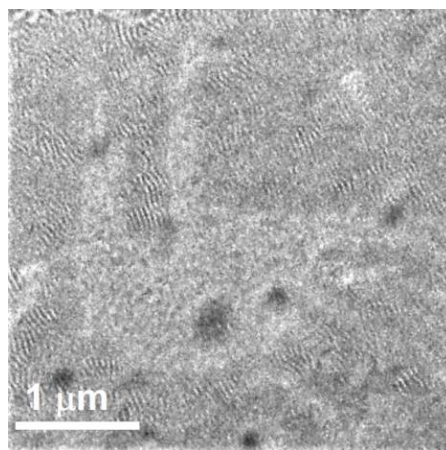


**Figure 2.4.** TEM image of solution casted PS-*b*-P4VP(PCDA)<sub>1</sub>

To obtain equilibrium structures, often, thermal treatments were used above the glass transition temperatures ( $T_g$ ) of the blocks.<sup>51</sup> But in block copolymer supramolecules, other than  $T_g$  of polymers in block copolymers, the melting point of the small molecules

also plays a significant role in the self-assembly process.<sup>40, 52, 53</sup> It has been reported that heating/annealing the block copolymer supramolecules close to or above the melting temperature of the small molecules control the overall supramolecular morphology and domain spacing. Thus, we focused on thermal annealing of the block copolymer supramolecules above the melting temperature of PCDA  $\sim 64 \pm 1$  °C shown in Figure 2.5.

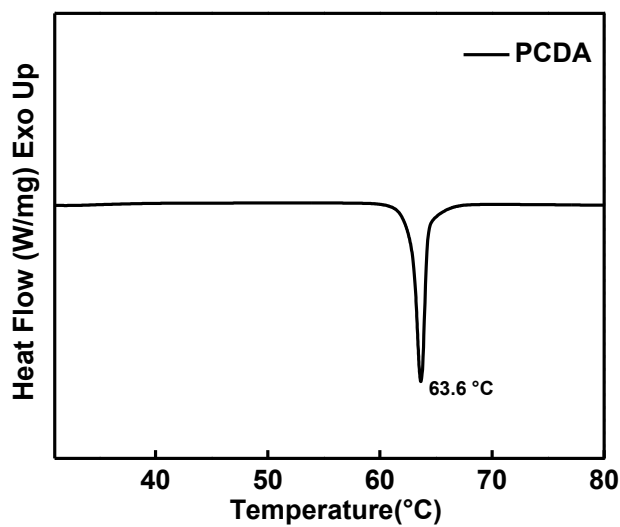


**Figure 2.5.** DSC thermogram of pure PCDA measured during first heating.

The SAXS and WAXS patterns of the thermally annealed sample are shown in Figure 2.3(c and d). The SAXS pattern shows peaks up to four scattering maxima at  $q = 0.17, 0.34, 0.51,$  and  $0.68 \text{ nm}^{-1}$  with an integer ratio of 1:2:3:4 between the first and higher-order reflections. The lamellar periodicity is increased to 35.7 nm compared to that of the solvent vapor annealed sample (31.5 nm). At the same time, the peak corresponding to the assembly of the PCDA monomers has also slightly shifted its position to  $q = 1.4 \text{ nm}^{-1}$  ( $d = 4.48 \text{ nm}$ ). Compared to the solvent vapor annealed sample, the thermally annealed sample shows ordered hierarchical assemblies containing both block copolymer lamellae (35.7 nm) and the 4.48 nm lamellae from the PCDA assemblies within the P4VP block. There is an increase in the sharpness and intensity of the peaks related to both block copolymer morphology and the PCDA assembly within the block copolymer microdomains.

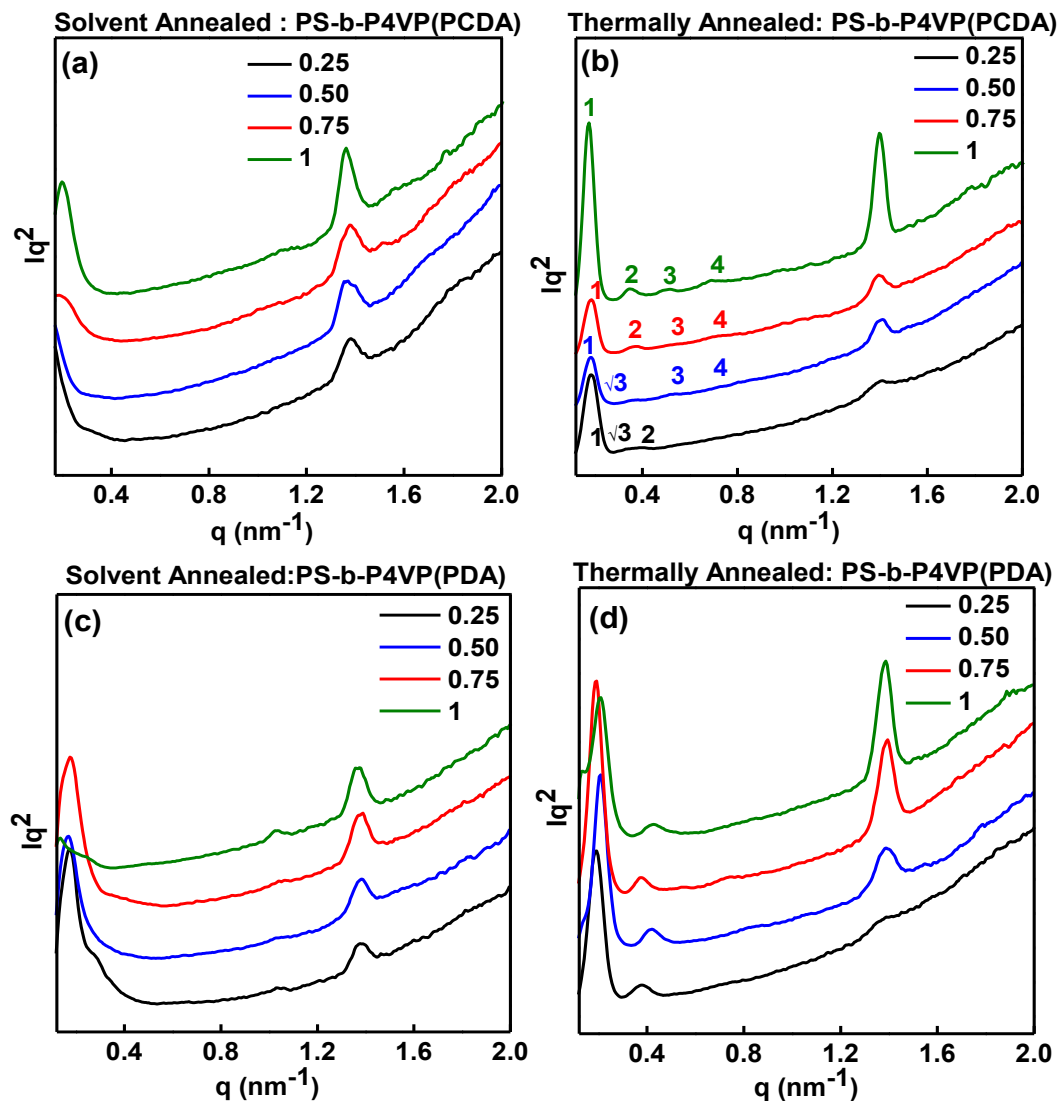


**Figure 2.6.** SAXS patterns of  $\text{PS-}b\text{-P4VP(PCDA)}_r$  supramolecular complexes for (a) solvent-vapor annealed samples and (b) thermally annealed samples and SAXS patterns of  $\text{PS-}b\text{-P4VP(PDA)}_r$  supramolecular complexes after polymerization (UV-irradiation) for (c) solvent-vapor annealed samples and (d) thermally annealed samples.

The influence of the PCDA content on the block copolymer morphology was investigated both in the solvent annealed and thermally annealed  $\text{PS-}b\text{-P4VP(PCDA)}_r$  supramolecules shown in Figure 2.6 (a and b). The stoichiometric ratio ( $r$ ) of PCDA to 4VP unit was varied from 0.25, 0.5, 0.75, and 1. The SAXS patterns shown in Figure 2.6a were obtained for the solvent-vapor annealed samples. These  $\text{PS-}b\text{-P4VP(PCDA)}_r$  complexes

---

---

show only one peak corresponding to the domain spacing of the block copolymer supramolecules. It is clear from the SAXS patterns that in solvent-vapor annealed samples, the domain spacing corresponding to the block copolymer self-assembly decreases with the increase in the molar ratio of PCDA. As higher-order peaks are absent, it is not possible to identify the morphology of the block copolymer in these samples. At higher  $q$ , a peak at  $q = 1.36 \text{ nm}^{-1}$  is observed in all the samples, which is corresponding to the molecular packing of PCDA within the block copolymer microdomains. As discussed in the previous section, the solvent-vapor annealed samples showed poor block copolymer morphology. However, PCDA monomers packing is better within the block copolymer microdomains as evident from the intensity of the peak at  $q = 1.36 \text{ nm}^{-1}$ .

The influence of the PCDA content on the block copolymer morphology was investigated in the thermally annealed PS-*b*-P4VP(PCDA)<sub>r</sub> supramolecules shown in Figure 2.6b, which is obtained after thermal annealing of the samples at 90 °C. The PS-*b*-P4VP(PCDA)<sub>0.25</sub> sample shows peaks with a ratio of 1: $\sqrt{3}$ :2, indicating the formation of hexagonally packed cylinders, whereas the PS-*b*-P4VP(PCDA)<sub>0.5</sub> sample shows a mixed morphology of hexagonally packed cylinders and lamellae. The samples with a higher molar ratio, PS-*b*-P4VP(PCDA)<sub>0.75</sub>, shows a well-defined lamellar morphology similar to the PS-*b*-P4VP(PCDA)<sub>1</sub>. These results indicated that the volume fraction of the P4VP(PCDA) complex and the interface space for the grafted structures play a critical role in determining the final morphology of the block copolymer supramolecules as discussed in the literature.<sup>39, 54, 55</sup> At the same time, the peak at  $q = 1.36 \text{ nm}^{-1}$ , which is corresponding to the molecular packing of PCDA within the block copolymer microdomains shows intense peak in the case of PS-*b*-P4VP(PCDA)<sub>1</sub> and other samples with lower molar ratios show less intense peak indicating that the molecular packing of PCDA monomer is not well organized within the block copolymer microdomains.

---

---

The WAXS pattern of the thermally annealed sample shown in Figure 2.3d exhibit apparently similar pattern to that of the solvent vapor annealed sample albeit the slight differences in the peak positions and intensities. Such differences may arise due to the confined crystallization of PCDA within the block copolymer lamellae during the cooling process from annealing temperature. Most importantly, the layered structure of PCDA reappears after the annealing process. We have verified the FTIR spectrum of the thermally annealed sample and it remains the same as that of the solvent vapor annealed sample (Figure 2.7) indicating the restoration of hydrogen bonding between pyridine units and PCDA. In this way, the supramolecular strategy allows for the fine tuning of the molecular packing of the PCDA monomers by varying the annealing conditions.

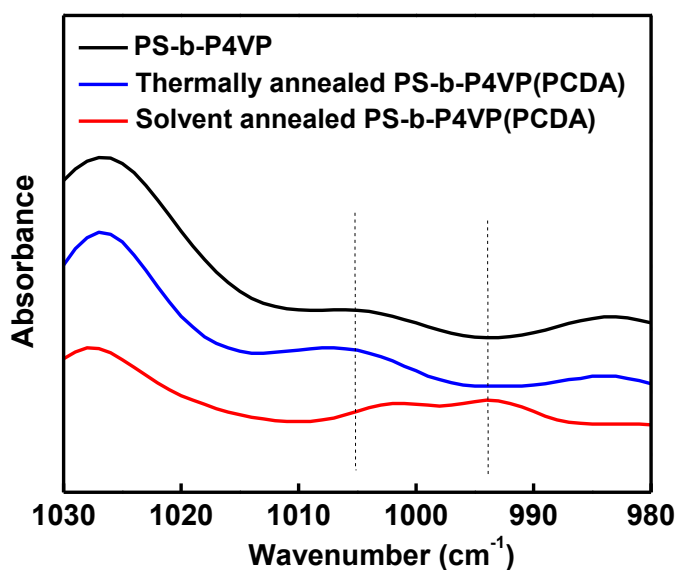


**Figure 2.7.** Comparison of FTIR spectra of PS-*b*-P4VP, thermally annealed PS-*b*-P4VP(PCDA)<sub>1</sub>, and solvent vapor annealed PS-*b*-P4VP(PCDA)<sub>1</sub> in the region of 1030-980 cm<sup>-1</sup>.

### 2.5.2. Topochemical Polymerization of PCDA within the Block Copolymer Microdomains

In order to investigate the molecular assembly of PCDA within the block copolymer microdomains, both solvent vapor annealed and thermally annealed PS-*b*-P4VP(PCDA)<sub>1</sub> samples were topochemically polymerized after exposure to 254 nm UV irradiation at room temperature for 20 min and then heated up to 190 °C (just above the melting temperature of the red phase). As seen in Figure 2.1b, the hydrogen-bonding is retained between polymerized PCDA (PDA) and 4VP chains even after the topochemical polymerization. Figure 2.8 shows the photographs and UV-Vis spectra of solvent vapor annealed (SA) and thermally annealed (TA) samples before polymerization, after polymerization (UV-irradiation) and melt-cooled samples.

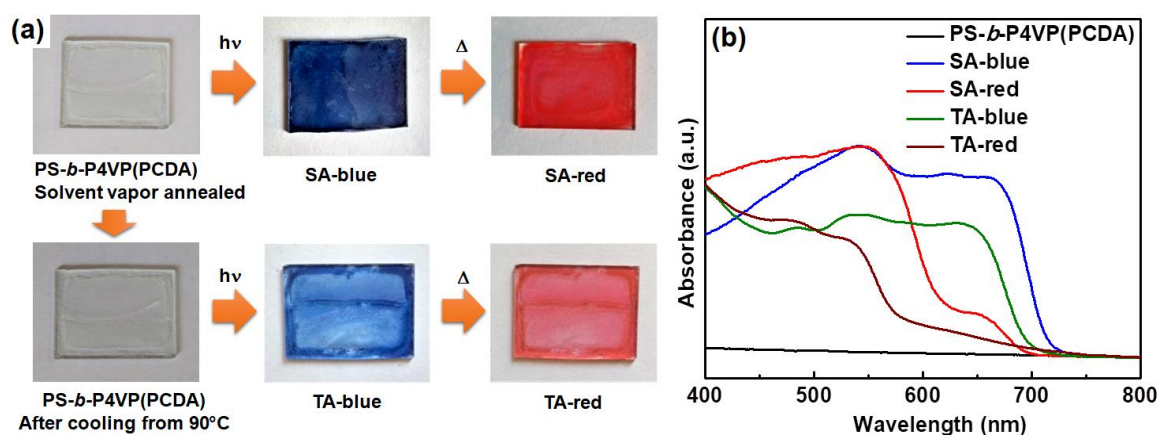


**Figure 2.8.** (a) Photographs of solvent vapor annealed and thermally annealed PS-*b*-P4VP(PCDA)<sub>1</sub>, UV irradiated and melt-cooled samples under visible light (b) UV-Vis absorption spectra of PS-*b*-P4VP(PCDA)<sub>1</sub> before UV irradiation (black line), solvent vapor annealed sample after UV irradiation (blue line, labeled as SA-blue), melt-cooled spectrum of SA-blue (red line, labeled as SA-red), thermally annealed sample after UV irradiation (green line, labeled as TA-blue), and melt-cooled spectrum of TA-blue (brown line, labeled as TA-red)

After UV-irradiation, both the samples show blue colour under visible light, but the UV-Vis spectra of both solvent vapor annealed and thermally annealed samples show dominant absorption peak for blue phase and minor red phase (540 nm). However, absorbance maxima of the blue phase are different for these samples. It has been reported that longer  $\pi$ -conjugated backbone normally fetch in bathochromically shifted absorption/emission bands.<sup>50, 56</sup> The solvent vapor annealed sample shows the absorption maxima at 660 nm (dark blue) and the thermally annealed sample shows the same at 630 nm (light blue). These results suggest that the molecular packing of the PCDA in the solvent vapor annealed sample is significantly different from that in the thermally annealed sample and here we speculate that this difference in the molecular packing might greatly affect the topochemical reaction degree of PCDA. The solvent vapor annealed sample shows a high degree of topochemical reaction compared to that of the thermally annealed sample, hence the colour of both blue phase and red phase are darker in solvent vapor annealed samples compared to thermally annealed samples. On the other hand, melt-cooled samples (heated up to 190 °C and then cooled to room temperature) show red colour and the UV-Vis spectra confirm the disappearance of the absorption peaks corresponding to the blue phase and the simultaneous appearance of absorption maxima at 540 nm, which corresponds to the red phase.

Further evidence for the formation of the blue phase and the red phase is obtained by Raman spectroscopy measurements. Figure 2.9 shows the Raman spectra of PS-*b*-P4VP(PCDA)<sub>1</sub> sample before polymerization, after polymerization (UV-irradiation) and melt-cooled samples. Before polymerization, PS-*b*-P4VP(PCDA)<sub>1</sub> sample shows the dominant acetylenic stretching band at 2278 cm<sup>-1</sup> and a weak band at 2100 cm<sup>-1</sup>.<sup>27, 57</sup> It is worth mentioning here that the band at 2100 cm<sup>-1</sup> does not exist in purified PCDA monomer

suggesting that some of the monomers are polymerized during the preparation of block copolymer supramolecules.

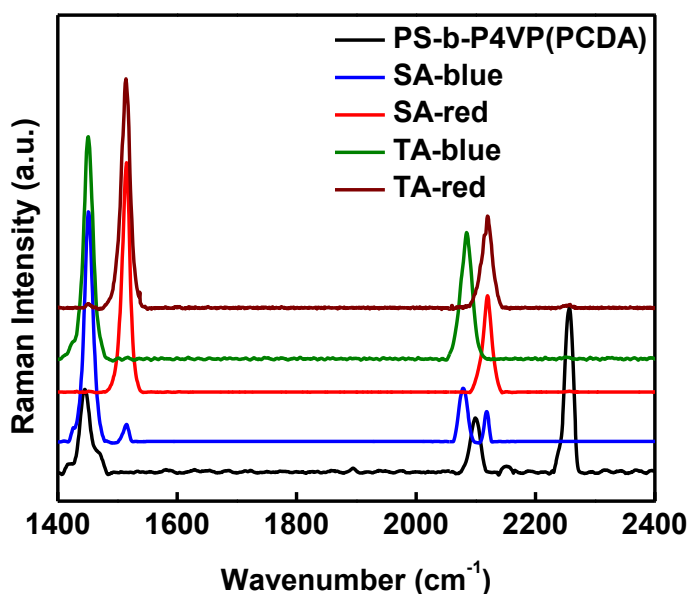


**Figure 2.9.** Raman spectra of PS-*b*-P4VP(PCDA)<sub>1</sub> before UV irradiation (black line), solvent vapor annealed sample after UV irradiation (blue line, labeled as SA- blue), melt-cooled spectrum of SA-blue (red line, labeled as SA-red), thermally annealed sample after UV irradiation (green line, labeled as TA-blue), and melt-cooled spectrum of TA-blue (brown line, labeled as TA-red).

When the solvent vapor annealed sample is irradiated with UV light, the band corresponding to the acetylenic stretching of PCDA disappears and new bands associated with conjugated alkyne-alkene groups appear at 2089 cm<sup>-1</sup> (C≡C) and 1445 cm<sup>-1</sup> (C=C). These bands are assigned to the blue phase of polymerized PCDA (PDA).<sup>27, 58</sup> In addition to these bands, two minor peaks are observed at 2118 cm<sup>-1</sup> and 1514 cm<sup>-1</sup>, which are due to the formation of a minor fraction of the red phase along with the blue phase. On heating and cooling (melt-cooled sample) of this UV irradiated solvent vapor annealed sample, the bands corresponding to the blue phase completely disappeared and the bands associated with the red phase (2118 and 1514 cm<sup>-1</sup>) appeared.<sup>59</sup> The red phase formed during heating

remains as such even after cooling to room temperature, which indicates the irreversible nature of the red phase. On the other hand, upon UV irradiation, the thermally annealed sample shows bands characteristic of blue phase at  $2089\text{ cm}^{-1}$  ( $\text{C}\equiv\text{C}$ ) and  $1445\text{ cm}^{-1}$  ( $\text{C}=\text{C}$ ). No traces of the red phase are observed in the UV irradiated samples. Similar to the solvent vapor annealed samples, the melt-cooled sample shows the pure red phase. It has been demonstrated that the colour change from blue to red is related to the conformational change of the PDA backbone from planar to nonplanar and the side chain conformation plays a critical role in controlling the conformational change of eneyne backbone.<sup>25</sup> Though the Raman spectroscopy is very helpful to understand the polymerization, it is not so worthwhile in understanding the topochemical reaction degree of PCDA.

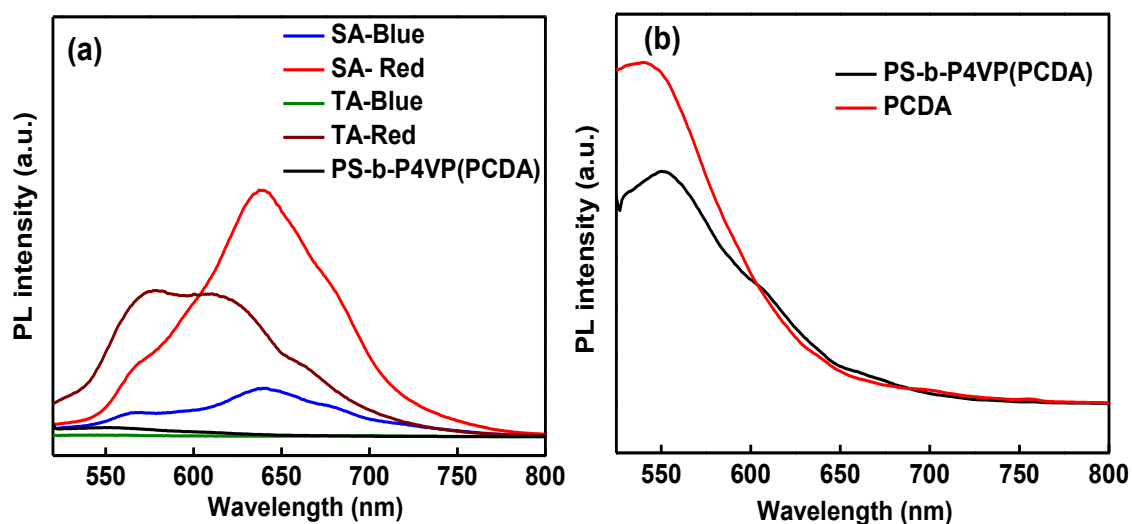


**Figure 2.10.** (a) Emission spectra ( $\lambda_{\text{ex}} = 500\text{ nm}$ ) of  $\text{PS-}b\text{-P4VP(PCDA)}_1$  before UV irradiation (black line), solvent vapor annealed sample after UV irradiation (blue line, labeled as SA- blue), melt-cooled spectrum of SA-blue (red line, labeled as SA-red), thermally annealed sample after UV irradiation (green line, labeled as TA-blue), and melt-cooled spectrum of TA-blue (brown line, labelled as TA-red), and (b) Emission spectra ( $\lambda_{\text{ex}} = 500\text{ nm}$ ) of pure PCDA and  $\text{PS-}b\text{-P4VP(PCDA)}_1$  complex.

---

Photoluminescence (PL) spectroscopy is useful to understand the degree of topochemical polymerization.<sup>35</sup> The variation of PL intensities in solvent vapor annealed samples and thermally annealed samples were studied and Figure 2.10 shows the PL spectra of various samples. The block copolymer supramolecule (PS-*b*-P4VP(PCDA)<sub>1</sub>) shows a weak emission at 550 nm (zoomed spectrum shown in Figure 2.10b) corresponding to the hierarchically ordered PCDA monomer within the block copolymer microdomains. When the solvent vapor annealed sample is exposed to the UV-irradiation (SA-blue), a weak peak at 640 nm is observed along with the monomer peak at 570 nm. It was reported that the blue phase of PDA is non-emissive and the peak at 640 nm can be assigned to the red phase of PDA.<sup>25</sup> As discussed in the preceding section, the UV- and Raman spectra revealed that SA-blue sample shows a minor fraction of the red phase along with the dominant blue phase. On heating and cooling of this sample (melt-cooled sample (SA-red)), the relative heights of the PL peaks increased significantly indicating the conversion of the blue phase to the red phase. On the other hand, in agreement with the UV- and Raman spectra, the thermally annealed sample (TA-blue) is non-emissive indicating either the formation of the pure blue phase or the sample remaining in the monomer state. On heating and cooling of this sample (melt-cooled sample (TA-red)), a new spectrum is observed compared to that of the solvent vapor annealed sample with two broad PL peaks at 578 nm and 612 nm. The hypsochromic shift of emission bands indicates the formation of shorter  $\pi$ -conjugated backbone due to the low degree of topochemical polymerization.<sup>50</sup> The ratio of the intensity of PDA peak relative to the emission peak of PCDA monomer is less than 1 in thermally annealed sample also confirms that PCDA monomers do not polymerize effectively compared to the solvent vapor annealed samples.

In the preceding section, hierarchical self-assembly of PCDA monomers within the block copolymer microdomains was discussed with the help of SAXS and WAXS. It is

---

obvious that the molecular packing of the PCDA and the ordering of block copolymer supramolecules depend upon the annealing conditions as well as molar ratio of PCDA. We are interested in understanding the changes in the hierarchical structures during the topochemical polymerization of both solvent vapor annealed samples and thermally annealed samples. Upon the UV irradiation, PS-*b*-P4VP(PCDA)<sub>1</sub> samples were polymerized and these samples are labeled as PS-*b*-P4VP(PDA)<sub>1</sub>. The room temperature SAXS data of PS-*b*-P4VP(PCDA)<sub>r</sub> complexes having different PCDA content were compared in Figure 2.6(c,d) after the UV-irradiation for both solvent-vapor annealed and thermally annealed samples. Upon the UV-irradiation, SAXS patterns of the solvent-vapor annealed samples (Figure 2.6c) show a broad peak at around  $q = 1.03 \text{ nm}^{-1}$  corresponding to the polymerized PDA. On the other hand, thermally annealed samples Figure 2.6d did not show this peak indicating that the molecular packing of PCDA is not appropriate for the polymerization. Figure 2.11 shows the temperature-dependent Lorentz-corrected SAXS and WAXS patterns of solvent vapor annealed PS-*b*-P4VP(PDA)<sub>1</sub> sample upon heating (up to 190 °C) and cooling to room temperature at a rate of 10°C/min. The room temperature SAXS pattern of PS-*b*-P4VP(PDA)<sub>1</sub> shows three peaks at  $q = 0.2 \text{ nm}^{-1}$  (31.4 nm),  $1.03 \text{ nm}^{-1}$  (6.1 nm), and  $1.36 \text{ nm}^{-1}$  (4.6 nm). The peak at lower  $q \sim 0.2 \text{ nm}^{-1}$  (31.4 nm) is corresponding to the domain spacing of the block copolymer microphase separation and it remains as such upon the UV irradiation. At the same time, the peak at  $q = 1.36 \text{ nm}^{-1}$  (4.6 nm), which is corresponding to the assembly of PCDA monomers within the block copolymer microdomains also remains as such upon the polymerization indicating that the topochemical reaction proceeded within the hierarchically ordered block copolymer microdomains. We assign this peak to the blue phase of PDA since corresponding d-spacing is consistent with the lamellar thickness of the blue phase of pure PDA bilayer

crystal. In addition to this, a new peak appears at  $q = 1.03 \text{ nm}^{-1}$  (6.1 nm), where the d-spacing is larger than the blue phase of PDA crystals.

The corresponding room temperature WAXS pattern (Figure 2.11b) shows (00 $l$ ) peaks at lower  $2\theta$  indicating that the layered structure is retained upon the polymerization and at higher  $2\theta$  multiple crystalline reflections were observed corresponding to the monoclinic structure of the blue phase.<sup>60</sup> It has to be noted that no diffraction peaks are observed for the PS-*b*-P4VP block copolymer as both the blocks are amorphous (Figure 2.2c).

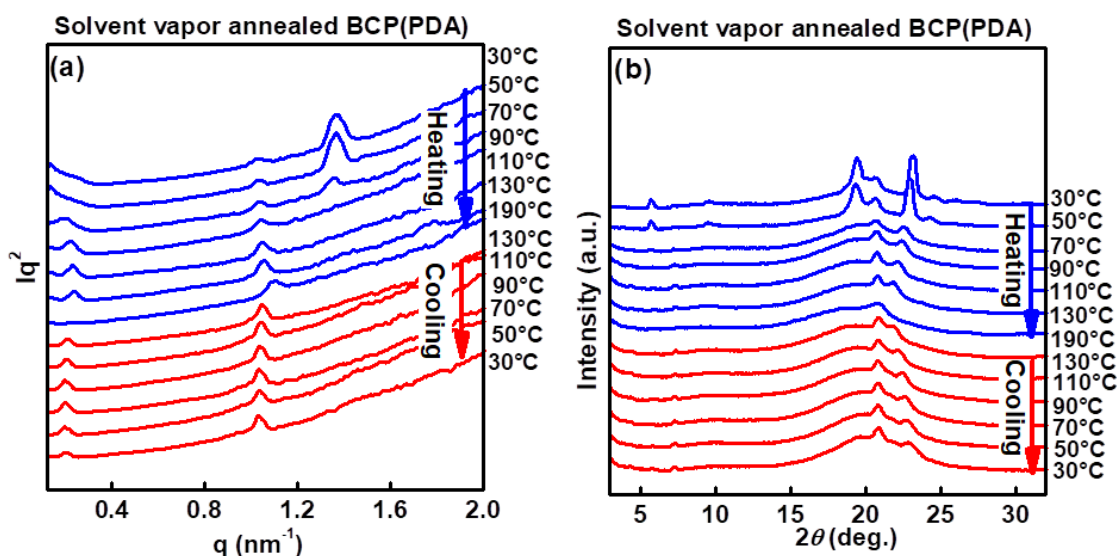


**Figure 2.11.** Temperature-dependent (a) Lorentz-corrected SAXS and (b) WAXS patterns of solvent vapor annealed PS-*b*-P4VP(PDA)<sub>1</sub> after the UV irradiation.

Upon heating, as seen in Figure 2.11a, the peak corresponding to the blue phase ( $q = 1.36 \text{ nm}^{-1}$  (4.6 nm)) disappeared in the temperature range of 60–75 °C, and the intensity of the peak  $q = 1.03 \text{ nm}^{-1}$  (6.1 nm) is increased above this temperature range. Based on the UV, Raman and PL results, this peak can be assigned to the red phase of PDA. One of the possible reasons for the appearance of red PDA phase upon the UV irradiation at room temperature in solvent vapor annealed samples is the change in the tilt angle of the side

chain of PDA with respect to the layer planes in the confined space created within the block copolymer microdomains.<sup>36</sup> In Figure 2.11b, a clear crystal-to-crystal transition is observed in the same temperature range and it can be assigned to the blue-to-red transition of PDA crystals within the block copolymer microdomains. The bilayer thickness of the red PDA phase (6.1 nm) within the block copolymer microdomains is larger than that of the blue phase (4.62 nm). Such an increase in the d-spacing of the lamellar thickness was reported in the literature due to the partial distortion of the arrayed p-orbitals, which is responsible for the increase in interchain distance.<sup>61</sup> But in the present study, there could be other reasons for the enlargement of lamellar thickness. The PCDA molecules are hydrogen-bonded with P4VP chains of PS-*b*-P4VP and upon polymerization, the hydrogen-bonding retained as evident from the SAXS and FTIR, and it may create a force to pull the side chains of PDA to form a more extended chain conformation.<sup>36</sup> Another possible reason is that the confined space within the block copolymer microdomains may change the tilt angle of the side chain of PDA with respect to the layer planes.

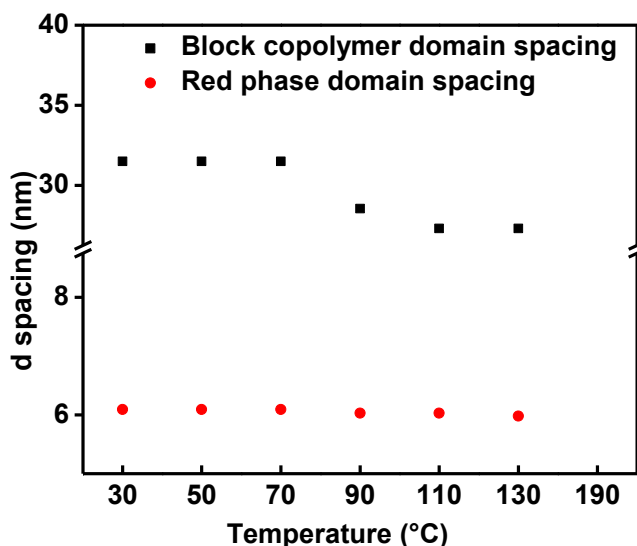


**Figure 2.12.** The d-spacings corresponding to the phase separated morphology and the hierarchically ordered PDA estimated from Figure 2.11 during the heating process.

On heating, the d-spacings of the phase separated morphology and the hierarchically ordered PDA chains decreased shown in Figure 2.12. It might be due to the mobility of polymer chains and the conformational change of the side chain of PDA. On further heating, the crystalline reflections corresponding to the red phase disappeared at 190 °C indicating the melting of the red phase as seen in Figure 2.11b. The DSC thermogram further confirms the melting of the red phase at 187 °C (Figure 2.13).

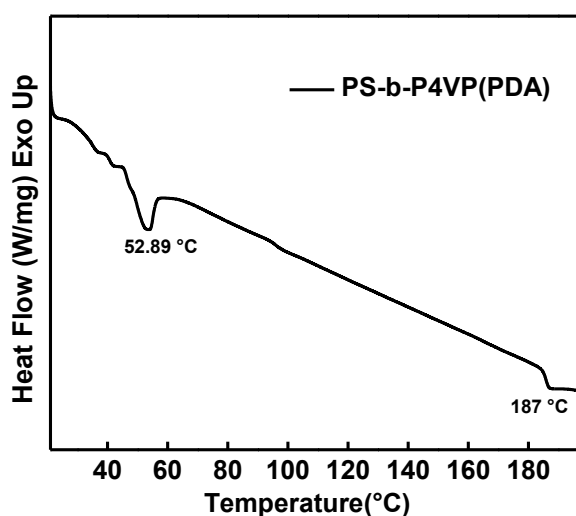


**Figure 2.13.** DSC thermogram of melt-cooled PS-*b*-P4VP(PDA)<sub>1</sub> measured during first heating.

At the same temperature, the microphase separated morphology of the block copolymer supramolecules collapsed due to the melting of the hierarchically ordered PDA chains. However, upon cooling, both red phase of PDA and microphase separated morphology of the block copolymer supramolecules reappeared simultaneously in WAXS and SAXS, respectively. These results suggested that in solvent vapor annealed block copolymer supramolecules, though the order of the phase separated block copolymer morphology is not that effective, the molecular packing of the PCDA monomers favour the topochemical polymerization.

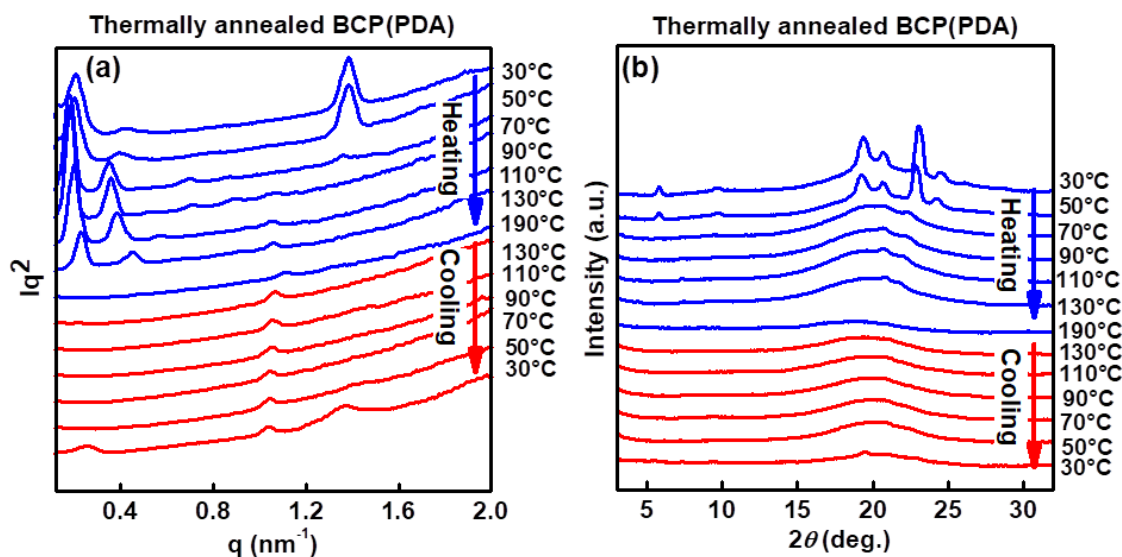


**Figure 2.14.** Temperature-dependent (a) Lorentz-corrected SAXS and (b) WAXS patterns of thermally annealed  $\text{PS-}b\text{-P4VP(PDA)}_1$  after the UV irradiation.

The effect of thermal annealing on the block copolymer morphology and its influence on topochemical polymerization was further studied to understand the molecular packing of PCDA monomers in thermally annealed samples. As discussed in the preceding section, thermal annealing of the block copolymer supramolecules ( $\text{PS-}b\text{-P4VP(PCDA)}_1$ ) above the melting temperature of PCDA leads to the improved order in block copolymer morphology. When this sample was irradiated with UV light, the order of the block copolymer is retained as such and this sample was labeled as thermally annealed  $\text{PS-}b\text{-P4VP(PDA)}_1$ . Figure 2.14 shows the temperature-dependent Lorentz-corrected SAXS and WAXS patterns of thermally annealed  $\text{PS-}b\text{-P4VP(PDA)}_1$  sample upon heating (up to 190 °C) and cooling to room temperature at a rate of 10°C/min. The room temperature SAXS pattern shows peaks corresponding to the improved block copolymer morphology at lower  $q$  and another peak at  $q = 1.38 \text{ nm}^{-1}$  (4.5 nm) corresponding to the hierarchically ordered PDA. It has to be noted that in agreement with the spectroscopy results, no peak corresponding to the red phase is observed in this sample at room temperature. The corresponding room temperature WAXS pattern in Figure 2.14b shows a similar pattern to

---

---

that of the solvent vapor annealed sample albeit slight differences in the peak positions. Upon heating, above 70 °C, the peak at  $q = 1.38 \text{ nm}^{-1}$  (4.5 nm) disappeared and at the same time the low  $q$  scattering peaks corresponding to the block copolymer assemblies becomes more pronounced. Above this temperature, a weak SAXS peak at  $q = 1.07 \text{ nm}^{-1}$  (5.8 nm) corresponding to the red phase of PDA appeared. The corresponding WAXS patterns above 70 °C revealed that the crystalline reflections corresponding to the PCDA monomers melted at this temperature and less intense peaks corresponding to the red phase PDA were observed at  $2\theta = 20.7$  and  $22.4^\circ$ . This observation suggests that the SAXS peak at  $q = 1.38 \text{ nm}^{-1}$  (4.5 nm) is corresponding to both unreacted PCDA monomers and polymerized PDA (blue phase). These results are in good agreement with the UV and PL spectroscopy data. These results suggest that in thermally annealed samples the packing of the PCDA monomers is inappropriate for topochemical polymerization. On further heating, above 190 °C, the red phase of PDA melts (see the WAXS patterns in Figure 2.14b) and simultaneously as seen in Figure 2.14a, the SAXS peaks at low  $q$  disappeared indicating the collapse of microphase separated morphology to a disordered state. On cooling, the block copolymer morphology is not recovered. However, the SAXS peak at  $q = 1.07 \text{ nm}^{-1}$  (5.8 nm) corresponding to the red phase reappeared. On further cooling to room temperature, both SAXS and WAXS patterns confirmed the recrystallization of unreacted PCDA monomers. In this way, thermally annealed samples behave differently compared to that of the solvent annealed samples.

Based on the insights garnered from FTIR, UV/Vis, Raman, PL spectroscopy and SAXS/WAXS, we can summarize how the molecular packing of PCDA is critically important to the overall assembly of block copolymer supramolecules and the subsequent topochemical polymerization of hydrogen-bonded PCDA within the block copolymer microdomains as schematically depicted in Figure 2.15. Upon the addition of PCDA to the

---

---

---

---

PS-*b*-P4VP, PCDA selectively forms the hydrogen-bonding with the 4VP chains, and as a result, the lamellar morphology was formed. The hydrogen-bonded PCDA molecules form the hierarchical structures within the P4VP domains. Such obtained supramolecules are annealed further by both solvent vapor annealing process and thermal annealing process to tune the microphase segregation of block polymer supramolecules and the molecular packing of the hierarchically ordered PCDA monomers. SAXS results revealed that the solvent vapor annealed sample shows the poor microphase segregation of block copolymer supramolecules. But these samples afford the formation of longer  $\pi$ -conjugated PDA upon the topochemical polymerization. On the other hand, the SAXS pattern of the thermally annealed sample shows the well-ordered microphase segregation of block copolymer supramolecules. However, the topochemical polymerization did not proceed effectively compared to the solvent vapor annealed samples and leads to the formation of PDAs with shorter  $\pi$ -conjugated backbones. As shown in Figure 2.15, the molecular packing of PCDA monomers is sensitive to the annealing process, and it is appropriate for the topochemical polymerization in solvent vapor annealed samples. On heating to 190°C, the blue phase of the block copolymer supramolecules transformed to red phase at temperature around 70 °C due to heat-induced thermochromic transition. The red phase consists of a non-polar backbone configuration in concurrence with the distorted alkyl side chains.

---

---

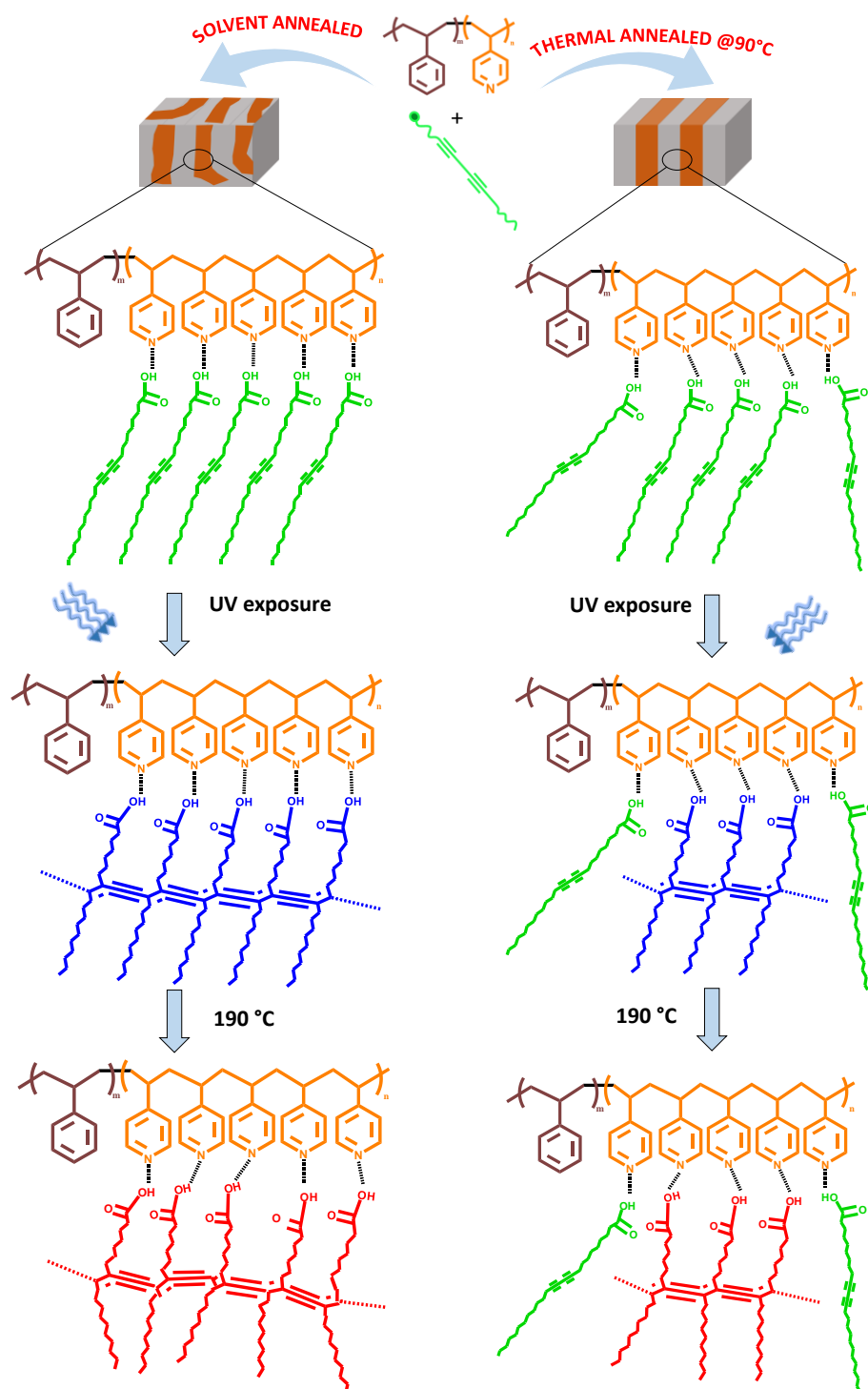


**Figure 2.15.** Schematic illustration of the hierarchical self-assembly of the PCDA monomers within the block copolymer microdomains in solvent vapor annealed and thermally annealed samples followed by topochemical polymerization and thermochromic transition. Note that this is a simplified representation provided for the better understanding.

## 2.6. Conclusions

In conclusion, we have successfully demonstrated the hierarchical self-assembly of photopolymerizable PCDA monomers within the block copolymer microdomains in the solid state through non-covalent interactions. Two different annealing approaches were used to tune the hierarchical ordering and the molecular orientation of PCDA molecules within the block copolymer microdomains. UV-vis, Raman, PL spectroscopy and temperature-dependent WAXS and SAXS allowed us to understand the topochemical polymerization during UV irradiation and heating. PCDA monomers were found to self-assemble effectively in solvent vapor annealed samples and afford the formation of longer  $\pi$ -conjugated PDA upon the topochemical polymerization compared to that of the thermally annealed samples. Though the microphase segregated block copolymer morphology was improved significantly upon thermal annealing, the molecular alignment of the PCDA became inappropriate for the effective topochemical polymerization. This work provides some new insights into the polymerization of hierarchically ordered photopolymerizable monomers and offers new materials for devices and sensors, which are worth investigating further.

## 2.7. References

- [1] Zimmerman, H. E.; Nesterov, E. E. *J. Am. Chem. Soc.* **2002**, 124 (11), 2818-2830.
- [2] MacGillivray, L. R.; Papaefstathiou, G. S.; Frišćić, T.; Hamilton, T. D.; Bučar, D.-K.; Chu, Q.; Varshney, D. B.; Georgiev, I. G. *Acc. Chem. Res.* **2008**, 41 (2), 280-291.
- [3] Ramamurthy, V.; Venkatesan, K. *Chem. Rev.* **1987**, 87 (2), 433-481.
- [4] Schmidt, G. M. J., Photodimerization in the solid state. In *Pure and Applied Chemistry*, 1971; Vol. 27, p 647.
- [5] Baughman, R. H. *J. Polym. Sci., Polym. Phys. Ed.* **1974**, 12 (8), 1511-1535.
- [6] Lauher, J. W.; Fowler, F. W.; Goroff, N. S. *Acc. Chem. Res.* **2008**, 41 (9), 1215-1229.
- [7] Matsumoto, A.; Odani, T.; Sada, K.; Miyata, M.; Tashiro, K. *Nature* **2000**, 405, 328.
- [8] Farina, M.; Audisio, G.; Gramegna, M. T. *Macromolecules* **1971**, 4 (2), 265-266.

- 
- 
- [9] Wegner, G. *Makromol. Chem.* **1972**, 154 (1), 35-48.
- [10] Zhu, L.; Trinh, M. T.; Yin, L.; Zhang, Z. *Chem. Sci* **2016**, 7 (3), 2058-2065.
- [11] Jia, X.; Zhu, M.; Bian, Q.; Yue, B.; Zhuang, Y.; Wu, B.; Yu, L.; Ding, J.; Zhang, J.; Zhu, L. *Macromolecules* **2018**, 51 (20), 8038-8045.
- [12] Kim, T.; Chan, K. C.; Crooks, R. M. *J. Am. Chem. Soc.* **1997**, 119 (1), 189-193.
- [13] Baughman, R. H.; Chance, R. R. *J. Polym. Sci., Polym. Phys. Ed.* **1976**, 14 (11), 2037-2045.
- [14] Yarimaga, O.; Jaworski, J.; Yoon, B.; Kim, J.-M. *Chem. Commun.* **2012**, 48 (19), 2469-2485.
- [15] Song, J.; Cisar, J. S.; Bertozzi, C. R. *J. Am. Chem. Soc.* **2004**, 126 (27), 8459-8465.
- [16] Nishide, J.; Oyamada, T.; Akiyama, S.; Sasabe, H.; Adachi, C. *Adv. Mater* **2006**, 18 (23), 3120-3124.
- [17] Jonas, U.; Shah, K.; Norvez, S.; Charych, D. H. *J. Am. Chem. Soc.* **1999**, 121 (19), 4580-4588.
- [18] McQuade, D. T.; Pullen, A. E.; Swager, T. M. *Chem. Rev.* **2000**, 100 (7), 2537-2574.
- [19] Lu, Y.; Yang, Y.; Sellinger, A.; Lu, M.; Huang, J.; Fan, H.; Haddad, R.; Lopez, G.; Burns, A. R.; Sasaki, D. Y.; Shelnutt, J.; Brinker, C. J. *Nature* **2001**, 410, 913.
- [20] Gu, Y.; Cao, W.; Zhu, L.; Chen, D.; Jiang, M. *Macromolecules* **2008**, 41 (7), 2299-2303.
- [21] Qian, X.; Städler, B. *Chem. Mater.* **2019**, 31 (4), 1196-1222.
- [22] Charych, D.; Nagy, J.; Spevak, W.; Bednarski, M. *Science (New York, N.Y.)* **1993**, 261 (5121), 585-588.
- [23] Tieke, B.; Lieser, G.; Wegner, G. *J. Polym. Sci. Pol. Chem* **1979**, 17 (6), 1631-1644.
- [24] Inokuma, Y.; Kawano, M.; Fujita, M. *Nat. Chem.* **2011**, 3, 349.
- [25] Okada, S.; Peng, S.; Spevak, W.; Charych, D. *Acc. Chem. Res.* **1998**, 31 (5), 229-239.
- [26] Kolusheva, S.; Shahal, T.; Jelinek, R. *J. Am. Chem. Soc.* **2000**, 122 (5), 776-780.
- [27] Chae, S. K.; Park, H.; Yoon, J.; Lee, C. H.; Ahn, D. J.; Kim, J.-M. *Adv. Mater* **2007**, 19 (4), 521-524.
- [28] Yoon, J.; Chae, S. K.; Kim, J.-M. *J. Am. Chem. Soc.* **2007**, 129 (11), 3038-3039.
- [29] Chance, R. R. *Macromolecules* **1980**, 13 (2), 396-398.
- [30] Schott, M. *J. Phys. Chem. B* **2006**, 110 (32), 15864-15868.
- [31] Yoon, B.; Lee, S.; Kim, J.-M. *Chem. Soc. Rev.* **2009**, 38 (7), 1958-1968.
- [32] Yu, L.; Hsu, S. L. *Macromolecules* **2012**, 45 (1), 420-429.
- 
-

- 
- 
- [33] Itoh, K.; Nishizawa, T.; Yamagata, J.; Fujii, M.; Osaka, N.; Kudryashov, I. *J. Phys. Chem. B* **2005**, 109 (1), 264-270.
- [34] Li, L.; Rosenthal, M.; Zhang, H.; Hernandez, J. J.; Drechsler, M.; Phan, K. H.; Rütten, S.; Zhu, X.; Ivanov, D. A.; Möller, M. *Angew. Chem. Int. Ed.* **2012**, 51 (46), 11616-11619.
- [35] Zhu, L.; Tran, H.; Beyer, F. L.; Walck, S. D.; Li, X.; Ågren, H.; Killops, K. L.; Campos, L. M. *J. Am. Chem. Soc.* **2014**, 136 (38), 13381-13387.
- [36] Wu, S.; Shi, F.; Zhang, Q.; Bubeck, C. *Macromolecules* **2009**, 42 (12), 4110-4117.
- [37] Wu, J.; Lu, X.; Shan, F.; Guan, J.; Lu, Q. *RSC Adv.* **2013**, 3 (45), 22841-22844.
- [38] Ikkala, O.; ten Brinke, G. *Science* **2002**, 295 (5564), 2407-2409.
- [39] Lee, K. H.; Bai, P.; Rancatore, B. J.; He, B.; Liu, Y.; Xu, T. *Macromolecules* **2016**, 49 (7), 2639-2645.
- [40] Rancatore, B. J.; Kim, B.; Mauldin, C. E.; Fréchet, J. M. J.; Xu, T. *Macromolecules* **2016**, 49 (3), 833-843.
- [41] Sidorenko, A.; Tokarev, I.; Minko, S.; Stamm, M. *J. Am. Chem. Soc.* **2003**, 125 (40), 12211-12216.
- [42] Kuila, B. K.; Gowd, E. B.; Stamm, M. *Macromolecules* **2010**, 43 (18), 7713-7721.
- [43] Nandan, B.; Gowd, E. B.; Bigall, N. C.; Eychmüller, A.; Formanek, P.; Simon, P.; Stamm, M. *Adv. Funct. Mater.* **2009**, 19 (17), 2805-2811.
- [44] Rancatore, B. J.; Bai, P.; Xu, T. *Macromolecules* **2016**, 49 (11), 4155-4163.
- [45] Ruokolainen, J.; Saariaho, M.; Ikkala, O.; ten Brinke, G.; Thomas, E. L.; Torkkeli, M.; Serimaa, R. *Macromolecules* **1999**, 32 (4), 1152-1158.
- [46] Sinturel, C.; Vayer, M.; Morris, M.; Hillmyer, M. A. *Macromolecules* **2013**, 46 (14), 5399-5415.
- [47] Kuila, B. K.; Chakraborty, C.; Malik, S. *Macromolecules* **2013**, 46 (2), 484-492.
- [48] Bai, P.; Kim, M. I.; Xu, T. *Macromolecules* **2013**, 46 (14), 5531-5537.
- [49] Angkaew, S.; Wang, H.-Y.; Lando, J. B. *Chem. Mater.* **1994**, 6 (8), 1444-1451.
- [50] Fujimori, A.; Ishitsuka, M.; Nakahara, H.; Ito, E.; Hara, M.; Kanai, K.; Ouchi, Y.; Seki, K. *J. Phys. Chem. B* **2004**, 108 (35), 13153-13162.
- [51] Guarini, K. W.; Black, C. T.; Yeung, S. H. I. *Adv. Mater.* **2002**, 14 (18), 1290-1294.
- [52] Rancatore, B. J.; Mauldin, C. E.; Fréchet, J. M. J.; Xu, T. *Macromolecules* **2012**, 45 (20), 8292-8299.
- 
-

- 
- 
- [53] Valkama, S.; Ruotsalainen, T.; Nykänen, A.; Laiho, A.; Kosonen, H.; ten Brinke, G.; Ikkala, O.; Ruokolainen, J. *Macromolecules* **2006**, 39 (26), 9327-9336.
- [54] Tran, H.; Gopinadhan, M.; Majewski, P. W.; Shade, R.; Steffes, V.; Osuji, C. O.; Campos, L. M. *ACS Nano* **2013**, 7 (6), 5514-5521.
- [55] Nandan, B.; Vyas, M. K.; Böhme, M.; Stamm, M. *Macromolecules* **2010**, 43 (5), 2463-2473.
- [56] Kuhn, H. J. *chem. Physics* 17, 1198 (1949). *Fortschr. Chem. org. Naturstoffe [Wien]* **1959**, 17, 404.
- [57] Wenzel, M.; Atkinson, G. H. *J. Am. Chem. Soc.* **1989**, 111 (16), 6123-6127.
- [58] Giorgetti, E.; Muniz-Miranda, M.; Margheri, G.; Giusti, A.; Sottini, S.; Alloisio, M.; Cuniberti, C.; Dellepiane, G. *Langmuir* **2006**, 22 (3), 1129-1134 DOI: 10.1021/la0514157.
- [59] Patlolla, A.; Zunino, J.; Frenkel, A. I.; Iqbal, Z. Thermochromism in polydiacetylene-metal oxide nanocomposites. *J. Mater. Chem.* **2012**, 22 (14), 7028-7035.
- [60] Pang, J.; Yang, L.; McCaughey, B. F.; Peng, H.; Ashbaugh, H. S.; Brinker, C. J.; Lu, Y. *J. Phys. Chem. B* **2006**, 110 (14), 7221-7225.
- [61] Lee, J.; Pyo, M.; Lee, S.-h.; Kim, J.; Ra, M.; Kim, W.-Y.; Park, B. J.; Lee, C. W.; Kim, J.-M. *Nat. Commun.* **2014**, 5, 3736.
- 
-



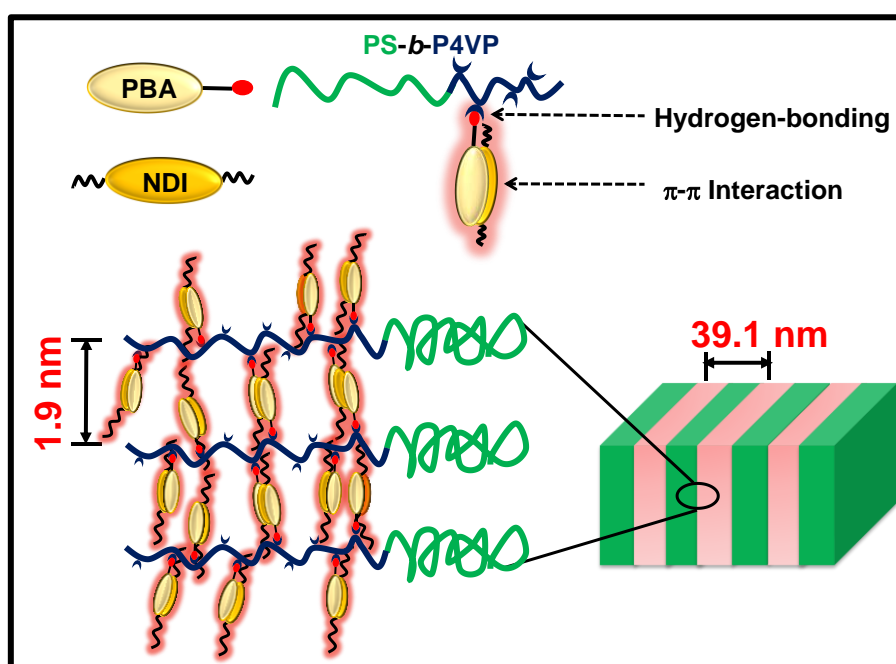
---

---

# Directed Assembly of Hierarchical Supramolecular Block Copolymers: A Strategy to Create Donor- Acceptor Charge Transfer Stacks

---

---



### 3.1. Abstract

*The hierarchical self-assembly of the charge-transfer (CT) complexes in the solid state is of paramount importance to dictate the performance of electronic devices. In this work, we describe a three-component hierarchical self-assembly approach to generate stable alternate donor-acceptor (D-A) assemblies within block copolymer microdomains by involving the supramolecular approach in self-assembly of block copolymers. So far, the assembly between a single small molecule and block copolymer were explored to obtain block copolymer supramolecules. Here we report block copolymer supramolecules*

*composed of two small molecules (donor and acceptor) and polystyrene-block-poly(4-vinylpyridine) (PS-*b*-P4VP). 1-Pyrenebutyric acid (PBA, donor) forms hydrogen bonding with P4VP and aromatic interactions with naphthalene diimide (NDI, acceptor) to generate charge-transfer (CT) complexes within the block copolymer domains in the solid state. Using FTIR, SAXS, WAXS, TEM, UV/Vis spectroscopy and photoluminescence spectroscopy measurements, we demonstrate the formation of hierarchical structures and charge-transfer complexes between PBA and NDI. Space charge limited current analysis showed the enhanced charge carrier mobility in PS-*b*-P4VP (PBA+NDI) supramolecules compared to the physical blends of PBA+NDI. The organization of donor and acceptor molecules within the block copolymer microdomains open up new insight in the area of electronic devices because of its advantages such as solution processability, controlled formation of hierarchical assemblies and the CT interaction in the solid state.*

### **3.2. Introduction**

The assembly of molecules via stacking of electron-rich (donors) and electron-deficient (acceptors) aromatic units at the nano- and mesoscale has been proven to be a key in most of the practical applications such as solar cells, organic light-emitting diodes (OLEDs), field-effect transistors (FETs) and thermochromic materials.<sup>1-5</sup> These assemblies of molecules often result in the modification of the electronic structure of the system and the formation of charge transfer (CT) complexes.<sup>6-8</sup> Over the past several years, CT complexation between the aromatic molecules has been studied extensively, and a few articles reviewed the progress made on the complexation of donor-acceptor interactions for a diverse range of materials such as organogels, foldamers, supramolecular polymers, liquid crystalline materials, and so on.<sup>4, 9-18</sup> The attention of these donor-acceptor interactions shifted to solid state as these interactions are promising for further self-assembly of the molecules to give crystalline or supramolecular structures geared towards

---

---

---

material applications.<sup>19, 20</sup> However, for the applications of these materials as active components of electronic devices, solution processability and the long-range order of the CT complexes are mandatory.

The solution process of small molecules into uniform thin films remains a major challenge due to their tendency to crystallize and dewetting of thin films. Moreover, the control over the orientation and packing of the donor/acceptor molecules in the tens of nanometer range is one of the major hurdles to increase the donor/acceptor interfaces. Many approaches have been explored to overcome these limitations. Among these, incorporation of donors and acceptors into the polymer chains shows several interesting properties such as high charge carrier mobilities, good solubility, processability and strong and broad absorption of light in the visible region.<sup>19, 21-23</sup> Moreover, these systems demonstrate improved mechanical properties, which is an advantage especially for applications that rely on flexible substrates.<sup>21</sup> However, the control over the morphology is one of the major challenges due to the phase separation. To overcome this problem, the donor and acceptor molecules are linked in a polymer chain, either as an alternating copolymer or block copolymer.<sup>19, 22, 23</sup> These systems can produce thermodynamically stable microphase separated morphologies, which are highly suitable for the device applications.<sup>19</sup> However, the reports on fully conjugated block copolymers are still rare because of the challenges involved in the synthesis.

Noncovalent polymer side-chain modification has emerged as a powerful tool for the creation of nanostructured materials with hierarchical morphologies and desirable properties.<sup>24, 25</sup> Ikkala and ten Brinke demonstrated the formation of hierarchical structures through the complexation of a small molecule with the block copolymer by hydrogen bonding.<sup>26-29</sup> Later, several groups adopted this supramolecular assembly (SMA) approach to generate nanostructured composites for diverse applications.<sup>30-40</sup> Among these, the

---

---

---

---

works on organic semiconductor-containing supramolecules attracted the great interest of researchers as this approach creates a new avenue to tailor the electronic properties of composites in addition to the structural control.<sup>34-36, 38, 39</sup> However, the major focus in this field is so far on the addition of a single small molecule to polymers for the formation of SMA. In contrast, the multicomponent assembly is rarely achieved, despite its high promises for the creation of novel nanosized composite materials, possibly because of the commonly encountered problem of phase separation.

Herein, we report the first example of the three-component assembly of pyrene butyric acid (PBA) (donor), naphthalene diimide (NDI) (acceptor) molecules and block copolymer using block copolymer SMA approach. PBA is a relatively good electron donor and NDI is a well-studied  $\pi$ -conjugated electron acceptor, which can be used to construct CT complexes.<sup>41-44</sup> Within the past few years, various molecular design strategies have been used to enhance the assembly and electronic interactions between donor and acceptor molecules in the solution state and gel state using noncovalent interactions such as hydrogen bonding, metal-coordination and aromatic-aromatic interactions.<sup>12, 13, 42, 45-50</sup> But for the concern of practical applications in devices, A-D-A stacks in the solid state are more appealing. In this work, the PBA molecules are hydrogen-bonded with poly(4-vinyl pyridine) of polystyrene-*b*-poly(4-vinyl pyridine) (PS-*b*-P4VP) and resulted in the formation of cylindrical morphology in bulk. Further addition of NDI molecules to this assembly favoured the formation of CT complexes by aromatic-aromatic interactions without disturbing the hydrogen bonding between the PBA and P4VP. As a consequence, the cylindrical morphology of the block copolymer changed to lamellar morphology. Further, the assembly of PBA and NDI molecules within the block copolymer microdomains is confirmed by the small-angle and wide-angle X-ray scattering measurements. The alternate stacking of PBA-NDI molecules within the P4VP domain

---

---

which is visibly evidenced by the colour change is further confirmed by UV/Visible and photoluminescence spectroscopy. The charge carrier mobility of the confined CT complexes was studied using space charge limited current (SCLC) measurements. We envisaged that the SMA approach is an effective route to better control the CT complexes with useful electronic and optical properties.

### **3.3. Experimental Section**

**3.3.1. Materials:** PS-*b*-P4VP with number-averaged molecular masses ( $M_n$ ): PS 54000 g mol<sup>-1</sup>, P4VP 6500 g mol<sup>-1</sup>, and PDI ( $D$ ) = 1.06, was purchased from Polymer Source, Inc. Homopolymer P4VP with number-averaged molecular mass ( $M_n$ ): P4VP 60000 g mol<sup>-1</sup> was purchased from Sigma Aldrich. 1-Pyrene butyric acid (PBA), 2,7-dihexylbenzo[*lmn*][3,8]phenanthroline-1,3,6,8(2H,7H)-tetrone (NDI) and 1,4-dioxane were purchased from Sigma Aldrich. The solvent used was of analytical grade and carefully dried before use.

**3.3.2. Sample Preparation:** PS-*b*-P4VP and PBA (1 mol 4-vinylpyridine monomer unit: 0.5 mol PBA) were dissolved separately in 8 ml 1,4-dioxane. The block copolymer solution was added drop-by-drop to the PBA solution while maintaining the mixing temperature close to the boiling point of the solvent with continuous stirring. The resultant solution was kept 3 days for the complete hydrogen-bonding formation. After 3 days, the 0.0193 g of NDI in 2ml 1,4-dioxane solution (1 mol of PBA: 1 mol of NDI) prepared separately was added to the SMA solution and stirred it for 1 day for the formation of CT complexes. To prepare the bulk samples, the solutions were transferred into the petri dish, and the solvent was allowed to slowly evaporate for a week. Such samples were kept in a vacuum oven at 40 °C for 12 hrs to remove the residual solvent. The physical blends of PBA and NDI were prepared by solution blending. 1:1 weight ratio of small molecules was dissolved in 1,4-dioxane and the solution was poured into the petri dish, allowing the solvent to evaporate

at ambient conditions, and dried.

### 3.4. Characterization

Wide-angle and small-angle X-ray scattering measurements (WAXS/SAXS) were carried out on XEUSS SAXS/WAXS system using a Genixmicro source from Xenocs and a mar345dtb image plate detector (Mar-Research, Hamburg, Germany). As casted samples from polymer solution were directly used to obtain both WAXS and SAXS data in the transmission mode. The generator was operated at 0.6 mA and 50 kV. The X-ray beam was collimated with FOX2D mirror and two pairs of scatterless slits from Xenocs. The fiber diagrams were processed using the Fit2D software. Silver behenate was used as the standard sample for calibration of the scattering vectors of WAXS and SAXS. The sample-detector distance was set at 217.5 mm and 1049 mm in the direction of the beam for WAXS and SAXS data collections, respectively. Linkam THMS 600 hot stage connected to the LNP 95 cooling system was placed in the X-ray path to carry out the temperature-dependent measurements. The powder sample was heated from 30 to 240 °C at a rate of 10 °C/min. The X-ray patterns were obtained at the interval of 10 °C on holding the sample at that temperature for 10 min.

Proton nuclear magnetic resonance spectra ( $^1\text{H}$  NMR) were recorded using Bruker spectrophotometer operating at 500 MHz ( $\text{CDCl}_3$  as solvent). Chemical shifts for  $^1\text{H}$  NMR spectra are reported as  $\delta$  in units of parts per million (ppm) downfield from  $\text{SiMe}_4$  ( $\delta$  0.0) and relative to the signal of chloroform-d ( $\delta$  7.25, singlet). The concentration of the sample was taken as 4mg/ml. FTIR measurements were performed on a PerkinElmer series Spectrum Two FT-IR spectrometer. The FTIR spectra were recorded over the wavenumber range of 4000–400  $\text{cm}^{-1}$ . The spectra were obtained by averaging 32 scans at a resolution of 2  $\text{cm}^{-1}$ . The morphologies of prepared SMA were analyzed with TEM (JEOL 2010 transmission electron microscope operating at 300 kV). The TEM samples were prepared

---

---

by drop casting the SMA solution in 1,4-dioxane (2mg/ml) on to the copper grid. To enhance the contrast of the TEM image, iodine vapor was used to stain the samples which selectively interact with the P4VP and small molecules microdomain. UV-visible spectra were recorded with a Shimadzu UV-3600, UV-visible-NIR spectrophotometer. The PL spectra of the solid samples were performed in a Spex-Fluorolog FL22 spectrofluorimeter equipped with a double grating 0.22 m Spex 1680 monochromator and a 450W Xe lamp as the excitation source operating in the front face mode. The photoexcitation was made at an excitation wavelength of 340 nm.

The charge carrier mobility of the block copolymer supramolecules and the physical blend of PBA+NDI were studied using SCLC measurements. 150 nm thick ITO (Indium Tin Oxide) coated glass of size 2.5cm × 2.5cm with a sheet resistance of 15Ω/sq (purchased from Kintec, Taiwan) was used as the substrate where ITO is the bottom electrode of the sandwich structure. The ITO on the glass substrate was patterned using lithography with scotch tape acting as the etch mask. The patterned ITO/glass substrates were then cleaned using detergent and a soft brush to remove the contaminants on the ITO surface. Subsequently, all the substrates were cleaned by ultra-sonication in hot water, chloroform, acetone, IPA and DI water for 10 minutes each. Just before drop casting the solution, UV ozone treatment was done for all the substrates to remove residual volatile organic contaminants from the ITO/glass surface and to increase the surface adhesiveness. Both PS-*b*-P4VP (PBA+NDI) & (PBA+NDI) samples dissolved in 1,4-dioxane was then drop cast on the substrate and kept it in a vacuum chamber for a prolonged time to remove the residual solvents and to achieve a thin film of thickness around 1μm. To complete the sandwich structure, 100 nm aluminum top electrode was deposited through a shadow mask using Angstrom Engineering thermal evaporation system at room temperature at a deposition rate of approximately 1 Å/ s under a chamber base pressure of 2×10<sup>-4</sup> Pa. The

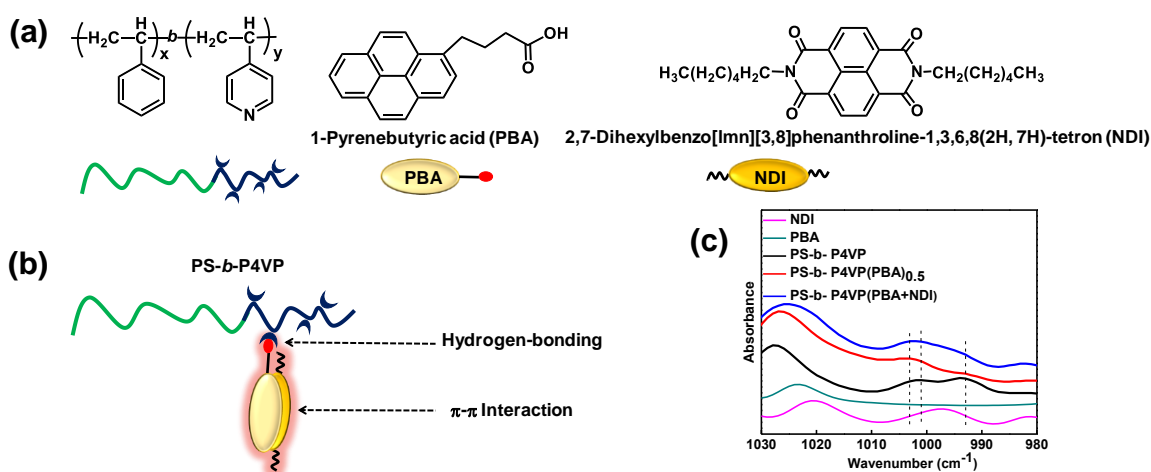
---

---

active area of the device was  $4\text{mm}^2$ . The dielectric constant was estimated from the capacitance of the device that was measured using a LCR meter (Hioki 3532-50LCR Hi Tester, Japan). The current-voltage measurements were performed by using a Keithley-2450 source measure unit in the range  $\pm 4\text{V}$ .

### 3.5. Results and Discussion

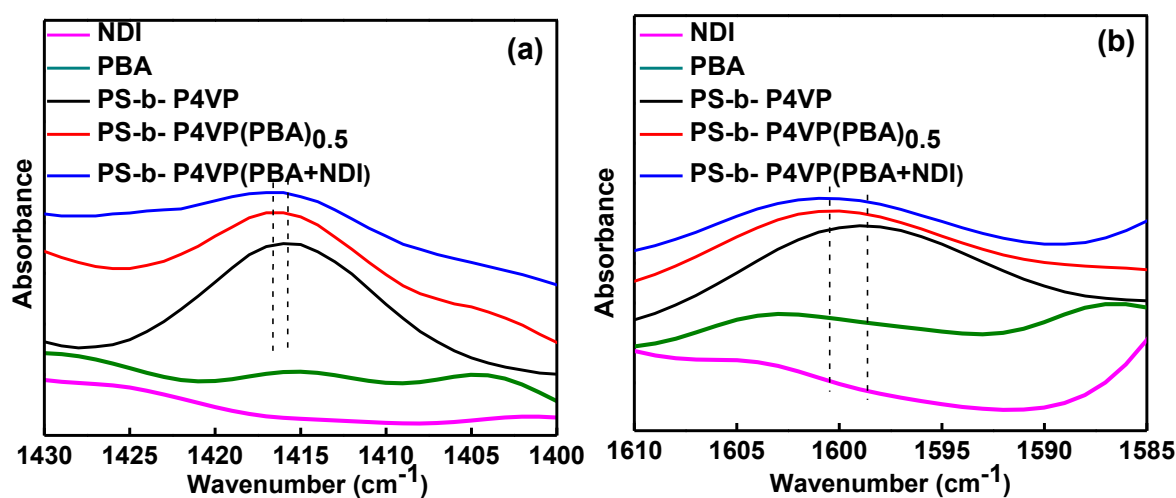
Figure 3.1a shows the molecular structure of the block copolymer (PS-*b*-P4VP), donor molecule (PBA) and acceptor molecule (NDI). The PS-*b*-P4VP was blended with PBA in 1,4-dioxane as the solvent medium. The stoichiometric ratio between the 4VP unit and PBA was fixed at 0.5 (PS-*b*-P4VP(PBA)<sub>0.5</sub>). To this, NDI solution was added with the fixed stoichiometric ratio of donor to acceptor molecule at 1 to form the supramolecular assembly (PS-*b*-P4VP(PBA+NDI)).



**Figure 3.1.** (a) Molecular structure of the block copolymer (PS-*b*-P4VP), donor molecule (PBA) and acceptor molecule (NDI) (b) schematic representation of SMA formation and D-A stacking within the P4VP domain of block copolymer (c) FTIR spectra of NDI, PBA, PS-*b*-P4VP, PS-*b*-P4VP(PBA)<sub>0.5</sub>, and PS-*b*-P4VP(PBA+NDI) in the region of 1030-980  $\text{cm}^{-1}$ .

As shown schematically in Figure 3.1b, PBA molecules selectively associate with the 4-vinylpyridine repeating unit of PS-*b*-P4VP via hydrogen bonding and the NDI

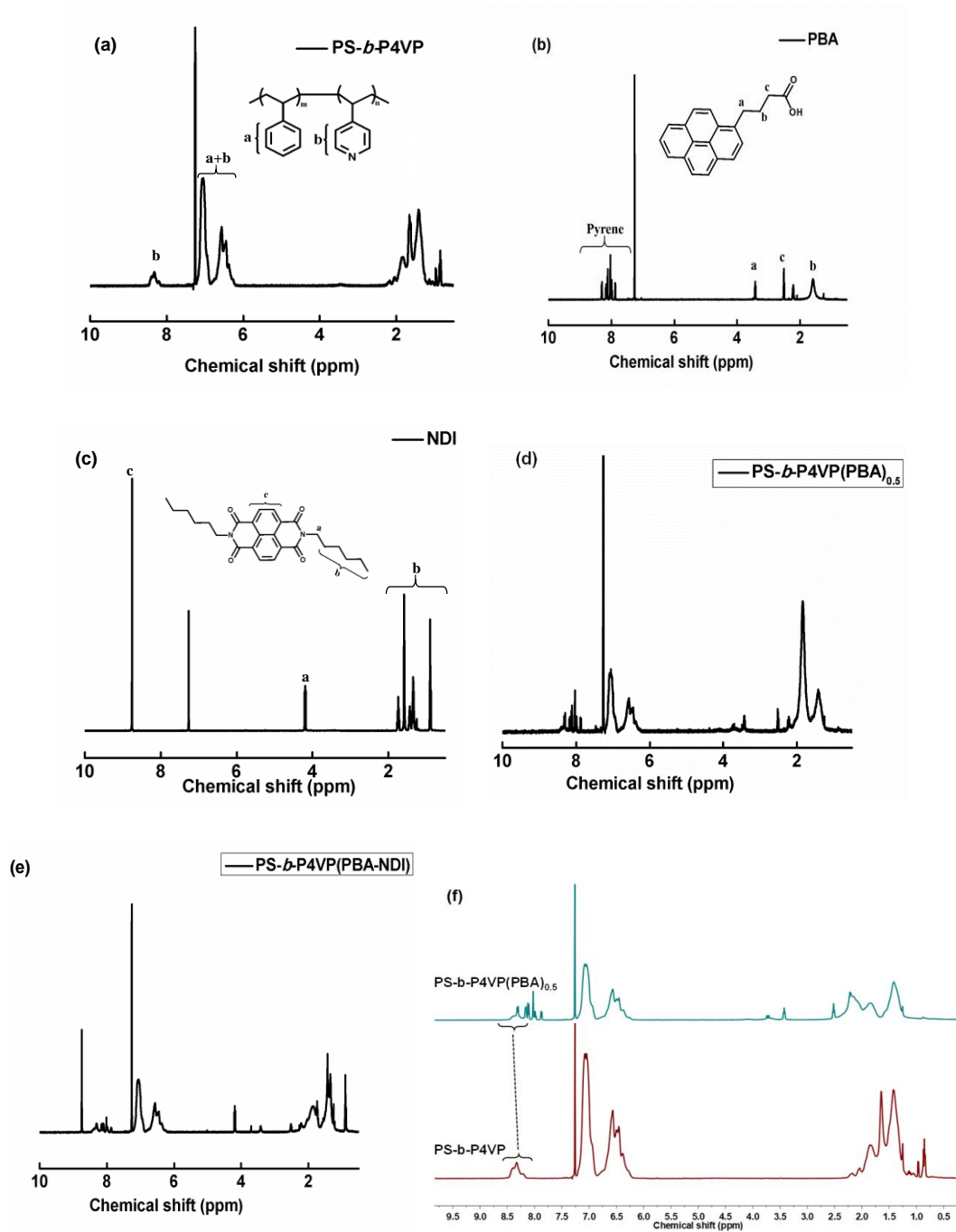
molecules associates with PBA through  $\pi$ - $\pi$  (donor-acceptor) interactions. Figure 3.1c and Figure 3.2 shows the FTIR spectra of PS-*b*-P4VP, PBA, NDI, PS-*b*-P4VP(PBA)<sub>0.5</sub> and PS-*b*-P4VP(PBA+NDI) in different regions. Free pyridine groups in the PS-*b*-P4VP block copolymer shows the absorption at 993 cm<sup>-1</sup> corresponding to the symmetric ring stretching mode (which is absent in the PBA spectrum).<sup>27, 29</sup> After the addition of PBA, the free pyridine ring absorption band at 993 cm<sup>-1</sup> becomes broad and the intensity of the peak decreases significantly.



**Figure 3.2.** FT-IR spectra of NDI, PBA, PS-*b*-P4VP, PS-*b*-P4VP(PBA)<sub>0.5</sub>, and PS-*b*-P4VP(PBA+NDI) in the different regions (a) 1430-1400 cm<sup>-1</sup> and (b) 1610-1585 cm<sup>-1</sup>.

At the same time, the hydrogen-bonded pyridine groups have absorption at 1004 cm<sup>-1</sup>.<sup>51</sup> Other regions (1430 to 1400 and 1610 to 1585 cm<sup>-1</sup>) also provide evidence for the formation of hydrogen bonding between 4VP units and PBA as shown in Figure 3.2 by shifting the characteristic peaks of P4VP at 1415 cm<sup>-1</sup> and 1597 cm<sup>-1</sup>.<sup>51</sup> It has to be noted that theoretically only 50% of 4VP units can be hydrogen bonded with PBA as the stoichiometric ratio between the 4VP unit and PBA was 0.5. On further addition of NDI, the FTIR spectrum remains the same as that of the PS-*b*-P4VP(PBA)<sub>0.5</sub>, indicating that the hydrogen bonding between pyridine units and PBA retain as such without any major change other than the slight change in the intensities of peaks due to the overlapping IR bands of

pure NDI.



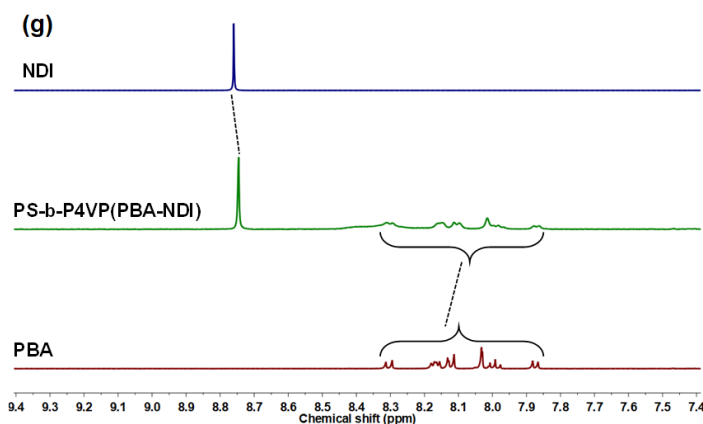
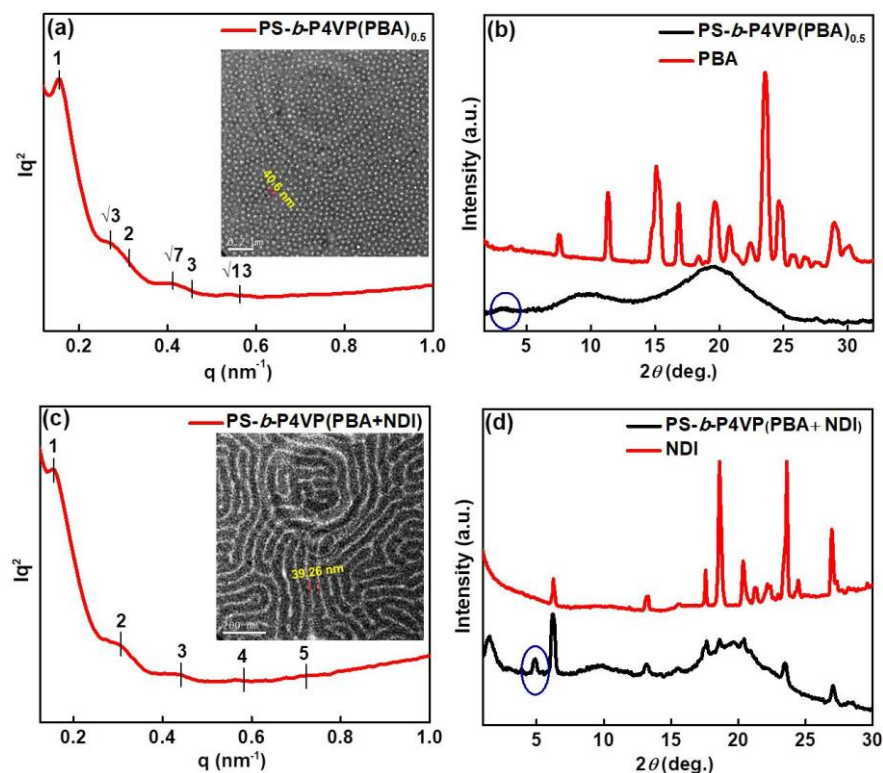


**Figure 3.3.**  $^1\text{H}$  NMR spectra of (a) PS-*b*-P4VP (b) PBA (c) NDI (d) PS-*b*-P4VP(PBA) $_{0.5}$  (e) PS-*b*-P4VP(PBA+NDI), (f) PS-*b*-P4VP and PS-*b*-P4VP(PBA) $_{0.5}$  showing the complex formation.

Figure 3.3 shows the  $^1\text{H}$  NMR spectra of (a) PS-*b*-P4VP (b) PBA (c) NDI (d) PS-*b*-P4VP(PBA) $_{0.5}$  (e) PS-*b*-P4VP(PBA+NDI), (f) comparison of  $^1\text{H}$  NMR spectra of PS-*b*-P4VP and PS-*b*-P4VP(PBA) $_{0.5}$ , and (g) comparison of  $^1\text{H}$  NMR spectra of NDI, PS-*b*-P4VP(PBA+NDI) and PBA. The  $^1\text{H}$  NMR spectra displaying the downfield shifts (8.21–8.27 ppm) of the two aromatic pyridine protons near to nitrogen occurs because of the hydrogen bonding between the carboxylic group of PBA and lone pair of electrons on the nitrogen atom of pyridine.<sup>38</sup>

The microphase separation of block copolymer supramolecular assembly and the molecular level dispersion, molecular ordering of PBA and NDI within the block copolymer microdomains were systematically investigated using both small-angle and wide-angle X-ray scattering (SAXS/WAXS) and transmission electron microscope (TEM). It has to be noted that the block copolymer PS-*b*-P4VP with number-average molecular masses ( $M_n$ ) PS 54000  $\text{g mol}^{-1}$ , P4VP 6500  $\text{g mol}^{-1}$ , and PDI ( $\bar{D}$ ) = 1.06 used here favours the spherical morphology in bulk according to the volume fraction of PS (89%) and P4VP (11%) with the domain spacing of 14.7 nm. Figure 3.4a and 3.4b show the Lorentz-corrected SAXS and WAXS patterns of PS-*b*-P4VP(PBA) $_{0.5}$ . The SAXS pattern of PS-*b*-

P4VP(PBA)<sub>0.5</sub> prominently features peaks at  $q = 0.155, 0.269, 0.310, 0.410, 0.470,$  and  $0.560 \text{ nm}^{-1}$  and the ratios of the higher order peak positions can be assigned to  $\sqrt{3}:2:\sqrt{7}:3:\sqrt{13}$  relative to the first order peak position, which is characteristic of hexagonally packed cylinders. The inset of Figure 3.4a shows the corresponding TEM image and it reflects the hexagonally ordered cylindrical morphology of PS-*b*-P4VP(PBA)<sub>0.5</sub> with an average center-to-center spacing of  $40.6 \pm 1 \text{ nm}$ , which is close to the domain spacing calculated from the first ordered SAXS reflection (40.5 nm). The WAXS pattern of pure PBA is compared with that of PS-*b*-P4VP(PBA)<sub>0.5</sub> in Figure 3.4b and it shows crystalline reflections corresponding to the monoclinic structure and the presence of the reflections at  $2\theta = 3.7^\circ$  (100),  $7.4^\circ$  (200) and  $11.2^\circ$  (300) indicating the multilayer-type structure of PBA.<sup>52</sup> However, these reflections are not observed in the SMA complex of PS-*b*-P4VP(PBA)<sub>0.5</sub>, indicating that no macrophase separation is observed between PS-*b*-P4VP and PBA. The WAXS pattern of PS-*b*-P4VP(PBA)<sub>0.5</sub> shows two broad amorphous halos at  $2\theta = 9.8^\circ$  and  $19.6^\circ$  and an additional peak at lower  $2\theta = 3.2^\circ$  ( $d = 2.7 \text{ nm}$ ). Kuila et al. reported the appearance of lower  $2\theta$  peak in PS-*b*-P4VP(PBA)<sub>1.0</sub> at slightly different position (where the stoichiometric ratio between 4VP and PBA is 1) and it was ascribed to the arrangement of PBA molecules within the block copolymer domains.<sup>33</sup> The estimated molecular length of the PBA molecule is  $1.3 \text{ nm}$ .<sup>53</sup> The spacing (2.7 nm) estimated from the WAXS peak is almost matching with double the length of PBA molecules (2.6 nm). It means the PBA molecules are arranged within the comb lamellae of the P4VP(PBA)<sub>0.5</sub> domain as two layers without interdigitation.



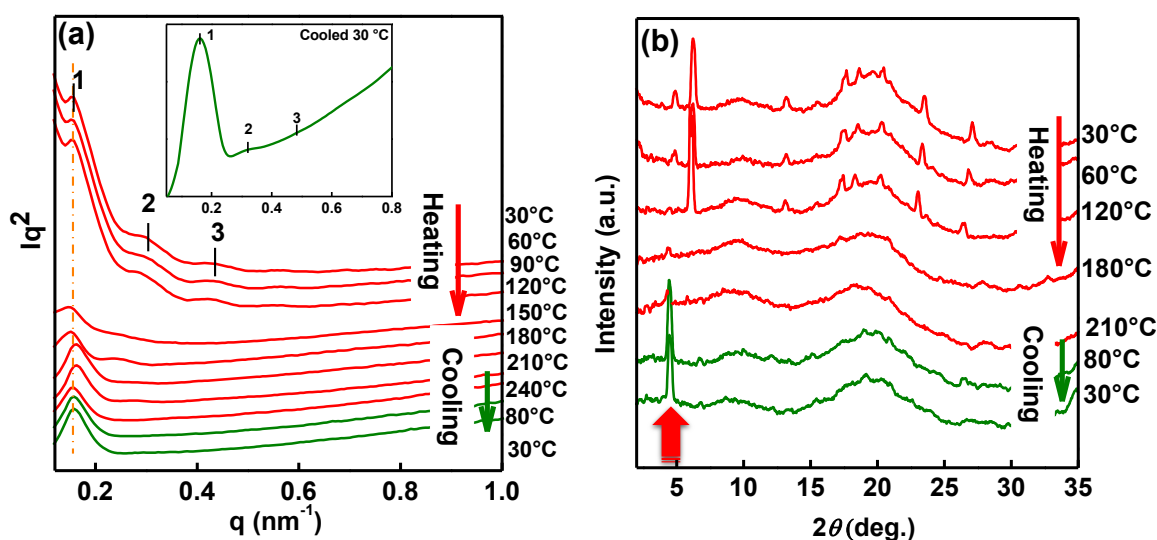
**Figure 3.4.** (a) Lorentz-corrected SAXS pattern of PS-*b*-P4VP(PBA)<sub>0.5</sub> (Inset, corresponding TEM image), (b) WAXS patterns of PBA and PS-*b*-P4VP(PBA)<sub>0.5</sub> (c) Lorentz-corrected SAXS pattern PS-*b*-P4VP(PBA+NDI) (Inset, corresponding TEM image), and (d) WAXS patterns of NDI and PS-*b*-P4VP(PBA+NDI).

Figure 3.4c and 3.4d show the Lorentz-corrected SAXS and WAXS patterns of PS-*b*-P4VP(PBA+NDI). With the addition of NDI to PS-*b*-P4VP(PBA)<sub>0.5</sub> complex, the positions of the SAXS peaks changed to  $q = 0.157, 0.313, 0.462, 0.620,$  and  $0.760 \text{ nm}^{-1}$  and the ratios of the higher order peak positions can be assigned to 2:3:4:5 relative to the first order peak position. The morphology changed from the hexagonally packed cylinders to lamellar morphology upon the addition of NDI to the PS-*b*-P4VP(PBA)<sub>0.5</sub> complex. The inset of Figure 3.4c shows the corresponding TEM image and in agreement with the SAXS, the lamellar morphology was observed with an average center-to-center spacing of  $39.3 \pm 1 \text{ nm}$ . This value is close to the domain spacing calculated from the first ordered SAXS reflection (40.3 nm). These results indicated that most of the NDI molecules are selectively

incorporated into the P4VP domains because of its interactions with PBA and the overall volume fraction of P4VP increases and as a result the block copolymer morphology changed from cylindrical to the lamellar. The WAXS pattern (Figure 3.4d) of PS-*b*-P4VP(PBA+NDI) shows several crystalline reflections over the amorphous halo of P4VP. To understand the origin of these crystalline reflections, the WAXS pattern of PS-*b*-P4VP(PBA+NDI) was compared with that of pure NDI in Figure 3.4d. It is obvious that the pure NDI is highly crystalline and some of the NDI crystalline reflections are still seen in the WAXS pattern of PS-*b*-P4VP(PBA+NDI) but the intensity is lower and the reflections are broadened somewhat. It is worth mentioning here that no peaks from PBA are observed even after the addition of NDI, indicating that the hydrogen bonding between PBA and 4VP remain intact as evidenced by the infrared spectra. However, a new reflection was observed at  $2\theta = 4.8^\circ$  ( $d = 1.84$  nm), which is different from the lower angle peak observed in the WAXS pattern of PS-*b*-P4VP(PBA)<sub>0.5</sub>. This peak is due to the assembly of hydrogen-bonded PBA and NDI via  $\pi$ - $\pi$  interaction within the block copolymer domains (hierarchical assemblies), and the details of this peak will be discussed below. The presence of NDI reflections indicates that some NDI molecules are self-sorted and agglomerated within the P4VP domains. A careful observation of TEM image (inset of Figure 3.4c) shows the agglomerated NDI molecules within the P4VP domains. Xu and co-workers observed the macrophase separation between the hydrogen-bonded block copolymer supramolecules during the solvent evaporation due to the rapid crystallization of small molecules.<sup>35,37</sup> They have successfully demonstrated that thermal annealing of these supramolecules enhanced the mobility of the small molecules to form the hierarchical structures.<sup>37</sup> Inspired from these works, variable temperature WAXS and SAXS measurements were carried out to understand the formation of hierarchical structures of PS-*b*-P4VP(PBA+NDI) during thermal treatment. Figure 3.5 shows the temperature-dependent SAXS and WAXS patterns

---

of PS-*b*-P4VP(PBA+NDI) sample upon heating (up to 240 °C) and cooling to room temperature at a rate of 10°C/min. The data collection time at each temperature is 10 min for both WAXS and SAXS. Upon heating the PS-*b*-P4VP(PBA+NDI) sample, no change in the SAXS pattern is observed below 120 °C (close to the  $T_g$  of P4VP block). When the temperature reached above 120 °C, significant changes in the intensities and the full width at half maximum (FWHM) of the SAXS peaks were observed, which might be due to the segmental mobility of both PS and P4VP blocks. However, the position of the first order peak, which is corresponding to the domain spacing of block copolymer remains more or less the same. On increasing the temperature to 180 °C (close to the melting temperature of PBA ~184-186 °C), the  $q$  value of the first order peak increased marginally ( $q = 0.163 \text{ nm}^{-1}$ ) and the peak became sharper.



**Figure 3.5.** Temperature-dependent (a) Lorentz-corrected SAXS and (b) WAXS patterns of PS-*b*-P4VP(PBA+NDI) (Inset of (a), zoomed SAXS pattern of the room temperature cooled sample).

On further increasing the temperature to 240 °C, which is above the melting temperature of NDI (~210 °C), the  $q$  value shifted back to its original position ( $q = 0.157 \text{ nm}^{-1}$ ) and remains the same upon cooling to room temperature. As seen in the inset of

Figure 3.5a, the lamellar morphology of the block copolymer is retained as such with the same domain spacing even though the assembly of small molecules improved significantly within the block copolymer domains in the room temperature cooled sample. The TEM image of the thermally annealed sample further confirms the formation of lamellar morphology as shown in Figure 3.6.

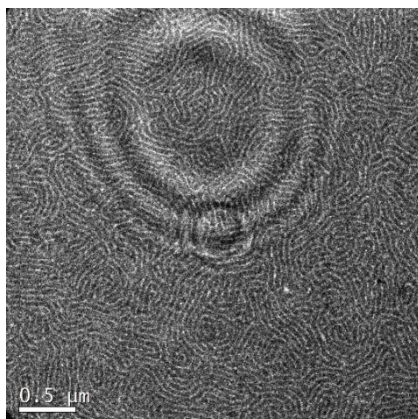


**Figure 3.6.** TEM image of thermally annealed PS-*b*-P4VP (PBA+NDI)

As discussed above, the room temperature WAXS pattern shows crystalline reflections over the amorphous halo of P4VP corresponding to the macrophase-separated NDI. Upon heating, these reflections disappeared completely at 180 °C, which is well below the melting temperature of NDI. It means the small molecules disperse in the molecular level within the block copolymer microdomains below its melting temperature. Upon cooling, no crystalline reflections are observed other than the strong peak at  $2\theta = 4.5^\circ$  ( $d = 1.96$  nm) corresponding to the hierarchical assemblies of small molecules. It has to be noted that either PBA or NDI was not crystallized upon cooling. Xu and co-workers reported that in block copolymer supramolecules, the crystallization of small molecules significantly changes the domain spacing of the block copolymer and the crystallization process of the small molecules is thermally reversible.<sup>37</sup> In our study, although the crystallization tendency of NDI is stronger, the presence of hydrogen-bonded PBA plays a crucial role in suppressing the crystallization of NDI because of the strong  $\pi$ - $\pi$  interaction

---

---

between PBA and NDI. As seen in Figure 4.6b, the peak at  $2\theta = 4.5^\circ$  ( $d = 1.96$  nm) is very much sensitive to the temperature and this peak is very useful to understand the coassembly process of PBA and NDI within the block copolymer microdomains. As discussed above, the WAXS pattern of PS-*b*-P4VP(PBA)<sub>0.5</sub> shows a peak at  $2\theta = 3.2^\circ$  ( $d = 2.7$  nm) corresponding to the assembly of hydrogen-bonded PBA molecules within the P4VP domains. Upon the addition of NDI, this peak is completely disappeared and a new peak at  $2\theta = 4.8^\circ$  ( $d = 1.84$  nm) appeared in the solution-casted PS-*b*-P4VP(PBA+NDI) sample. As NDI molecules do not have any preferential interactions with P4VP chains, it cannot form ordered structures within the P4VP domains. It means, the NDI molecules are selectively interacted with the PBA molecules through  $\pi$ - $\pi$  interaction (donor-acceptor interaction (D-A stack)) to form the charge transfer complexes (CT complexes) and disturbed the assembly of PBA within the P4VP domains. However, as evident from the room temperature WAXS pattern, some of the NDI molecules are agglomerated and these NDI molecules are not involved in the formation of D-A stacks. On heating, the peak at  $2\theta = 4.8^\circ$  ( $d = 1.84$  nm) completely disappeared in the temperature range of 120-150 °C, where the crystalline reflections of NDI remain unchanged. It has been shown that in block copolymer supramolecules the hydrogen bond weakens at the higher temperature and the bonds start to break above 110 °C.<sup>29, 37</sup> Here we speculate that the disappearance of the peak at  $2\theta = 4.8^\circ$  is due to the breakage of the assembly of D-A stacks within P4VP domains because of the combined effect of mobility of the PS and P4VP domains (above  $T_g$ ) as well as the breakage of the hydrogen-bonds between PBA and 4VP. On further heating, this peak again appeared with low intensity when the agglomerates of NDI are completely broken and it may be because of the increase in the population of loose PBA and NDI molecules. At this temperature, each NDI molecule interacts with PBA through  $\pi$ - $\pi$  interaction (donor-acceptor interaction) and upon cooling, this interaction did not allow

---

---

PBA or NDI to crystallize independently. When the cooling temperature reached below 120 °C (close to the  $T_g$  of P4VP), the intensity of peak increased substantially due to the formation of perfect hierarchical assemblies. The FTIR spectrum of the room temperature cooled sample (from melt) is similar to that of the spectrum of PS-*b*-P4VP(PBA+NDI) showed in Figure 3.1c, indicating the reformation of hydrogen bonds between PBA and 4VP. These results suggested that the thermal processing of the supramolecular complexes favours the co-assembly of D-A charge-transfer complexes quite significantly.

The formation of PBA and NDI charge-transfer complexes within the block copolymer microdomains was further understood by monitoring the visual colour change and UV/Vis spectroscopy. The addition of NDI solution to the PS-*b*-P4VP(PBA)<sub>0.5</sub> solution results in a visible colour change from pale yellow (SMA solution) to light red in the solution state (Figure 3.7a). For the comparison, the physical blend of PBA and NDI (without block copolymer) was prepared in a 1:1 ratio and it gives a light red colour in 1,4 dioxane similar to the PS-*b*-P4VP(PBA+NDI) solution (Figure 3.7b). When the solvent is evaporated, in the case of PS-*b*-P4VP(PBA+NDI), a dark purple-reddish colour was observed in the solid state (Figure 3.7c) and importantly, the colour was changed to pale yellow in the case of the physical blend of PBA and NDI (Figure 3.7d). It means, in the case of the physical blend, the red colour is stable only in the solution state, and up on solidification, the colour disappears, indicating the self-sorted state of PBA and NDI. It has been reported that the red colour appears due to the formation of charge-transfer complexes (alternating D-A stacks) between donor and acceptor chromophores, which can be characterized by the UV/Vis absorption band observed in the range of 400–700 nm.<sup>14, 46</sup> <sup>1</sup>H NMR spectra of NDI, PS-*b*-P4VP(PBA+NDI) and PBA shown in Figure 3.3(g) displaying the up-field shifts of aromatic protons because of CT complexation.<sup>54</sup>

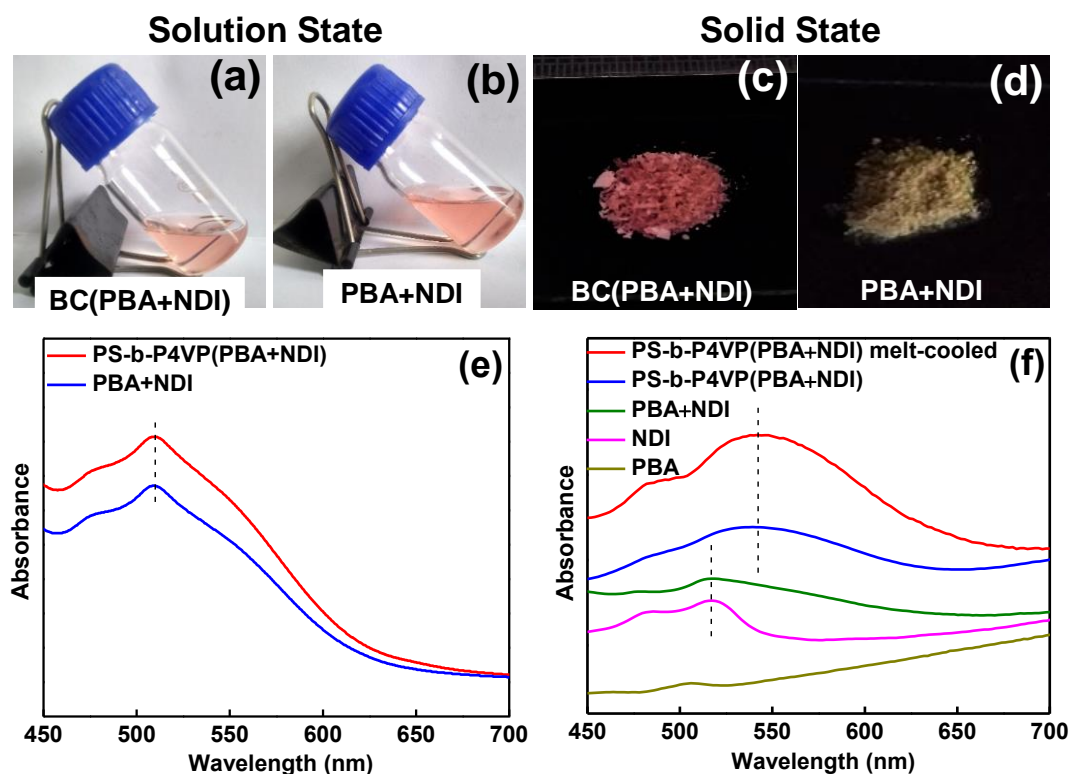


**Figure 3.7.** The visual appearance of (a) PS-*b*-P4VP(PBA+NDI), (b) physical blend (PBA+NDI) solutions in 1,4-dioxane, (c) PS-*b*-P4VP(PBA+NDI) powder, (d) physical blend (PBA+NDI) powder after the evaporation of solvent, (e) UV/Vis spectra of (a) and (b), and (f) UV/Vis spectra of PBA, NDI, physical blend (PBA+NDI), PS-*b*-P4VP(PBA+NDI), and melt-cooled PS-*b*-P4VP(PBA+NDI) in the solid state.

The UV/Vis absorption spectra of PS-*b*-P4VP(PBA+NDI) and PBA+NDI blend samples in the CT-band region were shown both in the solution state and solid state in Figures 3.7e and 3.7f, respectively. In solution state, both PS-*b*-P4VP(PBA+NDI) and PBA+NDI shows a similar spectrum with a broad absorption band at around 510 nm. The broad absorption band in this wavelength region is associated with the CT complexation process between the  $\pi$ -electron-rich PBA and  $\pi$ -electron-deficient NDI moiety. However, when the solvent is evaporated, different spectra were observed for block copolymer supramolecules and the physical blend of PBA+NDI. In the solid state, even though samples show significant scattering, the PS-*b*-P4VP(PBA+NDI) shows red-shifted

absorption band at around 540 nm, which unambiguously indicate the formation of the CT complexes (alternate DA stacks) between PBA and NDI within the block copolymer microdomains, in agreement with the visual red colour. Remarkably, the intensity of this red-shifted absorption band is more dominant in the melt-cooled sample, thus suggesting the formation of greater number of D-A stacks, which is already proved on the basis of variable temperature WAXS and SAXS. It is worth mentioning here that the C-T band in the solid-state exhibits a significant redshift compared to that of the solution and it may be possibly due to the delocalization of electron density along the D-A stacks.<sup>55</sup> On the other hand, the physical blend shows a different spectrum, which is similar to the spectrum of pure NDI in the solid state. The colour of the blend was changed from light red to pale yellow upon the solvent evaporation. These results clearly indicate that in the case of the physical blend, upon solvent evaporation the alternate DA stacks destabilizes and favours the formation of self-sorted aggregates of PBA and NDI. In the case of block copolymer supramolecules, the donor molecules (PBA) are hydrogen-bonded with the 4VP chains and the acceptor molecules (NDI) interact with PBA through charge transfer complexation. Such interactions prevent the self-sorting of PBA and NDI in multi-component self-assembly and as a result, the alternate DA stacks stabilizes within the block copolymer microdomains in the solid state and this assembly was stable even after 6 months.

Further evidence for CT complexation is confirmed by solid-state photoluminescence (PL) measurements, which shows significant quenching of the PBA emission in the block copolymer supramolecules (PS-*b*-P4VP(PBA+NDI)). The PL data was recorded after exciting all the samples at a wavelength of 340 nm. Figure 3.8 shows the visual images (under UV illumination) and PL spectra of PBA, NDI, PBA+NDI, PS-*b*-P4VP, PS-*b*-P4VP(PBA)<sub>0.5</sub>, and PS-*b*-P4VP(PBA+NDI). In the solid state, pure PBA shows yellowish-green fluorescence (Figure 3.8a) with emission maxima at 476 nm due to

the excimer formation from the aggregation of PBA molecules. In the case of the physical blend of PBA and NDI, the yellowish-green fluorescence (Figure 3.8b) is retained in the solid state indicating the self-sorting of PBA and NDI. It is obvious from Figure 4.8f that the PL spectrum of the physical blend of PBA and NDI looks like the overlap of PL spectra of PBA (Figure 3.8e) and NDI (Figure 3.8f). On the other hand, when the PBA was added to the PS-*b*-P4VP, the emission peaks were blue shifted and less broadened compared to that of pure PBA and these results are in good agreement with the literature.<sup>33</sup> As the stoichiometric ratio of PBA to 4VP chains is 0.5 and the P4VP is atactic, there is a possibility of having both closely packed PBA and isolated PBA within the P4VP domains. As a result, hydrogen-bonded PBA exhibits both monomer and excimer emission in PS-*b*-P4VP(PBA)<sub>0.5</sub>. Although PS-*b*-P4VP(PBA)<sub>0.5</sub> shows intense blue fluorescence (Figure 3.8c), the emission intensity is reduced drastically upon the addition of NDI indicating the significant quenching of the PBA emission in PS-*b*-P4VP(PBA+NDI). Up on the addition of NDI to PS-*b*-P4VP(PBA)<sub>0.5</sub>, the emission of PBA is reduced drastically indicating that NDI molecules are sandwiched in between PBA molecules to generate the alternate D-A stacks within the P4VP domains of the block copolymer supramolecules and the intense blue colour changed to white under UV light illumination (Figure 3.8d).

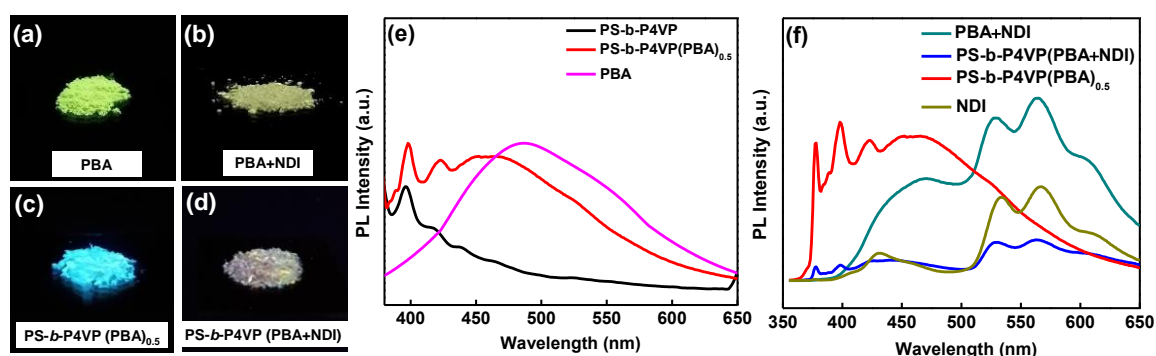


**Figure 3.8.** The visual appearance of (a) PBA, (b) physical blend (PBA+NDI), (c) PS-*b*-P4VP(PBA)<sub>0.5</sub>, (d) PS-*b*-P4VP(PBA+NDI) under UV light illumination, PL spectra of (e)

PBA, PS-*b*-P4VP, and PS-*b*-P4VP(PBA)<sub>0.5</sub> and (f) NDI, PS-*b*-P4VP(PBA)<sub>0.5</sub>, PS-*b*-P4VP(PBA+NDI) and physical blend (PBA+NDI) in the solid state.

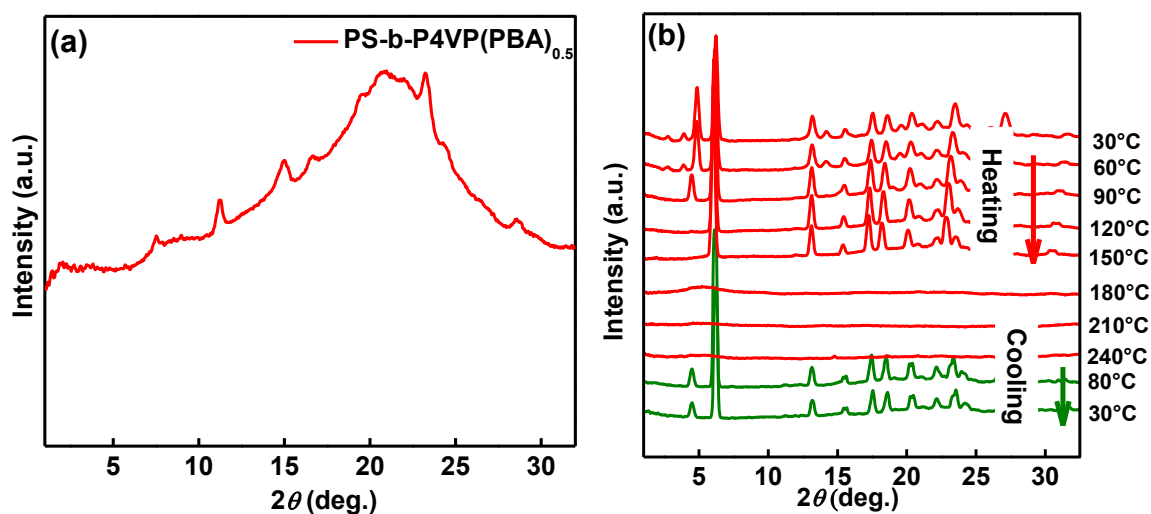


**Figure 3.9.** (a) WAXS pattern of P4VP(PBA)<sub>0.5</sub> and (b) Temperature-dependent WAXS patterns of P4VP(PBA+NDI).

We also investigated the role of homopolymer P4VP in stabilizing the charge transfer complexes using PBA and NDI through non-covalent interactions. The homopolymer P4VP with number-averaged molecular mass is ( $M_n$ ): P4VP 60000 g mol<sup>-1</sup> was used in this work. FTIR spectra confirmed the formation of hydrogen bonding between P4VP and PBA. Wide-angle X-ray diffraction results revealed that PBA added P4VP (P4VP(PBA)<sub>0.5</sub>) supramolecules resulted in the partial aggregation of PBA as shown in Figure 3.9a. In the case of the block copolymer, no such aggregation was observed PS-*b*-P4VP(PBA)<sub>0.5</sub>. With the addition of NDI to P4VP(PBA)<sub>0.5</sub> complex, at room temperature P4VP(PBA+NDI) shows several crystalline reflections over the amorphous halo of P4VP as shown in Figure 3.9b. Similar to block copolymer supramolecules, a new reflection was observed at  $2\theta = 4.8^\circ$  ( $d = 1.84$  nm) corresponding to the hierarchical assemblies of small molecules within P4VP. Up on heating to 240 °C and cooling, the peak corresponding to the hierarchical assemblies of small molecules was reappeared along with the crystalline reflections of NDI. These results indicated that though the C-T complexes are forming in

the case of homopolymer similar to the block copolymer supramolecules, however, the majority of the PBA and NDI molecules were agglomerated in homopolymer complexes compared to block copolymer supramolecules, which might be due to the high molecular weight of the homopolymer P4VP used.

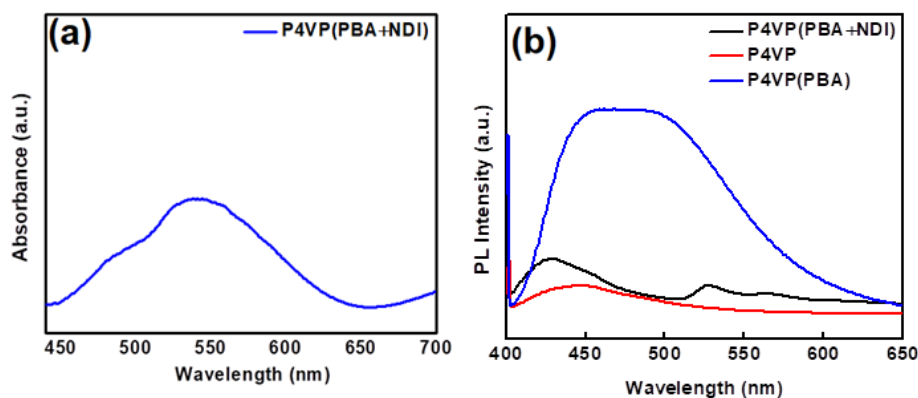


**Figure 3.10.** (a) UV/Vis spectra of P4VP(PBA+NDI) and (b) PL spectra of P4VP, P4VP(PBA)<sub>0.5</sub> and P4VP(PBA+NDI) in the solid state.

The formation of PBA and NDI charge-transfer complexes within the homopolymers were further understood by monitoring the UV/Vis spectroscopy and solid-state photoluminescence spectrum as shown in Figure 3.10. In the solid state, the P4VP(PBA+NDI) shows absorption band at around 540 nm, similar to the block copolymer supramolecules (PS-*b*-P4VP(PBA+NDI)) indicating the formation of the CT complexes (alternate DA stacks) between PBA and NDI within the homopolymer chains. At the same time, the PL spectrum of P4VP(PBA+NDI) shows significant quenching of the PBA emission in the homopolymer supramolecules.

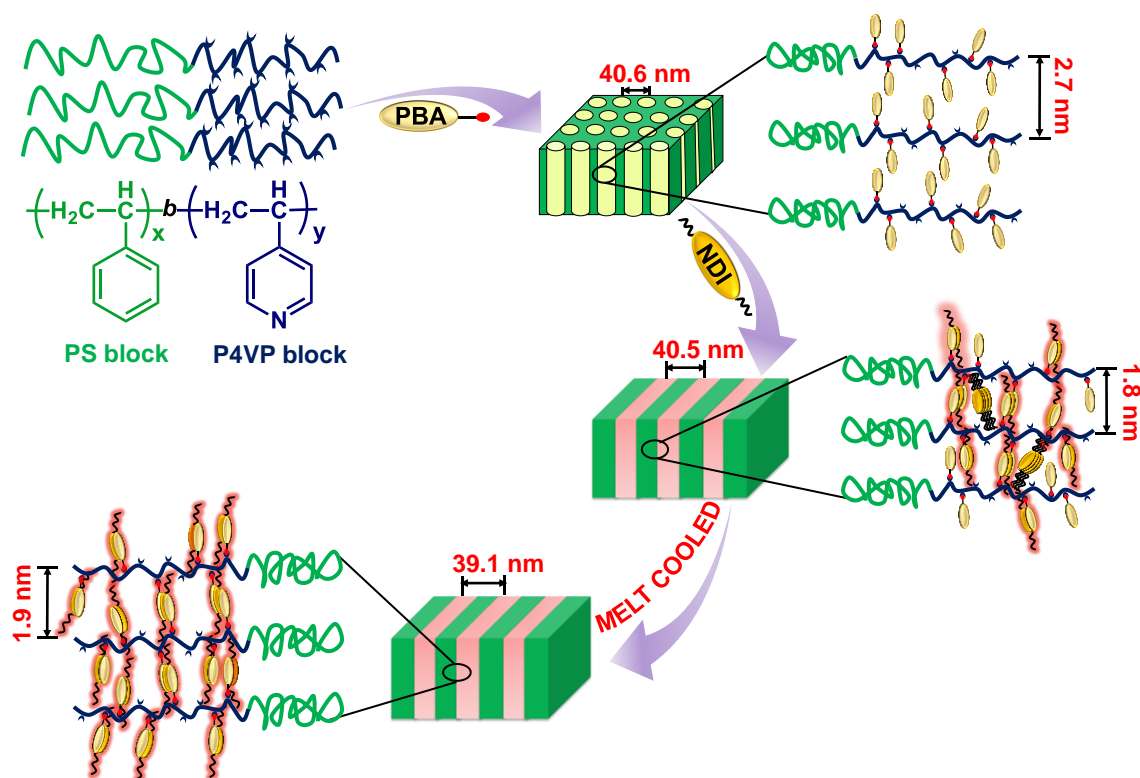


**Figure 3.11.** Schematic illustration of the hierarchical self-assembly of the donor and acceptor molecules within the block copolymer microdomains.

On the basis of the closer examination of the insights garnered from FTIR, SAXS/WAXS, UV/Vis spectroscopy, and photoluminescence spectroscopy, it is now possible to summarize the formation of hierarchical structures upon the addition of PBA and NDI to the block copolymer as schematically described in Figure 3.11. Upon the addition of PBA to the block copolymer, PBA selectively associates with 4VP chains via hydrogen bonding and hexagonally packed cylindrical morphology was formed with an average center-to-center spacing of  $40.6 \pm 1$  nm. The hydrogen-bonded PBA molecules form the hierarchical structures within the P4VP domains with the spacing of 2.7 nm. This spacing is closer to the double the length of PBA structure indicating the arrangement of PBA as layers within P4VP domain without interdigitation.<sup>53</sup> When the NDI molecules are added, the hexagonal cylindrical morphology of the block copolymer supramolecules changed to the lamellar morphology by retaining the average center-to-center spacing of

40.5 ± 1 nm. At the same time, the spacing of the small molecules arrangement reduced drastically to 1.8 nm and this value is well correlated with the length of energy minimized NDI structure.<sup>56</sup> It means charge-transfer interactions between PBA and NDI facilitates the closer packing of small molecules alternately within the P4VP domains by retaining the hydrogen-bonding between PBA and 4VP chains. The SAXS, WAXS and UV/Vis results revealed that thermally processed sample shows better D-A stacking driven by charge-transfer interactions and avoid the crystallization of small molecules in the multi-component assembly.

To further understand the charge carrier mobilities of these materials, space charge limited current (SCLC) measurements were performed using both block copolymer supramolecules and the physical blend of PBA+NDI.<sup>38, 57</sup> The film thicknesses of PS-*b*-P4VP(PBA+NDI) and the physical blend of PBA+NDI measured using the Dektak XT stylus profilometer were 2900 nm and 200 nm, respectively. Figure 7a shows the current *versus* voltage graph on log scale observed in the sandwich structure of ITO/(PBA+NDI)/Al, in which the region having a slope 2 is the SCLC region. Effective charge carrier mobility was estimated from the slope of the I *versus* V<sup>2</sup> graph of the SCLC region (Figure 7b) using the Mott-Gurney equation<sup>58</sup> given by

$$I = \frac{9\mu_{\text{eff}} \epsilon_0 \epsilon_r A V^2}{8d^3} \quad (1)$$

Where I is the current,  $\epsilon_0$  is the permittivity of free space,  $\epsilon_r$  is the dielectric constant,  $\mu_{\text{eff}}$  is the effective electron mobility measured, A is the active device area, d is the thickness of the drop cast film and V is the voltage applied.

The current versus voltage on the log scale and current versus voltage characteristics of the ITO/PS-*b*-P4VP(PBA+NDI)/Al sandwich structure are shown in Figure 3.12c and 3.12d, respectively.

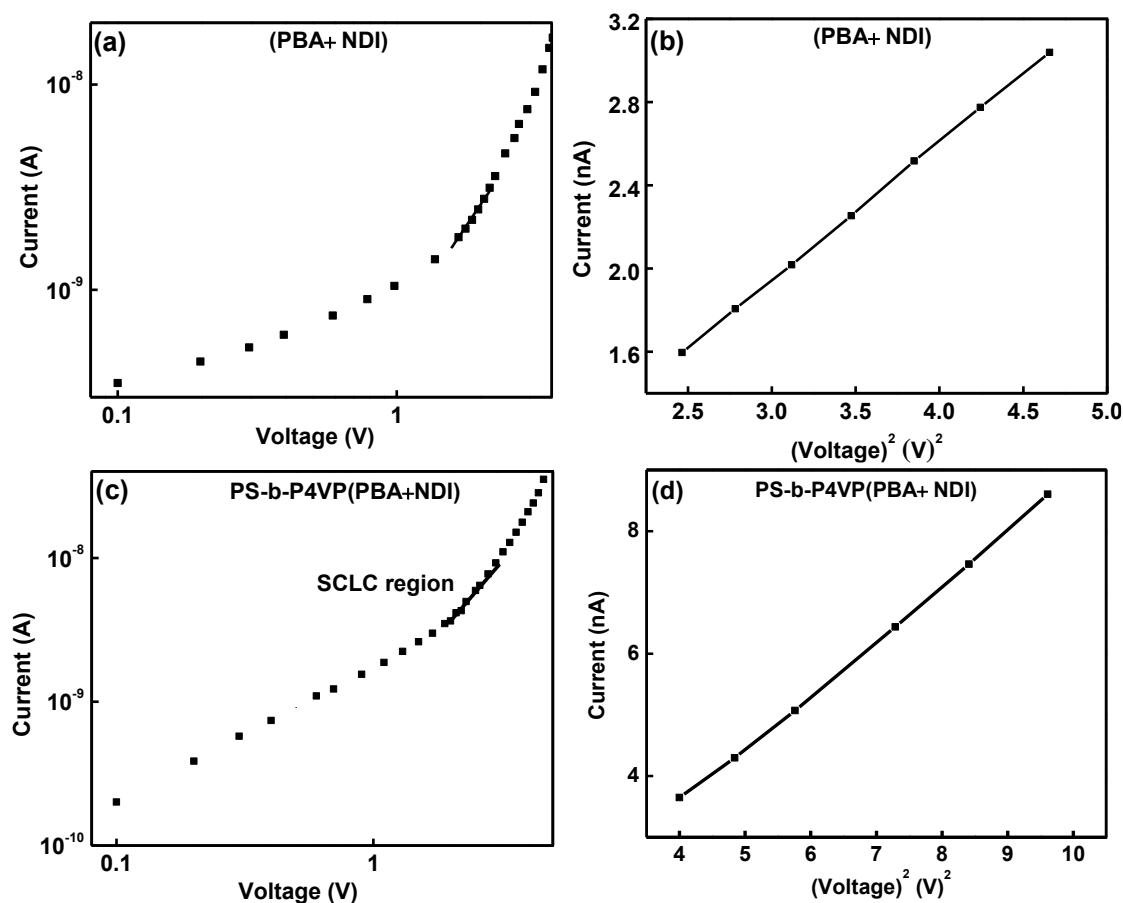


**Figure 3.12.** (a, c) Current *versus* voltage on the log scale and (b, d) current *versus* voltage<sup>2</sup> characteristics of the physical blend of PBA+NDI and PS-*b*-P4VP(PBA+NDI) with ITO and Al electrodes.

The PS-*b*-P4VP(PBA+NDI) film and Al form a Schottky contact at their interface and generate a depletion region. When the device was forward biased, the barrier height at the interface between Al and PS-*b*-P4VP (PBA+NDI) film decreased, turning on the device. At reverse voltage, the barrier height increased and it blocked the current flow.<sup>59</sup> The same mechanism was occurring in the device fabricated with (PBA+NDI) also. The calculated values of mobility using equation 1 are  $5.77 \times 10^{-10} \text{ cm}^2/\text{Vs}$  and  $1.9 \times 10^{-6} \text{ cm}^2/\text{Vs}$  for the physical blend of PBA+NDI and PS-*b*-P4VP(PBA+NDI), respectively. We observed good electron mobility in block copolymer supramolecules (PS-*b*-P4VP(PBA+NDI)) compared with the physical blend of PBA+NDI.

---

---

### 3.6. Conclusions

In conclusion, we have successfully demonstrated the unprecedented three-component hierarchical self-assembly to generate the alternate coassembly of donor and acceptor molecules within the block copolymer microdomains in the solid state through the non-covalent interactions. Addition of two small molecules to the block copolymer resulted in the formation of efficient charge-transfer complexes and this process is different from the previously reported block copolymer supramolecular assembly approach using a small molecule. Complexation of two small molecules with a block copolymer through noncovalent interactions leads to the morphological changes of the block copolymer from the disordered state to cylinders to lamellae. At the same time, noncovalent aromatic donor-acceptor interactions favoured the interdigitation of donor molecules to form the co-assembly of D-A charge-transfer complexes within the block copolymer microdomains and the SCLC mobility measurements proved the higher charge mobility in the case of block copolymer supramolecules compared to that of the physical blend of donor and acceptor. The major advantages of this process are solution processability and the controlled formation of hierarchical assemblies in bulk, which are very much useful for device applications such as organic photovoltaic (OPV), light harvesting, optical waveguides, etc.

### 3.7. References

- [1] Gabriel, G. J.; Sorey, S.; Iverson, B. L. *J. Am. Chem. Soc.* **2005**, 127 (8), 2637-2640.
  - [2] Cubberley, M. S.; Iverson, B. L. *J. Am. Chem. Soc.* **2001**, 123 (31), 7560-7563.
  - [3] Ostroverkhova, O. *Chem. Rev.* **2016**, 116 (22), 13279-13412.
  - [4] Hains, A. W.; Liang, Z.; Woodhouse, M. A.; Gregg, B. A. *Chem. Rev.* **2010**, 110 (11), 6689-6735.
  - [5] Alvey, P. M.; Reczek, J. J.; Lynch, V.; Iverson, B. L. *J. Org. Chem.* **2010**, 75 (22), 7682-7690.
- 
-

- 
- 
- [6] Liu, K.; Wang, C.; Li, Z.; Zhang, X. *Angew. Chem. Int. Ed.* **2011**, 50 (21), 4952-4956.
- [7] Brédas, J.-L.; Norton, J. E.; Cornil, J.; Coropceanu, V. *Acc. Chem. Res.* **2009**, 42 (11), 1691-1699.
- [8] Newton, M. D. *Chem. Rev.* **1991**, 91 (5), 767-792.
- [9] Hunter, C. A. *Chem. Soc. Rev.* **1994**, 23 (2), 101-109.
- [10] Hoeben, F. J. M.; Jonkheijm, P.; Meijer, E. W.; Schenning, A. P. H. J. *Chem. Rev.* **2005**, 105 (4), 1491-1546.
- [11] Mishra, A.; Ma, C.-Q.; Bäuerle, P. *Chem. Rev.* **2009**, 109 (3), 1141-1276.
- [12] Ghosh, S.; Ramakrishnan, S. *Angew. Chem. Int. Ed.* **2005**, 44 (34), 5441-5447.
- [13] Rao, K. V.; Jayaramulu, K.; Maji, T. K.; George, S. J. *Angew. Chem.* **2010**, 122 (25), 4314-4318.
- [14] Rao, K. V.; Jayaramulu, K.; Maji, T. K.; George, S. J. *Angew. Chem. Int. Ed.* **2010**, 49 (25), 4218-4222.
- [15] Maitra, U.; Vijay Kumar, P.; Chandra, N.; J. D'Souza, L.; D. Prasanna, M.; R. Raju, A. *Chem. Commun.* **1999**, (7), 595-596.
- [16] Reczek, J. J.; Villazor, K. R.; Lynch, V.; Swager, T. M.; Iverson, B. L. *J. Am. Chem. Soc.* **2006**, 128 (24), 7995-8002.
- [17] Bent, H. A. *Chem. Rev.* **1968**, 68 (5), 587-648.
- [18] Schmidt-Mende, L.; Fechtenkötter, A.; Müllen, K.; Moons, E.; Friend, R. H.; MacKenzie, J. D. *Science* **2001**, 293 (5532), 1119-1122.
- [19] Reczek, J. J.; Iverson, B. L. *Macromolecules* **2006**, 39 (17), 5601-5603.
- [20] Jonkheijm, P.; Stutzmann, N.; Chen, Z.; de Leeuw, D. M.; Meijer, E. W.; Schenning, A. P. H. J.; Würthner, F. *J. Am. Chem. Soc.* **2006**, 128 (29), 9535-9540.
- [21] Kim, T.; Kim, J.-H.; Kang, T. E.; Lee, C.; Kang, H.; Shin, M.; Wang, C.; Ma, B.; Jeong, U.; Kim, T.-S.; Kim, B. J. *Nat. Commun.* **2015**, 6, 8547.
- [22] Huettner, S.; Sommer, M.; Hodgkiss, J.; Kohn, P.; Thurn-Albrecht, T.; Friend, R. H.; Steiner, U.; Thelakkat, M. *ACS nano* **2011**, 5 (5), 3506-3515.
- [23] Lindner, S. M.; Hüttner, S.; Chiche, A.; Thelakkat, M.; Krausch, G. *Angew. Chem. Int. Ed.* **2006**, 45 (20), 3364-3368.
- [24] Yamauchi, K.; Lizotte, J. R.; Long, T. E. *Macromolecules* **2003**, 36 (4), 1083-1088.
- [25] Brunsveld, L.; Folmer, B. J. B.; Meijer, E. W.; Sijbesma, R. P. *Chem. Rev.* **2001**, 101 (12), 4071-4098.
- 
-

- 
- 
- [26] Valkama, S.; Ruotsalainen, T.; Nykänen, A.; Laiho, A.; Kosonen, H.; ten Brinke, G.; Ikkala, O.; Ruokolainen, J. *Macromolecules* **2006**, 39 (26), 9327-9336.
- [27] Ikkala, O.; ten Brinke, G. *Chem. Commun.* **2004**, (19), 2131-2137.
- [28] Ikkala, O.; ten Brinke, G.. *Science* **2002**, 295 (5564), 2407-2409.
- [29] Ruokolainen, J.; Saariaho, M.; Ikkala, O.; ten Brinke, G.; Thomas, E. L.; Torkkeli, M.; Serimaa, R. *Macromolecules* **1999**, 32 (4), 1152-1158.
- [30] Sidorenko, A.; Tokarev, I.; Minko, S.; Stamm, M. *J. Am. Chem. Soc.* **2003**, 125 (40), 12211-12216.
- [31] Nandan, B.; Gowd, E. B.; Bigall, N. C.; Eychmüller, A.; Formanek, P.; Simon, P.; Stamm, M. *Adv. Funct. Mater.* **2009**, 19 (17), 2805-2811.
- [32] Kuila, B. K.; Gowd, E. B.; Stamm, M. *Macromolecules* **2010**, 43 (18), 7713-7721.
- [33] Kuila, B. K.; Chakraborty, C.; Malik, S. *Macromolecules* **2013**, 46 (2), 484-492.
- [34] Rancatore, B. J.; Bai, P.; Xu, T. *Macromolecules* **2016**, 49 (11), 4155-4163.
- [35] Lee, K. H.; Bai, P.; Rancatore, B. J.; He, B.; Liu, Y.; Xu, T. *Macromolecules* **2016**, 49 (7), 2639-2645.
- [36] Rancatore, B. J.; Kim, B.; Mauldin, C. E.; Fréchet, J. M. J.; Xu, T. *Macromolecules* **2016**, 49 (3), 833-843.
- [37] Rancatore, B. J.; Mauldin, C. E.; Fréchet, J. M. J.; Xu, T. *Macromolecules* **2012**, 45 (20), 8292-8299.
- [38] Narayan, R.; Kumar, P.; Narayan, K. S.; Asha, S. K. *Adv. Funct. Mater.* **2013**, 23 (16), 2033-2043.
- [39] Hagaman, D.; Enright, T. P.; Sidorenko, A. *Macromolecules* **2012**, 45 (1), 275-282.
- [40] Zhao, Y.; Thorkelsson, K.; Mastroianni, A. J.; Schilling, T.; Luther, J. M.; Rancatore, B. J.; Matsunaga, K.; Jinnai, H.; Wu, Y.; Poulsen, D.; Fréchet, J. M. J.; Paul Alivisatos, A.; Xu, T. *Nat. Mater.* **2009**, 8, 979.
- [41] Das, A.; Ghosh, S. *Angew. Chem. Int. Ed.* **2014**, 53 (4), 1092-1097.
- [42] Rajdev, P.; Molla, M. R.; Ghosh, S. *Langmuir* **2014**, 30 (8), 1969-1976.
- [43] Al Kobaisi, M.; Bhosale, S. V.; Latham, K.; Raynor, A. M.; Bhosale, S. V. *Chem. Rev.* **2016**, 116 (19), 11685-11796.
- [44] Das, A.; Molla, M. R.; Maity, B.; Koley, D.; Ghosh, S. *Chem.: Eur. J.* **2012**, 18 (32), 9849-9859.
- [45] Cooke, G.; Rotello, V. M. *Chem. Soc. Rev.* **2002**, 31 (5), 275-286.
- [46] Das, A.; Ghosh, S. *Angew. Chem. Int. Ed.* **2014**, 53 (8), 2038-2054.
- 
-

- 
- [47] Das, A.; Ghosh, S. *Chem. Commun.* **2016**, 52 (42), 6860-6872.
- [48] Balzani, V.; Gómez-López, M.; Stoddart, J. F. *Molecular Machines. Acc. Chem. Res.* **1998**, 31 (7), 405-414.
- [49] Ajayaghosh, A.; George, S. J. *J. Am. Chem. Soc.* **2001**, 123 (21), 5148-5149.
- [50] Hunter, C. A.; Lawson, K. R.; Perkins, J.; Urch, C. J. *J. Chem. Soc., Perkin Trans 2* **2001**, (5), 651-669.
- [51] Ikkala, O.; Ruokolainen, J.; ten Brinke, G.; Torkkeli, M.; Serimaa, R. *Macromolecules* **1995**, 28 (21), 7088-7094.
- [52] Olszak, T. A.; Willig, F.; Durfee, W. S.; Dreissig, W.; Bradaczek, H. *Acta Crystallogr. C* **1989**, 45 (5), 803-805.
- [53] Sofos, M.; Goldberger, J.; Stone, D. A.; Allen, J. E.; Ma, Q.; Herman, D. J.; Tsai, W.-W.; Lauhon, L. J.; Stupp, S. I. *Nat. Mater.* **2008**, 8, 68.
- [54] Pramanik, B.; Ahmed, S.; Singha, N.; Das, B. K.; Dowari, P.; Das, D. *Langmuir* **2019**, 35 (2), 478-488.
- [55] Kim, J. H.; Lindeman, S. V.; Kochi, J. K. *J. Am. Chem. Soc.* **2001**, 123 (21), 4951-4959.
- [56] Ofir, Y.; Zelichenok, A.; Yitzchaik, S. *J. Mater. Chem.* **2006**, 16 (22), 2142-2149.
- [57] Ahmed, F.; Halder, S.; Dutta, B.; Islam, S.; Sen, C.; Kundu, S.; Sinha, C.; Ray, P. P.; Mir, M. H. *New J. Chem.* **2017**, 41 (19), 11317-11323.
- [58] Geurst, J. A. *physica status solidi (b)* **1966**, 15 (1), 107-118.
- [59] Zhu, M.; Cui, T.; Varahramyan, K. *Microelectron. Eng.* **2004**, 75 (3), 269-274.
-

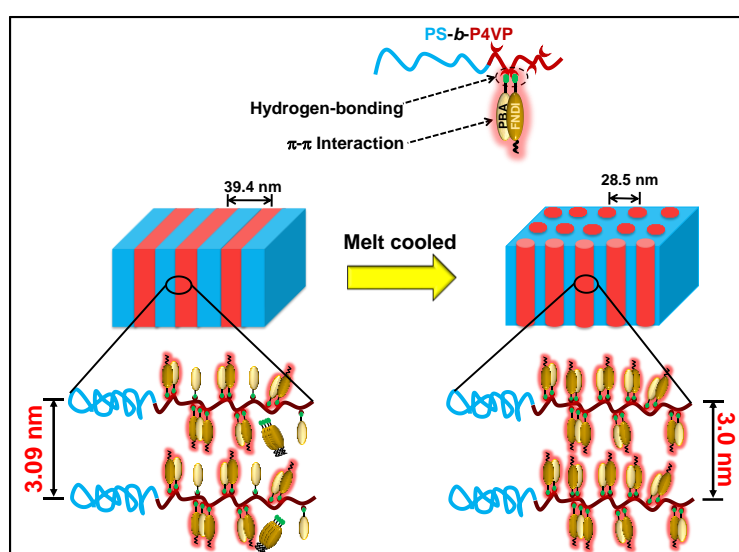
---

---

## Co-assembly of Functionalized Donor-Acceptor Molecules within the Block Copolymer Domains via Supramolecular Approach

---

---



### 4.1. Abstract

Among the supramolecular designs, the functional groups on the  $\pi$ -systems exhibit several features, including the strong choice for  $\pi$ - $\pi$  interactions, excellent charge-transfer (CT) complexation, semiconductivity and photophysical properties. This chapter describes the three-component self-assembly of functionalized small molecules (donor and acceptor) and polystyrene-block-poly(4-vinylpyridine) (PS-b-P4VP) block copolymer. Herein, we depict the role of the functional groups on both donor (1-pyrenebutyric acid, PBA) and acceptor (functionalized naphthalene diimide, FNDI) molecules on the hierarchical assembly as well as the D-A stacking within the block copolymer domains. Both the molecules can form H-bonding with P4VP chains, and apart from this,  $\pi$ - $\pi$  stacking

*between the PBA and FNDI molecules is also possible within the block copolymer domains. These noncovalent interactions lead to the formation of hierarchical structures and charge-transfer complexes between PBA and FNDI, where the bilayer D-A stacks formed within the block copolymer microdomains. It was also observed that the introduction of a functional group on FNDI molecules favors the formation of stable D-A stacks in the physical blend. Overall, the organization of both functionalized donor and acceptor molecules within the block copolymer domain exhibits enhanced charge carrier mobility, which is potentially useful in the field of electronic devices.*

## **4.2. Introduction**

Over the past few years, supramolecular chemistry has gained interest in the interdisciplinary areas that span chemistry, biology, physics, nanotechnology and materials science.<sup>1-5</sup> By taking advantage of the powerful supramolecular approach, research is going on to generate a diverse range of nanostructured materials by exploiting various noncovalent interactions, such as hydrogen bonding,<sup>6</sup> charge-transfer (CT)  $\pi$ - $\pi$  stacking interaction,<sup>7</sup> metal-ligand coordination,<sup>8</sup> etc. Supramolecular assembly of  $\pi$ -structures, particularly chromophores, has acquired more interest in multidisciplinary fields to fulfil the required photophysical and unidirectional charge-transport characteristics for practical applications.<sup>9-12</sup> For instance, charge-transfer assembly of alternate stacking of donor-acceptor (D-A) chromophores is of great importance because of their inherent conducting properties and ferroelectric behaviour.<sup>9, 13</sup> Donor-acceptor (D-A) complexation or the charge transfer complexation has been extensively studied in diverse range of materials including supramolecular photosystems,<sup>14</sup> foldamers,<sup>15</sup> liquid crystals,<sup>16</sup> nanoparticles,<sup>17</sup> organogels,<sup>18</sup> hydrogels<sup>19</sup> and so on.

The self-assembly with significant stability in most of the above-mentioned systems could only be accomplished by improving the CT complex with the simultaneous influence

---

---

---

of additional noncovalent forces such as hydrogen bonding, electrostatic interaction, metal-ligand coordination and solvophobic interaction. Among these noncovalent interactions, it is particularly interesting to achieve the hydrogen bonding mediated assembly of donor-acceptor complexes.<sup>9,20,21</sup> The presence of functional moieties such as alcohols, carboxylic acids, amide, urea, etc. imparts the hydrogen bonding, which offers directionality, tunability, and selectivity which are necessary to modulate the self-assembly process. This structural diversity, directional nature, and the ability to access a wide range of building blocks with attached H-bonding functional groups have encouraged chemists to investigate the controlled self-assembly of various systems, including  $\pi$  systems to tune the optical and electronic properties of the material.<sup>9,20,22,23</sup>

Several authors systematically investigated the impact of functionalization on donor-acceptor complexes, particularly by imparting hydrogen bonds forming functionalization on the donor and acceptor units in solution state.<sup>6,9,12,24-26</sup> It has been proved that the hydrogen bonding side chains along with the complementary aromatic  $\pi$ - $\pi$  interactions could control the donor-acceptor interactions for diverse applications such as solar cells and organic light-emitting diodes (OLEDs) as well as in basic biological processes such as photosynthesis.<sup>27-30</sup> From the perspective of device applications, it is extremely desirable to solution process the small molecules into uniform thin films with the improved long-range order of D-A assemblies. Incorporation of small molecules (donors and acceptors) into the polymer chains shows interesting properties such as processability, high charge carrier mobility and enhanced solubility. However, the incorporation of small molecules into the polymer backbones or side chains by covalent bonding as either a block copolymer or an alternating copolymer is rare because of the complexity involved in the synthesis. In this regard, the prominent scientists Ikkala and ten Brinke put forward a promising approach to develop hierarchical nanostructures of small

---

---

molecules with block copolymers using noncovalent polymer side-chain modification.<sup>31-34</sup> This approach was later followed by several groups to produce nanostructured composites by incorporating features with electronic, optical or stimuli-responsive characteristics for various applications.<sup>35-38</sup>

In the previous chapter, we have reported the generation of stable alternative D-A stacks within the block copolymer domains by three-component hierarchical supramolecular assembly. We reported the formation of three-component assembly by using two small molecules such as 1-pyrene butyric acid (PBA) and naphthalene diimide (NDI) with PS-*b*-P4VP block copolymer. In that case, only the PBA molecules formed hydrogen bonding with P4VP domains and the addition of NDI molecules to this assembly facilitated the creation of CT complexes through  $\pi$ - $\pi$  interactions, which is confirmed by the visual colour change and also using UV/Visible and photoluminescence spectroscopy. The physical blend of PBA and NDI without block copolymer exhibited a self-sorted assembly in solid state, which highlights the role of the block copolymer in stable D-A assembly in solid state. The space charge limited current (SCLC) analysis shows that block copolymer supramolecules having higher charge mobility compared to that of the physical blend of donor and acceptor molecules.<sup>39</sup>

In the present work, we investigate the co-assembly of functionalized donor (PBA) and acceptor (functionalized naphthalene-diimide (FNDI)) molecules within the block copolymer domains via hydrogen bonding driven supramolecular assembly. Here, the length of the alkyl chain is identical in both molecules so that it can form a comb kind of structure by hydrogen bonding with other weak interactions involving  $\pi$ - $\pi$  interaction and CT interactions. These noncovalent interactions lead to the formation of hierarchical structures and charge-transfer complexes between PBA and FNDI within the block copolymer microdomains, which are confirmed by SAXS, WAXS, TEM, UV/Vis

---

spectroscopy and photoluminescence spectroscopy measurements. Unlike the previous work, the hydrogen bonding of acceptor molecules with 4 VP chains favored the formation of bilayer of D-A stacks within the block copolymer microdomains. At the same time, the physical blend also favored the formation of stable D-A stacks. The SCLC measurement showed enhanced charge carrier mobility of the confined D-A stacks in the case of SMAs using functionalized donor and acceptor molecules.

### 4.3. Experimental Section

**4.3.1. Materials:** PS (54000 g mol<sup>-1</sup>)-*b*-P4VP(6500 g mol<sup>-1</sup>) with  $D = 1.06$  was purchased from Polymer Source, Inc. 1-Pyrenebutyric acid (PBA), 1,4,5,8-naphthalene tetracarboxylic acid dianhydride, n-hexyl amine, potassium hydroxide (KOH), 4-aminobutanoic acid, 1,4-dioxane, HPLC-grade dimethylformamide (DMF), and methanol were purchased from Sigma-Aldrich. The solvents used were of analytical grade and carefully dried prior to use. Synthetic details and the characterization data for the carboxyl functionalized naphthalene diimide (FNDI) compounds are given below.

#### 4.3.2. Synthesis of Functionalized Naphthalene Diimide (FNDI)

The synthesis of FNDI was carried out using reported literature procedure<sup>40</sup> as shown in Figure 4.1.

**4.3.2.1. Synthesis of Compound-1:** In a 500 mL RB flask 2.0 g of 1,4,5,8-naphthalenetetracarboxylic acid dianhydride (7.46 mmol) was dissolved in 350 mL water. The solution was then heated after the addition of 1 M aqueous KOH solution (35 mL) with vigorous stirring until the compound dissolved completely. Once the clear solution is formed, 1 M H<sub>3</sub>PO<sub>4</sub> was added until the pH was adjusted to 6.4. To that solution, 0.98 mL of n-hexyl amine (7.46 mmol) was added and again, the pH was readjusted to 6.4 with 1 M H<sub>3</sub>PO<sub>4</sub>. The resultant solution was refluxed overnight. After cooling the mixture, the filtrate was acidified with 5 mL acetic acid and the obtained precipitate was then filtered and

repeatedly washed with water and dried in a vacuum oven to get compound-1 as an off-white solid (1.02 g (51% yield)). NMR spectrum of compound-1 is shown in Figure 4.2a.

**4.3.2.2. Synthesis of Compound-2:** 1 g of the compound-1 (2.85 mmol) was first dissolved in dimethylformamide (DMF, 15 mL) by heating at 60 °C. To that solution 0.605 g of  $\gamma$ -aminobutyric acid (5.87 mmol) and 1.02 mL of DIPEA (5.87 mmol) are added sequentially. The reaction mixture was held at 90 °C for 12 h. The reaction mixture was allowed to cool and the solvent was evaporated using a rota evaporator. The obtained crude residue was suspended in 100 mL water/methanol (2:1) and hydrochloric acid (6 N) was added to adjust the pH to 3. The obtained solid was repeatedly washed with water by centrifugation and then kept it in a vacuum oven for drying to get 0.8 g of compound-2 (80 % yield) as a light brown solid. NMR spectrum of compound-2 is shown in Figure 4.2b.

**4.3.3. SMA Preparation:** The SMA of block copolymer (PS-*b*-P4VP) and PBA (1 mol of 4-vinylpyridine monomer unit:0.5 mol of PBA) were prepared first in 1,4-dioxane separately. The PS-*b*-P4VP solution was slowly added to the PBA solution at around 100 °C with continuous stirring. Such prepared solution was allowed to age at room temperature for 3 days for the complete hydrogen-bonding formation. To this solution, the separately prepared FNDI solution (1 mol of 4-vinylpyridine monomer unit:0.5 mol of FNDI) was added with continuous stirring and kept for 3 days. Such prepared SMA solution was transferred to the petri dish and allowed to evaporate the solvent slowly. The resultant samples were dried in a vacuum oven at 40 °C for 12 h. The physical blend of PBA and FNDI were prepared by solution blending by mixing 1:1 weight ratio of small molecules in 1,4-dioxane and the solution was poured into the petri dish and allowed the solvent to evaporate at ambient conditions.

#### 4.4. Characterization

The XEUSS SAXS/WAXS system with a Genixmicro source from Xenocs was used to conduct the wide-angle and small-angle X-ray scattering measurements (WAXS/SAXS). Both WAXS and SAXS data were collected in transmission geometry and the generator was operated at 0.6 mA and 50 kV. Fox2D mirror and two pairs of scatterless slits from Xenocs were used to collimate the X-ray beam. The Fit2D software was used to process the fiber diagrams. WAXS and SAXS scattering vectors were calibrated using the standard silver behenate sample. Sample to detector distances were fixed at 220.5 mm and 1048.2 mm for WAXS and SAXS, respectively. In order to perform the temperature-dependent measurements, Linkam THMS 600 hot stage connected to LNP 95 cooling system was used. The samples were heated from room temperature to 280 °C at a rate of 10 °C/min and the X-ray patterns were acquired at 10 °C interval and the samples were equilibrated at each temperature for 10 min.

Proton nuclear magnetic resonance spectra ( $^1\text{H}$  NMR) were recorded in  $\text{CDCl}_3$  using Bruker spectrophotometer operating at 500 MHz. In  $^1\text{H}$  NMR spectra, the chemical shifts ( $\delta$ ) were recorded as in units of parts per million (ppm). Mass spectra were recorded under EI/HRMS at 60,000 resolution using Thermo Scientific Exactive Mass Spectrometer. FTIR measurements were recorded on the Spectrum Two FT-IR spectrometer of the PerkinElmer series. The FTIR spectra were recorded over the 4000–400  $\text{cm}^{-1}$  wavenumber range at a resolution of 2  $\text{cm}^{-1}$  by averaging 32 scans. The TEM (JEOL 2010 transmission electron microscope operating at 300 kV) was used to analyze the morphologies of SMAs and the samples were prepared by drop-casting the SMA solution in 1,4-dioxane (2 mg/ml) on to the copper grid. The iodine vapor was used to stain the samples to enhance the contrast of the TEM image and the iodine selectively interacts with the P4VP domain. The Shimadzu UV-3600, UV-visible-NIR spectrophotometer was used to capture UV-visible

spectra. The Spex-Fluorolog FL22 spectrofluorimeter equipped with a double grating 0.22 m Spex 1680 monochromator and a 450W Xe lamp (excitation source operating in the front face mode) was used to measure the PL spectra of the sample in solid state. The sample was excited at a wavelength of 340 nm.

The charge carrier mobility of SMAs and the physical blend of PBA+FNDI were studied using SCLC measurements. Prepare a sandwich structure of patterned ITO coated glass and aluminium (Al) substrates were fabricated for the SCLC studies. Both PS-*b*-P4VP (PBA+FNDI) & (PBA+FNDI) samples were dissolved in 1,4-dioxane and drop casted on the substrate to achieve a thin film of thickness around 5  $\mu\text{m}$  which is measured by using Dektak XT stylus profilometer. The active area of the device was 4  $\text{mm}^2$ . The LCR meter (Hioki 3532-50LCR Hi Tester, Japan) was used to measure the capacitance of the device, from which the dielectric constant was estimated. The current-voltage measurements were carried out using a Keithley-2450 source measure unit within a range of  $\pm 4\text{V}$ .

## 4.5. Results and Discussion

### 4.5.1. Characterization of Functionalized Naphthalene Diimide (FNDI)

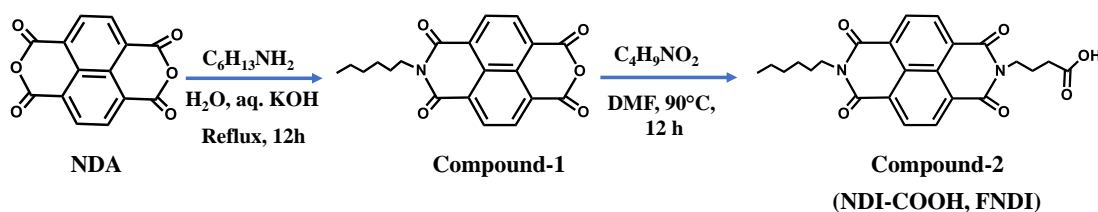


**Figure 4.1.** Scheme of the synthesis of the functionalized NDI (FNDI).

The FNDI was obtained in extremely pure form by repeated purification procedures. The structure of the synthesized product was confirmed by using  $^1\text{H}$  NMR and mass spectroscopy.

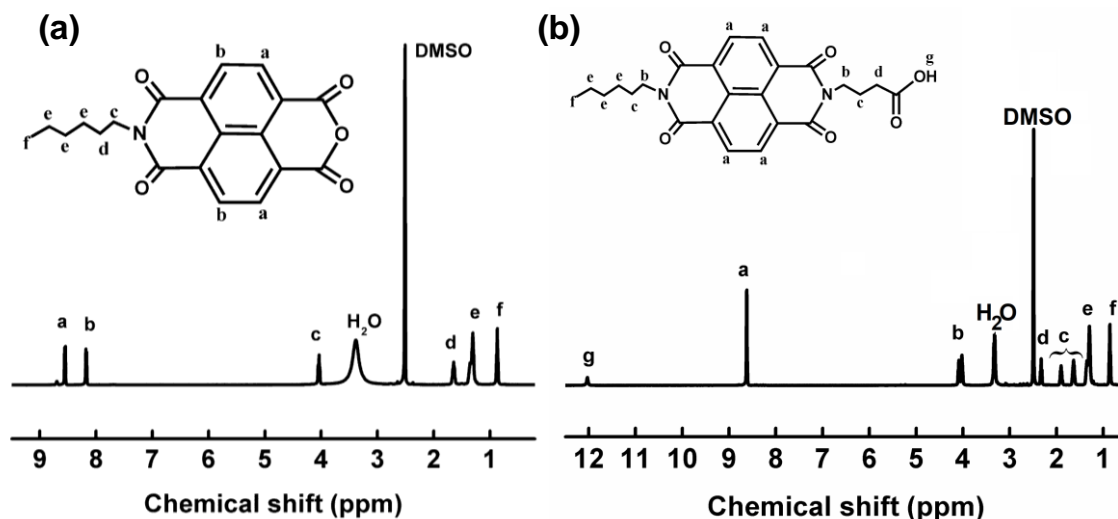


**Figure 4.2.** The <sup>1</sup>H NMR spectra of synthesized (a) compound-1 and (b) compound-2 (FNNDI).

Figure 4.2 compares the <sup>1</sup>H NMR spectra of intermediate product and final product (FNNDI) during the synthesis, which is recorded in deuterated DMSO at room temperature (25 °C).

The details from the <sup>1</sup>H NMR spectra and mass analysis are given below

**Compound-1:**  $\delta/\text{ppm} = 8.56\text{-}8.54$  (d, 2H),  $8.19\text{-}8.18$  (d, 2H),  $4.03\text{-}4.01$  (t, 2H),  $1.65\text{-}1.61$  (m, 2H),  $1.35\text{-}1.28$  (m, 6H),  $0.86\text{-}0.84$  (t,  $J = 6\text{Hz}$ , 3H).

ESI-HRMS ( $m/z$ ): calc for  $\text{C}_{20}\text{H}_{17}\text{NO}_5^+$  [ $\text{M} + \text{H}$ ]<sup>+</sup>: 352.35, found: 352.27.

**Compound-2 (FNNDI):**  $\delta/\text{ppm} = 12.02$  (s, 1H),  $8.62$  (s, 4H),  $4.08$  (t, 2H),  $4.02$  (t, 2H), 2, 32 (br. 1H),  $1.99$  (t, 2H),  $1.65$  (t, 2H),  $1.30\text{-}1.25$  (m, 6H),  $0.86\text{-}0.84$  (t, 3H).

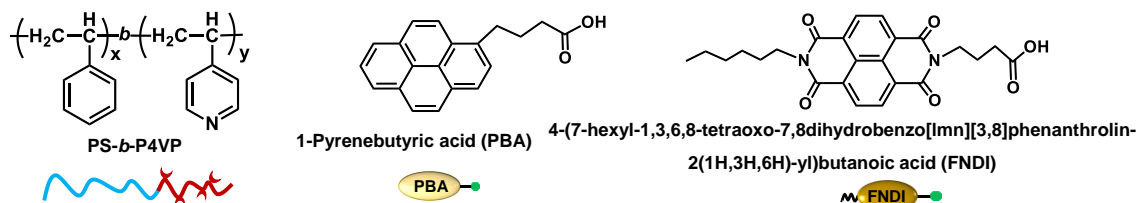
ESI-HRMS ( $m/z$ ): calc for  $\text{C}_{20}\text{H}_{17}\text{NO}_5^+$  [ $\text{M} + \text{H}$ ]<sup>+</sup>: 437.46, found: 437.17.

The type and the position of the corresponding peaks in <sup>1</sup>H NMR and the mass obtained from the mass spectroscopy confirm the formation of COOH functionalized naphthalene diimide molecule.

#### 4.5.2. Hierarchical Assembly of D-A Molecules within the Block Copolymer Domains

FNNDI having carboxylic acid functionality on one side was synthesized with equal

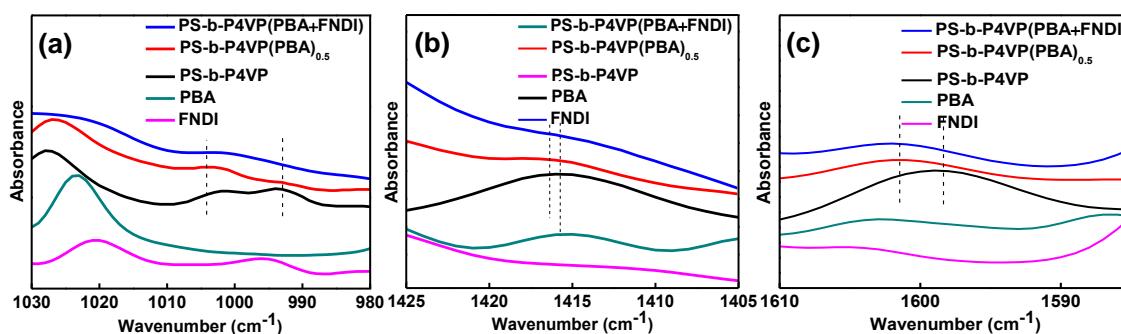
spacer length to that of PBA to enable the hydrogen bonding formation with P4VP. Figure 4.3 shows the chemical structures of the block copolymer (PS-*b*-P4VP), donor (PBA) and acceptor (FNDI) molecules used for the formation of supramolecular assembly.



**Figure 4.3.** Chemical structure of the block copolymer (PS-*b*-P4VP), donor molecule (PBA) and carboxylic acid functionalized acceptor molecule (FNDI).

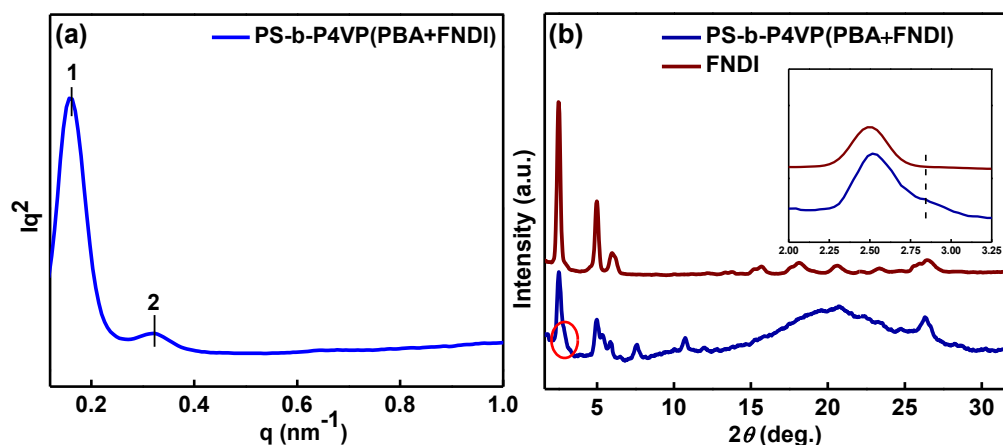
First, donor molecules were blended with PS-*b*-P4VP with the stoichiometric ratio (PBA:4VP) of 0.5 (PS-*b*-P4VP(PBA)<sub>0.5</sub>), therefore, only 50% of the 4VP units in PS-*b*-P4VP were hydrogen-bonded with PBA molecules and another 50% of 4VP units are free. To this solution, FNDI solution was added with the stoichiometric ratio of FNDI and 4VP groups fixed at 0.5 (PS-*b*-P4VP(PBA+FNDI)). This allows the rest of the 4VP units in block copolymer to form hydrogen bonding with FNDI molecules. Figure 4.4 shows the FTIR spectra of the PS-*b*-P4VP, PBA, FNDI, PS-*b*-P4VP(PBA)<sub>0.5</sub> and PS-*b*-P4VP(PBA+FNDI) in three different regions. From the FTIR spectra, the absorption peak at 993 cm<sup>-1</sup> corresponds to the symmetric ring stretching of the free pyridine group in the PS-*b*-P4VP block copolymer. This peak becomes broad after the addition of PBA and the peak intensity reduces substantially confirming the formation of H-bonding between PBA and 50% of 4VP groups. Simultaneously, upon the complexation, the intensity of the absorption band at 1004 cm<sup>-1</sup> further confirms the hydrogen bonding between pyridine units and PBA. After the addition of acceptor (FNDI) molecules, the absorption peak at 993 cm<sup>-1</sup> completely disappeared as shown in Figure 4.4a and the peak corresponding to hydrogen-bonded pyridine (1004 cm<sup>-1</sup>) remains intact, which means that the functionalized acceptor molecule also takes part in hydrogen bonding with free 4VP groups. The formation of

hydrogen bonding of 4VP units with PBA and FNDI is further confirmed by the shift of peaks in other regions (1430 to 1400 and 1610 to 1585  $\text{cm}^{-1}$ ) of the FTIR spectra as shown in Figure 4.4b and 4.4c.



**Figure 4.4.** FTIR spectra of FNDI, PBA, PS-*b*-P4VP, PS-*b*-P4VP(PBA)<sub>0.5</sub>, and PS-*b*-P4VP(PBA+FNDI) in the different regions of (a) 1030-980  $\text{cm}^{-1}$  (b) 1425-1405  $\text{cm}^{-1}$  and (c) 1610-1585  $\text{cm}^{-1}$ .

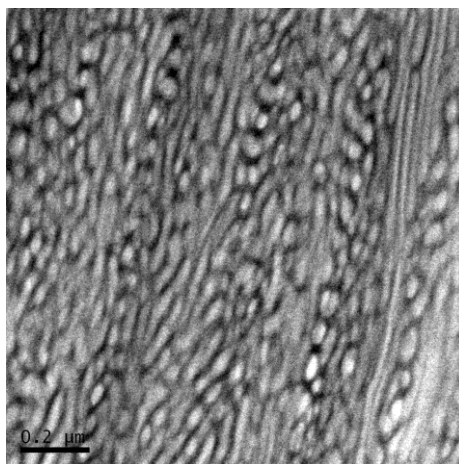
SAXS/WAXS and TEM were used to understand the microphase separation of block copolymer supramolecules, molecular level dispersion and hierarchical arrangement of small molecules (PBA and FNDI) within the block copolymer microdomains. The block copolymer (PS (54000  $\text{g mol}^{-1}$ )-*b*-P4VP(6500  $\text{g mol}^{-1}$ ) with  $D = 1.06$ ) used in this study favors the spherical morphology in bulk. As discussed in the previous chapter, upon the addition of PBA molecules, the morphology of block copolymer supramolecules (PS-*b*-P4VP(PBA)<sub>0.5</sub>) changed to hexagonally packed cylinders with the domain spacing of  $40.5 \pm 1$  nm. The WAXS studies revealed that PBA molecules are homogeneously dispersed without any agglomeration and arranged within the comb lamellae of P4VP(PBA)<sub>0.5</sub> domains with the domain spacing of 2.7 nm (two layers of PBA without interdigitation).<sup>39</sup>



**Figure 4.5.** (a) Lorentz-corrected SAXS pattern of PS-*b*-P4VP(PBA+FNDI), and (b) WAXS patterns of FNDI and PS-*b*-P4VP(PBA+FNDI).

Upon the addition of FNDI (stoichiometric ratio: 1 mol of 4-vinylpyridine monomer unit:0.5 mol of FNDI) to PS-*b*-P4VP(PBA)<sub>0.5</sub> complex, FNDI selectively interacts with 4VP chains through hydrogen bonding and as a result, the overall volume fraction of P4VP(PBA+FNDI) changes and that leads to the change in the morphology of block copolymer supramolecules. Figure 4.5a depicts the Lorentz-corrected SAXS pattern of PS-*b*-P4VP(PBA+FNDI). The positions of the SAXS peaks are at  $q = 0.159$  and  $0.320 \text{ nm}^{-1}$ , and the peak positions are in the ratio of 1:2 indicates the formation of lamellar morphology. The domain spacing estimated from the first-order peak is  $39.4 \pm 1 \text{ nm}$ . However, the corresponding TEM image shown in Figure 4.6 reveals the dominant lamellar morphology mixed with the cylindrical morphology with an average center-to-center spacing of  $38 \pm 1 \text{ nm}$ , which is in good agreement with the spacing calculated from the SAXS pattern. These results indicated that FNDI molecules selectively incorporated into the P4VP domains and to understand the dispersion of FNDI within the P4VP domains, WAXS pattern was collected at room temperature. Figure 4.5b shows the WAXS patterns of PS-*b*-P4VP(PBA+FNDI) and FNDI. The WAXS pattern of PS-*b*-P4VP(PBA+FNDI) shows some crystalline reflections corresponding to FNDI molecules superimposed on the broad

amorphous halo of the block copolymer, indicating the agglomeration of FNDI molecules, but the peaks are broader with relatively less intensity. No other peaks are seen from the crystallization of PBA indicating that the hydrogen bonding between PBA and 4VP chains remains intact, which was further confirmed from the FTIR spectrum. However, a careful observation of the WAXS pattern revealed a weak reflection at lower  $2\theta = 2.8^\circ$  ( $d=3.15$  nm), which is neither from FNDI nor from PBA. This peak is also different from the peak observed in the WAXS pattern of PS-*b*-P4VP(PBA)<sub>0.5</sub>. Based on these observations, this peak could be assigned to the hierarchical assembly of hydrogen bonded PBA and FNDI within the block copolymer domains. It has been demonstrated that thermal annealing of the block copolymer supramolecules improves the ordering of the small molecules within the block copolymer microdomains. Variable temperature SAXS and WAXS measurements of PS-*b*-P4VP(PBA+FNDI) sample were carried out to understand the formation of the hierarchical assembly during the thermal annealing process.



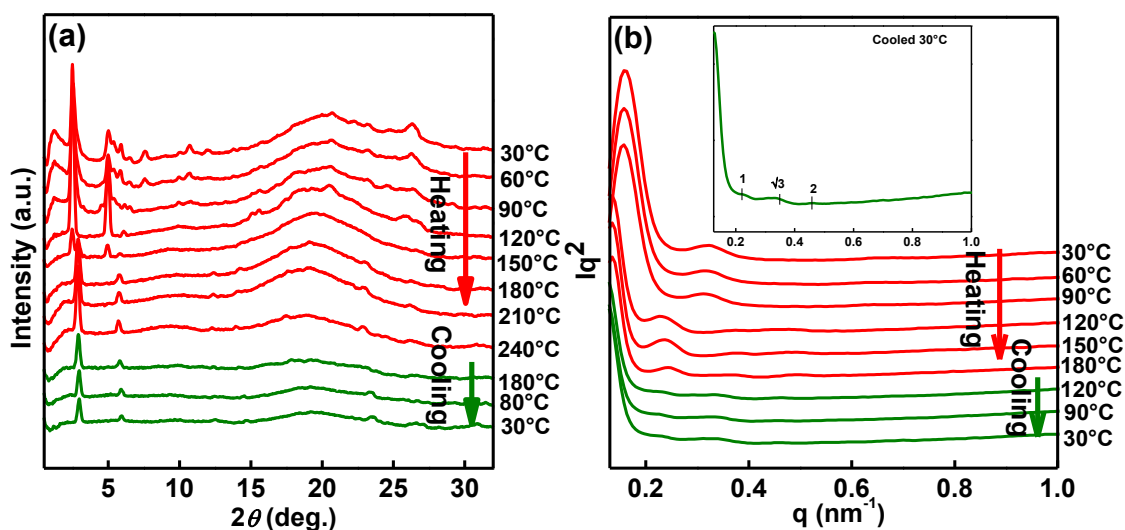
**Figure 4.6.** TEM image of PS-*b*-P4VP(PBA+FNDI) supramolecules

Figure 4.7 depicts the temperature-dependent WAXS and SAXS patterns of PS-*b*-P4VP(PBA+FNDI) sample during heating (up to 240 °C) and cooling to room temperature at a rate of 10 °C/min. As discussed in the preceding section, WAXS pattern of PS-*b*-P4VP(PBA+FNDI) shows multiple crystalline reflections superimposed over the

amorphous halo of block copolymer and these reflections are corresponding to the macrophase-separated (crystallized) FNDI. The intensity of these reflections reduced drastically above 120 °C, i.e., above the glass transition temperature of PS and P4VP and disappeared completely around 180 °C, which is well below the melting temperature of FNDI ( $T_m = 225$  °C). Simultaneously, two new reflections at  $2\theta = 2.9^\circ$  ( $d = 3.04$  nm) and  $2\theta = 5.9^\circ$  ( $d = 1.49$  nm) appeared above 120 °C and the intensity of these peaks increased significantly above 180 °C. The disappearance of crystalline reflections above the  $T_g$  of block copolymer indicates the molecular level dispersion of FNDI within the block copolymer domains and the appearance of new reflections with the ratio of 1:2 indicates the formation of lamellar morphology of PBA and FNDI within the block copolymer microdomains. Upon cooling, the X-ray reflections corresponding to the hierarchical assembly remained as such, however no crystalline reflections corresponding to the PBA or FNDI were observed indicating that neither PBA nor FNDI was crystallized during cooling. It is worth recalling that the WAXS pattern of the PS-*b*-P4VP(PBA)<sub>0.5</sub> shows a peak at  $2\theta = 3.2^\circ$  ( $d = 2.7$  nm) corresponding to the bilayer assembly of hydrogen bonded PBA within P4VP domains. After the addition of FNDI, this peak is completely vanished and upon heating above 120 °C, the appearance of X-ray reflections at  $2\theta = 2.9^\circ$  ( $d = 3.04$  nm) and  $2\theta = 5.9^\circ$  ( $d = 1.49$  nm) indicates the formation of bilayer assembly of PBA and FNDI within the P4VP microdomains. It means, the breakage of agglomeration of FNDI above 120 °C favored the formation of stable D-A stacks because of the  $\pi$ - $\pi$  interactions and these interactions suppressed the crystallization of small molecules during cooling. These results are different from the recently reported block copolymer supramolecules PS-*b*-P4VP(PBA+NDI), where non-functionalized NDI was used as one of the small molecules. In that case, monolayer assembly of PBA and NDI was formed with the spacing of 1.84 nm.<sup>39</sup> Whereas in the present case, the functionalized NDI also forms hydrogen

---

bonding with P4VP chains and as a result D-A stacks (CT complexes) are formed as bilayer and the spacing calculated was 3.04 nm, which is higher than the length of energy minimized structure of FNDI (1.98 nm). These results suggested that thermal annealing above the  $T_g$  of block copolymer plays a crucial role in the dispersion of small molecules within the block copolymer microdomains and favored the formation of stable charge-transfer complexes. During cooling, the hydrogen bonding of PBA and FNDI with P4VP chains together with the  $\pi$ - $\pi$  interaction between PBA and FNDI suppressed the crystallization of PBA or FNDI within the block copolymer domains.



**Figure 4.7.** Temperature-dependent (a) WAXS and (b) Lorentz-corrected SAXS patterns of PS-*b*-P4VP(PBA+FNDI) (Inset of (b), zoomed SAXS pattern of the room temperature cooled sample).

As discussed above, the room temperature SAXS pattern of PS-*b*-P4VP(PBA+FNDI) shows the dominant lamellar morphology. Upon heating, the SAXS pattern remains the same up to 90 °C and above 120 °C ( $T_g$  of block copolymer), a drastic change in the SAXS pattern was observed. Peak positions are shifted to  $q = 0.21 \text{ nm}^{-1}$ ,  $0.36 \text{ nm}^{-1}$ , and  $0.45 \text{ nm}^{-1}$  and the ratio of the peak positions are 1:  $\sqrt{3}$ : 2. It means that above 120 °C, the morphology of the block copolymer is changed from lamellar to cylindrical. WAXS

studies also revealed that at this temperature, the FNDI molecules dispersed homogeneously within the block copolymer microdomain and it favored the formation of CT complexes. It means that the formation of CT complexes and the interactions between PBA and FNDI favored the change in the domain spacing of the block copolymer and at the same time, the morphology is also changed. During cooling, the cylindrical morphology is retained (inset of Figure 4.7b), where the small molecules are organized as lamellae within the block copolymer cylinders.

#### 4.5.3. Formation of Charge-Transfer Complex

The formation of charge-transfer complexes between PBA and FNDI within the block copolymer domains and the physical blend of PBA and FNDI was confirmed by a visual colour change and UV-Vis spectroscopy. The physical blend of PBA and FNDI was prepared in 1:1 ratio without block copolymer. As seen from the visual images (Figure 4.8a and 4.8b), both PS-*b*-P4VP(PBA+FNDI) and the physical blend of PBA+FNDI samples show a purple-red colour in the solid state indicating the formation of alternating D-A stacks, i.e., charge transfer (CT) complexes between PBA and FNDI molecules.

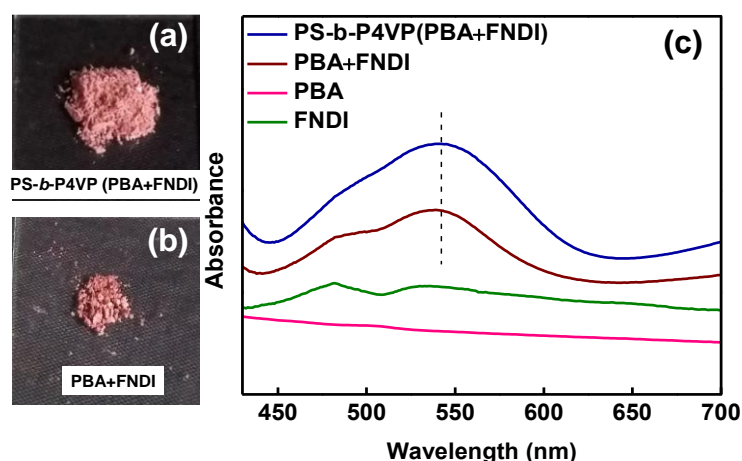


**Figure 4.8.** The visual appearance of (a) PS-*b*-P4VP(PBA+FNDI), and (b) physical blend (PBA+FNDI) and (c) UV/Vis spectra of PS-*b*-P4VP(PBA+FNDI), (PBA+FNDI), FNDI and PBA in solid state.

To further confirm this, UV/Vis spectroscopy study was carried out, which shows an absorption band in the range of 400-700 nm, a characteristic peak of charge-transfer complexes.<sup>19, 41</sup> Figure 4.8c shows the UV/Vis absorption spectra of PBA, FNDI, PS-*b*-P4VP(PBA+FNDI) and the physical blend of PBA+FNDI in the solid state in CT-band region. Even though the samples show significant scattering, both physical blend of PBA+FNDI and PS-*b*-P4VP(PBA+FNDI) show a broad band around 540 nm, which is associated with the CT complex formation between the  $\pi$  electron-rich PBA and  $\pi$  electron-deficient FNDI moieties. In the case of PS-*b*-P4VP(PBA+FNDI) supramolecules, both donor and acceptor molecules are hydrogen-bonded with the P4VP chains, but the presence of alkyl chain with the equal length between the chromophore and COOH group favors the formation of CT complexes through  $\pi$ - $\pi$  interactions. Both the hydrogen-bonding with P4VP chains and  $\pi$ - $\pi$  interactions between PBA and FNDI stabilize the DA stacks within the block copolymer microdomains and this assembly was found to be stable even after 6 months. It has to be noted that the physical blend of PBA+FNDI also shows the formation of CT complexes in the solid state, which is completely different from the observation made in the previous chapter where self-sorting of PBA and NDI (without COOH group) was observed in the case of physical blend. It means that the presence of COOH group in both donor and acceptor molecules favored the formation of D-A stacking in the physical blend and inhibits the self-sorting behaviour. However, the intensity of the absorption band of PS-*b*-P4VP(PBA+FNDI) is prominent compared to that of the physical blend (PBA+FNDI), suggesting the effective formation of D-A stacks within the block copolymer microdomains. The formation of D-A stacks was further confirmed using <sup>1</sup>H NMR spectra in the solution state. Figure 4.9 shows the <sup>1</sup>H NMR spectra of PBA, FNDI, PS-*b*-P4VP(PBA+FNDI) and (PBA+FNDI). An up-field shift in the aromatic protons of PBA and FNDI in both PS-*b*-P4VP(PBA+FNDI) supramolecules and physical blend indicates

---

the CT complex formation in solution state.<sup>42</sup>

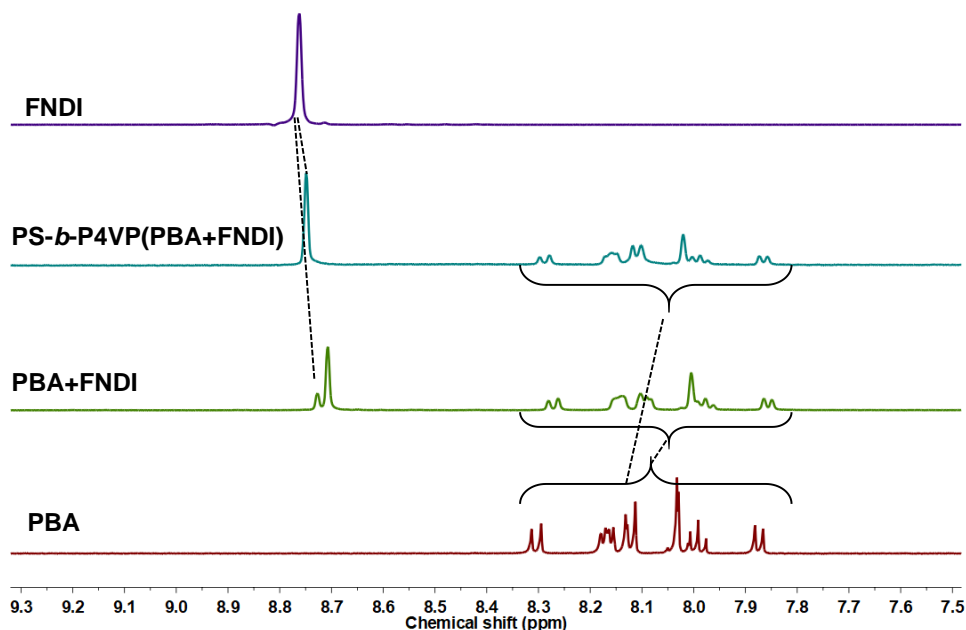


**Figure 4.9.**  $^1\text{H}$  NMR spectra of FNDI, PS-*b*-P4VP(PBA+FNDI), PBA+FNDI and PBA displaying the up-field shifts of aromatic protons because of CT complexation.

To further confirm the formation of CT complex in block copolymer supramolecules, solid-state photoluminescence (PL) measurements were carried out. All samples were excited at 340 nm and the corresponding PL spectra were recorded. Figure 4.10 shows the visual images (under UV light illumination) and PL spectra of PBA, PS-*b*-P4VP, PS-*b*-P4VP(PBA)<sub>0.5</sub>, FNDI, PS-*b*-P4VP(PBA+FNDI) and PBA+FNDI in the solid state. As discussed in the previous chapter, pure PBA shows yellowish-green fluorescence in the solid state with strong broad emission peak from 400 to 600 nm. The emission peaks of PBA were blue shifted and less broadened after complexation with block copolymer (PS-*b*-P4VP(PBA)<sub>0.5</sub>) and exhibits both monomer and excimer emission. As explained in the previous chapter, it might be due to the closely packed PBA and isolated PBA within the P4VP domains. Pure FNDI shows fjord blue colour in the solid state with an emission maxima at 461 nm due to the excimer formation from the aggregation of FNDI molecules.

As shown in Figure 4.10e and inset of 4.10h, upon the addition of FNDI to PS-*b*-P4VP(PBA)<sub>0.5</sub>, a drastic quenching of fluorescence of PBA was observed indicating the formation of alternate D-A stacks within the P4VP domains of the block copolymer. At the same time, under UV light illumination, the blue colour of PBA and fjord blue colour of FNDI changed to red colour upon the formation of CT complexes between PBA and FNDI within the block copolymer microdomains. On the other hand, the visual image and the PL spectrum of the physical blend (PBA+FNDI) are almost similar to that of the block copolymer supramolecular system indicating the formation of D-A stacks (Figure 4.10f and inset of 4.10h). These results are consistent with the UV-Vis spectroscopy results.

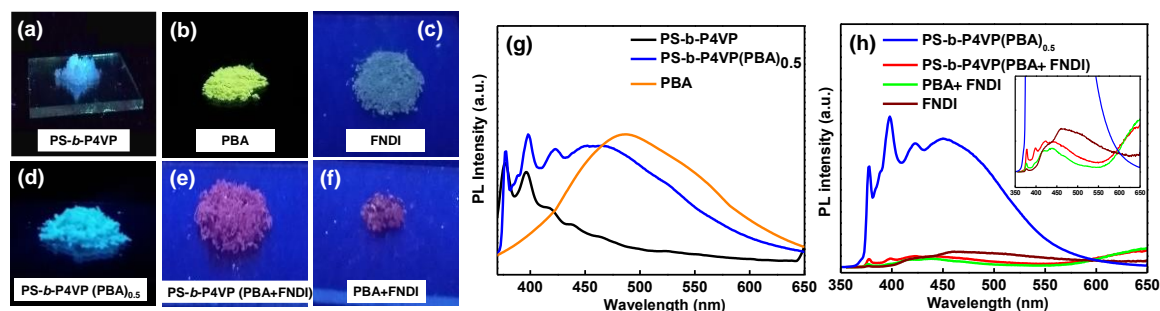


**Figure 4.10.** The visual appearance of (a) PS-*b*-P4VP, (b) PBA, (c) FNDI, (d) PS-*b*-P4VP(PBA)<sub>0.5</sub>, (e) PS-*b*-P4VP(PBA+FNDI), and (f) physical blend (PBA+FNDI) under UV light illumination. PL spectra of (g) PBA, PS-*b*-P4VP, PS-*b*-P4VP(PBA)<sub>0.5</sub> and (h) FNDI, PS-*b*-P4VP(PBA)<sub>0.5</sub>, PS-*b*-P4VP(PBA+FNDI) and physical blend (PBA+FNDI) in the solid state.

Based on the experimental findings from FTIR, SAXS/WAXS, UV/Vis spectroscopy and PL spectroscopy studies, the generation of hierarchical structures in block copolymer supramolecules could be rationalized as schematically shown in Figure 4.11. As analogous to the previous chapter, PBA, the donor molecule selectively forms hydrogen bonding with the pyridine units to form P4VP(PBA) comb block resulting in a hexagonally packed cylindrical morphology with an average center-to-center spacing of  $40 \pm 1$  nm. The

hierarchical assembly of PBA molecules within the P4VP domain is coordinated without any interdigitation that is apparent from the domain spacing (2.7 nm) obtained from the WAXS, which is twice the length of the PBA molecule (1.3 nm).<sup>43</sup> After the incorporation of acceptor molecule (FNDI), obtained a mixed morphology with dominant lamellae and minor fraction of cylinders, due to the increased volume fraction of P4VP(PBA+FNDI). As evident from the temperature-dependent WAXS studies, upon annealing, improved order in the arrangement of small molecules was observed and the ratio of WAXS peaks at lower  $2\theta$  (1:2) indicates the formation of lamellar structure within the lamellae of block copolymer supramolecules. Unlike the previous chapter, after the addition of acceptor molecules (length of energy minimized structure of FNDI is 1.98 nm), the spacing of the arrangement of small molecules increased to 3.0 nm indicating the formation of bilayer assembly of small molecules within the P4VP domains. The presence of  $-\text{COOH}$  group in the FNDI molecule favored the formation of H-bonding with 4VP chains and as a result, CT complexes are formed between the PBA and FNDI molecules which are hydrogen bonded with the same P4VP chains. This situation facilitates the formation of bilayer assembly of PBA and FNDI within the 4VP chains by retaining the hydrogen bonding between PBA and 4VP chains as well as FNDI and 4VP chains. UV/Vis spectroscopy and photoluminescence spectroscopy results confirmed the formation of charge transfer complex between PBA and FNDI through  $\pi$ - $\pi$  interaction. These results are different from that of the previous chapter, where the monolayer assembly was observed within the P4VP chains with the domain spacing of 1.9 nm in the case of NDI as acceptor (without COOH group). Thermal annealing of block copolymer supramolecules shows the excellent hierarchical assembly of small molecules within the block copolymer domains and it is due to the combined effect of both H-bonding between the donor as well as the acceptor molecules with 4VP and  $\pi$ - $\pi$  interaction between the PBA and FNDI.

---

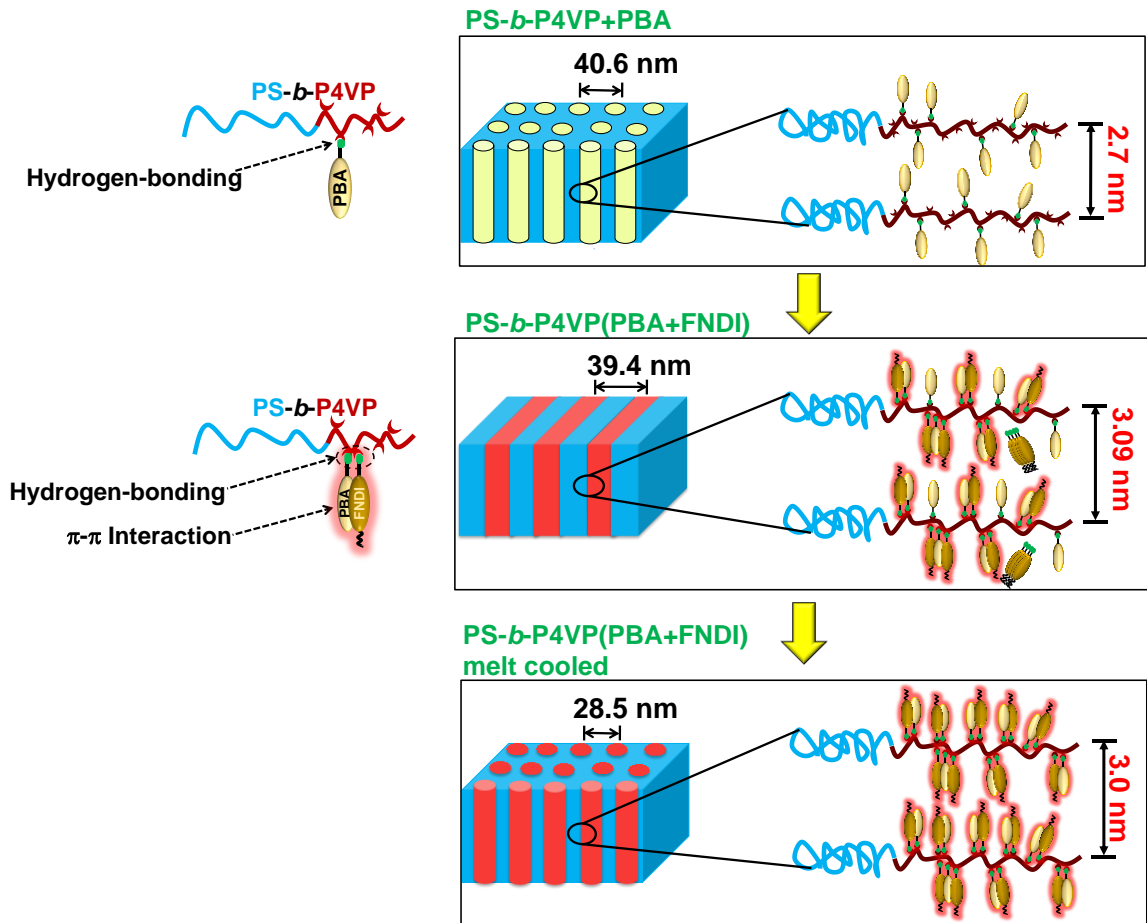


**Figure 4.11.** Schematic illustration of the hierarchical self-assembly of the donor (PBA) and acceptor molecules (FNDI) within the block copolymer microdomains.

The charge carrier mobilities of PS-*b*-P4VP(PBA+FNDI) and the physical blend of PBA+FNDI were evaluated using space charge limited current (SCLC) measurements using the method reported in the previous chapter. Effective charge carrier mobility was calculated using the Mott-Gurney equation given by,

$$I = \frac{9\mu_{eff} \epsilon_0 \epsilon_r AV^2}{8d^3}$$

Where  $I$  is the current,  $\mu_{eff}$  is the effective electron mobility measured,  $\epsilon_0$  is the permittivity of free space,  $\epsilon_r$  is the dielectric constant,  $A$  is the active device area,  $V$  is the voltage applied and  $d$  is the thickness of the film.

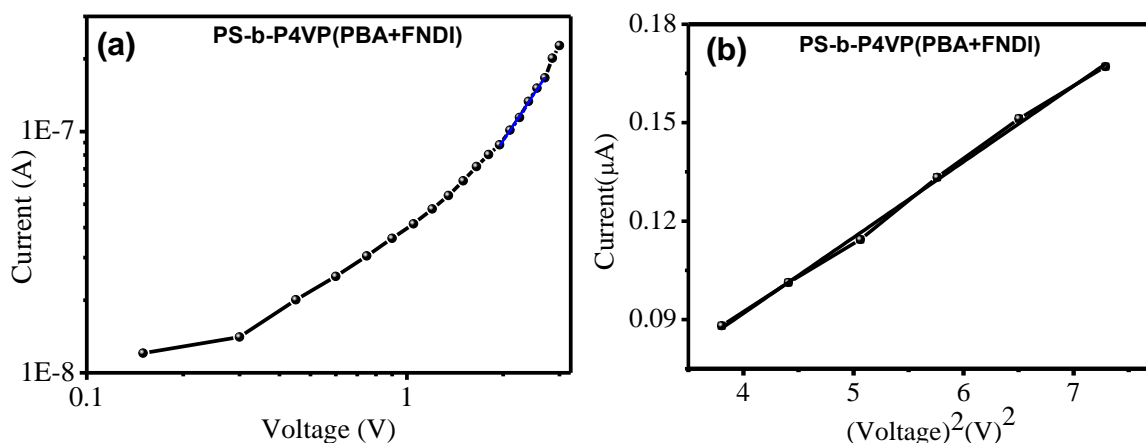


**Figure 4.12.** (a) Current versus voltage on the log scale and (b) current versus voltage<sup>2</sup> characteristics of the PS-*b*-P4VP(PBA+FNDI) with ITO and Al electrodes.

The film thickness measured for the block copolymer supramolecules (PS-*b*-P4VP(PBA+FNDI)) using the Dektak XT stylus profilometer was 3700 nm. But in the case of physical blend, it was difficult to obtain a uniform film due to the dewetting and rapid crystallization of small molecules.<sup>44, 45</sup> Figure 4.12 shows the current versus voltage plot on log scale observed in the sandwich structure of ITO/(PS-*b*-P4VP(PBA+FNDI))/Al where the region having a slope 2 is the SCLC region. The estimated bulk mobility of the PS-*b*-P4VP(PBA+FNDI) sample is  $1.01 \times 10^{-4}$  cm<sup>2</sup>/(Vs) which is higher than the charge carrier mobility obtained in our previous report using PS-*b*-P4VP(PBA+NDI) where NDI was used without COOH group. The charge carrier mobility value obtained here is comparable to the many conjugated polymers that have been used in OLEDs and OPVs.<sup>30,</sup>

46

## 4.6. Conclusions

In summary, we have investigated the multicomponent assembly of PS-*b*-P4VP and functionalized donor (1-pyrenebutyric acid, PBA) and acceptor (functionalized naphthalene diimide, FNDI) molecules. Both donor and acceptor molecules form hydrogen bonding with P4VP chains of the block copolymer and it resulted in the formation of bilayer

assembly of alternate donor-acceptor stacks within the P4VP domains. Thermal annealing of the block copolymer supramolecules resulted in the effective formation of stable hierarchical assemblies where efficient charge-transfer complexes are formed as bilayer lamellae within the block copolymer microdomains. These observations are different from the reported block copolymer supramolecules using PBA and non-functionalized NDI molecules, where the monolayer assembly of donor and acceptor was formed due to the interdigitation of donor and acceptor molecules because of the  $\pi$ - $\pi$  interactions. It was also observed that the introduction of a functional group on FNDI molecules favors the formation of stable D-A stacks in the physical blend as well. These results suggested that the incorporation of both functionalized donor and acceptor molecules within the block copolymer microdomains favors the stable CT complexes and as a result, the enhanced charge carrier mobility was observed, which may facilitate the design of devices in the field of electronics.

#### 4.7. References

- [1] Seiffert, S.; Sprakel, J. *Chem. Soc. Rev.* **2012**, 41 (2), 909-930.
- [2] De Greef, T. F. A.; Smulders, M. M. J.; Wolfs, M.; Schenning, A. P. H. J.; Sijbesma, R. P.; Meijer, E. W. *Chem. Rev.* **2009**, 109 (11), 5687-5754.
- [3] Li, S.-L.; Xiao, T.; Lin, C.; Wang, L. *Chem. Soc. Rev.* **2012**, 41 (18), 5950-5968.
- [4] Brunsveld, L.; Folmer, B. J. B.; Meijer, E. W.; Sijbesma, R. P. *Chem. Rev.* **2001**, 101 (12), 4071-4098.
- [5] Huang, F.; Scherman, O. A. *Chem. Soc. Rev.* **2012**, 41 (18), 5879-5880.
- [6] Das, A.; Ghosh, S. *Angew. Chem* **2014**, 126 (4), 1110-1115.
- [7] Das, A.; Ghosh, S. *Angew Chem Int Ed Engl* **2014**, 53 (8), 2038-54.
- [8] Kaliyappan, T.; Kannan, P. *Prog. Polym. Sci.* **2000**, 25 (3), 343-370.
- [9] Das, A.; Ghosh, S. *ChemComm* **2016**, 52 (42), 6860-6872.
- [10] Aida, T.; Meijer, E. W.; Stupp, S. I. *Science* **2012**, 335 (6070), 813-817.
- [11] Kim, F. S.; Ren, G.; Jenekhe, S. A. *Chem. Mater.* **2011**, 23 (3), 682-732.

- 
- 
- [12] Hoeben, F. J. M.; Jonkheijm, P.; Meijer, E. W.; Schenning, A. P. H. J. *Chem. Rev.* **2005**, 105 (4), 1491-1546.
- [13] Yeh, M.-Y.; Lin, H.-C. *Phys. Chem. Chem. Phys.* **2014**, 16 (44), 24216-24222.
- [14] Bhosale, R.; Míšek, J.; Sakai, N.; Matile, S. *Chem. Soc. Rev.* **2010**, 39 (1), 138-149.
- [15] Bradford, V. J.; Iverson, B. L. *J. Am. Chem. Soc.* **2008**, 130 (4), 1517-1524.
- [16] Pisula, W.; Kastler, M.; Wasserfallen, D.; Robertson, J. W. F.; Nolde, F.; Kohl, C.; Müllen, K. *Angew. Chem* **2006**, 45 (5), 819-823.
- [17] Li, J.; Guo, L.; Zhang, L.; Yu, C.; Yu, L.; Jiang, P.; Wei, C.; Qin, F.; Shi, J. *Dalton Trans* **2009**, (5), 823-831.
- [18] Shao, H.; Nguyen, T.; Romano, N. C.; Modarelli, D. A.; Parquette, J. R. *J. Am. Chem. Soc.* **2009**, 131 (45), 16374-16376.
- [19] Rao, K. V.; Jayaramulu, K.; Maji, T. K.; George, S. J. *Angew Chem Int Ed Engl* **2010**, 49 (25), 4218-22.
- [20] González-Rodríguez, D.; Schenning, A. P. H. J. *Chem. Mater.* **2011**, 23 (3), 310-325.
- [21] Yagai, S.; Kitamura, A. *Chem. Soc. Rev.* **2008**, 37 (8), 1520-1529.
- [22] Ajayaghosh, A.; Praveen, V. K. *Acc. Chem. Res* **2007**, 40 (8), 644-656.
- [23] Yagai, S. *Bull. Chem. Soc. Jpn.* **2015**, 88 (1), 28-58.
- [24] Molla, M. R.; Das, A.; Ghosh, S. *Chem.: Eur. J.* **2010**, 16 (33), 10084-10093.
- [25] Sikder, A.; Ghosh, B.; Chakraborty, S.; Paul, A.; Ghosh, S. *Chem.: Eur. J.* **2016**, 22 (6), 1908-1913.
- [26] Syamakumari, A.; Schenning, A. P. H. J.; Meijer, E. W. *Chem.: Eur. J.* **2002**, 8 (15), 3353-3361.
- [27] Wasielewski, M. R. *Chem. Rev.* **1992**, 92 (3), 435-461.
- [28] Guldi, D. M. *Chem. Soc. Rev.* **2002**, 31 (1), 22-36.
- [29] Alam, M. M.; Jenekhe, S. A. *Chem. Mater.* **2004**, 16 (23), 4647-4656.
- [30] Yu, G.; Gao, J.; Hummelen, J. C.; Wudl, F.; Heeger, A. J. *Science* **1995**, 270 (5243), 1789-1791.
- [31] Ikkala, O.; ten Brinke, G. *Science* **2002**, 295 (5564), 2407-9.
- [32] Hanski, S.; Houbenov, N.; Ruokolainen, J.; Chondronicola, D.; Iatrou, H.; Hadjichristidis, N.; Ikkala, O. *Biomacromolecules* **2006**, 7 (12), 3379-3384.
- [33] Ruokolainen, J.; Mäkinen, R.; Torkkeli, M.; Mäkelä, T.; Serimaa, R.; Brinke, G. t.; Ikkala, O. *Science* **1998**, 280 (5363), 557-560.
- 
-

- 
- 
- [34] Ruokolainen, J.; Torkkeli, M.; Serimaa, R.; Komanschek, B. E.; Ikkala, O.; ten Brinke, G. *Phys. Rev. E* **1996**, 54 (6), 6646-6649.
- [35] Wu, C.; Zhou, S. *Macromolecules* **1995**, 28 (15), 5388-5390.
- [36] Osuji, C.; Ferreira, P. J.; Mao, G.; Ober, C. K.; Vander Sande, J. B.; Thomas, E. L. *Macromolecules* **2004**, 37 (26), 9903-9908.
- [37] Zhou, Y.; Ahn, S.-k.; Lakhman, R. K.; Gopinadhan, M.; Osuji, C. O.; Kasi, R. M. *Macromolecules* **2011**, 44 (10), 3924-3934.
- [38] Morikawa, Y.; Nagano, S.; Watanabe, K.; Kamata, K.; Iyoda, T.; Seki, T. *Adv. Mater* **2006**, 18 (7), 883-886.
- [39] Deepthi, K.; Amal, R. R. B.; Rajeev, V. R.; Unni, K. N. N.; Gowd, E. B. *Macromolecules* **2019**, 52 (7), 2889-2899.
- [40] Singha, N.; Gupta, P.; Pramanik, B.; Ahmed, S.; Dasgupta, A.; Ukil, A.; Das, D. *Biomacromolecules* **2017**, 18 (11), 3630-3641.
- [41] Das, A.; Ghosh, S. *Angew. Chem* **2014**, 53 (8), 2038-2054.
- [42] Pramanik, B.; Ahmed, S.; Singha, N.; Das, B. K.; Dowari, P.; Das, D. *Langmuir* **2019**, 35 (2), 478-488.
- [43] Sofos, M.; Goldberger, J.; Stone, D. A.; Allen, J. E.; Ma, Q.; Herman, D. J.; Tsai, W.-W.; Lauhon, L. J.; Stupp, S. I. *Nat. Mater* **2009**, 8 (1), 68-75.
- [44] Katz, H. E.; Bao, Z.; Gilat, S. L. *Acc. Chem. Res* **2001**, 34 (5), 359-369.
- [45] Ma, B.; Woo, C. H.; Miyamoto, Y.; Fréchet, J. M. J. *Chem. Mater.* **2009**, 21 (8), 1413-1417.
- [46] Zhu, Z.; Waller, D.; Gaudiana, R.; Morana, M.; Mühlbacher, D.; Scharber, M.; Brabec, C. *Macromolecules* **2007**, 40 (6), 1981-1986.
- 
-



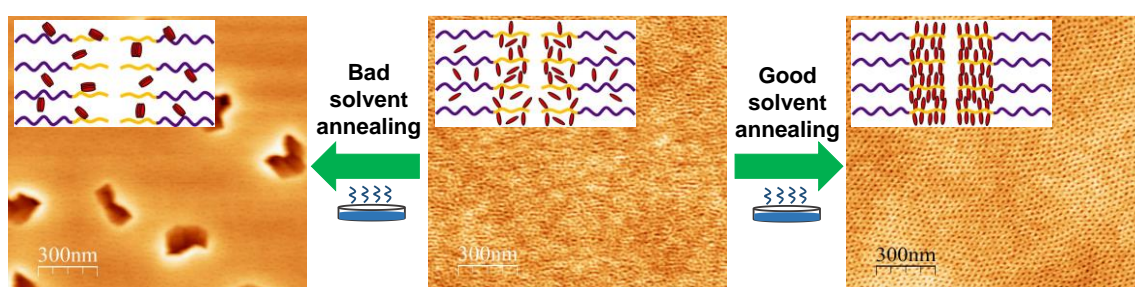
---

---

# Factors Influencing the Formation of Block Copolymer-based Supramolecular Assemblies in Bulk and Thin Films

---

---



### 5.1. Abstract

*The factors that control the formation of supramolecular assemblies (SMAs) by hydrogen bonding using polystyrene-block-poly(4-vinyl pyridine) (PS-*b*-P4VP) and biphenyl systems containing different functionalities were investigated both in bulk as well as in thin films. 4-Hydroxybiphenyl (4HB) (hydroxyl functionalized), biphenyl-4-carboxylic acid (BPCA) (carboxyl functionalized) and 4'-hydroxy-4-biphenylcarboxylic acid (HBCA) (with both hydroxyl and carboxyl functionalities) were chosen as small molecules. Phase behaviour of SMAs in bulk was studied by temperature-dependent wide-angle and small-angle X-ray scattering. All the SMAs showed the macrophase separation of small molecules in solvent casted samples. Heating or annealing above the glass transition temperature of block copolymers turned out to be a crucial factor in the effective formation of SMAs in the case of 4HB. On the other hand, SMAs formation is not that effective in the case of the carboxylic group-containing small molecules (BPCA and HBCA). Heating or annealing of*

*as casted films above the melting temperature of small molecules leads to the homogeneous dispersion of BPCA and HBCA in SMAs due to the breakage of hydrogen-bonds. In thin films, SMAs formation by solvent vapor annealing is sensitive to the selectivity of solvents to constituted blocks and small molecules. Breaking of self-association of small molecules by heating above the melting temperature of small molecules or annealing in a good solvent for both block copolymers and the small molecules is a key factor in the formation of SMAs in bulk and thin films. The present study provides a guideline for the basic design of effective SMAs using different kinds of small molecules, block copolymers and annealing conditions.*

## **5.2. Introduction**

Self-assembly of block copolymers is of immense interest in the field of nanotechnology because of its ability to form ordered periodic structures in the nanoscopic length scale.<sup>1-7</sup> Due to the inherent immiscibility of different polymeric segments, block copolymers undergo microphase separation in bulk as well as in thin films. Further, the research community developed a strategy to introduce functionalities into the block copolymer systems by combining the supramolecular chemistry with block copolymer self-assembly.<sup>8-22</sup> The block copolymer-based supramolecular assemblies (SMAs) are produced by the association of small molecules with one of the polymer blocks by noncovalent interaction such as hydrogen bonding, electrostatic interactions,  $\pi$ - $\pi$  interactions, van der Waals forces, etc.<sup>9-11, 18-20, 23-28</sup> One of the important aspects of block copolymer based SMAs is the tunability of morphologies using a single block copolymer by varying the stoichiometry between small molecules and block copolymer and thereby avoiding the burden of synthesizing new block copolymers.<sup>9, 11, 17, 23, 29</sup> These morphological transitions occur due to the change in the volume fraction of constituting blocks with respect to the incorporation of small molecules. In the case of sufficiently long small molecules, the

---

---

---

resulting SMAs show hierarchical structures (structure-within-structure) with larger-length scale formed by block copolymer self-assembly and the smaller length scale corresponding to the small molecules assembly within the block copolymer microdomains.<sup>9, 13, 21, 22, 30, 31</sup> Another major advantage of SMAs is the removal of small molecules by selective dissolution and to create a nanoporous material, which provides fascinating opportunities for nanotechnology applications.<sup>11, 12</sup>

Extensive studies have been carried out to explore the phase behaviour of block copolymer-based SMAs in bulk and thin films. Among these, the works on SMAs based on poly(styrene)-*block*-poly(4-vinyl pyridine) (PS-*b*-P4VP) and mono-functionalized 3-pentadecyl phenol (PDP) have been discussed elaborately in the literature.<sup>8, 10, 13, 18, 19, 22, 32-36</sup> Ikkala and ten Brinke demonstrated that the annealing of PS-*b*-P4VP(PDP) leads to the formation of ordered hierarchical structures.<sup>8, 10, 22, 33</sup> Upon annealing, multiple order-order transitions were observed in these SMAs due to the diffusion of PDP molecules within the polymer blocks. In certain cases, macrophase separation of small molecules was observed depending on the annealing conditions.<sup>16, 37</sup> Xu et al. incorporated organic semiconductors within the block copolymer SMAs and observed that these molecules macrophase separate from the block copolymers in solution cast films due to their strong crystallization tendency.<sup>14, 38-40</sup> Upon annealing, these molecules interact with the nitrogen of the 4-vinyl pyridine groups through hydrogen bonding leading to the change in the block copolymer domain spacing. They have also reported that incorporation of small molecules with two binding sites changes the kinetic pathways of the SMAs formation due to the change in the enthalpic and entropic interactions between small molecules and block copolymers.<sup>40</sup> Recently, we have reported the alternate co-assembly of donor and acceptor molecules within the block copolymer SMAs in the solid-state through non-covalent interactions.<sup>23</sup> Here we observed that as prepared block copolymer SMAs contain macrophase-separated

---

---

small molecules, while heating close to the melting temperature of the small molecules favours the formation of effective interactions between the small molecules and P4VP domains resulting in hierarchical structures. Though some reports are available in the literature on the role of small molecules on the phase behaviour of SMAs, it is not clear how the glass transition temperature ( $T_g$ ) of polymers in block copolymer and melting temperature of small molecules affect the annealing induced phase behaviour of block copolymer SMAs.

Apart from bulk, a large number of studies have been carried out on thin films of block copolymer SMAs due to their application potency. Ten Brinke et al. and Tung et al. mainly focused on the formation of PS-*b*-P4VP(PDP) and discussed the terrace formation and microdomain orientation depending upon the solvents used for the solvent vapor annealing process.<sup>13, 19, 41, 42</sup> Stamm and co-workers have investigated the SMA formation between PS-*b*-P4VP and 2-(4'-hydroxyphenylazo) benzoic acid (HABA), which possesses both carboxyl and hydroxyl functional group for hydrogen bonding with P4VP. They found that depending on the molar ratio between HABA and 4VP units, the SMA exhibits a morphological transition from cylinders to lamellae both in the case of bulk as well as in thin films.<sup>11, 12, 29, 43, 44</sup> Furthermore, the selectivity of the solvent as well as the degree of swelling plays a crucial role for switching the orientation of cylindrical microdomains of P4VP/HABA in thin films.<sup>11, 12, 29, 44</sup> Bazuin and co-workers studied the SMA formation by choosing a small molecule with single functionality and compared the influence of hydroxy-functionalized small molecule with identical carboxylic acid-functionalized small molecule in SMA thin films.<sup>20, 27, 45, 46</sup> For that purpose, they selected naphthol (NOH) and naphthoic acid (NCOOH) as small molecules. Based on their studies, they claimed that stripe morphologies were obtained with NCOOH, whereas dot morphology was attained with NOH under similar conditions. The stripe morphology is favoured not only by

---

---

NCOOH but also by dip-coating rates, higher solution concentrations, ratio of small molecules to 4VP, etc. Importantly they discussed the possible reasons for the stripe morphology with respect to the fraction of small molecules and degree of P4VP selectivity in thin films and concluded that NCOOH has greater hydrogen bond strength with P4VP than NOH.<sup>20</sup> Wu and Bubeck studied the influence of chemical structures and molar ratio of small molecules on the solvent vapor annealing induced macro- and microphase separation of block copolymer SMAs using carboxyl- and phenol containing azo compounds and PS-*b*-P4VP.<sup>47</sup> They reported that phenolic groups as hydrogen-bonding moieties suppress the macrophase separation in SMAs compared to the carboxylic group containing small molecules due to the self-associated hydrogen bonds of carboxylic groups. Though some studies are available in the literature on the formation of thin films using block copolymer SMAs with mono-functionalized and multi-functionalized small molecules, no systematic study is available to understand the influence of chemical structure and selectivity of solvent to small molecules on the solvent vapor induced phase behaviour of SMAs in thin films.

Herein, we aim to understand the influence of the chemical structure of small molecules on the formation of block copolymer SMAs both in bulk and thin films using PS-*b*-P4VP. For that purpose, we have chosen three identical biphenyl systems as small molecules, one with hydroxyl functionalized groups (4-hydroxybiphenyl (4HB)), the other with carboxylic functionalized groups (Biphenyl-4-carboxylic acid (BPCA)) and the last one having both functionalities (4'-hydroxy-4-biphenylcarboxylic acid (HBCA)) (Figure 5.1). Temperature-dependent wide-angle and small-angle X-ray scattering was used to understand the phase behaviour of SMAs in bulk. It was shown that the glass transition temperature of polymers played a crucial role in the effective SMA formation in the case of a hydroxyl-functionalized small molecule (4HB). On the other hand, both BPCA and

---

---

HBCA show the macrophase separation of small molecules in SMAs and the small molecules remain in the crystalline state up to their melting temperature, which may be due to the self-associated hydrogen bonds of carboxylic groups within small molecules. It will be shown that in thin films, the selectivity of the solvents to small molecules and to the block copolymer has a significant effect on the microphase separation of SMAs. Solvent vapor annealing of SMAs using a bad solvent leads to the crystallization of small molecules within the SMAs and that resulted in poorly ordered morphologies due to a variation of volume fractions with the P4VP block. Complete macrophase separation of small molecules was also observed. It was also shown that using a good solvent for small molecules and block copolymers, the formation of perpendicular cylindrical morphology was observed irrespective of the functional groups present in small molecules without any traces of macrophase separation of small molecules.

### 5.3. Experimental Section

**5.3.1. Materials:** PS-*b*-P4VP with  $M_n = 35500 \text{ g mol}^{-1}$  for PS,  $M_n = 4400 \text{ g mol}^{-1}$  for P4VP and PDI ( $D$ ) = 1.06, which favours the spherical morphology in bulk according to the volume fraction of PS (89%) and P4VP (11%) was supplied by Polymer Source, Inc. 4-hydroxybiphenyl (4HB), 4'-hydroxy-4-biphenyl carboxylic acid (HBCA) and biphenyl-4-carboxylic acid (BPCA), tetrahydrofuran, toluene, dichloromethane and chloroform were purchased from Sigma-Aldrich. Silicon wafers were purchased from Semiconductor Processing Co. and used as substrates to prepare SMA thin films after cleaning using a standard procedure reported elsewhere.<sup>12, 51</sup>

**5.3.2. Sample Preparation:** The supramolecular assemblies of PS-*b*-P4VP block copolymer with various small molecules (1 mol of 4VP monomer unit: 1 mol of small molecule) were prepared in toluene/THF (75:25) solvent mixture. PS-*b*-P4VP and small molecules were dissolved separately in the solvent mixture. The PS-*b*-P4VP solution was

---

---

---

added slowly to the small molecule solution at a temperature close to boiling point of the solvent in an ultrasonic bath. Such prepared 1 wt% solution was kept for one week to ensure the hydrogen-bonding formation between 4VP and small molecules. Bulk samples were prepared by evaporating solvents slowly. Thin films were prepared by dip-coating from the filtered solutions (1 wt% 1,4-dioxane) at a rate of 1.0 mm s<sup>-1</sup>. Dip-coated thin films were further annealed in a sealed glass chamber containing saturated vapors of solvents. The colour of the swollen SMA thin films changes at room temperature when the swelling ratio was approximately 2.5. Then the glass chamber was opened and allowed the solvent to evaporate rapidly. For the AFM imaging, solvent vapor annealed thin films were further rinsed in methanol for about 20 min to generate the nanoporous films by dissolving the small molecules.

#### **5.4. Characterization**

Wide-angle and small-angle X-ray scattering (WAXS/SAXS) measurements were carried out on a XEUSS SAXS/WAXS system from Xenocs (operated at 0.6 mA and 50 kV) and a mar345dtb image plate detector. All the measurements were carried out in the transmission mode using Cu K $\alpha$  radiation ( $\lambda = 1.54 \text{ \AA}$ ). The recorded fiber diagrams were processed using the Fit2D software. The detector was set at 221.75 mm and 1050 mm in the X-ray beam direction for WAXS and SAXS data collections and the scattering vector range was calibrated using a silver behenate standard. Variable temperature measurements were performed using a Linkam THMS 600 hot stage connected to the LNP 95 cooling system. The hot stage was placed in the X-ray path and the X-ray patterns were obtained at the interval of 20 °C. The data collection time was 10 min and the heating rate was set at 10 °C/min. Grazing-incidence small-angle X-ray scattering (GISAXS) measurements were performed at HASYLAB (DESY, Hamburg, Germany) on the beamline BW4 of the

---

---

DORIS III storage ring. The wavelength of the X-ray used was  $\lambda = 0.138$  nm. The scattering patterns were recorded on a 2D detector (MARCCD; 2048 x 2048 pixel). 1-Dimensional intensity profiles are reported as  $q$  vs.  $I$ , where  $q = (4\pi/\lambda) \sin(\theta)$ ,  $\lambda$  is the wavelength of incident X rays, and  $\theta$  is the scattering angle. Infrared spectra were recorded in the reflectance mode with a Bruker IFS 66v FTIR spectrometer over the wavenumber range of 4000-400  $\text{cm}^{-1}$  using SMA thin films deposited on cleaned silicon wafers. Atomic force microscopy (AFM) imaging of SMA thin films was probed using a Dimensions 3100 scanning force microscope (NanoScope IV Controller) in the tapping mode. Differential scanning calorimetry (DSC) measurements were carried out using TA Q2000 under nitrogen atmosphere at a rate of 10  $^{\circ}\text{C}/\text{min}$ .

## 5.5. Results and Discussion

The PS-*b*-P4VP block copolymer was solution blended with three different small molecules (shown in Figure 5.1) in toluene/THF (75:25) solvent mixture and the stoichiometric ratio between the 4VP unit and small molecule was fixed at 1.0 in all the SMAs. All three small molecules are designed to have the same backbone structure with different functional moieties to construct the SMAs so that the influence of functional groups on the SMA formation can be studied systematically.

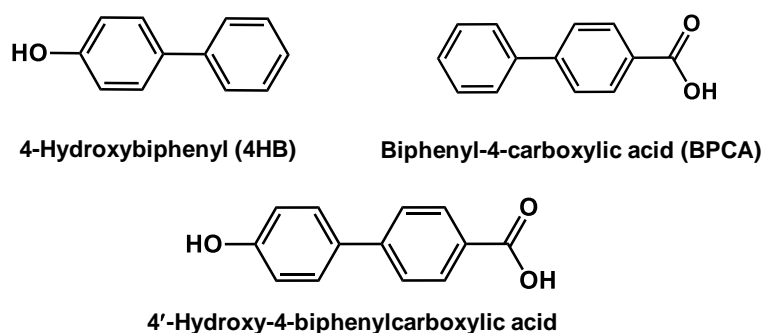


**Figure 5.1.** Chemical structures of three different small molecules used in this study.

The formation of SMAs with three small molecules was confirmed by FTIR spectra, as shown in Figure 5.2, 5.3 and 5.4. PS-*b*-P4VP block copolymer contributes an absorption

peak at  $993\text{ cm}^{-1}$  corresponding to the free pyridine group (symmetric ring stretching mode), which is shifted to higher wavenumbers after forming the SMAs with small molecules.<sup>8, 10, 13, 27, 48</sup> After the formation of the hydrogen bonding with the pyridine group, the absorption band shifts to  $1005\text{ cm}^{-1}$ ,  $1008\text{ cm}^{-1}$  and  $1014\text{ cm}^{-1}$  for PS-*b*-P4VP(4HB)<sub>1</sub>, PS-*b*-P4VP(BPCA)<sub>1</sub> and PS-*b*-P4VP(HBCA)<sub>1</sub>, respectively. The wavenumber shift is larger in the case of COOH containing small molecules indicating the formation of stronger hydrogen-bonding between COOH and pyridine groups. Roland et al. reported a similar observation using SMAs containing 1-naphthol and 1-naphthoic acid as small molecules.<sup>20, 27, 45, 46</sup> As seen from Figures 5.3 and 5.4, the shift of another free pyridine band at  $1415\text{ cm}^{-1}$  also follows the same trend. Clear spectral changes in the region of  $1610\text{--}1585\text{ cm}^{-1}$  further confirm the hydrogen-bonding between pyridine groups and small molecules.<sup>49</sup> This spectral region is corresponding to the aromatic groups of block copolymer and small molecules. It is worth mentioning here that a small peak at  $993\text{ cm}^{-1}$  after the SMAs formation indicates the presence of few free pyridine groups that may be due to the macrophase separation of small molecules in as casted films and details will be discussed in the following sections.

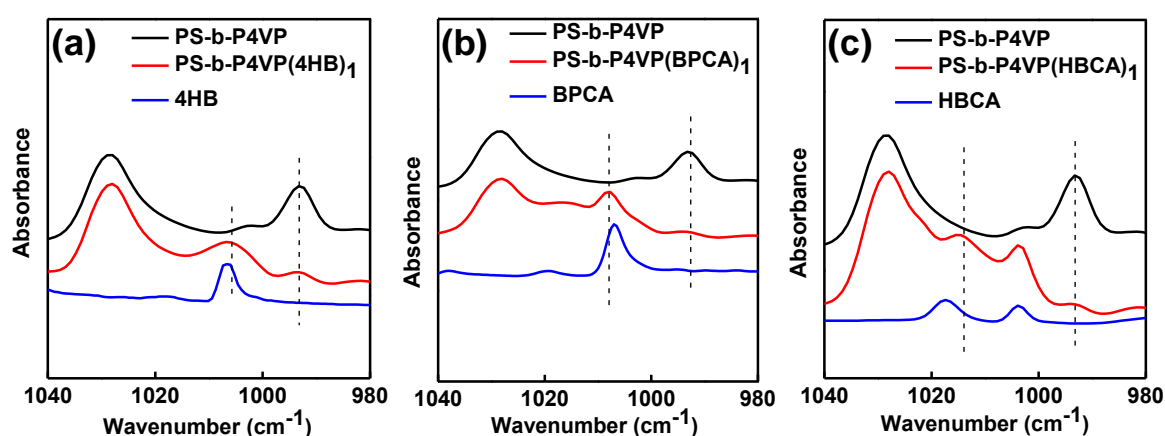


**Figure 5.2.** FTIR spectra of (a) PS-*b*-P4VP, PS-*b*-P4VP(4HB)<sub>1</sub>, and 4HB (b) PS-*b*-P4VP, PS-*b*-P4VP(BPCA)<sub>1</sub>, and BPCA (c) PS-*b*-P4VP, PS-*b*-P4VP(HBCA)<sub>1</sub>, and HBCA in the region of  $1040\text{--}980\text{ cm}^{-1}$ .

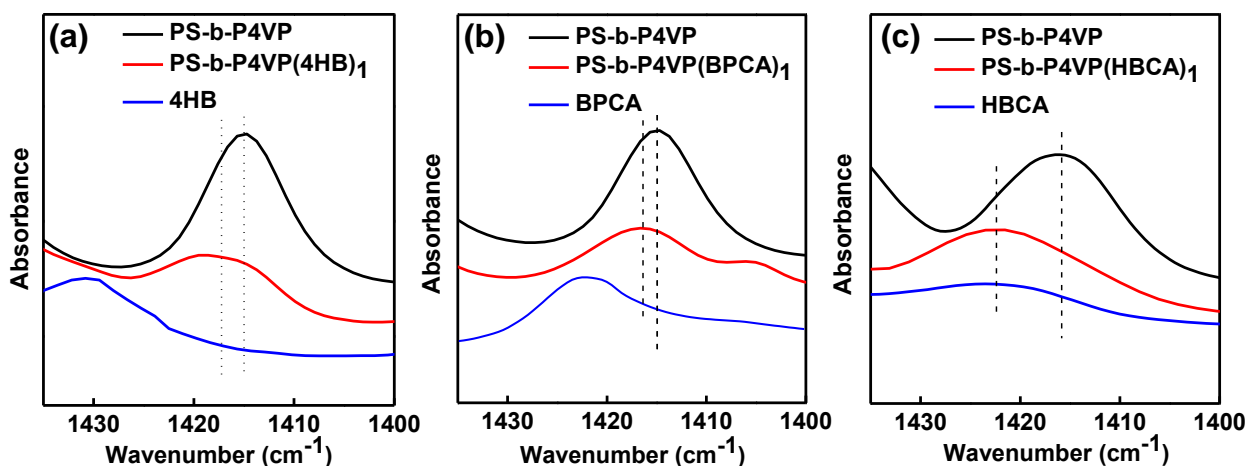


**Figure 5.3.** FTIR spectra of (a) PS-*b*-P4VP, PS-*b*-P4VP(4HB)<sub>1</sub> and 4HB (b) PS-*b*-P4VP, PS-*b*-P4VP(BPCA)<sub>1</sub> and BPCA (c) PS-*b*-P4VP, PS-*b*-P4VP(HBCA)<sub>1</sub> and HBCA in the region of 1435-1400 cm<sup>-1</sup>.

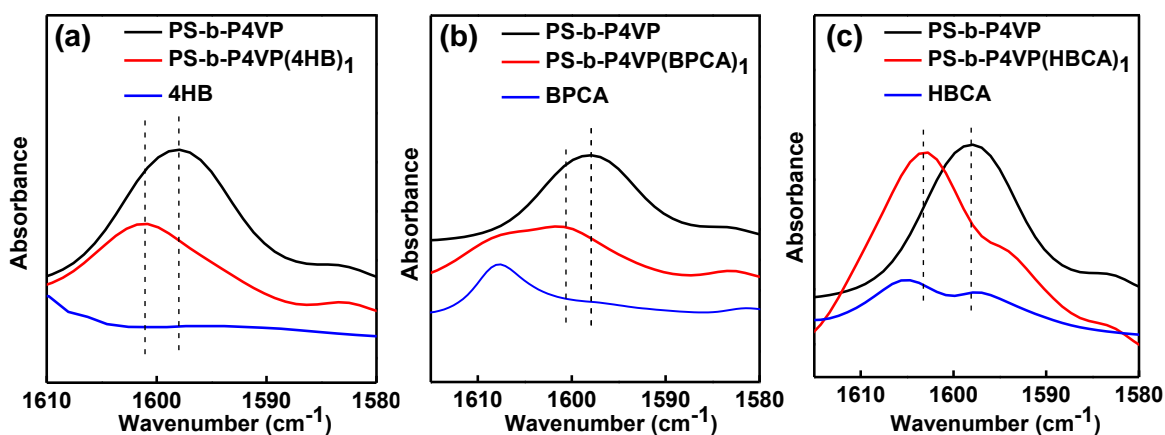


**Figure 5.4.** FTIR spectra of (a) PS-*b*-P4VP, PS-*b*-P4VP(4HB)<sub>1</sub> and 4HB (b) PS-*b*-P4VP, PS-*b*-P4VP(BPCA)<sub>1</sub> and BPCA, (c) PS-*b*-P4VP, PS-*b*-P4VP(HBCA)<sub>1</sub> and HBCA in the region of 1580-1610 cm<sup>-1</sup>.

### 5.5.1. Effect of Small Molecules on the SMA Formation in Bulk

The macro- and microphase separation structures and morphologies in block copolymer SMAs were investigated by both wide-angle and small-angle X-ray scattering (WAXS/SAXS). Figure 5.5 shows the temperature-dependent WAXS and SAXS patterns of PS-*b*-P4VP(4HB)<sub>1</sub> upon heating (up to 210 °C) at a rate of 10°C/min. At every 20 °C interval, the sample was allowed to equilibrate for 10 min for the data collection for both

---

---

WAXS and SAXS. The WAXS pattern of pristine 4HB is shown in Figure 5.5a for the comparison and it shows multiple reflections corresponding to the crystal structure of 4HB. The room temperature WAXS pattern of the solvent casted PS-*b*-P4VP(4HB)<sub>1</sub> shows less intense crystalline reflections corresponding to the 4HB superimposed with the amorphous halo of PS-*b*-P4VP indicating the macrophase-separation of some of the 4HB within the block copolymer SMAs. The corresponding SAXS pattern shows a broad peak centered at  $q = 0.22 \text{ nm}^{-1}$  ( $d = 28.2 \text{ nm}$ ). Based on the room temperature WAXS and SAXS patterns, we are speculating that in solvent casted samples, some of the free 4HB molecules might be stabilized as aggregates both in PS and P4VP microdomains and that resulted in the poorly ordered morphology of SMAs. Similar kinds of observations were made in other SMAs reported in the literature.<sup>16, 37, 40, 47</sup> Upon heating, the WAXS reflections corresponding to the pure 4HB disappeared completely at around 100 °C and only the peaks corresponding to the amorphous PS-*b*-P4VP is seen above 100 °C. It means that the macrophase separated 4HB molecules dispersed at the molecular level due to the segmental mobility of PS chains and diffused into the P4VP domains. These results suggest that the interactions between 4HB molecules are weak and the segmental mobility of polymer chains can facilitate the dispersion of 4HB molecules at molecular level. The corresponding SAXS patterns above 100 °C show well-resolved sharp peaks at  $q = 0.216, 0.368$  and  $0.432 \text{ nm}^{-1}$ , whose positions are in the ratio of 1: $\sqrt{3}$ :2 indicating the formation of cylindrical morphology. The SAXS patterns revealed the effective microphase separation of SMAs above 100 °C, which might be due to the complete diffusion of 4HB molecules to the P4VP domains and the formation of hydrogen-bonding between the dispersed 4HB molecules and P4VP domains. As seen in Figure 5.5c, the domain spacing (periodicity) increased slightly at this temperature, which could be due to the diffusion of 4HB molecules to the P4VP domain. It has to be noted that the molecular dispersion of 4HB molecules occurred well

---

---

below the melting temperature of 4HB ( $T_m = 165 \pm 1$  °C) which could be possibly related to increased segmental mobility ( $T_g$ ) of PS and P4VP domains. Xu and coworkers reported similar kind of observation in the case of oligothiophene containing SMAs where the oligothiophenes diffuse through PS domains to form the hydrogen bonds with 4VP chains well below the melting temperature of small molecules.<sup>16, 40</sup> On further heating, at around 165 °C, the domain spacing of SMA increased gradually with the temperature up to 210 °C. This behaviour is different from the work reported by Xu and coworkers, where they reported the decrease in the domain spacing at the melting of P4VP(oligothiophene) domains.<sup>16</sup> This anomalous behaviour might be due to the rigidity of the small molecule used for the formation of SMAs. Based on the WAXS and SAXS results, the arrangement of small molecules within the block copolymer SMAs during annealing is schematically depicted in Figure 5.5d. Solution casted PS-*b*-P4VP(4HB)<sub>1</sub> shows the domain spacing  $28.2 \pm 1$  nm, where some of the 4HB molecules are agglomerated both in PS and P4VP domains. Upon heating, above the  $T_g$  of PS, the complete dispersion of 4HB molecules within P4VP domains was observed and at the same time, the hexagonally packed cylindrical morphology was formed with the domain spacing of  $29.0 \pm 1$  nm. It means the thermal annealing facilitated the diffusion of 4HB molecules to P4VP domains, and as a result, the effective microphase separation was observed with a slight increase in the domain spacing.

---

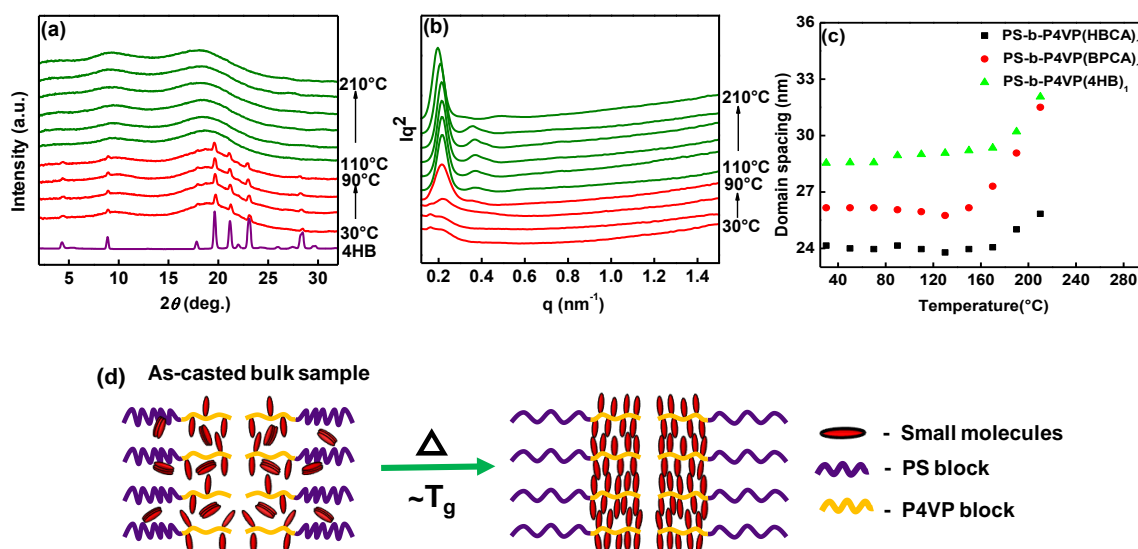


**Figure 5.5.** Temperature-dependent (a) WAXS patterns, (b) Lorentz-corrected SAXS patterns of PS-*b*-P4VP(4HB)<sub>1</sub>, (c) *d*-spacing estimated from the first ordered peak from Figure 5.5b and (d) schematic illustration explaining the arrangement of small molecules within the block copolymer SMAs before and after annealing. For the comparison, the WAXS pattern of pristine 4HB is shown in Figure 5.5a at the bottom.

Figure 5.6 shows the temperature-dependent WAXS and SAXS patterns of PS-*b*-P4VP(BPCA)<sub>1</sub> and PS-*b*-P4VP(HBCA)<sub>1</sub> upon heating at a rate of 10°C/min up to 230 °C and 300 °C, respectively. For the comparison, room temperature WAXS patterns of small molecules, i.e., BPCA and HBCA are incorporated in Figures 5.6a and 5.6c. Room temperature WAXS patterns of solution casted PS-*b*-P4VP(BPCA)<sub>1</sub> and PS-*b*-P4VP(HBCA)<sub>1</sub> show the reflections corresponding to the respective small molecules superimposed on the broad amorphous halo of the block copolymer. This indicates the macrophase separation of small molecules within the block copolymer SMAs similar to the aforementioned solution casted PS-*b*-P4VP(4HB)<sub>1</sub> at room temperature. The corresponding SAXS patterns of PS-*b*-P4VP(BPCA)<sub>1</sub> and PS-*b*-P4VP(HBCA)<sub>1</sub> show single peaks at  $q = 0.24 \text{ nm}^{-1}$  ( $d = 26.2 \text{ nm}$ ) and  $q = 0.257 \text{ nm}^{-1}$  ( $d = 24.4 \text{ nm}$ ), respectively. No higher-ordered peaks were observed at room temperature, indicating the poorly ordered morphology of

SMAAs in both the cases. Compared to PS-*b*-P4VP(4HB)<sub>1</sub>, the domain spacings of PS-*b*-P4VP(BPCA)<sub>1</sub> and PS-*b*-P4VP(HBCA)<sub>1</sub> decreased by ~ 2 nm and ~ 4 nm, respectively and that might be because of the change in the volume fraction of P4VP(BPCA) and P4VP(HBCA) domains due to the agglomeration of small molecules as seen in the room temperature WAXS patterns of SMAAs. Upon heating, the WAXS reflections corresponding to small molecules remained as such in SMAAs up to 190 °C and 250 °C for PS-*b*-P4VP(BPCA)<sub>1</sub> and PS-*b*-P4VP(HBCA)<sub>1</sub>, respectively. Unlike the PS-*b*-P4VP(4HB)<sub>1</sub>, in these cases,  $T_g$  of PS in block copolymer did not show much influence on the molecular level dispersion of small molecules. As a result, the macrophase separated small molecules remained until the temperature reached close to the melting temperature of small molecules (see Figure 5.7). However, the gradual decrease in the intensity of WAXS reflections corresponding to small molecules was observed above the  $T_g$  of PS, indicating the slow diffusion of small molecules into the P4VP domains. In both cases, the WAXS reflections corresponding to small molecules disappeared at the higher temperatures close to the melting temperature of small molecules. It has to be noted that carboxylic group is present in both these small molecules. It was reported that the self-association of hydrogen bonding is strong in the small molecules containing carboxylic groups.<sup>47</sup> Unlike the case of PS-*b*-P4VP(4HB)<sub>1</sub> as discussed above, the segmental mobility of polymer chains is not enough to break the self-association of carboxylic groups in (PS-*b*-P4VP(BPCA)<sub>1</sub> and PS-*b*-P4VP(HBCA)<sub>1</sub>) below their melting temperature.

---

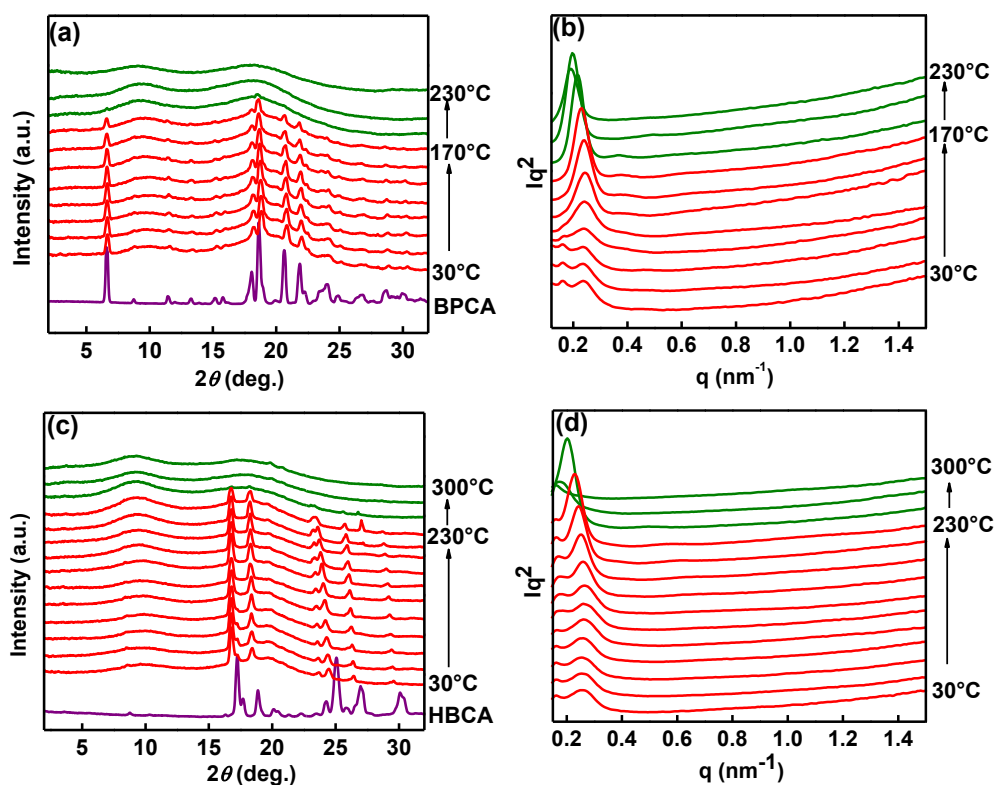


**Figure 5.6.** Temperature-dependent (a and b) WAXS patterns and Lorentz-corrected SAXS patterns of PS-*b*-P4VP(BPCA)<sub>1</sub> and (c and d) WAXS patterns and Lorentz-corrected SAXS patterns of PS-*b*-P4VP(HBCA)<sub>1</sub>. For the comparison, WAXS patterns of BPCA and HBCA are shown in Figure 5.6a and Figure 5.6c, respectively.

During heating, a gradual increase in the intensity of the first-ordered peak was observed in the SAXS patterns of PS-*b*-P4VP(BPCA)<sub>1</sub> above the  $T_g$  of PS in the block copolymer. At the same time, the weak second ordered peak appeared with the increase in the temperature, indicating the formation of ordered microphase separated morphology of block copolymer SMA. The ratio of peak positions suggests the formation of mixed morphologies (spherical and cylindrical order) at higher temperatures, just below the melting temperature of BPCA. The formation of mixed morphologies might be due to the macrophase separation of BPCA, which results in the variation of the stoichiometric ratio between 4VP and small molecules.<sup>47</sup> When the temperature reaches close to the melting, as reported by ten Brinke and co-workers, there is a possibility of complete breakage of

hydrogen-bonds between 4VP chains and small molecules.<sup>50</sup> As seen from Figure 5.5c, the domain spacing of PS-*b*-P4VP(BPCA)<sub>1</sub> increased significantly above 150 °C, indicating the order-to-order transition in this temperature range due to the diffusion of small molecules within the block copolymer domains. As the higher-ordered peaks in SAXS patterns are not clearly visible, it is difficult to understand the morphology in these samples. Almost similar kind of observation is made in the SAXS patterns of PS-*b*-P4VP(HBCA)<sub>1</sub> during heating, albeit the difference in the order-to-order transition temperature. On further heating, the order-to-disorder transition of SMA was also observed at a temperature above 270 °C. The WAXS and SAXS results of PS-*b*-P4VP(BPCA)<sub>1</sub> and PS-*b*-P4VP(HBCA)<sub>1</sub> indicated that the small molecules with COOH groups behave quite differently from the small molecules containing only the hydroxyl groups. In the case of BPCA and HBCA, the presence of COOH groups leads to strong self-association, and as a result, the hydrogen bonding between carboxylic groups of BPCA and HBCA retained until the melting temperature of the small molecules. Due to this, the macrophase separated morphology was observed up to the melting temperature of small molecules in the case of PS-*b*-P4VP(BPCA)<sub>1</sub> and PS-*b*-P4VP(HBCA)<sub>1</sub>. Whereas in the case of a hydroxyl-containing small molecule (4HB), due to the weaker hydrogen bonding, major rearrangements occurred close to the  $T_g$  of polymers, and as a result, the macrophase separation of small molecules was completely resolved. A similar kind of observation was made in thin films of block copolymer SMAs containing azo compounds as small molecules with COOH and OH groups.<sup>47</sup> These results suggest that thermal annealing is not a suitable method for the SMAs with carboxylic groups containing small molecules and thermal annealing at higher temperatures could lead to the sublimation or degradation of small molecules. That results in the variation of the stoichiometric ratio between 4VP and small molecules in SMAs, leading to the formation of mixed morphologies or disordered morphologies.

---

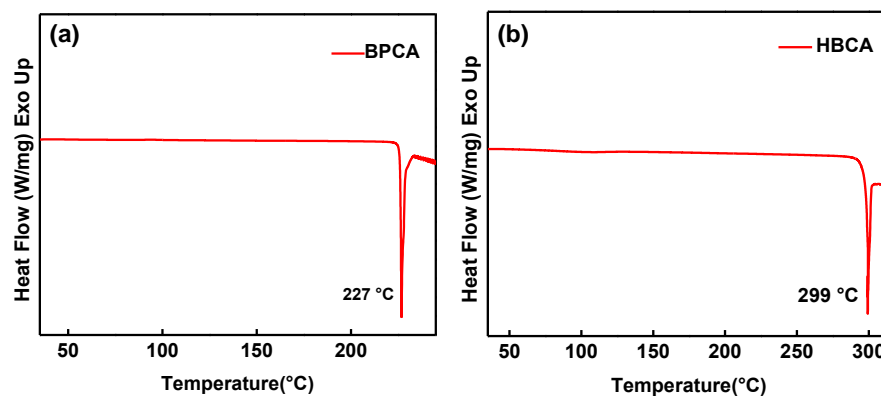


**Figure 5.7.** DSC thermogram of (a) BPCA and (b) HBCA molecule measured during first heating.

### 5.5.2. Effect of Small Molecules on the SMA Formation in Thin Films

Thin films of PS-*b*-P4VP(4HB)<sub>1</sub>, PS-*b*-P4VP(BPCA)<sub>1</sub> and PS-*b*-P4VP(HBCA)<sub>1</sub> were deposited on cleaned silicon wafers by dip-coating method at a withdrawal rate of 1 mm/sec from 1 wt% 1,4-dioxane solutions. The influence of the type of small molecules on film thickness is negligible and the film thicknesses measured in all the cases were  $26 \pm 2$  nm. In order to understand the effect of solvent on the microphase separation and microdomain orientation in the SMAs, chloroform and toluene/THF (75/25 V/V) were used for solvent vapor annealing. All the films were solvent vapor annealed under similar conditions using a glass chamber with an airtight cap (volume of the chamber = 250 cm<sup>3</sup> and area = 27 cm<sup>2</sup>). Thin film morphologies were evaluated by atomic force microscopy (AFM) images. It has to be noted that all the films were removed from the chamber and rinsed in methanol for 20 min to remove the small molecules to generate porous films so that contrast can be enhanced in the AFM images. Figure 5.8 shows a series of AFM height images of thin films of different SMAs before and after solvent vapor annealing in chloroform and toluene/THF mixture. Figures 5.8 (a, d, g) shows the AFM images of the as-casted thin films of three different SMAs using 1,4-dioxane solutions. In all the three cases, films exhibit disordered morphology due to the rapid evaporation of the solvent

during dip-coating. No macrophase separation of small molecules was observed in all the films indicating that the 1,4-dioxane is a good solvent to prepare the SMA solutions. It has to be noted that bulk samples showed macrophase separation of small molecules compared to the thin films. It might be due to the sample preparation conditions wherein the solvent evaporation rate is slow in bulk samples compared to that of the dip-coated thin films. On further annealing in chloroform and toluene/THF vapors, these thin films behave differently with respect to the small molecules used for the preparation of SMAs.

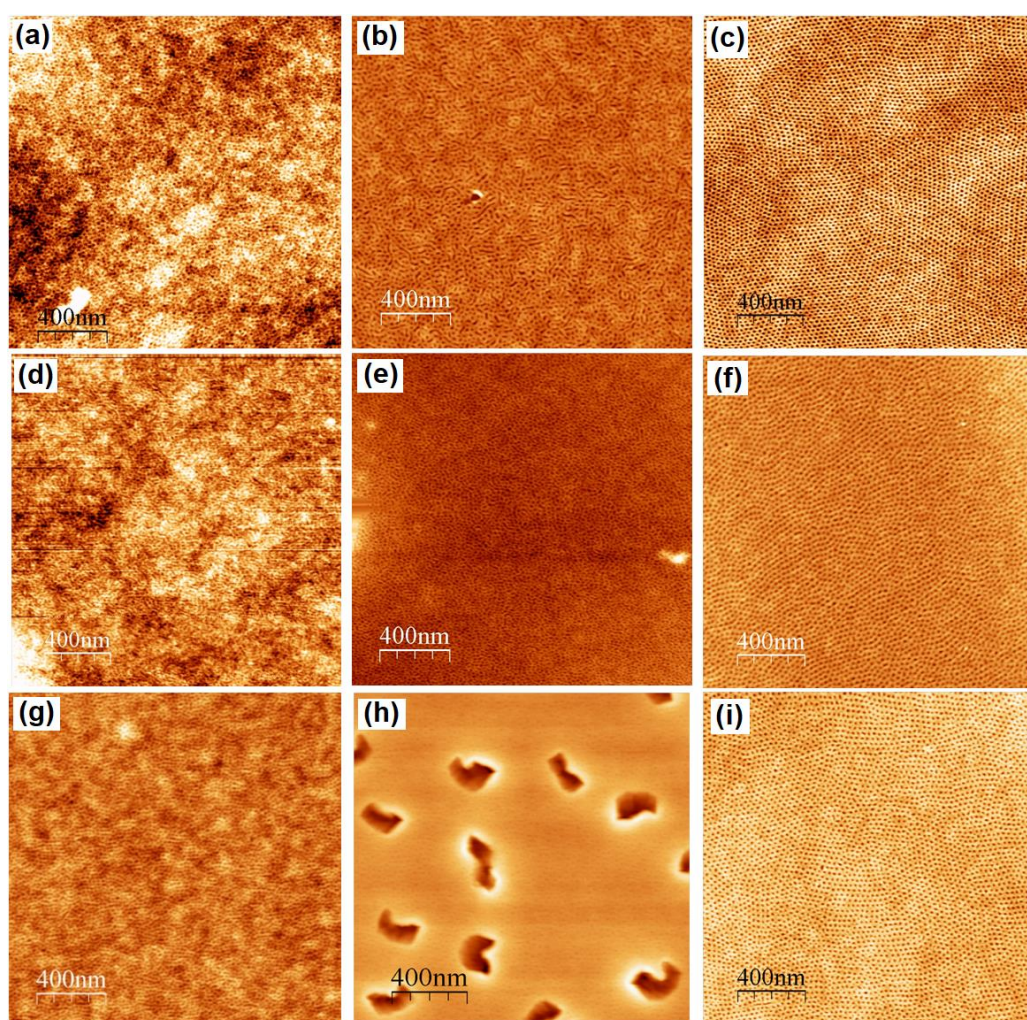


**Figure 5.8.** AFM height images of (a, d, g) as-cast films, (b, e, h) chloroform vapor annealed films and (c, f, i) toluene/THF vapor annealed films of PS-*b*-P4VP(4HB)<sub>1</sub>, PS-*b*-P4VP(BPCA)<sub>1</sub>, and PS-*b*-P4VP(HBCA)<sub>1</sub>, respectively. All the images were obtained after removal of the small molecules by rinsing in methanol for 20 min.

---

---

Figures 5.8b and 5.8c show the AFM images of SMA films prepared using the hydroxyl group-containing small molecule, i.e., 4HB after solvent vapor annealing in chloroform and toluene/THF mixture. No macrophase separation of small molecules was observed in both cases. Chloroform vapor annealed sample shows a clear microphase separation with disordered morphology where the cylindrical microdomains are oriented both parallel and perpendicular to the substrate. We have reported earlier that chloroform is a nonselective solvent for PS-*b*-P4VP and favoured the in-plane cylindrical morphology both in PS-*b*-P4VP and the SMA based on 2-(4'-hydroxybenzeneazo)benzoic acid (HABA) (PS-*b*-P4VP(HABA)<sub>1</sub>) using the films having the similar thickness.<sup>12, 29, 44, 51, 52</sup> In these two cases, as chloroform is a nonselective solvent, it is expected to be absorbed by both the domains equally and enhance the segmental mobility of both the blocks. It was also reported that the absorption of solvent molecules by constituted blocks could reduce the interaction parameter ( $\chi$ ) between the two blocks.<sup>29, 53</sup> Detailed pathways for the formation of in-plane cylinders using chloroform as a solvent was discussed in previous reports using PS-*b*-P4VP thin films.<sup>52</sup> But in the present case, chloroform is a moderate solvent for 4HB at room temperature, and as a result, the scenario is different compared to that of the PS-*b*-P4VP or PS-*b*-P4VP(HABA)<sub>1</sub>. Table 5.1 gives the selectivity of the solvents to the small molecules used in this study. The swelling of P4VP(4HB) domains in chloroform may not be that effective compared to pure P4VP and chloroform may not be distributed equally between PS and P4VP(4HB) domains. Selective swelling of constituted blocks results in the changes of volume fraction of the two phases and the  $\chi$  change may not be that effective. We are speculating here that the thickness of the PS-*b*-P4VP(4HB)<sub>1</sub> films in the swollen state is one of the key factors in controlling the microdomain orientation. On the other hand, films annealed in a mixture of toluene/THF vapors showed well-defined hexagonally packed cylindrical microdomains oriented perpendicular to the substrate (Figure 5.8c) with

---

---

the domain spacing of  $27 \pm 1$  nm and a pore diameter of  $8 \pm 1$  nm. The 1,4-dioxane vapor annealed sample also showed similar morphology. It has to be noted that both toluene/THF mixture and 1,4-dioxane are good solvents for 4HB and these solvents favoured the perpendicular morphology without any traces of macrophase separation of small molecules. As the AFM provides only the information about the surface morphology, we further used grazing-incidence small-angle X-ray scattering (GISAXS) to investigate the internal morphology of PS-*b*-P4VP(4HB)<sub>1</sub> thin films as a representative. Figure 5.9 shows the 2D GISAXS image and the corresponding in-plane profile of film annealed in a mixture of toluene/THF vapors after washing with methanol. As observed in thermally annealed bulk samples, the scattering vectors are located at the ratios of  $1:\sqrt{3}:2$  indicating the formation of perpendicularly oriented cylindrical morphology. The *d*-spacing estimated from the first-ordered reflection was  $\sim 26$  nm, which is well matching with the domain spacing estimated from the AFM image.

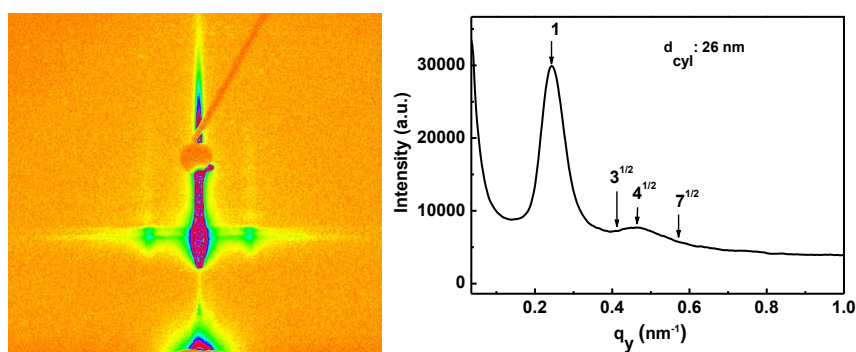


**Figure 5.9.** 2-Dimensional GISAXS pattern and the corresponding in-plane profile of annealed PS-*b*-P4VP(4HB)<sub>1</sub> thin film in a mixture of toluene/THF after removal of 4HB by rinsing in methanol.

It is worth mentioning that PS-*b*-P4VP thin films demonstrated the switching behaviour of the cylindrical microdomains upon annealing in different solvent vapors depending on the selectivity of the solvent to constituent blocks, solvent evaporation rate and the geometry of drying.<sup>52</sup> Sidorenko et al. demonstrated such switching phenomena in

SMA based on PS-*b*-P4VP diblock copolymer with HABA (PS-*b*-P4VP(HABA)<sub>1</sub>).<sup>44</sup> However, unlike in block copolymer thin films and PS-*b*-P4VP(HABA)<sub>1</sub> thin films, chloroform vapors are unable to switch the orientation of the cylinders from perpendicular to parallel in the case of PS-*b*-P4VP(4HB)<sub>1</sub>. This may be due to the weak interaction of chloroform with the 4-hydroxybiphenyl, which is attached to the P4VP block. From these results, we may say that the selectivity of the solvent to constituted blocks and small molecules is responsible for the switching behaviour in block copolymer SMA thin films.

**Table 5.1.** Solubility of polymers and small molecules in various solvents.

Polymer / Small Molecule	Tol/THF (75/25 V/V)	1,4-Dioxane	Chloroform	Methanol
PS	Soluble	Soluble	Soluble	Not soluble
P4VP	Soluble	Not readily soluble	Soluble	Soluble
4-Hydroxybiphenyl (4HB)	Readily soluble	Soluble	Soluble	Readily soluble
Biphenyl-4-carboxylic acid (BPCA)	Readily soluble	Soluble	Soluble at 60 °C	Readily soluble
4'-Hydroxy-4-biphenylcarboxylic acid (HBCA)	Readily soluble	Soluble	Not soluble	Readily soluble

Figures 5.8e and 5.8f show the AFM images of SMA films prepared using the carboxylic group-containing small molecule, i.e., BPCA after solvent vapor annealing in chloroform and toluene/THF mixture. Here it has to be noted that chloroform is not a good solvent for BPCA at room temperature, and as a result, the swelling of P4VP(BPCA) microdomains may not be that effective. Chloroform vapor annealed PS-*b*-P4VP(BPCA)<sub>1</sub> sample shows disordered morphology where the partial agglomeration of BPCA molecules was observed in the AFM image. This could be due to the different reasons. First, the

selectivity of the solvent, i.e., chloroform, is a nonsolvent for BPCA at room temperature and it promotes the crystallization or agglomeration of BPCA molecules in the swollen films. Second, the presence of carboxylic groups promotes the self-associated hydrogen bonds within the small molecules and leads to the formation of aggregates. Wu and Bubeck reported that the self-association of carboxylic groups in small molecules increases the attraction between small molecules and drives the macrophase separation in SMAs.<sup>47</sup> As some of the small molecules are aggregated, the stoichiometric ratio between 4VP and BPCA is less than 1, and as a result, the volume fraction of P4VP(BPCA) decreases in thin films. Such a difference in volume fraction and selectivity of the solvent to small molecules lead to the formation of disordered morphology in chloroform annealed thin films. On the other hand, PS-*b*-P4VP(BPCA)<sub>1</sub> films annealed in the vapors of toluene/THF mixture showed hexagonally packed cylinders oriented perpendicular to the substrate (Figure 5.8f) with the domain spacing of  $26 \pm 1$  nm and a pore diameter of  $8 \pm 1$  nm. In this case, no macrophase separation of BPCA molecules was observed which might be due to the better interactions between BPCA and toluene/THF mixture. It was reported that the  $T_g$  of block copolymers decrease upon solvent vapor uptake, where the decrease depends on the quality of the solvent to the block copolymers.<sup>52, 54, 55</sup> In this case, the mixture of toluene/THF is a relatively good solvent for PS-*b*-P4VP(BPCA)<sub>1</sub> compared to chloroform. The segmental mobility of PS and P4VP(BPCA) domains are high in the case of swollen film in the toluene/THF mixture and it facilitates the dispersion of BPCA molecules (BPCA is soluble in this solvent) at molecular level and helps in the formation of hydrogen bonding between 4VP and BPCA molecules.

---

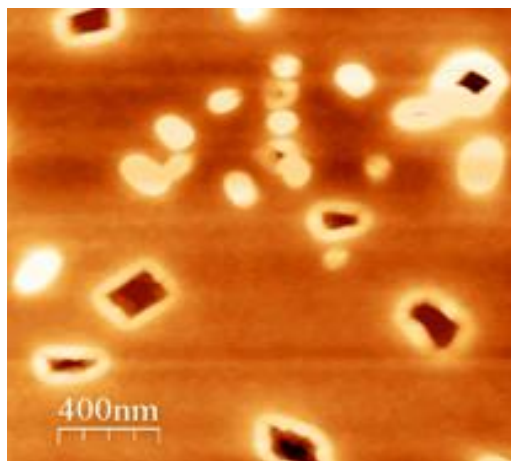


**Figure 5.10.** AFM image of the PS-*b*-P4VP(HBCA)<sub>1</sub> annealed using chloroform vapors.

Figures 5.8h and 5.8i show the AFM images of SMA films prepared using both hydroxyl and carboxylic groups containing small molecule, i.e., HBCA after solvent vapor annealing in chloroform and toluene/THF mixture. As mentioned in Table 1, chloroform is a nonsolvent for HBCA and P4VP(HBCA) domains are expected to show limited swelling in chloroform vapors compared to the other two small molecules discussed above. Chloroform vapor annealed PS-*b*-P4VP(HBCA)<sub>1</sub> sample shows different morphology where the macrophase separation of small molecules from the block copolymer is clearly evident on the surface of the thin film. In this case, as chloroform is a nonsolvent for HBCA, upon annealing SMA films in the chloroform vapors, the hydrogen-bonding formed between HBCA and 4VP breaks and the small molecules self-associate to form tiny crystals on the surface of thin films (Figure 5.10). Wu and Bubeck reported the formation of crystals on the surface of thin films in block copolymer SMAs using carboxylic groups containing azo compounds and it was assigned to the formation of self-associated hydrogen bonds and  $\pi$ - $\pi$  stacking of the small molecules.<sup>47</sup> It has to be noted that they have not studied the effect of solvents on the microphase separation of SMAs. These results suggest that selectivity of the solvent to small molecules plays a crucial role in the macrophase separation of small molecules than the functional group present. Interestingly, PS-*b*-P4VP(HBCA)<sub>1</sub> film

annealed in the vapors of toluene/THF mixture did not show any traces of macrophase separation of HBCA and the film shows perpendicularly oriented hexagonally packed cylinders (Figure 5.8i) with the domain spacing of  $26 \pm 1$  nm and a pore diameter of  $8 \pm 1$  nm. As explained in the previous example, good solubility of the small molecule (HBCA) helps in the formation of ordered structure. So again, selectivity of the solvent to the small molecule and the solubility of the constituted blocks and small molecules are crucial in controlling the microphase separation and the microdomain orientation in block copolymer SMA films.

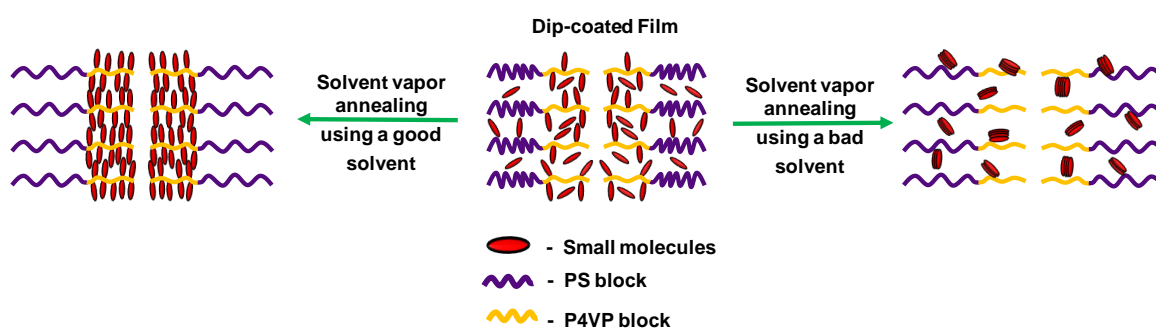


**Figure 5.11.** Schematic illustration of the phase behaviour of SMA thin films upon solvent vapor annealing using good and bad solvents (for small molecules).

Based on the experimental results obtained and discussed in the preceding section on thin films, the phase behaviour of SMAs thin films in the presence of various small molecules is schematically depicted in Figure 5.11. Dip-coated thin films from 1,4-dioxane solutions resulted in the formation of disordered morphology in all the SMAs without any macrophase separation of small molecules. 1,4-Dioxane is a good solvent for all the small molecules used in this study and upon the rapid evaporation of this solvent during dip-coating the macrophase separation of small molecules is not favoured. Irrespective of the functional groups present on the small molecules, solvent vapor annealing in good solvent for both small molecules and block copolymer resulted in the microphase separation of SMAs without any traces of agglomerated small molecules. When the good solvent was

---

---

used for the solvent vapor annealing, the mobility of block copolymer and small molecules will be high in the swollen films (similar to the melt in bulk samples) and upon the evaporation of solvent from the swollen films, microphase separation occurs due to the formation of hydrogen-bonds between small molecules and 4VP chains of block copolymer. On the other hand, when the bad solvent (for small molecules) was used for the solvent vapor annealing of SMA thin films, the dispersion of small molecules in the swollen films is limited, and upon the evaporation of the solvent, small molecules aggregate to form clusters. Even though the self-association of the carboxylic group-containing small molecules favours the aggregation of small molecules, the selectivity of the solvent to small molecules plays a crucial role in the phase behaviour of SMAs.

## **5.6. Conclusions**

In summary, we have successfully identified the factors influencing the formation of SMAs both in bulk and thin films using PS-*b*-P4VP and small molecules with different functional groups. In bulk, all the samples showed macrophase separated and crystallized small molecules in as casted samples. Upon thermal annealing, in SMAs containing hydroxyl-functionalized small molecule (4HB), the glass transition temperature of block copolymers played a crucial role in the diffusion of agglomerated small molecules and facilitated the effective formation of SMAs with the cylindrical morphology. In the case of SMAs containing carboxylic group functionalized small molecules, macrophase separation of small molecules was observed up to the melting temperature of small molecules due to the strong self-association of carboxylic groups. These results confirm that thermal annealing is not an appropriate method for the formation of SMAs using carboxylic group functionalized small molecules. In thin films, selectivity of the solvents to constituted blocks and small molecules played a major role in solvent vapor annealing. It was demonstrated that a bad solvent leads to macrophase separated structures with disordered

---

---

morphology and a good solvent leads to effective formation of SMAs with perpendicularly oriented hexagonally packed cylindrical morphology irrespective of the functional groups present in the small molecule. Breaking self-associated small molecules by heating above the glass transition temperature of block copolymers or using a good solvent for both block copolymer and the small molecules are important factors in the formation of SMAs in bulk and thin films. This work provides a guideline to choose the right small molecules and right annealing methods for the effective formation of block copolymer based SMAs.

## 5.7. References

- [1] Leibler, L. *Macromolecules* **1980**, 13, (6), 1602-1617.
- [2] Bates, F. S.; Fredrickson, G. H. *Physics today* **1999**, 52, (2), 32-38.
- [3] Darling, S. B. *Prog. Polym. Sci.* **2007**, 32, (10), 1152-1204.
- [4] Kim, H.-C.; Park, S.-M.; Hinsberg, W. D. *Chem. Rev.* **2010**, 110, (1), 146-177.
- [5] Bang, J.; Jeong, U.; Ryu, D. Y.; Russell, T. P.; Hawker, C. J. *Adv. Mater.* **2009**, 21, (47), 4769-4792.
- [6] Hamley, I. W., *Developments in block copolymer science and technology*. John Wiley & Sons: 2004.
- [7] Hamley, I. W., *The physics of block copolymers*. Oxford University Press New York: 1998; Vol. 19.
- [8] Ruokolainen, J.; Saariaho, M.; Ikkala, O.; ten Brinke, G.; Thomas, E. L.; Torkkeli, M.; Serimaa, R. *Macromolecules* **1999**, 32, (4), 1152-1158.
- [9] Ikkala, O.; ten Brinke, G. *Science* **2002**, 295, (5564), 2407-2409.
- [10] Ikkala, O.; ten Brinke, G. *Chem. Commun.* **2004**, (19), 2131-2137.
- [11] Sidorenko, A.; Tokarev, I.; Minko, S.; Stamm, M. *J. Am. Chem. Soc.* **2003**, 125, (40), 12211-12216.
- [12] Nandan, B.; Gowd, E. B.; Bigall, N. C.; Eychmüller, A.; Formanek, P.; Simon, P.; Stamm, M. *Adv. Funct. Mater.* **2009**, 19, (17), 2805-2811.
- [13] Tung, S.-H.; Kalarickal, N. C.; Mays, J. W.; Xu, T. *Macromolecules* **2008**, 41, (17), 6453-6462.
- [14] Rancatore, B. J.; Bai, P.; Xu, T. *Macromolecules* **2016**, 49, (11), 4155-4163.
- [15] Bai, P.; Kim, M. I.; Xu, T. *Macromolecules* **2013**, 46, (14), 5531-5537.

- 
- 
- [16] Rancatore, B. J.; Mauldin, C. E.; Fréchet, J. M. J.; Xu, T. *Macromolecules* **2012**, 45, (20), 8292-8299.
- [17] Kuila, B. K.; Gowd, E. B.; Stamm, M. *Macromolecules* **2010**, 43, (18), 7713-7721.
- [18] Valkama, S.; Ruotsalainen, T.; Nykänen, A.; Laiho, A.; Kosonen, H.; ten Brinke, G.; Ikkala, O.; Ruokolainen, J. *Macromolecules* **2006**, 39, (26), 9327-9336.
- [19] van Zoelen, W.; Asumaa, T.; Ruokolainen, J.; Ikkala, O.; ten Brinke, G. *Macromolecules* **2008**, 41, (9), 3199-3208.
- [20] Roland, S.; Gaspard, D.; Prud'homme, R. E.; Bazuin, C. G. *Macromolecules* **2012**, 45, (13), 5463-5476.
- [21] van Zoelen, W.; ten Brinke, G. *Soft Matter* **2009**, 5, (8), 1568-1582.
- [22] Ruokolainen, J.; Mäkinen, R.; Torkkeli, M.; Mäkelä, T.; Serimaa, R.; Brinke, G. t.; Ikkala, O. *Science* **1998**, 280, (5363), 557-560.
- [23] Deepthi, K.; Amal, R. R. B.; Rajeev, V. R.; Unni, K. N. N.; Gowd, E. B. *Macromolecules* **2019**, 52, (7), 2889-2899.
- [24] Faul, C. F. J.; Antonietti, M. *Adv. Mater.* **2003**, 15, (9), 673-683.
- [25] Pollino, J. M.; Weck, M. *Chem. Soc. Rev.* **2005**, 34, (3), 193-207.
- [26] Hoeben, F. J. M.; Jonkheijm, P.; Meijer, E. W.; Schenning, A. P. H. J. *Chem. Rev.* **2005**, 105, (4), 1491-1546.
- [27] Roland, S.; Pellerin, C.; Bazuin, C. G.; Prud'homme, R. E. *Macromolecules* **2012**, 45, (19), 7964-7972.
- [28] Krishnan, D.; Raj R B, A.; Gowd, E. B. *Polym. Chem.* **2019**, 10, (23), 3154-3162.
- [29] Nandan, B.; Vyas, M. K.; Böhme, M.; Stamm, M. *Macromolecules* **2010**, 43, (5), 2463-2473.
- [30] Huang, W.-H.; Chen, P.-Y.; Tung, S.-H. *Macromolecules* **2012**, 45, (3), 1562-1569.
- [31] Zhao, Y.; Thorkelsson, K.; Mastroianni, A. J.; Schilling, T.; Luther, J. M.; Rancatore, B. J.; Matsunaga, K.; Jinnai, H.; Wu, Y.; Poulsen, D.; Fréchet, J. M. J.; Paul Alivisatos, A.; Xu, T. *Nat. Mater.* **2009**, 8, 979.
- [32] Hofman, A. H.; Chen, Y.; ten Brinke, G.; Loos, K. *Macromolecules* **2015**, 48, (5), 1554-1562.
- [33] Hofman, A. H.; Reza, M.; Ruokolainen, J.; ten Brinke, G.; Loos, K. *Macromolecules* **2014**, 47, (17), 5913-5925.
- [34] Vukovic, I.; ten Brinke, G.; Loos, K. *Macromolecules* **2012**, 45, (23), 9409-9418.
- [35] Kao, J.; Tingsanchali, J.; Xu, T. *Macromolecules* **2011**, 44, (11), 4392-4400.
- 
-

- [36] Sun, H.-S.; Lee, C.-H.; Lai, C.-S.; Chen, H.-L.; Tung, S.-H.; Chen, W.-C. *Soft Matter* **2011**, 7, (9), 4198-4206.
- [37] Korhonen, J. T.; Verho, T.; Rannou, P.; Ikkala, O. *Macromolecules* **2010**, 43, (3), 1507-1514.
- [38] Rancatore, B. J.; Kim, B.; Mauldin, C. E.; Fréchet, J. M. J.; Xu, T. *Macromolecules* **2016**, 49, (3), 833-843.
- [39] Rancatore, B. J.; Mauldin, C. E.; Tung, S.-H.; Wang, C.; Hexemer, A.; Strzalka, J.; Fréchet, J. M. J.; Xu, T. *ACS nano* **2010**, 4, (5), 2721-2729.
- [40] Lee, K. H.; Bai, P.; Rancatore, B. J.; He, B.; Liu, Y.; Xu, T. *Macromolecules* **2016**, 49, (7), 2639-2645.
- [41] van Zoelen, W.; Polushkin, E.; ten Brinke, G. *Macromolecules* **2008**, 41, (22), 8807-8814.
- [42] Tung, S.-H.; Xu, T. *Macromolecules* **2009**, 42, (15), 5761-5765.
- [43] Gowd, E. B.; Rama, M. S.; Stamm, M., Nanostructures based on self-assembly of block copolymers. In *Nanofabrication*, Springer: 2012; pp 191-216.
- [44] Tokarev, I.; Krenek, R.; Burkov, Y.; Schmeisser, D.; Sidorenko, A.; Minko, S.; Stamm, M. *Macromolecules* **2005**, 38, (2), 507-516.
- [45] Roland, S.; Prud'homme, R. E.; Bazuin, C. G. *ACS Macro Lett* **2012**, 1, (8), 973-976.
- [46] Roland, S.; Gamys, C. G.; Grosrenaud, J.; Boissé, S.; Pellerin, C.; Prud'homme, R. E.; Bazuin, C. G. *Macromolecules* **2015**, 48, (14), 4823-4834.
- [47] Wu, S.; Bubeck, C. *Macromolecules* **2013**, 46, (9), 3512-3518.
- [48] Ruokolainen, J.; ten Brinke, G.; Ikkala, O.; Torkkeli, M.; Serimaa, R. *Macromolecules* **1996**, 29, (10), 3409-3415.
- [49] Ikkala, O.; Ruokolainen, J.; ten Brinke, G.; Torkkeli, M.; Serimaa, R. *Macromolecules* **1995**, 28, (21), 7088-7094.
- [50] Bondzic, S.; de Wit, J.; Polushkin, E.; Schouten, A. J.; ten Brinke, G.; Ruokolainen, J.; Ikkala, O.; Dolbnya, I.; Bras, W. *Macromolecules* **2004**, 37, (25), 9517-9524.
- [51] Gowd, E. B.; Nandan, B.; Vyas, M. K.; Bigall, N. C.; Eychmüller, A.; Schlörb, H.; Stamm, M. *Nanotechnology* **2009**, 20, (41), 415302.
- [52] Gowd, E. B.; Koga, T.; Endoh, M. K.; Kumar, K.; Stamm, M. *Soft Matter* **2014**, 10, (39), 7753-7761.
- [53] Li, Y.; Wang, X.; Sanchez, I. C.; Johnston, K. P.; Green, P. F. *J. Phys. Chem. B* **2007**, 111, (1), 16-25.

- [54] Di, Z.; Posselt, D.; Smilgies, D.-M.; Papadakis, C. M. *Macromolecules* **2010**, 43, (1), 418-427.
- [55] Paik, M. Y.; Bosworth, J. K.; Smilgies, D.-M.; Schwartz, E. L.; Andre, X.; Ober, C. K. *Macromolecules* **2010**, 43, (9), 4253-4260.



### Overall Summary

---

---

#### 6.1. Summary

The overall concept of the thesis is to understand the assembly of small molecules within the block copolymer microdomains using the supramolecular self-assembly process. Several thermodynamic and kinetic factors affect the overall assembly of block copolymer based supramolecules. These include polymer-small molecule interactions, BCP microphase separation, interaction parameter, polymer chain deformation, melting, crystallinity and packing of the small molecule, etc. The following questions were addressed to understand the effective formation of block copolymer based supramolecules. What are the factors that influence the formation of block copolymer based supramolecular in bulk and thin films? Whether the microphase separation of the block copolymers improves the topochemical polymerization of hierarchically ordered monomers? The major focus in this field was so far on the addition of a single small molecule to polymers for the formation of block copolymer based supramolecules. Is it possible to achieve the multi-component assembly in block copolymer based supramolecules? We tried to address some of these questions with the support of experimental evidence in this thesis. The major findings of the present thesis are summarized below.

The 1<sup>st</sup> chapter comprises a general introduction about the supramolecular assembly of block copolymers. The phase behaviour of block copolymer supramolecules in bulk and thin films and the factors that are affecting the block copolymer supramolecules were described here in detail. The chapter concludes with a short description of the applications of the block copolymer supramolecular based structures in various fields.

In the 2<sup>nd</sup> chapter, we have successfully demonstrated the hierarchical self-assembly of photopolymerizable diacetylene (PCDA) monomers within the polystyrene-*b*-poly(4-vinyl pyridine) (PS-*b*-P4VP) block copolymer microdomains in the solid-state through noncovalent interactions, i.e., hydrogen bonding. The hierarchical ordering and the molecular orientation of PCDA molecules within the block copolymer microdomains are controlled by the microphase separation of the block copolymer supramolecules, which is further controlled by different annealing techniques. The hierarchically ordered PCDA molecules are then converted into an optoelectronically active material by photoirradiation followed by subsequent heating. The PCDA monomers were found to self-assemble effectively in solvent vapor annealed samples and afford the formation of longer  $\pi$ -conjugated PDA upon the topochemical polymerization compared to that of the thermally annealed samples. Though the microphase segregated block copolymer morphology was improved significantly upon thermal annealing, the molecular alignment of the PCDA became inappropriate for the effective topochemical polymerization.

In the 3<sup>rd</sup> chapter for the first time, we have demonstrated the three-component hierarchical self-assembly to create the alternate co-assembly of donor and acceptor molecules within the block copolymer microdomains. The 1-pyrene butyric acid (PBA) molecules (donor) are hydrogen-bonded with 4-vinyl pyridine of PS-*b*-P4VP and resulted in the formation of cylindrical morphology in bulk. Further addition of naphthalene diimide (NDI, acceptor) molecules to this assembly favoured the formation of charge-transfer (CT) complexes by aromatic-aromatic interactions without disturbing the hydrogen bonding between the PBA and P4VP, and the cylindrical morphology changed to the lamellar morphology. The noncovalent aromatic donor-acceptor interactions favoured the interdigitation of donor molecules to form the co-assembly of D-A CT complexes within the block copolymer microdomains and the SCLC mobility measurements proved the

---

---

higher charge mobility in the case of block copolymer supramolecules compared to that of the physical blend of donor and acceptor molecules.

In the 4<sup>th</sup> chapter, a detailed investigation was carried out on the effect of functionalization on both donor and acceptor molecules for the D-A stacking and the formation of hierarchical assembly within the block copolymer domains. Here, the length of the alkyl chain in both the molecules is kept same, so that these molecules form comb kind of structures via hydrogen bonding and that should allow the  $\pi$ - $\pi$  interaction between D and A. Unlike the previous chapter, here the interdigitation of molecules was not observed because of the hydrogen bonding capability of both D and A molecules that restricted the interdigitation of these molecules within the block copolymer domains. It was also observed that the noncovalent interactions lead to the formation of hierarchical structures and charge-transfer complexes between functionalized PBA and NDI within block copolymer microdomains. Functionalization of acceptor molecules favour the formation of stable D-A stacks in the physical blend as well. Based on these two chapters, we may say that the multi-component assembly of small molecules and block copolymers are possible to generate novel structures and the functionalization of D and A is a key factor in controlling the hierarchical assembly of small molecules within the block copolymer microdomains. This opens up new insight in the area of electronic devices because of its advantages such as solution processability, controlled formation of hierarchical assemblies and the CT interaction in the solid state.

The 5<sup>th</sup> chapter discussed the factors influencing the formation of SMAs both in bulk and thin films using PS-*b*-P4VP and small molecules with different functional groups. For that purpose, we have chosen three identical biphenyl systems as small molecules, one with hydroxyl functionalized groups (4-hydroxybiphenyl (4HB)), the other with carboxylic functionalized groups (biphenyl-4-carboxylic acid (BPCA)) and the last one having both

---

---

functionalities (4'-hydroxy-4-biphenylcarboxylic acid (HBCA)). In bulk, the as-casted sample shows macrophase separated morphology in all the three SMAs. Upon thermal annealing, the glass transition temperature ( $T_g$ ) of the block copolymer played a key role in SMAs with the hydroxy-functionalized small molecules and promoted the effective SMAs with cylindrical morphology. In the case of SMAs with the carboxylic acid-functionalized small molecules, the macrophase separation is observed up to the melting temperature of small molecules, which may be due to the self-associated hydrogen bonds of carboxylic groups within small molecules. In thin films, the selectivity of the solvent to the polymer and small molecules has a crucial role in the formation of SMAs. It was demonstrated that a good solvent leads to effective formation of SMAs with well-defined morphology and a bad solvent leads to macrophase separated structures with disordered morphology irrespective of the functional groups present in the small molecules.

The knowledge generated in this thesis provides a guideline for the basic design of effective SMAs using different kinds of small molecules, block copolymers and annealing conditions.

## 6.2. Future Perspectives

The results obtained in the present study provide excellent scope for further research, as discussed below.

- Preliminary studies showed that the hierarchically ordered PCDA molecules within the block copolymer domains are converted into an optoelectronically active material by photoirradiation followed by subsequent heating. It will be interesting to study the influence of alkyl chain length and functional groups on monomers on the formation of hierarchical structures and its influence on the properties of the materials upon topochemical polymerization.

- 
- 
- Next-generation semiconductors can be obtained using the block copolymer based supramolecules by choosing a variety of organic and inorganic additives that can selectively incorporate into one of the blocks of the self-assembled BCPs. The developed materials can be tested as active materials in bulk heterojunction solar cell devices.
  - The effect of nanoscopic confinement of donor and acceptor (D-A) assembly will be interesting to explore in thin films state to understand the optoelectronic properties.
- 
-



---

---

## Papers Presented at Conferences

### *Oral Presentations*

1. Directed Assembly of Hierarchical Supramolecular Block Copolymers: A Strategy to Create Donor-Acceptor Charge Transfer Stacks. **K. Deepthi**, R. B. Amal Raj and E. Bhoje Gowd, **National Seminar on Advanced Functional Materials (NSAFM-2019)** held at Kerala University, Trivandrum. (*Best oral presentation award*)
2. Directed Assembly of Hierarchical Supramolecular Block Copolymers: A Strategy to Create Donor-Acceptor Charge Transfer Stacks. **K. Deepthi**, R. B. Amal Raj and E. Bhoje Gowd, **MRSI Annual Technical Meeting-2019**, held at CSIR-NIIST, Thiruvananthapuram, Kerala.
3. Directed Assembly of Hierarchical Supramolecular Block Copolymers: A Strategy to Create Donor-Acceptor Charge Transfer Stacks. **K. Deepthi**, R. B. Amal Raj and E. Bhoje Gowd, **Indian Institute of Metals (IIM-2019)**, held at CSIR-NIIST, Thiruvananthapuram, Kerala.

### *Poster Presentations*

1. Directed Assembly of Hierarchical Supramolecular Block Copolymers: A Strategy to Create Donor-Acceptor Charge Transfer Stacks. **K. Deepthi**, R. B. Amal Raj and E. Bhoje Gowd, **International Conference on Polymer Science and Technology (MACRO-2018)**, held at IISER Pune, Maharashtra.
2. Alternate Stacking of D-A system via Supramolecular Assembly of Block Copolymers, **K. Deepthi**, R. B. Amal Raj and E. Bhoje Gowd, **Polymer Conference for Young Researchers (PCYR-2018)**, held at CSIR-NIIST, Thiruvananthapuram, Kerala.

3. Alternate Stacking of D-A system via Supramolecular Assembly of Block Copolymers, **K. Deepthi**, R. B. Amal Raj and E. Bhoje Gowd, **International Conference on Recent Trends in Materials Science and Technology (ICMST-2018)** held at VSSC, Thiruvananthapuram, Kerala.
  4. Directed Assembly of Hierarchical Supramolecular Block-Copolymers: A Strategy to Create Donor-Acceptor Charge-Transfer Stacks, **K. Deepthi**, R. B. Amal Raj and E. Bhoje Gowd, **National Conference on Luminescence and its Applications (NCLA-2018)** held at CSIR-NIIST, Thiruvananthapuram, Kerala.
  5. Influence of Additives on the Formation of Block Copolymer-based Supramolecules in Bulk and Thin Films, **K. Deepthi**, and E. Bhoje Gowd, **Short Course on Polymer Science & Indo-Japan Joint Symposium on Polymeric Materials**, 31<sup>st</sup> January-1<sup>st</sup> February, 2017, held at Thiruvananthapuram, Kerala. (*Best poster presentation award*)
  6. Influence of Additives on the Formation of Block Copolymer-based Supramolecules in Bulk and Thin Films, **K. Deepthi**, and E. Bhoje Gowd, **International Conference on Polymer Science and Technology (MACRO-2017)**, held at Thiruvananthapuram, Kerala.
  7. Structural Evolution of Poly(L-lactide) Block upon Heating of the Amorphous ABA Triblock Copolymers Containing Poly(L-lactide) A Blocks, **Deepthi Krishnan**, S. Nagarajan, E. Bhoje Gowd, **National Conference on Recent Trends in Materials Science and Technology (NCMST-2016)** held at IIST, Thiruvananthapuram, Kerala.
- 
-

8. Structural Evolution of Poly(L-lactide) Block upon Heating of the Amorphous ABA Triblock Copolymers Containing Poly(L-lactide) A Blocks, **Deepthi Krishnan**, S. Nagarajan, E. Bhoje Gowd, **National Conference on Materials Research Society of India (MRSI-2016)** held at NEIST, Assam.
- 
-



---

---

## List of Publications

### *Related to Thesis*

1. Directed Assembly of Hierarchical Supramolecular Block Copolymers: A Strategy to Create Donor-Acceptor Charge Transfer Stacks.  
**K. Deepthi**, R. B. Amal Raj, V. R. Rajeev, K. N. N. Unni, E. B. Gowd\*  
*Macromolecules*, 2019, 52, 2889-2899.
2. Topochemical Polymerization of Hierarchically Ordered Diacetylene Monomers within the Block Copolymer Domains.  
**K. Deepthi**, R. B. Amal Raj, E. B. Gowd\*  
*Polymer Chemistry*, 2019, 10, 3154–3162.
3. Recent Advances in Block Copolymer-Based Functional Supramolecules.  
**K. Deepthi**, R. B. Amal Raj, E. B. Gowd\*  
*Bulletin of Material Science*, 2019. (In press)
4. Factors Influencing the Formation of Block Copolymer-based Supramolecular in Bulk and Thin Films.  
**K. Deepthi**, Manfred Stamm, E. B. Gowd\*  
(Submitted to *Soft Matter*).
5. Co-assembly of Functionalized Donor-Acceptor Molecules within the Block Copolymer Domains via Supramolecular Approach.  
**K. Deepthi**, R. B. Amal Raj, E. B. Gowd\*  
(Manuscript under preparation).

***Not Related to Thesis***

1. Structural Evaluation of Poly(L-lactide) Block upon Heating of the Glassy ABA Triblock Copolymers Containing Poly(L-lactide) A Blocks.

S Nagarajan, **K. Deepthi**, E B Gowd\*

*Polymer*, 2016, 105, 422-430.

***Book Chapter***

1. Crystallization Behavior of Crystalline–Amorphous and Crystalline–Crystalline Block Copolymers Containing Poly (l-lactide).

S. Nagarajan, **K. Deepthi**, V. P. Sivaprasad, E. B. Gowd\*

*Crystallization in Multiphase Polymer Systems, Elsevier*, 2018, 93-122.

---

---

